The role of Nrf2 in protection of the neurovascular unit following stroke

Srivastava, Salil

Awarding institution:
King's College London

The role of Nrf2 in protection of the neurovascular unit following stroke

A thesis submitted for the degree of
Doctor of Philosophy
King's College London

Salil Srivastava

Cardiovascular Division
BHF Center of Research Excellence
King's College London
Franklin Wiklins Building
Waterloo Campus
London SE1 9NH, UK

February 2014

मां और डैडा

यह आप लोगों के लिए है

Abstract

Cerebral stroke contributes to approximately 10% of deaths worldwide and is the most common cause of adult morbidity. The cost of stroke to the UK is approximately £8.9 billion per annum, of which 5% accounts for costs incurred by the National Health Service. About 85% of cerebral stroke patients experience cerebral ischaemia-reperfusion injury, with recombinant tissue-plasminogen activator (rt-PA) being the only approved form of treatment. rtPA treatment is only efficacious within in a limited time window (3 – 4.5h) after the onset of ischaemia, however, it is coupled with severe side-effects. This thus warrants the requirement of further research into improved therapeutic strategies to protect the brain against ischaemia-induced damage.

Accumulating evidence implicates a major role for oxidative stress in the pathophysiology of stroke, resulting in the loss of cells that form the neurovascular unit. Research currently focuses on protecting astrocytes and neurons, but has failed to identify the need for protecting of the cerebrovascular endothelium, important for the maintenance of brain function and environment. The redox sensitive transcription factor NF-E2 related factor 2 (Nrf2) orchestrates an adaptive response in upregulating phase II detoxifying enzymes and antioxidant stress proteins. However, little is known about the temporal and spatial distribution of Nrf2 in different brain cell types after cerebral ischaemia and reperfusion injury. Furthermore, post-stroke administration of the dietary isothiocyanate sulforaphane (SFN), an Nrf2 inducer, has been shown to protect the ischaemic brain. However, the effects of sulforaphane pre-conditioning *in vivo* remain to be elucidated.

Male Sprague-Dawley rats (260 – 300g) were subjected to 70 min middle cerebral artery occlusion (MCAo) and reperfused for 4, 24 or 72h. Paraformaldehyde perfused-fixed brains were then excised and cryosectioned to obtain 10µm coronal brain sections. Total cellular and nuclear/cytoplasmic Nrf2 content was calculated using a novel quantitative immunohistochemical technique, based on the initial rate of 3,3'-diaminobenzidine (DAB) polymer formation, following the reaction of DAB with H_2O_2. Cytoplasmic Nrf2 content increased in cerebral cells after 4h reperfusion injury, whereas a significant increase in nuclear content was observed after 24h reperfusion injury. Total cellular Nrf2 content was also greater in stroke-affected regions 24h after 70 min MCAo and decreased in all regions of the ischaemic brain after 72h. To determine the effects of sulforaphane (SFN) treatment on Nrf2 *in vivo*, rats were administered SFN (5 mg/kg. *i.p.*) for 1, 2, 4 and 24h, or pre-treated with SFN 1h prior to 70 min MCAo and 24h reperfusion injury. SFN pre-treatment significantly reduced Nrf2 protein content in rats after 24h reperfusion injury. Furthermore, SFN treatment of naïve rats revealed a significant increase in Nrf2 protein content within 1h of administration.

To further elucidate the role of Nrf2 mediated protection in the cerebral endothelium, the mouse brain endothelial cell line, bEnd.3, was used as an *in vitro* model of the blood-brain barrier (BBB). SFN time- (4 – 24 h) and dose-dependently (0.5 – 2.5 μM) increased protein expression of HO-1 and NQO1, two Nrf2-regulated proteins. Furthermore, SFN (2.5μM) also induced Nrf2 nuclear translocation, 1 – 4h after treatment. bEnd.3 cells deprived of oxygen and glucose, as an *in vitro* model of cerebral ischaemia, revealed a time dependent increase in cell death, which was attenuated in cells pre-treated with SFN (2.5μM) for 12h.

This study thus reports the first quantitative analysis of the temporal and spatial distribution of Nrf2 following ischaemia and reperfusion injury. We provide evidence that SFN administration *in vivo* rapidly increases expression of Nrf2 and its target enzymes, and that pre-treatment protects the brain against oxygen-glucose deprivation. Our *in vitro* studies revealed SFN stimulates Nrf2-mediated HO-1 and NQO1 expression, conferring protection to the brain endothelium against ischaemia-induced damage. Thus, SFN pre-conditioning may provide a potential therapeutic strategy to limit BBB permeability and associated neurological deficits after cerebral stroke.

Acknowledgements

For my second MRes rotation I was informed that I would be joining Prof Giovanni E Mann's research group. My colleagues told me that Giovanni is a task-master and I am crazy for joining his research group. When I first met Gio it became clear, Gio is very passionate about his science, he lives for it and wants us to do the same. There is one memory I wish to share…. When I joined his research group, my presentation skills were not up to par. Before my last MRes presentation, Gio took me to the meeting room, left me there and said that I have 4 hours to practice and he will bring everyone to listen to me. In those 4 hours, I stopped and started many times, but by the time everyone listened it flowed, and Gio I saw you smile at the moment, so I knew I was heading in the right direction. After every presentation that I gave, Gio would always say to me this is the best I have seen you present, but we need to improve! I hope that one day I can present my work like you and fill the audience with the same confidence. It has been an honour for me to be your PhD student. Gio, you introduced me to Nrf2, and where people in the group have focused on its downstream targets, I have worked closely on this one protein for a couple of years, and now, I am attached to it like glue ☺ and will aim to advance this field further! Gio, thank you for guiding me through this PhD, taking my emails at ridiculous hours in the night, for being patient with me and looking after me for the past 4 years. I hope I have delivered and made you proud.

I guess compared to other students I have had three PhD supervisors rather than two. Prof GE Mann, Dr Paul Fraser and Dr Richard Siow. Throughout the course of this PhD, I have worked closely with Paul, both in the lab and analysing data. The time I spent writing the *J Physiol* paper with Paul was an invaluable experience, and is something I will never forget. Richard has been a greater mentor and also a friend in this PhD. His advice and input on science in general and *in vitro* work have been priceless, and our chats about technology has always made things fun too. Thank you to all three of my supervisors, for dealing with me over the past 4 years. I would also like to thank Dr Alessio Alfieri for his time to teach me the MCAo technique in rats and for his fluorescence work, with which this thesis would have shown an incomplete story. Thank Alessio for you help and for your patience while teaching me MCAo protocol.

There are many friends that I have made over the past few years! To my group, past members and new (Xinghua, Sarah, Tabasum, Bijal, Shane, Tom, Keith, Li Li, Alessio), thank you for the fun times and making this PhD experience an enjoyable one. Sarah Chapple, thank you for your support and encouragement through out this PhD and making the time in the lab interesting with your talks! Shane, Bijal and Li Li, thank you for making the lab enjoyable, and Tom, although I have not spent much time with you here, thank you for letting me borrow that marker pen. Keith, your work on improving our data analysis has helped me immensely and sped up our work. Thank you for working with me this year, with out your help, some of the data I present

in this thesis would not have been here. Also maybe its time you switch to an Apple computer. Aisah, your constant criticism and questions about my work made me work harder and harder, Thank you!! Our conversations have always left me asking more questions about science, and how can I forget, you have taught me so much about TRPA1. I would also like to thank other members of the vascular biology group (Khadija, Pratish, Jiaqi) for being friendly and smiley faces around this floor.

Finally, but definitely not last, I need to say thank you to my family. I will start of with Dada, it is because of him I decided to do a PhD. His constant research into the career paths available and his encouragement and support to apply for a PhD has yielded many results. Dada, I hope you are proud of me and always will be. Maa, you have taken care of me throughout this PhD, whenever I worked through the night, you would not sleep and kept checking on me to make sure I am OK and not asleep on the sofa. I am sorry I have not been able to do a lot at home recently but I will now! And my dear little brother, Saket, you have made heavy moments fun, with laughs and supported me throughout. I wish you all the best in your PhD Saket, and I will be there to support you throughout! Come on my little brother, lets make things different!

The journey of this PhD has been eventful and will be one I will remember and cherish for a long time to come.

List of publications

Original research articles and reviews

Alfieri A, **Srivastava S**, Siow RCM, Modo M, Fraser PA, Mann GE (2011). Targeting the Nrf2–Keap1 antioxidant defence pathway for neurovascular protection in stroke. *J Physiol*. **589**: 4125-4136.

Srivastava S, Alfieri A, Siow RCM, Mann GE and Fraser PA (2013). Temporal and spatial distribution of Nrf2 in rat brain following stroke: quantitation of nuclear to sytoplasmic Nrf2 content using a novel immunohistochemical technique, *J Physiol*. **591**: 3525-3538.

Alfieri A, **Srivastava S**, Siow RCM, Cash D, Modo M, Duchen MR, Fraser PA, Williams SC, Mann GE (2013). Sulforaphane preconditioning of the Nrf2/HO-1 defense pathway protects the cerebral vasculature against blood-brain barrier disruption and neurological deficits in stroke. *Free Radic. Biol. Med*., **65**: 1012-1022

Published Abstracts

Srivastava S, Alfieri A, Siow RCM, Mann GE and Fraser PA. Immunohistochemical quantification of the redox sensitive transcription factor Nrf2 in stroke. *Joint meeting of the British and American microcirculation societies,* July 2012, *Microcirculation* **PC103,** DOI:10.1111/micc.12018 (Poster Communication).

Alfieri A, **Srivastava S,** Siow RCM, Modo M, Duchen MR and Mann GE. Antioxidant defences in the gliovascular complex in stroke: heme oxygenase 1 and 2 expression in cerebral-microvessels after ischaemia-reperfusion injury. *Joint meeting of the British and American microcirculation societies,* July 2012, *Microcirculation* **PC4**, DOI:10.1111/micc.12018 (Poster Communication).

Alfieri A, **Srivastava S,** Siow RCM, Modo M, Duchen MR and Mann GE. Heme Oxygenase 1 Induction in the peri-infarct region after cerebral ischemia-reperfusion injury in rats is associated with reduced blood-brain barrier breakdown. *Society for Free Radical Research International*, September 2012, *Free Radic. Biol. Med.* **51**, S136-S137.

Srivastava S, Alfieri A, Siow RCM, Fraser PA and Mann GE. Quantification of Nrf2 content in core and peri-infarct regions of rat brains following ischemia-reperfusion injury. *Society for free radical biology and medicine (SFRBM)* November 2012, *Free Radic. Biol. Med.* **53**, S175 (Poster Communication).

Srivastava S, Alfieri A, Siow RCM, Fraser PA and Mann GE. Time dependent changes in the spatial distribution of Nrf2 after cerebral stroke. *British microcirculation society early career investigator symposium*, April 2013, (Poster Communication).

Alfieri A, **Srivastava S,** Siow RCM, Modo M, Duchen MR and Mann GE. Sulforaphane pre-treatment reduces blood-brain barrier disruption in experimental stroke by inducing heme oxygenase-1 expression in the glio-vascular complex of the peri-infarct region. *Experimental Biology,* April 2013, *FASEBJ,* **27**, 682.2 (Poster Communication).

Alfieri A, **Srivastava S,** Siow RCM, Modo M, Duchen MR and Mann GE. Spatial and temporal expression of Nrf2-inducible antioxidant defences in the gliovascular complex after stroke. *International union of physiological sciences (IUPS)*, July 2013, *Proceedings of the physiological society, Proc 37th IUPS,* PCA361.

Srivastava S, Alfieri A, Siow RCM, Fraser PA and Mann GE. Sulforaphane pre-treatment reduces Nrf2 content in core and peri-infarct brain regions in rats subjected to cerebral ischaemia-reperfusion injury. *International union of physiological sciences (IUPS)*, July 2013, *Proceedings of the Physiological Society, Proc 37th IUPS,* PCA362 (Poster Communication).

Unpublished Abstracts

Srivastava S, Alfieri A, Siow RCM, Modo M, Fraser PA and Mann GE. Role of Nrf2 in protection of the neurovascular unit following stroke. *BHF center of research excellence symposium, King's College London,* May 2011, poster communication (*Awarded poster prize*)

Srivastava S, Fraser PA, Siow RCM, Modo M, Mann GE and Alfieri A. Role of Nrf2 in protection of the neurovascular unit following cerebral ischaemia-reperfusion. *Young physiologists symposium: Imaging plasticity – from cells to brain, Univ Oxford,* July 2011, poster communication

Srivastava S, Alfieri A, Siow RCM, Mann GE and Fraser PA. Quantification of the redox sensitive transcription factor Nrf2 following cerebral ischaemia. *BHF 4-year PhD symposium, UCL*, March 2012, poster communication

Srivastava S, Alfieri A, Siow RCM, Mann GE and Fraser PA. Quantification of the redox sensitive transcription factor Nrf2 following cerebral ischaemia. *School of Medicine Graduate Showcase King's college London*, July 2012, poster communication

Srivastava S, Alfieri A, Siow RCM, Fraser PA and Mann GE. Quantification of Nrf2 content in core and peri-infarct regions of rat brains following ischemia-reperfusion injury. *London vascular biology forum (LVBF)*, December 2012, poster communication (*Awarded poster prize*)

Srivastava S, Alfieri A, Siow RCM, Fraser PA and Mann GE. Time dependent changes in the spatial distribution of Nrf2 after cerebral ischaemia-reperfusion injury. *BHF 4-year PhD Symposium, Univ Oxford*, April 2013, oral communication

Srivastava S, Alfieri A, Siow RCM, Fraser PA and Mann GE. Time dependent changes in the spatial distribution of Nrf2 after cerebral ischaemia. *BHF center of research excellence symposium King's College London*, April 2013, oral communication

List of Abbreviations

2,3-DHBA	2,3-dihydroxybenzoic acid
6-ODHA	6-hydroxydopamine
AHR	Aryl hydrocarbon receptor
AhR	Aryl hydrocarbon receptor
AITC	Allyl isothiocyanate
AMP	Adenosine monophosphate
AMPA	α-Amino-3-hydroxy-5-methyl-4-isoxazolepropionic acid
AMPK	Adenosine monophosphate activated kinase
AP-1	Activating protein 1
ARE	Antioxidant response element
ARNT	Aryl hydrocarbon receptor nuclear translocator protein
ATP	Adenosine triphosphate
B2M	β2 microglobulin
BaP	Benzo(a)pyrene
BBB	Blood brain barrier
Bcl-2	B-cell lymphoma 2
bEnd.3	Brain endothelial cell line
BL	Basal lamina
BRG1	Brahma related gene-1
BSA	Bovine serum albumin
BSO	Buthionine sulfoximine
BTB	Broad tram-track-bric-a-brack
bZip	Basic region-leucine zipper
cAMP	Cyclic AMP
cGMP	Cyclic guanosine monophosphate
Cl^-	Chloride ions
CO	Carbon monoxide
CREB	cAMP response element binding protein
CTR	C-terminal region
Cu-Zn SOD	Copper- and zinc-containing superoxide dismutase
CUL	Cullin
CysDA	Z-Leu-Leu-Leu-al
DAB	3’3-diaminobenzidine
DAPI	4',6-diamidino-2-phenylindole
ddH_2O	Double distilled water

DEM	Diethyl maleate
DGR	Double glycine repeat/kelch
DMEM	Dulbecco's modified Eagle's medium
DMOG	Dimethyloxloylglycine
DMSO	Dimethyl sulfoxide
DMTU	Dimethyluea
DNA	Deoxyribonucleic acid
ECL	Enhanced chemiluminescence
EpRE	Electrophilic response element
eNOS	Endothelial nitric oxide synthase
EpRE	Electrophile response element
ER	Endoplasmic reticulum
ESR	Electron spin resonance
FADH2	Flavin Adenine Dinucleotide
FCS	Fetal calf serum
FIH-1	Factor inhibiting HIF-1
G6PDH	Glutathione-6-phosphate dehydrogenase
GCL	Glutamate cysteine ligase
GCLC	Glutamate cysteine ligase catalytic domain
GCLM	Glutamate cysteine ligase modulatory domain
GCS	γ-glutamylcysteine synthetase
GEE	Glutathione ethyl ester
GFAP	Glial fibrillary acidic protein
GLUT1	Glucose transporter 1
GPx	Glutathione peroxidase
GS	Glutathione synthetase
GSH	Glutathione
GSNO	S-nitroso glutathione
GST	Glutathione *S*-transferases
GSTM1	Glutathione S-transferase Mu 1
H_2O_2	Hydrogen peroxide
HAT	Histone acyltransferases
HBA	p-hydroxybenzyl alcohol
HDAC3	Histone deacetylase
HIF-1	Hypoxia inducible factor 1
HIF-1α	Hypoxia inducible factor 1α

HIV	Human immunodeficiency virus
HMEC-1	Human microvascular endothelial cells
HO-1	Heme oxygenase 1
HO-2	Heme oxygenase 2
HPLC	High performance liquid chromatography
HRE	Hypoxia-responsive elements
HRP	Horseradish peroxidase
HUVECs	Human umbilical vein endothelial cells
i.p.	Intraperitoneal
ICAM1	Intracellular adhesion molecule-1
ICH	Intracerebral hemorrhage
IgG	Immunoglobulin G
IL-23	Interleukin-23
IL-8	Interleukin-8
IL-β	Interleukin- β
iNOS	Inducible nitric oxide synthase
IVR	Intervening repeat
Keap1	Kelch-like-ECH-associated protein 1
KO	Knockout
LAT1	Large neutral amino acid transporter 1
LCR	Locus control region
LDH	Lactate dehydrogenase
Maf	Musculoaponecrotic fibrosarcoma
MCA	Middle cerebral artery
MCAo	Middle cerebral artery occlusion
MDA	Malondialdehyde
MG132	N-(benzyloxycarbonyl)leucinylleucinylleucinal
mRNA	Messenger ribosomal nucleic acid
MTT	3-[4,5-dimethylthiazol-2-yl]-2,5 diphenyl tetrazolium bromide
Na^+	Sodium ion
NADH	Nicotinamide adenine dinucleotide
NF-E2	Nuclear factor erythroid 2
NF-κB	Nuclear factor kappa B
NICE	National Institute for Health and Clinical Excellence
NMDA	N-methyl-D-aspartate
nNOS	Neuronal nitric oxide synthase

NO	Nitric oxide
NOX	NADPH oxidases
NQO1	NADPH:quinone oxidoreductase 1
Nrf2	NF-E2 related factor 2
NRP/B	Nuclear restricted protein in brain
O_2	Oxygen
OGD	Oxygen and glucose deprivation
OPA	O-phthaldialdehyde
p-AKT	Phospho-Akt
p-ERK 1/2	Phospho extracellular signal regulated kinase
PAS	PER-ARNT-SIM
PDH	Prolyl hydroxylase
PDTC	Pyrrolidine dithiocarbamate ammonium salt
Pgp	P-glycoprotein
pMCAo	Permanent middle cerebral artery occlusion
Prx	Peroxiredoxins
PUFAs	Polyunsaturated fats
qRT-PCR	Quantitative real-time polymerase chain reaction
rBEC4	Rat brain endothelial cells
RECA1	Rat endothelial cell antigen 1
RNS	Reactive nitrogen species
ROS	Reactive oxygen species
RPL13A	60S ribosomal protein L13a
rtPA	Recombinant tissue plasminogen activator
S.E.M.	Standard error of the mean
SDHA	Succinate dehydrogenase complex, subunit A
SFN	Sulforaphane
SOD	Superoxide dismutase
STAIR	Stroke treatment academic industry roundtable
T25	25cm^2 tissue culture flask
T75	75cm^2 tissue culture flask
t-BHQ	Tert-Butylhydroquinone
TEER	Trans-endothelial electrical resistance
TGF-β	Transforming growth factor beta
tMCAo	Transient middle cerebral artery occlusion
tPA	Tissue plasminogen activator

Trx1	Thioredoxin 1
Ub	Ubiquitin
VCAM1	Vascular cell adhesion protein 1
VHL	Von Hipple-Lindau
WT	Wild type
XD	Xanthine Dehydrogenase
XO	Xanthine Oxidase

Table of Contents

List of figures

Chapter 1

Chapter 2

Chapter 3

Chapter 4

Chapter 7

List of tables

Chapter 1

Chapter 2

Chapter 7

Chapter 1 - Introduction

Chapter 1 – Introduction

Cerebral stroke contributes to approximately 10% of deaths worldwide and has been classed as the second most common cause of death after cardiovascular disease (Gaziano, 2005; Rothwell *et al.*, 2011). Cerebral stroke is the leading cause of adult morbidity and is coupled with emotional and socio-economic consequences for the patient, their relatives and health services (Dawson *et al.*, 2007; Kuper *et al.*, 2007; Saka *et al.*, 2009). Stroke costs the UK approximately £8.9 billion per annum, with 5% accounting for treatment costs to the National Health Service (NHS) (Weir & Dennis, 1997; Dawson *et al.*, 2007; Saka *et al.*, 2009). Accessible and better healthcare is enabling patients to live longer and increasing obesity and a sedentary life style are enhancing the risk of cardiovascular diseases, diabetes, and as a consequence, cerebral stroke (Pomerleau *et al.*, 2006). Patients can be classed as being at a high-risk of suffering from a stroke, however, the time frame during which a patient is likely to experience a stroke cannot be predicted. Furthermore, the administration of recombinant tissue plasminogen activator (rtPA) is the only approved form of treatment available to patients, but it is only efficacious if delivered within a defined therapeutic time-window (3 – 4.5h) after the onset of ischaemia. This poses a challenge for researchers to find therapeutic regimes that will improve neurological outcome following stroke.

The pathophysiology of stroke involves activation of multiple pathophysiological processes, which includes the increased generation reactive oxygen and nitrogen species (ROS/RNS), contributing to oxidative stress. Nuclear factor E2 related factor 2 (Nrf2), a redox-sensitive transcription factor, orchestrates the expression of cytoprotective enzymes following increased oxidative stress to restore cellular homeostasis. Cerebral stroke is known to result in the activation of Nrf2 and its downstream protein targets, however, the time course of Nrf2 activation following stroke remains unknown.

Stroke research has focused on dietary compounds that may target the Nrf2 defence pathway for protection of the brain against stroke. However, with the majority of studies focusing of post-stroke therapeutics, the protection afforded will be dependent on hospital accessibility and time frame of drug delivery. Moreover, stroke research has primarily focused on the protection of astrocytes and neurons using various activators of Nrf2, but has failed to focus on the cerebral endothelium, a critical component of the blood-brain barrier (BBB) and important for the maintenance of the brain parenchyma.

The current PhD project employed a rodent model of cerebral stroke to investigate the spatial and temporal distribution of Nrf2 and its mediated proteins in the cerebral endothelium and other cell types following stroke. The dietary Nrf2 activator sulforaphane was then administered *in vivo* to pre-condition rodents prior to experimental stroke and to investigate its effects on the

spatial distribution of Nrf2 and its target proteins. To further assess the role of sulforaphane mediated protection and pre-conditioning in the cerebrovascular endothelium, an *in vitro* model of the BBB was established and subjected to ischaemic-injury *in vitro.*

To introduce the topic, this chapter will discuss the pathophysiology of cerebral ischaemia and reperfusion injury, the effect of stroke on the neurovascular unit and the BBB. Moreover, the role of the Nrf2-Keap1 defence pathway and its role in protecting the brain against stroke will be reviewed.

1.1 Brain and the neurovascular unit

1.1.1 The Brain

The brain is central in regulating the energy supply of peripheral organs, such as the heart and muscle via efferent nerve pathways and, notably, is also able to "sense" energy use and energy demands via physiological sensors and afferent nerve pathways (Peters *et al.*, 2004). In the adult human, total brain mass accounts for approximately 2% of total body weight (Raichle & Gusnard, 2002), however, the brain demands approximately 20% of the body's oxygen (O_2) supply for its metabolic purposes at rest and receives 15% of cardiac output (Attwell & Laughlin, 2001; Raichle & Gusnard, 2002; Jain *et al.*, 2010b). The energy consumption of the brain is far greater than any other organ, including muscle (Peters *et al.*, 2004). Moreover, it is well established that even in mental disorders, the metabolic activity of the brain remains remarkably constant, although changes in the rate of O_2 consumption are noted following the development of a neurodegenerative disease state (Sokoloff *et al.*, 1955; Raichle & Gusnard, 2002). Imaging studies have also revealed that the brain's consumption of glucose is equal to the rate at which glutamate, a neurotransmitter, is converted to glutamine, providing a measure of synaptic release of glutamate (Attwell & Laughlin, 2001). An increase in glutamate activity also affects the brain's energy demand to meet metabolic function, changing O_2 consumption (Attwell & Laughlin, 2001; Jain *et al.*, 2010b). Interestingly, the brain does not have the capacity to store energy, hence it is reliant on an uninterrupted and continuous blood flow to provide O_2, glucose and nutrients to meet energy demands (Peters *et al.*, 2004). Furthermore, whilst muscle is able to metabolise glucose, fats and proteins to meet energy demand, the brain is exclusively dependent upon glucose (Peters *et al.*, 2004). To meet the brain's demand for a constant supply of O_2, glucose and other nutrients important for metabolism, the brain bestowed with an extensive vascular network (Duelli & Kuschinsky, 2001; Iadecola & Anrather, 2011). Notably, cerebral flow is under regulation by brain parenchymal cells, including neurons, and is thus regulated by the neurovascular unit (Abbott *et al.*, 2006; Abbott *et al.*, 2010).

1.1.2 The Neurovascular unit

The concept of the neurovascular unit was first introduced by Iadecola in 2004 (Iadecola, 2004), arising from the phenomenon of neurovascular coupling, i.e. the coupling and interactions between neural activity, providing energy demand, and the local cerebral blood flow, supplying the parenchyma with energy (Stanimirovic & Friedman, 2012). The term neurovascular unit defines the interactions of brain parenchymal cells (astrocytes, neurons, oligodendrocytes, microglia, pericytes) with the cerebrovascular endothelium (Abbott *et al.*, 2006; del Zoppo, 2010; Alfieri *et al.*, 2011) and is illustrated in Figure 1.1. Cerebral endothelial cells (see Section 1.1.2.3) forms the BBB, which are supported by the presence of discontinuous pericytes (Zlokovic, 2008; Abbott *et al.*, 2010). Both the endothelium and pericytes are enveloped and contribute to the formation of a basement membrane, a local perivascular extracellular matrix also known as the basal lamina (BL1), however, its composition is different from the extracellular matrix of glial end feet, giving rise to BL2. The extensive network of astrocytic foot processes surrounding the brain capillaries is necessary for the regulation of cerebral blood flow. Furthermore, neuronal projections onto surrounding smooth muscle cells communicate with the vasculature via the release of neurotransmitters to regulate cerebral blood flow (Abbott *et al.*, 2010). In this section, the role of the cerebrovascular endothelium, neurons and astrocytes in the neurovascular unit are discussed.

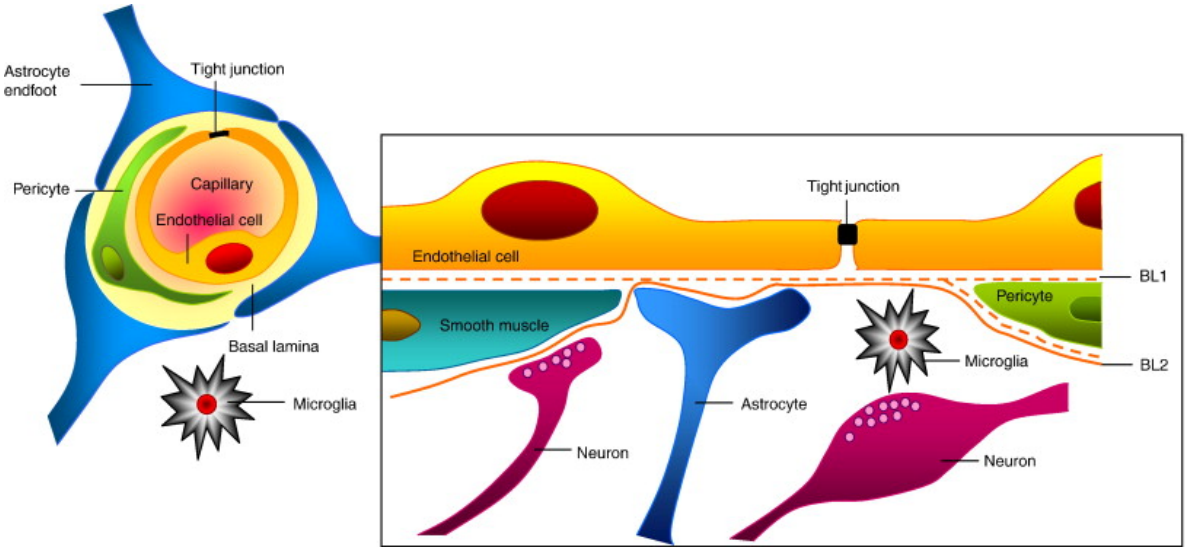

Figure 1.1 The neurovascular unit.
The neurovascular unit defines interactions of neural and non-neural cells involved in the regulation of cerebral blood flow. Tight appositions of endothelial cells, held together by tight-junctional complexes that line brain capillaries forms the blood-brain barrier, which is surrounded by pericytes in a discontinuous manner. The extracellular matrix of both pericytes and endothelial cells contributes to the enveloping basement membrane, which constitutes the basal lamina from endothelial cells and pericytes (BL1) and glial end foot processes (BL2). Astrocytic foot processes form an extensive network that surrounds the cerebral vasculature. Figure taken from (Abbott *et al.*, 2010).

1.1.2.1 Cerebrovascular endothelium

The cerebrovascular endothelium lines brain capillaries and forms the blood-brain barrier, a concept first described by the German scientist Paul Ehrlich in 1885 (Ribatti *et al.*, 2006). The BBB is composed of a tight apposition of endothelial cells, sealed by the presence of tight-junctional proteins and enveloped by a continuous basement membrane (Wolburg & Lippoldt, 2002; Hawkins & Davis, 2005; Stanimirovic & Friedman, 2012). Pericytes embrace the cerebrovascular endothelium on the abluminal surface via several long processes and serve not only as a scaffold for the cerebrovascular endothelium, but communicate via paracrine signalling pathways or via physical contact (Bergers & Song, 2005). Due to the close apposition of pericytes with the cerebral endothelium, it also is enveloped by the basement membrane (Bergers & Song, 2005; Stanimirovic & Friedman, 2012). The blood-brain barrier is described as having three major functions, which are (1) protection of the brain parenchyma from the blood milieu, (2) selective transport of substances from cerebral blood flow, and (3) metabolism and modification of blood- or brain-borne metabolites (Ribatti *et al.*, 2006). Paul Ehrlich further ratified the existence of this specialised barrier to the brain following the injection of vital dyes into adult animals, reporting the staining of all organs, excluding the brain and the spinal cord (Ribatti *et al.*, 2006). Further evidence for the existence of this "speacialised" barrier was provided by Bield and Krasu (1898) and Lewandowsky (Lewandowsky, 1900). They observed no pharmacological effects on the CNS following the intravenous injections of cholic acid or sodium ferrous cyanide (Bradbury, 1993; Hawkins & Davis, 2005; Ribatti *et al.*, 2006). Although Lewandowsky was the pioneer of the term "blood-brain barrier", its existence was still in question due to the finding that plasma proteins, such as albumin, bound certain dyes and prevented penetration from the blood into the tissue (Ribatti *et al.*, 2006). Goldmann however was the first to demonstrate the existence of this specialised barrier using the acidic dye Trypan blue. Injection of Trypan blue into the cerebral ventricular system of dogs and rabbits coloured the whole brain. However, intravenous injection of Trypan blue into the whole body of these animals results in whole body staining but excluding the brain and spinal cord (Ribatti *et al.*, 2006).

As mentioned previously, the cerebrovascular endothelium lines microvessels in the brain and acts as a physical barrier due to the presence of tight-junctional complexes (Hirase *et al.*, 1997; Abbott *et al.*, 2006). The presence of this specialised barrier forces blood-bourne substances to cross into the brain parenchyma via transcellular routes rather than the paracellular route available at other endothelial barriers (Abbott *et al.*, 2006). Furthermore, ions such as Na^+ and Cl^- are also forced to take paracellular routes to enter the brain milieu (Betz, 1986; Abbott *et al.*, 2006). However, gaseous molecules, such as molecular O_2, are able to freely pass through the

lipid bilayer. The selective movements of substances observed across the BBB is achieved by the presence of specific transport systems on both the luminal and abluminal surfaces of cerebral endothelial cells, such as GLUT1 for transport of glucose and vitamin C (Morgello *et al.*, 1995; Agus *et al.*, 1997; Zlokovic, 2008), LAT1 for the transport of large neutral amino acids (Boado *et al.*, 1999; Kido *et al.*, 2001), and the multidrug resistance gene product P-glycoprotein (Cordon-Cardo *et al.*, 1989; Schinkel *et al.*, 1994; Abbott *et al.*, 2006).

A particular characteristic of the cerebrovascular endothelium is the tightness of the endothelial layer, which has been examined by measuring levels of trans-endothelial electrical resistance (TEER). The cerebrovascular endothelium achieves TEER levels of >1000 ohm/cm^2, significantly greater than TEER values obtained in other vascular beds (2 – 20 ohm/cm^2) (Abbott *et al.*, 2006; Stamatovic *et al.*, 2008). The observed high levels of TEER are due to tight-junctional complexes present between adjacent endothelial cells. Proteins involved in these tight-junctional complexes include occludin, responsible for the regulation of tight-junctional proteins between endothelial cells (Furuse *et al.*, 1993; Hirase *et al.*, 1997). Histological studies of brain microvessels reveal a high expression of occludin at cell-cell contacts, which is absent in endothelial cells from other vascular beds (Hirase *et al.*, 1997). Claudins are another set of proteins found at tight-junctional complexes, contributing to the high levels of TEER observed in the BBB (Huber *et al.*, 2001; Abbott *et al.*, 2006). Moreover, junctional adhesion molecules (JAM) are also present at BBB endothelial tight junctions and are involved in the maintenance of tight-junctional complexes and leukocyte migration (Huber *et al.*, 2001; Abbott *et al.*, 2006). Kuchler-Bopp *et al.* demonstrated the induction of BBB like properties in human derived umbilical endothelial cell line (ECV 304) when co-cultured with astrocytes or with astrocyte conditioned medium (Kuchler-Bopp *et al.*, 1999). Moreover Hayashi *et al.* reported the induction of BBB specific transporters in human umbilical vein endothelial cells (HUVEC) co-cultured with astrocytes (Hayashi *et al.*, 1997). Interestingly, Pekny and colleagues have shown that astrocytes deficient for glial fibrillary acidic protein (GFAP), a filamentous protein upregulated in neurodegenerative diseases, are unable to induce BBB like properties in co-cultured aortic endothelial cells (Pekny *et al.*, 1998). Hence, these findings suggest that astrocytes directly influence the cerebrovascular endothelium.

It is well known that the integrity of the BBB is important for the protection of brain function, parenchymal cells and regulation of cerebral blood flow. Following the development of a neurodegenerative disease state, a loss of integrity of the BBB results in increased vasogenic oedema, which is defined by the extravasation of plasma proteins (Klatzo, 1987; Greenwood, 1991; Lakhan *et al.*, 2013). The increased vasogenic oedema is responsible for neuronal cell death observed after the development of a neurological disease state.

1.1.2.2 Neurons

Neurons define a class of cells that are specialised for intracellular communication as clearly illustrated by their morphology. Neurons are characterised by a cell body, consisting of a nucleus, axon and multiple dendrites, specialised for electrical signalling (Sa-Pereira *et al.*, 2012). Furthermore, it has been suggested that every neuron within the brain is associated with its own capillary supply, illustrating the importance of neurovascular communications (Zlokovic, 2008). Projections from GABA-ergic, noradrenergic, serotonergic and cholinergic neurons directly interact with endothelial cells and astrocytic foot processes (Sa-Pereira *et al.*, 2012). Tontsch *et al.* illustrated the importance of neurons in the induction of BBB-like structural properties and metabolism in cultured endothelial cells (Tontsch & Bauer, 1991), demonstrating that neurons may play a role in regulating cerebral vessel function. Moreover, the ability of neurons to increase TEER in cerebral endothelial cells *in vitro* has been associated with reduced permeability (Sa-Pereira *et al.*, 2012).

1.1.2.3 Astrocytes

Astrocytes are the major type of glial cell present in the brain and plays a major role in the neurovascular unit, with astrocytic end feet in close apposition with the cerebral endothelium forming the BBB (Figure 1.1) (Koehler *et al.*, 2006). Astrocytes communicate with cerebral endothelial cells via the release of ATP (Paemeleire & Leybaert, 2000; Koehler *et al.*, 2006). Astrocytes are further sub-divided into two morphological populations, protoplasmic and fibrous (Molofsky *et al.*, 2012). Protoplasmic astrocytes are resident in the grey matter and are in contact with the cerebrovascular endothelium, forming the neurovascular complex. Fibrous astrocytes populate the white matter and maintain the classical star like morphology with dense glial filaments (Molofsky *et al.*, 2012). Notably, fibrous astrocytes express the filamentous protein GFAP (glial fibrillary acidic protein), which has also been detected in reactive astrocytes undergoing gliosis noted in various neurodegenerative diseases such Alzheimer's disease, Parkinsons disease and cerebral ischaemia-reperfusion injury (Brahmachari *et al.*, 2006; Molofsky *et al.*, 2012). The mechanism by which astrocytic expression of GFAP is increased is unknown, although the involvement of nitric oxide (NO) has been reported following treatment of cultured primary astrocytes with S-nitroso glutathione (GSNO), an NO donor (Brahmachari *et al.*, 2006). Pekney *et al.*, further demonstrated that GFAP deficient astrocytes are unable to induce or maintain BBB characteristics (Pekny *et al.*, 1998), providing further evidence that astrocytes play a key role in preserving the BBB.

Within the neurovascular unit, astrocytes also act as an anatomical intermediary between neurons and the cerebrovascular endothelium (Petzold & Murthy, 2011). Morphological

analysis of the neurovascular unit reveals that perivascular astrocytic end feet cover almost the entire external surface of the cerebrovascular endothelium. Astrocytic end feet are enriched with astrocyte specific proteins, including aquaporin-4, connexin 43, purinergic receptors and potassium channels (Petzold & Murthy, 2011). Aquaporin 4 (AQP4) is a water channel protein involved in water homeostasis, but has also been implicated in cerebral oedema formation and regulation of BBB permeability (Fukuda & Badaut, 2012). Manley *et al.* have shown that AQP4 KO mice subjected to ischaemia and reperfusion injury *in vivo*, exhibit reduced cerebral oedema formation (~35%) improved neurological outcome following 24h reperfusion injury (Manley *et al.*, 2000). Interestingly, Friedman *et al*. reported decreased AQP4 expression 8h after acute ischaemia in regions of marked vascular damage (Friedman *et al.*, 2009). Thus this data suggests that cerebral odema formation and BBB breakdown may be owed to the presence of AQP4 on perivascular astrocytic endfeet.

Under pathophysiological conditions astrocytes promote cerebrovascular dysfunction and breakdown of the blood-brain barrier (Abbott *et al.*, 2006). Bradykinin released during stroke acts on bradykinin receptors on astrocytes and endothelium to increase intracellular Ca^{2+}, promoting cell death. Bradykinin also promotes the production of IL-6 via NF-κB, increasing cerebrovascular permeability. Interestingly, release of transforming growth factor beta (TGF-β) from perivascular astrocytes downregulates tissue plasminogen activator (tPA) production in the cerebrovascular endothelium, thereby reducing the ability to breakdown fibrin clots, responsible for cerebral artery occlusion (Abbott *et al.*, 2006). Hence, although astrocytes in the neurovascular unit play a important role in the communicating between other astrocytes and neurons, these may also have an important role in BBB breakdown and cerebral oedema formation following stroke.

1.2 Cerebral Stroke

Cerebral stroke is the leading cause of adult morbidity and the third most common cause of death in the developed world. As illustrated in Table 1.1, the majority of patients that die as a result of stroke are above 75 years of age, however, approximately 25% of stroke patients are under the age of 65. Cerebral stroke is also responsible for multiple secondary problems, which include depression, epilepsy and dementia (Pendlebury, 2009; Pendlebury & Rothwell, 2009a; Pendlebury, 2012). Notably, stroke patients account for more hospital bed days compared to other disorders (Rothwell *et al.*, 2004). Thus stroke associated care is coupled with high cost implications for health services and affected communities, with the UK Stroke Association estimating costs between £3.7 and £8 billion in 2010 (UK Stroke association statistics database, 2013). Moreover, a rapid rise in the aging population is expected to the increase the number of stroke patients and its associated burdens (Rothwell *et al.*, 2004). This highlights the

requirement for research into therapeutic strategies that will limit the neurological deficits associated with stroke.

Table 1.1 Percentage of death following stroke in the UK in 2010

Age Group	*Percentage affected*
< 35	0.3%
35 – 44	0.7%
45 – 54	1.9%
55 – 64	3.9%
65 – 74	10.6%
75 >	83%

Data from UK stroke association, January 2013

The risk factors associated with an increased incidence of cerebral stroke are hypertension, atherosclerosis, diabetes and increasing age (Wolf, 1985; Johansson, 1999; Sacco *et al.*, 1999; Grau *et al.*, 2001; Travis *et al.*, 2003). Patients may suffer from either one of two subtypes of stroke, namely ischaemic or haemorrhagic (Donnan *et al.*, 2008). As illustrated in Table 1.2, 85% of cerebral stroke patients suffer from cerebral ischaemia, whereas the remaining 15% of patients suffer from haemorrhagic stroke.

Table 1.2 Types of cerebral stroke and percentage of stroke patients affected in the UK in 2010

Types of cerebral stroke	*Sub-type of stroke*	*Percentage affected*
Ischaemic Stroke		85%
Haemorrhagic stroke		15%
	Intercerebral haemorrhage	10%
	Subarachnoid haemorrhage	5%

Data from stroke association, January 2013

1.2.1 Cerebral ischaemia and reperfusion injury

Cerebral stroke is characterised by neurological deficits attributed to the acute focal injury of the central nervous system originating due to a vascular cause (Sacco *et al.*, 2013). Cerebral stroke is clinically defined as the rapid development of the loss of brain function that lasts for more than 24h (Pendlebury & Rothwell, 2009b). As shown in Table 1.2, cerebral ischaemia affects approximately 85% of UK stroke patients and occurs as a consequence of either transient or permanent reduction in cerebral blood flow through a major cerebral artery, defining focal ischaemia, or after transient circulatory arrest, defining global ischemia. (Dirnagl *et al.*, 1999; Bramlett & Dietrich, 2004). In global ischaemia, total cerebral blood flow falls from 0.8 mL/g/min to zero in a matter seconds, which is followed by the loss of consciousness after approximately 10 seconds of ischaemia. Furthermore, irreversible brain damage and cell death are observed after a few minutes of global ischaemia (Endres & Dirnagl, 2002; Bramlett & Dietrich, 2004).

Focal ischaemia is a consequence of the cessation of blood flow, either transiently or permanent, through a cerebral artery. The severe reduction in blood flow occurs as a result of occlusion by either an emboli or local thrombosis, (Dirnagl *et al.*, 1999; Endres & Dirnagl, 2002). Moreover, focal ischaemia is further characterised histologically by the presence of an ischaemic core and penumbral regions (Endres & Dirnagl, 2002). As mentioned previously, the brain is dependent upon a continuous supply of oxygen and nutrients for metabolism and function (Endres & Dirnagl, 2002; Iadecola & Anrather, 2011). Hence, the sudden arrest of cerebral blood flow results in loss of neuronal activity, deterioration and disruption of ion homeostasis, contributing to the neurological deficits observed after stroke. The pathobiology of ischaemia is further discussed in Section 1.3 (Astrup *et al.*, 1981; Raichle, 1983; Bramlett & Dietrich, 2004; Alfieri *et al.*, 2011).

Table 1.3 Causes of ischaemic stroke

Cause of ischaemic stroke	***Percentage affected***
Atherosclerosis	50%
Blood clot	20%
Lacunar stroke	25%
Arterial dissection	5%

Data from stroke association, January 2013

Transient ischemia is followed by reperfusion, which defines the re-introduction of blood flow through the ischaemic vessel (Aronowski *et al.*, 1997), and occurs spontaneously after the

breakdown of the cerebral emboli or thrombus (Todd *et al.*, 1986). Although the re-introduction of oxygen should aid in the restoration of brain function, it contributes to increased oxidative stress and an upregulation of pro-inflammatory processes (Jean *et al.*, 1998; Peters *et al.*, 1998), as discussed in Section 1.3.4. In 1998, Peters *et al.* were the first to clearly illustrate a marked increase in reactive oxygen species generation upon reperfusion of the rat brain after 60 min middle cerebral artery occlusion (MCAo) (Peters *et al.*, 1998), contributing to oxidative stress.

Ischaemia induces cell death almost immediately after its induction, giving rise to the development of the infarct or ischaemic core. If re-canalisation therapy is delivered within a short time frame after the induction of ischaemia, then the volume of infarct can be limited (Ramos-Cabrer *et al.*, 2011). The likelihood however, of patients receiving such treatment within this defined duration is low. Severe reduction or occlusion of cerebral blood flow results in immediate ionic failure, increased neuronal depolarisations and increased glutamate release (Dirnagl *et al.*, 1999). These biochemical changes results in cell death following the initiation of the ischaemic cascade and development of the infarct core (Figure 1.2). Notably, tissue immediately surrounding the ischaemic core is hypoperfused during ischaemia and forms the ischaemic penumbra, as discussed further in Section 1.2.1.1.

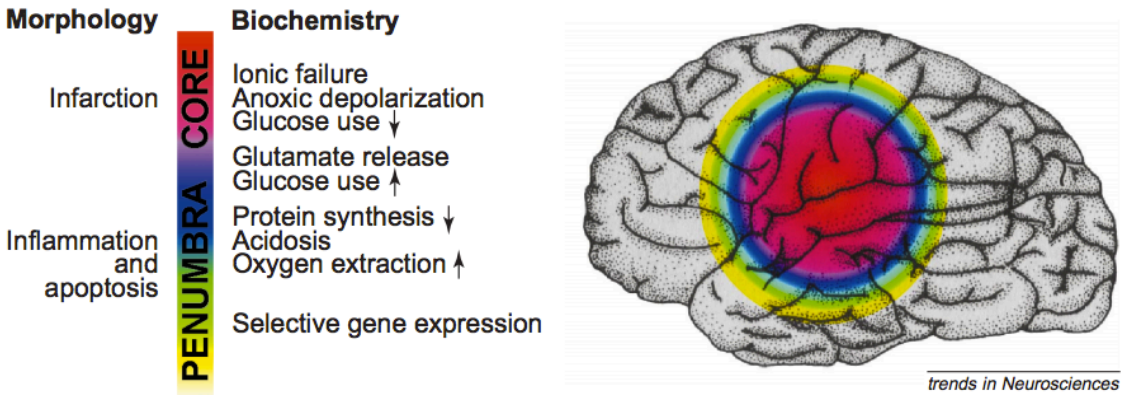

Figure 1.2 Definition of the ischaemic core and penumbra.
Ischaemic injury results in a cascade of biochemical changes, resulting in immediate cell death and development of the infarct core. Tissue surrounding the ischemic core is hypoperfused, however the level of cerebral blood-flow determines the biochemical changes observed within the penumbral tissue. Figure taken from (Dirnagl *et al.*, 1999)

1.2.1.1 Phenomena of the ischaemic penumbra

The ischaemic penumbra is defined as the region of hypoperfused tissue directly surrounding the ischemic core (Astrup *et al.*, 1981). The penumbral tissue is perfused at levels within

thresholds of functional impairment, which are too low to maintain electrical activity but sufficient to maintain ion homeostasis and brain function (Astrup *et al.*, 1981; Heiss, 2000; Ramos-Cabrer *et al.*, 2011). The phenomenon of the ischaemic penumbra was first described by Astrup *et al.* in 1989, after which, it has had rapidly become the prime focus of stroke research aimed at identifying therapeutic strategies to prevent further damage to the ischaemic penumbra after the initial ischaemic insult (Astrup *et al.*, 1981). The tolerance of brain tissue to ischaemic damage is dependent upon residual blood flow, and hence the development of the ischaemic penumbra has been described as a dynamic process (Heiss, 2000). Reduction in cerebral blood flow is responsible for the development of neurological deficits. As mentioned previously, normal brain blood flow in man ranges from 60 – 100 mL/100g/min (Heiss, 2000), and a reduction in cerebral blood flow results in changes in brain activity as summarised in Table 1.4.

Table 1.4 Effects of changes in cerebral blood flow on brain activity

Rate of cerebral blood flow (mL/100g/min)	***Impact on brain activity***
60 - 100	Maintenance of normal brain activity
< 55	Impact on normal neuronal function Inhibition of protein synthesis
< 35	Anaerobic glycolysis
< 20	Neurotransmitter release and disturbances in energy metabolism
< 6 – 15	Disturbances in ion homeostasis
0	Cerebral cell death and development of infarct core

Data acquired from (Heiss, 2000).

The size of the penumbral region is initially dependent upon the duration of ischaemia and the time frame in which normal cerebral blood flow can be restored. However, even after the restoration of normal blood flow to the penumbral tissue, further damage is still inflicted due to a cascade of pathophysiological molecular events propagating from the ischaemic core (Ramos-Cabrer *et al.*, 2011). The release of the neurotransmitter, glutamate, from the ischaemic core to the penumbral region induces irreversible cellular damage (Ramos-Cabrer *et al.*, 2011). Furthermore, other deleterious processes that can propagate from the ischaemic core to the penumbra include pro-inflammatory mediators, increased expression of leukocyte adhesion molecules and oxidative stress (Ramos-Cabrer *et al.*, 2011). The mechanisms underlying cellular damage following ischaemia and reperfusion injury are discussed in Section 1.3. Notably, protection of the ischaemic penumbra has now become a prime objective of stroke research, with recent strategies aimed at identifying therapeutic targets to increase endogenous cytoprotective mechanisms (Bandera *et al.*, 2006).

1.2.1.2 Treatment strategies available to patients of cerebral stroke

At present only one form of treatment approved by the FDA is available to patients with ischaemic stroke, namely administration of rtPA. However, the use of tPA is controversial (Liang *et al.*, 2008), as tPA is a multidomain serine protease capable of lysing fibrin stimulated clots or plasminogen into the serine protease plasmin (Keyt *et al.*, 1994). Plasmin then cleaves fibrin and other important components of blood clots to initiate a proteolytic cascade, resulting in fibrinolysis, i.e. breakdown of the blood clot and restoration of blood flow through the ischaemic artery (Gravanis & Tsirka, 2005).

In 1992, del Zoppo *et al.* initiated a study using synthetic rtPA to treat cerebral ischaemia patients and noted that complete re-canalisation of cerebral vessels was observed if rtPA was delivered within a short time frame after the onset of ischaemia. Patients that received rtPA 6h after the onset of ischaemia showed haemorrhagic transformation and worsened clinical status (del Zoppo *et al.*, 1992). This highlights that tPA treatment is only effective if delivered within a the defined time windows following initiation of the ischaemic insult.

In accordance with the updated National Institute for Health and Clinical Excellence (NICE) guidelines published in September 2012, treatment of ischaemic stroke patients with rtPA should only be undertaken within 4.5h after the onset of ischaemia. This renders only 3 – 5% of stroke patients eligible for treatment by rtPA. Furthermore, patients are only eligible if cerebral haemorrhage has been ruled out following assessment using appropriate imaging techniques. However, the majority of patients are ineligible for rtPA treatment due to inadequate access to a hospital unit within the narrow time frame available for treatment. Patients that are eligible for rtPA treatment may experience haemorrhagic transformation, a major side effect of rtPA treatment (del Zoppo *et al.*, 1992).

The actions of tPA are not limited to fibrinolysis, as tPA has been shown to exacerbate protein expression and activity of metalloproteinase-9, increasing the probability of haemorrhagic transformation (Wang *et al.*, 2004). Interestingly, Wang *et al.* demonstrated attenuation of ischaemic damage in tPA deficient mice following MCAo and reperfusion injury, however the injection of exogenous tPA in both wild type and tPA KO animals significantly increased cerebral infarct volume (Wang *et al.*, 1998). Thus, the high risks associated with rtPA treatment validate the need for alternative therapeutic strategies to treat stroke patients.

1.3 Pathophysiology of cerebral ischaemia and reperfusion injury

Section 1.2 established that cerebral ischaemia is the consequence of a severe reduction in cerebral blood flow. This results in changes in brain metabolism, with decreasing blood flow notably affecting protein synthesis, energy depletion, excitotoxicity and changes in ion homeostasis (Astrup *et al.*, 1981; Bramlett & Dietrich, 2004) a consequence of the ischaemic cascade. Destructive mechanisms are launched within moments of ischaemic injury, resulting in energy failure due to shifts in ionic balance and initiation of excitotoxic mechanisms (Endres *et al.*, 2008). Within hours after the initial ischaemic insult, pro-inflammatory and other mechanisms of cell death are activated (Figure 1.3). In comparison, endogenous neuroprotective mechanisms are not activated over the same time course and thus do not provide the necessary protection (Figure 1.3). Hence, this section discusses the pathophysiological mechanisms affecting the ischaemic brain, leading to cerebral cell death and associated neurological deficits.

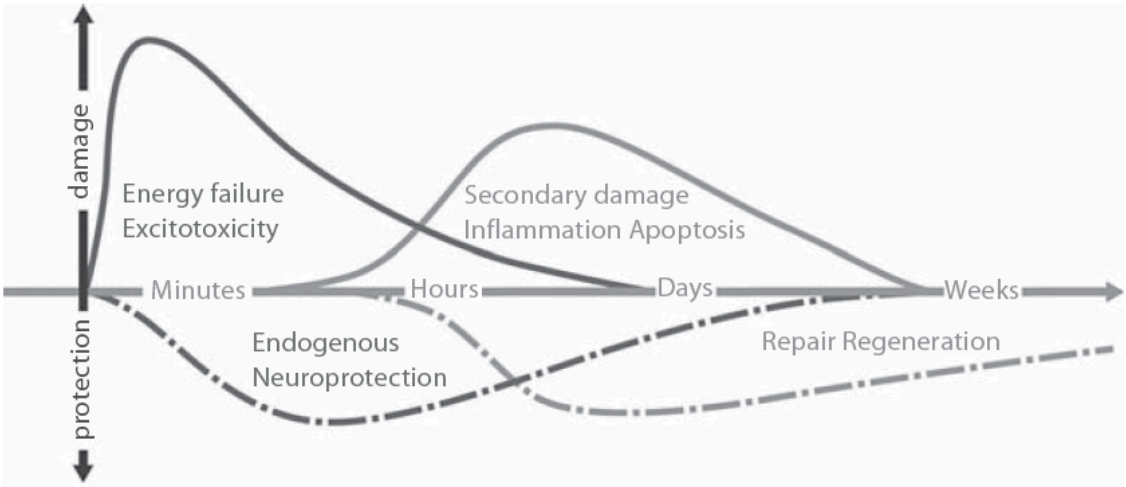

Figure 1.3 Pathobiology of stroke induced damage and endogenous repair.
This schematic aims to reflect the intensity or impact (y-axis) of the different elements of the ischaemic cascade as a function of time (x-axis). Immediately after the onset of ischaemia, the activation of excitotoxic mechanisms results in damage or lethality to neurons and glia. Excitotoxicity also initiates peri-infarct depolarisation, which later propagates to secondary damage and activates inflammation and programmed cell death. However, endogenous protective mechanisms are launched hours after the initial ischaemic insult. Moreover, the impact of protective mechanisms are less compared to destructive mechanisms. Figure taken from (Endres *et al.*, 2008).

1.3.1 Glutamate excitotoxicity

Glutamate is a major excitatory neurotransmitter released in the brain and regulates normal physiological activity (Meldrum, 2000; Kingwell, 2010). Glutamate has been reported to play an important role during development of the brain, as blockade of certain glutamate receptors results in neuronal cell death (Meldrum, 2000). Glutamate is also available via exogenous sources, most notably, the diet, however, there is no report of exogenous sources of glutamate having deleterious effects upon the brain (Meldrum, 2000).

Glutamate has been described as a non-essential amino acid, systhesised by many precursors, which include α-ketoglutarate and glutamine (Gonzales & Jaworski, 1997). α-ketoglutarate is a major component of the Krebs cycles and can be converted to glutamate via a single step reaction, where as glutamine is provided by glial cells for the production of glutamate within neurons (Gonzales & Jaworski, 1997; Mark *et al.*, 2001). Glutamate destined to act as a neurotransmitter is stored within synaptic vesicles of the cell. Upon stimulation, synaptic vesicles fuse with the neuronal membrane releasing glutamate into the synaptic cleft to interact with a subgroup of glutamate receptors expressed on the post-synaptic neuron (Gonzales & Jaworski, 1997). Three ionotropic glutamate receptors are N-methyl-D-aspartate (NMDA) receptor, AMPA receptor and kinate receptor. Released glutamate is then taken back up by the signal emitting pre-synaptic neurons and "re-packaged" into synaptic vesicles. However, further regulation of glutamate release is provided by glial cells, which rapidly convert glutamate to glutamine for transport back into the neuron as a precursor for glutamate production (Gonzales & Jaworski, 1997; Meldrum, 2000; Hazell, 2007).

Following traumatic brain injury or cerebral ischaemia, the severe depletion of intracellular energy stores affects cerebral ion homeostasis, resulting in excessive glutamate release (Figure 1.4) (Endres *et al.*, 2008). This excessive release of glutamate results in the initiation of pathophysiological mechanisms, resulting in cerebral cell death, and is termed glutamate excitoxicity. The released glutamate acts on ionotropic glutamate receptors, including NMDA, resulting in excessive Ca^{2+} influx and eventual Ca^{2+} overload. This also results in the activation of Ca^{2+} dependent enzymes, upregulating the activity of ATPase, DNAse, proteases, protein kinase C, calmodulin-dependent protein kinase II, phospholipases and nitric oxide synthase (Mark *et al.*, 2001). The marked increases in intracellular Ca^{2+} also induce mitochondrial damage and the activation of pro-apoptotic processes, further progressing the aetiology of cell death following cerebral ischaemia (Figure 1.4) (Endres *et al.*, 2008).

Another downstream effect of glutamate-mediated excitotoxicity is the increased generation of free radical species, as discussed in Section 1.3. Increased free radical generation gives rise to oxidative stress, resulting in DNA damage, protein and lipid oxidation, contributing to eventual

cell death (Figure 1.4). The increased presence of free radical species also results in the activation of pro-inflammatory processes, resulting in leukocyte recruitment to the ischaemic region and the activation of microglia, the brain's resident macrophages.

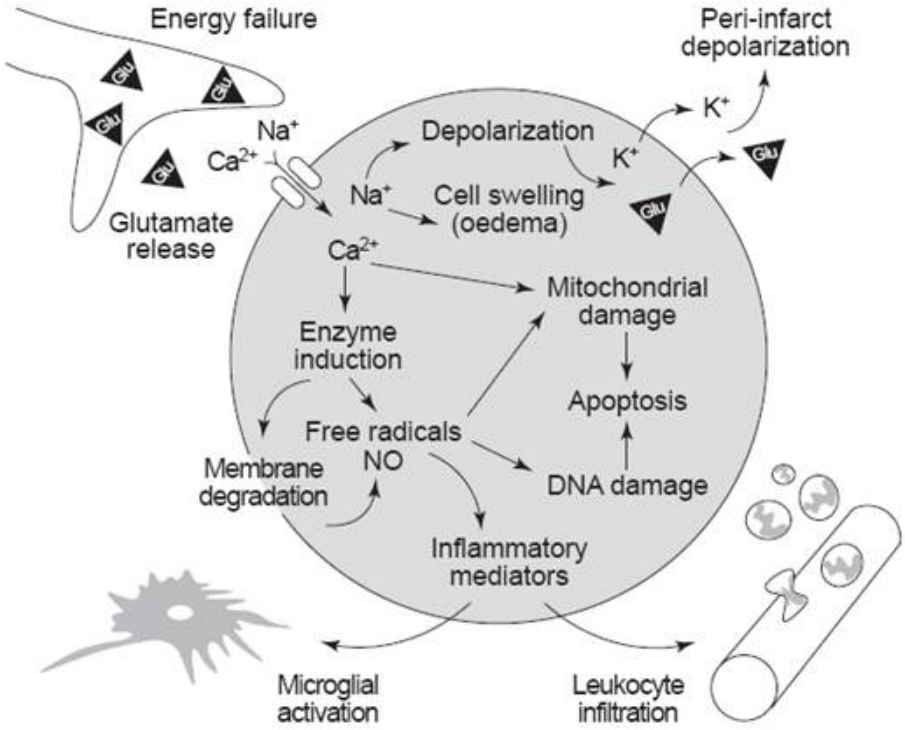

Figure 1.4 Schematic representation of the pathophysiological consequences associated with glutamate excitotoxicity.
Energy failure following stroke results in the depolarisation of neurons, and glutamate release. Activation of glutamate receptors increases intracellular Ca^{2+} and Na^{+}, whilst K^{+} is released into the extracellular environment. Increased extracellular K^{+} and glutamate results in peri-infarct depolarisations, i.e. the spreading of depolarisation to adjacent cells. Changes in the cellular osmotic gradient increase intracellular water content, resulting in oedema. Furthermore, increased Ca^{2+} activates multiple enzyme systems, including proteases, lipases and endonucleases. Raised intracellular Ca^{2+} also promotes free radical generation, resulting in membrane degradation, and DNA and mitochondrial damage, and ultimately activation of programmed cell death via pro-apoptotic pathways. Oxygen free radicals also induce the expression of pro-inflammatory mediators, activating microglia and promoting leukocyte migration (Dirnagl *et al.*, 1999).

1.3.2 Oxidative stress

Oxidative stress is defined as an imbalance between the increased generation of ROS and RNS against endogenous antioxidant defences, which increases the risk of oxidative damage and cell death both *in vitro* and *in vivo* (Figure 1.5) (Kohen & Nyska, 2002; Halliwell, 2007; Allen & Bayraktutan, 2009). The term ROS encompasses superoxide, hydrogen peroxide, and their secondary products, which include hydroxyl radical, peroxynitrite and hypochlorous acid (Halliwell, 1992; Cheng *et al.*, 2011). A basal level of oxidative damage to DNA, lipids and

proteins does occur, however under normal physiological conditions, there is a balance between the production of pro-oxidant and antioxidants species (Halliwell, 2006).

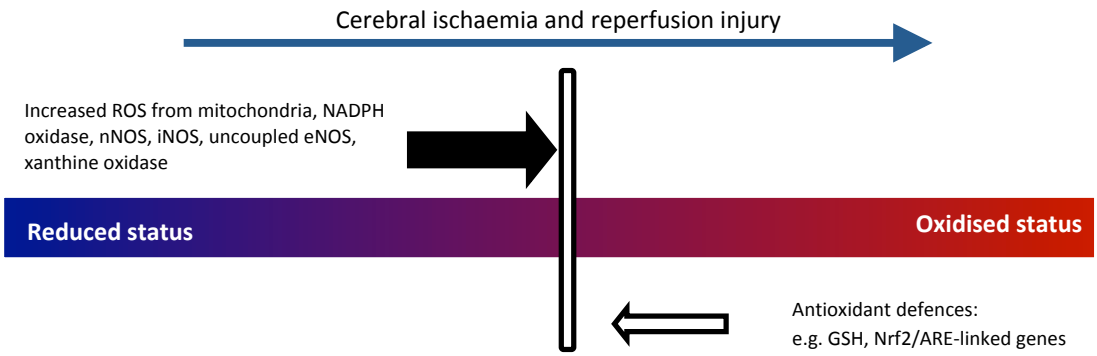

Figure 1.5 Altered redox status of cerebral tissue following cerebral ischaemia and reperfusion injury.
Cerebral ischaemia and reperfusion injury and other neurodegenerative disease states are characterised by an altered redox status, resulting from an imbalance between oxidative stress and antioxidant defences. Cerebral ischaemia and reperfusion injury results in the increased production of ROS and RNS from a range of sources, including mitochondria, NADPH oxidase, neuronal nitric oxid synthase (nNOS), inducible nitric oxide synthase (iNOS) and xanthine oxidase, shifting the redox balance of tissues towards an oxidised state. Figure adapted from (Cheng *et al.*, 2011).

ROS play an important role in intracellular signalling pathways and regulate multiple physiological functions. These include (1) the production of ROS in phagocytic cells by NADPH oxidases (NOX), (2) activation of the immune system following upregulation of T-lymphocyte activity, (3) regulation of cell adhesion to the vascular endothelium, (4) regulation of vascular tone following upregulation and activation of a secondary messenger, cyclic guanosine monophosphate (cGMP) and (5) ROS mediated cell death (Valko *et al.*, 2007; Allen & Bayraktutan, 2009). Basal concentrations of ROS are maintained in the cell via the balance between the rate of ROS production and its removal by various antioxidants (Valko *et al.*, 2007).

It is well established that the brain has a level high of oxygen consumption and hence is highly susceptible to increased ROS generation and oxidative damage (Halliwell, 2006). The high consumption of oxygen by the brain is due to the maintenance of ATP levels required for brain ion homeostasis (Halliwell, 2006). However, as the brain is also rich in polyunsaturated fats, and has a low antioxidant capacity, it is susceptible to increased damage during oxidative stress (Shohami *et al.*, 1997; Halliwell, 2006; Allen & Bayraktutan, 2009). Moreover, low levels of catalase in the brain have been reported (Halliwell, 2001), providing further evidence of a low antioxidant status. Interestingly, a major form of antioxidant defences in the brain is the storage

of catalytic metals, such as iron and copper. However, brain ischaemia or trauma increases the availability of these metal ions, accelerating the rate of free radical species generation (Halliwell, 1992). Increased oxidative stress following enhanced generation and accumulation of ROS has deleterious effects on the cellular environment, leading to cell death by apoptosis or necrosis, changes in cell proliferation and inhibition of cell division (Halliwell, 2007).

Enzymatic and non-enzymatic endogenous antioxidant defences are also available to protect the brain against oxidative stress. Superoxide dismutase (SOD) is one such enzymatic antioxidant, which catalyses the dismutation of superoxide to O_2 and H_2O_2. Catalase is another enzymatic antioxidant, which further dismutates H_2O_2 to water.

Following ischaemia and reperfusion injury in rats, Peters *et al.* have reported an increase in the generation of ROS (Peters *et al.*, 1998), and thus ROS have been implicated as key mediators of brain damage following ischaemic stroke (Allen & Bayraktutan, 2009). Overexpression of the enzymatic antioxidant copper-zinc superoxide dismutase (CuZnSOD) in mice subjected to 3h MCAo ad 3h reperfusion injury significantly reduces cerebral infarct volume and associated neurological deficits (Yang *et al.*, 1994). Kinouchi *et al.* reported similar results in SOD transgenic mice subjected to permanent focal cerebral ischaemia, highlighting reduced cerebral infarct and oedema volumes, and furthermore increased levels of the intracellular antioxidant glutathione in transgenic versus non-transgenic mice (Kinouchi *et al.*, 1991).

With respect to the cerebrovascular endothelium, oxidative stress has been reported to affect the integrity of the BBB, increasing cerebrovascular permeability and affecting the assembly of tight-junctional complexes in rats subjected to hypoxia and re-oxygenation (Lochhead *et al.*, 2010). Al Ahmad *et al.* provided further evidence *in vitro* that pro-oxidants affect the integrity of the BBB, increasing permeability (Al Ahmad *et al.*, 2012). This demonstrates that oxidative stress impacts the integrity of the BBB, increasing the probability of neurological deficits observed after stroke or in other neurodegenerative disease states. Although oxidative stress is regarded as one of the major pathophysiological processes affecting the ischaemic brain, there are multiple sources of ROS generation in the brain, which includes mitochondria, NADPH oxidases and xanthine oxidases. However, the major source of ROS production following cerebral ischaemia remains to be elucidated.

1.3.2.1 Mitochondrial ROS

Mitochondria are referred to as the powerhouse of the cell, regulating the production of ATP following aerobic respiration and oxidative phosphorylation involving the reducing agents NADH and FADH2, molecular oxygen and complex I-IV of the electron transport chain (Figure 1.6) (Groschner *et al.*, 2012; Chaturvedi & Flint Beal, 2013). Mitochondria also regulate calcium homeostasis, and harbour the release of pro-apototic factors (Christophe & Nicolas, 2006). Mitochondria reduce molecular O_2 to water via the electron transport chain and the terminal enzyme cytochrome c oxidase (Piantadosi & Zhang, 1996; Turrens, 1997). Notably, 90% of the molecular oxygen consumption in the normal brain is accounted for by the mitochondria (Piantadosi & Zhang, 1996). Under normal conditions, 1-2% of the consumed oxygen is converted to the superoxide anion (Turrens, 1997), generated at either complex 1, NADH dehydrogenase, or complex III, ubisemiquinone.

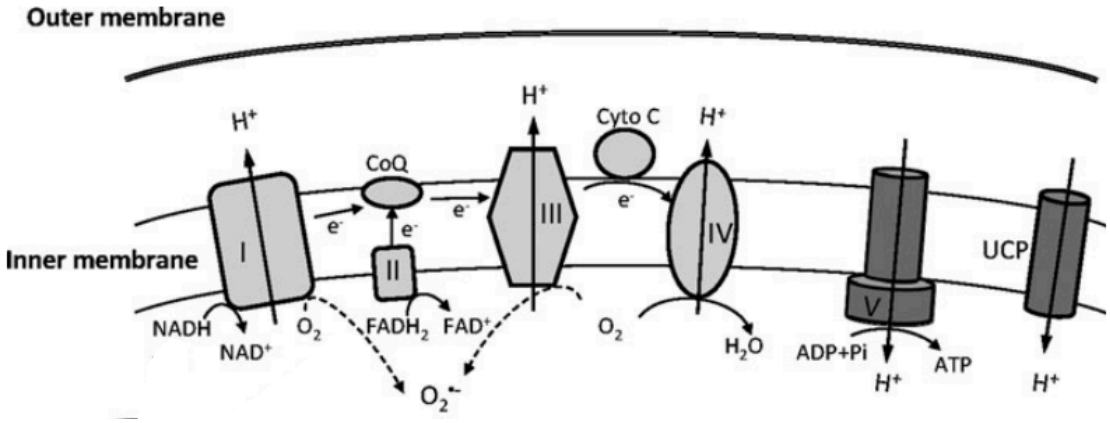

Figure 1.6 Mitochondrial electron transport chain.
Mitochondria are an important source of ROS the vascular system. The mitochondrial respiratory chain is formed of 4 protein complexes, complex I – IV, that transfer electrons from reducing agents NADH, at complex I, or $FADH_2$ (at complex II). Electrons are transferred to molecular oxygen, and protons pumped out into the inter membrane space via complex 4. Protons are transferred across from the intermembrane space by ATP synthase (V), generating ATP. Furthermore, uncoupling proteins (UCP) allow for protons to leak back from the intermembrane space. Figure adapted from (Cheng *et al.*, 2011).

Following ischaemic injury in the brain, structural changes have been observed in neuronal mitochondria, characterised by increased matrix density, swelling, condensation and calcium deposition (Solenski *et al.*, 2002), affecting mitochondrial function and stability. Furthermore, a 35% reduction in the rate of ATP production was also observed after 10 min cerebral ischaemia in dogs (Rosenthal *et al.*, 1987). Piantadosi *et al.* demonstrated an increase in the recovery of

2,3-dihydroxybenzoic acid (2,3-DHBA) following infusion of salicylic acid into the brain of rats subjected to transient global ischaemia and reperfusion injury. 2,3-DHBA increases were attenuated in rats treated with the mitochondrial complex I inhibitor and neuroleptic drug haloperidol (Piantadosi & Zhang, 1996), thus suggesting a role for complex I derived ROS following ischaemia. SOD1 or Cu-Zn SOD is present in the cellular cytoplasm whereas SOD2 or Mn-SOD is localised to the mitochondria. Permanent ischaemia for 24h in $SOD2^{-/-}$ mice demonstrated exacerbated neurological deficits and infarct volume and decreased mitochondrial viability, as indicated by rhodamine 123 accumulation (Murakami *et al.*, 1998). Moreover, overexpression of MnSOD in transgenic mice subjected to ischaemia and reperfusion injury of the heart show increased protection compared to matched wild-type littermates (Chen *et al.*, 1998). This provides critical evidence to suggest a role for mitochondrial produced ROS in the pathophysiology of cerebral ischaemia.

1.3.2.2 NADPH Oxidases

There are seven isoforms of NADPH oxidases (Nox) that exist in mammals; Nox1, Nox2, Nox3, Nox4, Nox5, Dual Oxidase 1 (Duox1) and Duox2 (von Lohneysen *et al.*, 2010; Konior *et al.*, 2013). NADPH oxidases are membrane bound structures, as demonstrated in Figure 1.7. Under normal conditions, Nox are quiescent, but upon activation, Nox generate superoxide (Ray & Shah, 2005). Interestingly, Duox1 and 2 have been shown to produce H_2O_2 (Guichard *et al.*, 2008). Although Nox were initially identified in phagocytic cells (Ray & Shah, 2005), Nox are differentially expressed in various cell types and vascular beds, with the expression of Nox2 and Nox4 noted on the vascular endothelium (Ray & Shah, 2005; Kahles *et al.*, 2007). Vascular Nox are formed of six trans-membrane domains, which are involved in electron transfer to reduce molecular oxygen to the superoxide anion (Konior *et al.*, 2013). Furthermore, the expression of Nox has been reported in various cerebral cell types and is summarised in Table 1.5.

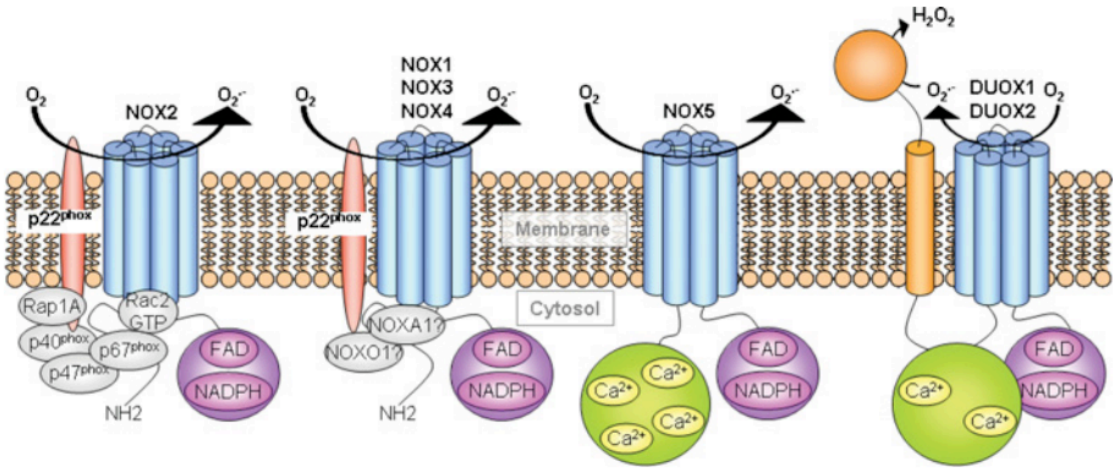

Figure 1.7 Structure and function of NADPH oxidases.
The NADPH oxidase (Nox) family consists of 7 known members (Nox1, Nox2, Nox3, Nox4, Nox5, Duox1 and Duox2) that catalyse the reduction to molecular oxygen to superoxide. The components of Nox are dispersed between the plasma membrane and cytoplasmic compartments. In the plasma membrane Nox isoforms are composed of 7 transmembrane domains and furthermore, Nox1 – 4 are also associated to $p22^{phox}$. Notably, DUOX1 and DUOX2 have an additional peroxidase like transmembrane domain. Activation of Nox is achieved following the recruitment of cytoplasmic factors to the transmembrane domains, allowing the oxidation of NADHP to $NADP^{+}$. The activation of Nox5, Duox1 and Duox2 is achieved following Ca^{2+} binding at the specific site. Figure taken from (Guichard *et al.*, 2008).

Table 1.5 Summary of NADPH Oxidases isoforms identified in cerebral cells

Cerebral cell type	***Nox isoform***	***Reference***
Astrocytes	Nox1	(Reinehr *et al.*, 2007), (Kahles *et al.*, 2010)
	Nox2	(Song *et al.*, 2011), (Abramov *et al.*, 2007)
	Nox4	(Jiang *et al.*, 2011)
Neurons	Nox1	(Coyoy *et al.*, 2008; Choi *et al.*, 2012), (Kahles *et al.*, 2010)
	Nox2	(Behrens *et al.*, 2007)
	Nox4	(Vallet *et al.*, 2005)
	Duox1	(Damiano *et al.*, 2012)
	Duox2	(Damiano *et al.*, 2012)
Cerebrovascular endothelium	Nox1	(Kahles *et al.*, 2010)
	Nox2	(Kahles *et al.*, 2007), (Girouard *et al.*, 2006)
	Nox 4	(Basuroy *et al.*, 2009)

Abbreviations: Nox, NADPH oxidase

Nox2, initially termed $gp91^{phox}$, has been extensively studied in the vasculature (Kahles *et al.*, 2010), although it was initially identified as being responsible for the toxic respiratory burst of superoxide in leukocytes (Konior *et al.*, 2013). The protein structure of Nox2 consists of two membrane bound subunits, $gp91^{Phox}$ and $p22^{phox}$. Four cytosolic components, $p47^{phox}$, $p67^{phox}$, $p40^{phox}$ and Rac, associate with the membrane bound domains to form an active enzyme (see Figure 1.5). ROS derived from Nox2 plays a major role in cell proliferation, mediated by p38-MAP kinase, and migration induced by vascular endothelial cell growth factor (VEGF) (Konior *et al.*, 2013). Interestingly, Chan *et al*. reported a reduction in superoxide generation in cerebral vessels of Nox2 $^{-/-}$ mice treated with angiotensin II (Chan & Baumbach, 2013), suggesting that Nox2 generated ROS may affect the cerebral vasculature.

In terms of Nox mediated damage following cerebral ischaemia, Kahles *et al.* have identified a detrimental role for Nox2 following reperfusion injury in mice, with significant attenuation of BBB permeability and lesion volume in Nox2 KO compared to wild type (WT) mice (Kahles *et al.*, 2007). Kahles *et al.* further demonstrated that pharmacological inhibition of Nox with apocynin, an inhibitor of Nox assembly and general flavoprotein inhibitor, also attenuated BBB permeability (Kahles *et al.*, 2007). Hong *et al.* reported increased Nox activity and superoxide generation on reperfusion injury in rats following MCAo (Hong *et al.*, 2006b). Interestingly, atorvastatin reduced Nox activity and lesion volume following MCAo and reperfusion injury, providing strong evidence that statins may also play a role in inhibiting Nox by preventing its assembly (Hong *et al.*, 2006b). Although Hong *et al.* did not identify the Nox isoforms responsible for superoxide generation, they provided evidence that Nox derived superoxide contributes to the aetiology of BBB breakdown. Interestingly, Hong *et al.* also highlighted that increased Nox activity was isolated to the ischaemic penumbra, further underpinning a role for Nox in ROS generation and oxidative stress following reperfusion injury (Hong *et al.*, 2006b). These studies and the others highlighted in Table 1.6 illustrate the role of Nox mediated cerebral damage, BBB breakdown and neurological deficits following cerebral ischaemia and reperfusion injury.

Table 1.6 Studies of NADPH oxidase mediated damage following stroke

Species	*Model*	*Nox isoform*	*Findings*	*Reference*
Mouse	60 min tMCAo and up to 24h reperfusion	Nox4	• Increased Nox4 mRNA and protein expression 12 and 24h after tMCAo • Increased Nox4 protein expression noted in neurons and cerebral microvessels • Nox4 KO mice show a 75% reduction in infarct volume, 24h after tMCAo • Treatment of mice with VAS2870, a global Nox inhibitor, yielded same results as Nox4 KO	(Kleinschnitz *et al.*, 2010)
Mouse	2h tMCAo and 22h reperfusion	Nox2	• Nox2 KO mice show a 50% reduction in infarct volume 22h after tMCAo • Nox2 KO mice and WT treated with apocynin show a reduction in BBB permeability after ischaemia	(Kahles *et al.*, 2007)
Mouse	60 min tMCAo and 24h reperfusion	Nox1	• Nox1 KO mice show a 55% reduction in infarct volume 24h after tMCAo • Nox1 mice show improved neurological outcome, and increased preservation of BBB integrity after stroke • Reduced oedema formation and decreased permeability in Nox1 KO mice compared to WT	(Kahles *et al.*, 2010)
Mouse	2h tMCAo and 24h reperfusion	Nox2	• Nox2 KO mice show a 50% reduction in cerebral infarct volume 24h after MCAo • Improved neurological outcome in Nox2 KO mice • Reduction in neuronal damage in Nox2 KO mice notable after histological analysis • Nox2 KO mice showed reduced glutamate release after cerebral ischaemia and reperfusion	(Wang *et al.*, 2013b)
Mouse	90min tMCAo and 24h reperfusion injury	Nox2	• Globular adiponectin (gAD) treatment reduced Nox2 expression after stroke • gAD treatment improved neurological outcome after stroke	(Song *et al.*, 2013)

Rats	2h tMCAo and 3 or 24h reperfusion	Global Nox	• Ethanol treatment reduced neurological deficit score after stroke • Increased Nox activity observed in animals 3h after ischaemia, but attenuated after ethanol treatment • Nox2 protein expression reduced in animals subjected to ischaemia and reperfusion injury and treated with ethanol	(Kochanski *et al.*, 2013)
Rats	2h tMCAo and 22h reperfusion	Global Nox	• Cerebral ischaemia and reperfusion injury increased Nox activity • Apocynin treatment 5 min prior to reperfusion significantly attenuated Nox activity	(Genovese *et al.*, 2011)

Abbrevations: gAD, globular adiponectin; Nox, NADPH Oxidase; tMCAo, transient middle cerebral artery occlusion

ROS production in the ischaemic brain can be separated into two distinct phases: an early phase, reflecting ROS production during ischaemia, and late phase, which reflects ROS production during reperfusion injury. Nox have been predicted to increase ROS production after reperfusion, contributing to the late phase (Lindsay *et al.*, 1991). Abramov *et al.* subjected hippocampal and cortical neurons from mice to *in vitro* oxygen and glucose deprivation (OGD) followed by re-oxygenation, an *in vitro* model of ischaemia-reperfusion injury, and reported an increase in superoxide generation, which was absent in neurons derived from Nox2 KO mice (Abramov *et al.*, 2007). Hence, these studies indicate that Nox play a key role in contributing to oxidative stress following cerebral ischaemia and reperfusion injury. Furthermore, as Nox require molecular oxygen for superoxide generation, it is more than likely that Nox contribute to ROS generation following the re-introduction of oxygen during cerebrovascular reperfusion.

1.3.2.3 Xanthine Oxidase

Xanthine oxidase is a major source of the superoxide anion and has been implicated as an important mediator in the pathogenesis of ischaemic injury (Manning *et al.*, 1984; Itoh *et al.*, 1986). Xanthine oxidase is a complex molybdo-flavoenzyme that catalyses the hydroxylation of hypoxanthine to xanthine and subsequently urate or uric acid (Harrison, 2002). However, xanthine oxidase is a modified form of xanthine dehydrogenase, which catalyses the conversion of hypoxanthine to uric acid via the production of xanthine as an intermediate derivative. Xanthine oxidase formed after protein oxidation of xanthine dehydrogenase, under conditions such as cerebral ischaemia, catalyses the breakdown of hypoxanthine and xanthine to produce superoxide by utilising molecular oxygen as the electron acceptor (Love, 1999).

Nox derived superoxide production has primarily been associated with reperfusion injury, while xanthine oxidase derived superoxide has been shown to occur during both ischaemia and reperfusion (Lindsay *et al.*, 1991). The expression of xanthine oxidase varies between tissues, with high xanthine oxidase activity noted in the liver but relatively low levels in the whole brain (Betz, 1985). Interestingly, xanthine oxidase expression is high in vascular endothelium and also in isolated cerebral microvessels (Betz, 1985). Although xanthine oxidase has been localised in cytoplasm of the endothelium, confocal microscopy has shown xanthine oxidase on surface of endothelial cells (Harrison, 2002). Hence, activation of xanthine oxidase will affect the integrity of the BBB.

McCord *et al*. hypothesised that the conversion of xanthine dehydrogenase to xanthine oxidase is initiated upon reduction of blood flow. An increase in intracellular calcium during ischaemia activates proteases that convert xanthine dehydrogenase to xanthine oxidase (McCord, 1985). Following ischaemic injury, depletion of cellular ATP results in elevated concentration of AMP, which is catabolised to hypoxanthine and utilised by xanthine oxidase to generate superoxide

(McCord, 1985). Kinuta *et al.*, have also shown increased xanthine oxidase activity in the ischaemic rat brain, following four vessel occlusion (Kinuta *et al.*, 1989).

Allopurinol is an inhibitor of xanthine oxidase activity, reducing oxidative stress in the vasculature and improving endothelial function. Treatment of patients with allopurinol, within 72h of confirmed ischaemic stroke, leads to a significant reduction in plasma levels of uric acid and intracellular adhesion molecule-1 (ICAM1) (Muir *et al.*, 2008). *In vivo* Martz *et al.* demonstrated a 35% reduction in stroke volume in male rats pre-treated with allopurinol, prior to MCAo, suggesting that xanthine oxidase contributes to ROS production and oxidative stress following ischaemic injury (Martz *et al.*, 1989). Allopurinol pre-treatment in spontaneously hypertensive rats yielded similar findings (Itoh *et al.*, 1986). Furthermore, permanent MCAo in rabbits pre-treated with allopurinol leads to reduced brain levels of uric acid and xanthine, measured using high performance liquid chromatography (HPLC) (Akdemir *et al.*, 2001). Hence, these studies demonstrate that xanthine oxidase derived ROS contributes to oxidative stress following cerebral ischaemia and reperfusion injury.

Table 1.7 Reported findings of expression and activity of xanthine oxidase in the ischaemic brain

Species	*Model*	*Findings*	*Reference*
Gerbil	3 or 6h Unilateral carotid artery occlusion and 48h reperfusion	• Level of brain oedema formation related to severity of neurological deficits • Pre-treatment of brains with DMTU 30min before reperfusion significantly attenuated oedema • Long term Tungeten treatment, prior to occlusion and reperfusion injury reduced brain oedema formation • Tungsten reduced XD and XO activity and brain hydrogen peroxide in animals subjected to occlusion and reperfusion injury • Allopurinol did not reduced brain XO and XD levels, it reduced oedema formation and brain hydrogen peroxide levels after occlusion and reperfusion	(Patt *et al.*, 1988)
Pig	In vitro primary endothelial cell culture subjected to anoxia and re-oxygenation	• Pre-treatment of brains with DMTU 30min before reperfusion significantly attenuated oedema • After 10h anoxia, a 55% increase in ROS was detected after 4h re-oxygenation • Re-oxygenation increased cell death by 40% • Inhibition of XO activity by oxypurinol reduced anoxia-re-xoygenation induced cell death	(Beetsch *et al.*, 1998)
Rats	Forebrain ischaemia and reperfusion injury	• Allopurinol pre-treatment significantly attenuated superoxide generation following ischaemia and reperfusion injury • ICAM-1 and MDA expression was significantly attenuated in allopurinol pre-treated rats subjected to ischaemia and reperfusion injury	(Ono *et al.*, 2009)
Rats	pMCAo	• Allopurinol pre-treated rats demosntrate reduced infarct volume after 3h MCAo	(Martz *et al.*, 1989)
Rats	pMCAo	• XO activity increased after 3h pMCAo returning to basal levels after 24h	(Sermet *et al.*, 2000)
Rabbits	pMCAo	• HPLC revealed an increase in xanthine after 4 and 24h pMCAo • Allopurinol pre-treatment significantly reduced xanthine expression in ischaemic brains	(Akdemir *et al.*, 2001)

Abbrevations: DMTU, Dimethyluea, XD Xanthine Dehydrogenase; XO Xanthine Oxidase, ICAM-1, intracellular adhesion molecule 1; MDA Malonyldeakdehyde' MCAo, Middle cerebral artery occlusion; pMCAo, permanent middle cerebral artery occlusion

1.4 Nrf2 and antioxidant defences

As mentioned in Section 1.3, oxidant species are involved in a range of biological processes, ranging from physiological signalling pathways to the increased production of lipid peroxides, protein oxidation and DNA damage. In many neurodegenerative and cardiovascular diseases, an increase in the production of oxidant species is known to contribute towards pathophysiology. In contrast to oxidant species, antioxidants terminate chain reactions initiated by oxidants via enzymatic or non-enzymatic pathways. The majority of antioxidants are reducing agents, such as intracellular glutathione, vitamins A, C and E and α-lipoic acid (Johansen *et al.*, 2005). Furthermore, in addition to the endogenous enzymatic antioxidants mentioned previously (SOD and catalase), there are also endogenous antioxidant enzymes and phase II detoxifying enzymes regulated by the redox sensitive transcription factor Nrf2, such as heme-oxygenase 1 and NADPH:quinone oxidoreducatse 1, which are discussed in Section 1.5 (Motohashi & Yamamoto, 2004; Taguchi *et al.*, 2011).

1.4.1 Nrf2/ARE Pathway

1.4.1.1 Nrf2

The redox sensitive transcription factor nuclear factor erythroid 2 related factor 2 (Nrf2) belongs to the CNC (cap "n" collar) group of bZip (basic region-leucine zipper) motif transcription factors (Motohashi & Yamamoto, 2004). Moi *et al.* reported the discovery of Nrf2 in 1994 following the screening of a K562 cDNA library. It was reported that this newly discovered transcription factor shared sequence homology with nuclear factor erythroid 2 (NF-E2), an erythroid specific transcription factor known to mediate the enhancer activity of the Locus control region (LCR) in regulation of the β-globin gene (Moi *et al.*, 1994). Although, Nrf2 was discovered in 1994, its DNA binding site, known as the antioxidant response element (ARE), also referred to as the electrophilic response element (EpRE), was characterised in 1991 (Rushmore *et al.*, 1991).

1.4.1.2 ARE and MARE

The accumulation of ROS, RNS and xenobiotics are major causes of cellular damage and eventual cell death, which occurs as a result of lipid peroxidation, DNA damage and protein modification. (Cheng *et al.*, 2011; Copple *et al.*, 2008; Kaspar *et al.*, 2009; Stepkowski & Kruszewski, 2011; Huang *et al.*, 2000; Nguyen *et al.*, 2000). Endogenous cytoprotective mechanisms are regulated by the redox sensitive transcription factor Nrf2, which regulates a battery of phase II detoxifying and antioxidant genes. The 5' flanking region of such genes harbours a *cis*-acting element, known as either the ARE or EpRE. This consensus sequence

allows for the recruitment of Nrf2 to the promoter region of Nrf2-regulated genes, and subsequent transcription and upregulation of cytoprotective proteins under conditions of increased oxidative, electrophilic or xenobiotic stress (Ishii *et al.*, 2000; Motohashi & Yamamoto, 2004; Taguchi *et al.*, 2011; Chapple *et al.*, 2012; Cheng *et al.*, 2013).

The ARE consensus sequence was identified to be similar to the Maf recognition binding element (MARE) (Itoh *et al.*, 1999). Maf proteins exist in two forms known as large Maf and small Maf proteins. Both forms of Maf proteins form hetrodimers with transcription factors, however, small Maf proteins dimerise with Nrf2, allowing for its binding to the ARE. Musculoaponecrotic fibrosarcoma (Maf) are bZip transcription factors that were reported to hetrodimerise, initially with Jun and Fos, via its leucine zipper structure, allowing for binding of small Maf heterodimers to the MARE sequence (Kataoka *et al.*, 1994). Interestingly, Mafs are also able to form homodimers, however the binding affinity of Mafs to the MARE sequence is dependent upon its binding partner (Kataoka *et al.*, 1994). Kataoka *et al.* suggested that Nrf2 may heterodimerise with small Maf proteins (Kataoka *et al.*, 1994), and Itoh *et al.* in 1997 provided evidence using an EMSA assay *in vitro* in *E.coli* that Nrf2 formes hetrodimers with the small Maf protein MafK, increasing the binding affinity to the mouse Ya1 (alpha class glutathione S-transferase gene) ARE gene by 400-fold (Itoh *et al.*, 1997). Notably, the Nrf2-MafK heterodimer also binds to the ARE sequence of a phase II detoxifying enzyme NQO1(Itoh *et al.*, 1997), discussed further in Section 1.5. *In vivo*, Motohashi *et al.* reported that MafG and MafF are also required for Nrf2 binding activity (Motohashi *et al.*, 2004). These findings thus clearly suggest that Nrf2 binding to the ARE promoter sequence is dependent on hetrodimerisation, and hence different heterodimer binding complexes may be responsible in regulating the observed protein induction.

1.4.1.3 Nrf2 domians and Nrf2-Keap1 interactions

Structural data for Nrf2 indicates that this protein consists of 7 domains, Neh 1 – 7. Figure 1.8 illustrates the possible arrangement of the functional Nrf2 protein domains and summarises their activity. The Neh1 domain of Nrf2 consists of the bZip motif, responsible for the hetrodimerisation of Nrf2 with small Maf proteins (Motohashi & Yamamoto, 2004). The Neh2 domain consists of the ETGE and DLG motif, which are required for the binding of Nrf2 to its cytosolic repressor Keap1 (Motohashi & Yamamoto, 2004), and is discussed later in this section. The Neh 4 and 5 domains of Nrf2 have been reported to bind to the cAMP response element binding protein (CBP), which recruits histone acyltransferases (HAT) to a transcriptional activation complex, allowing for modification of the chromatin structure. Furthermore, CBP also possesses HAT activity and acetylates histone and non-histone nuclear proteins (Katoh *et al.*, 2001). Mutations of the Neh4 and Neh5 domains in HEPA hepatoma

c1c7 cells markedly attenuates CBP binding to Nrf2 and Nrf2 activity, as examined using a luciferase reporter assay (Katoh *et al.*, 2001). The Neh7 domain has been found to repress Nrf2-ARE interaction following direct interaction of the Neh7 domain with the retinoic X receptor α (Wang *et al.*, 2013a).

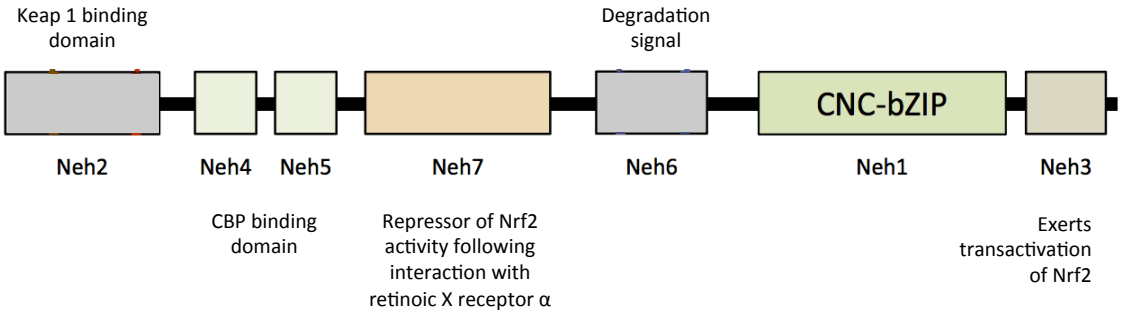

Figure 1.8 Functional domains of Nrf2 and associated activity.
The Nrf2 protein consists of 7 functional domains. The Neh1 domain plays a major role in the heterodimerisation of Nrf2 with small Maf proteins binding to the ARE. The Neh2 domain consists of the ETGE and DLG binding motifs, required for the anchoring of Nrf2 by the cytosolic repressor Keap1. Figure adapted from (Hayes & Dinkova-Kostova, 2014).

The activity of Nrf2 is repressed by its interaction by its cytosolic binding partner, Kelch-like-ECH-associated protein 1 (Keap1), via the Neh2 domain of Nrf2. Keap1 exists as a homodimer in the cytosol and possesses 4 functional domains; the broad tram-track-bric-a-brack domain (BTB domain), double glycine repeat/kelch domain (DGR), intervening repeat (IVR) and a C-terminal region (CTR) (Motohashi & Yamamoto, 2004; Taguchi *et al.*, 2011). Under normal conditions, Keap1 forms a ligase complex following its association with Cullin3 (Cul3), to form an E3 ligase complex (Taguchi *et al.*, 2011). This Keap1-Cul3 complex is responsible for the polyubiquitination of Nrf2, leading to its degradation by the 26S proteasome (Figure 1.9) (Taguchi *et al.*, 2011).

Under homeostatic conditions, the interaction between Keap1 and Nrf2 is described by the hinge and latch model, whereby Keap1 serves as a "gate" for the accumulation of Nrf2 in the nucleus. Keap1 exists in the cytosol as a homodimer and interacts with Nrf2 via the DGR/Kelch domain and the Neh2 domain of each respective protein. The Neh2 domain of Nrf2 harbours an ETGE motif that is responsible for the strong interaction of Nrf2 to the Kelch domain of Keap1. The Neh2 domain also encodes for the DLG motif, which orchestrates the presence of a weaker interaction between the Kelch domain of the second Keap1 protein homodimer. This difference in the affinity of the two motifs, possessed by the Neh2 domain, gives rise to the "hinge and

latch" model of Nrf2/Keap1. Nrf2 is constitutively degraded when bound to Keap1, thus preventing the accumulation of Nrf2 "free" Nrf2 in the cytosol.

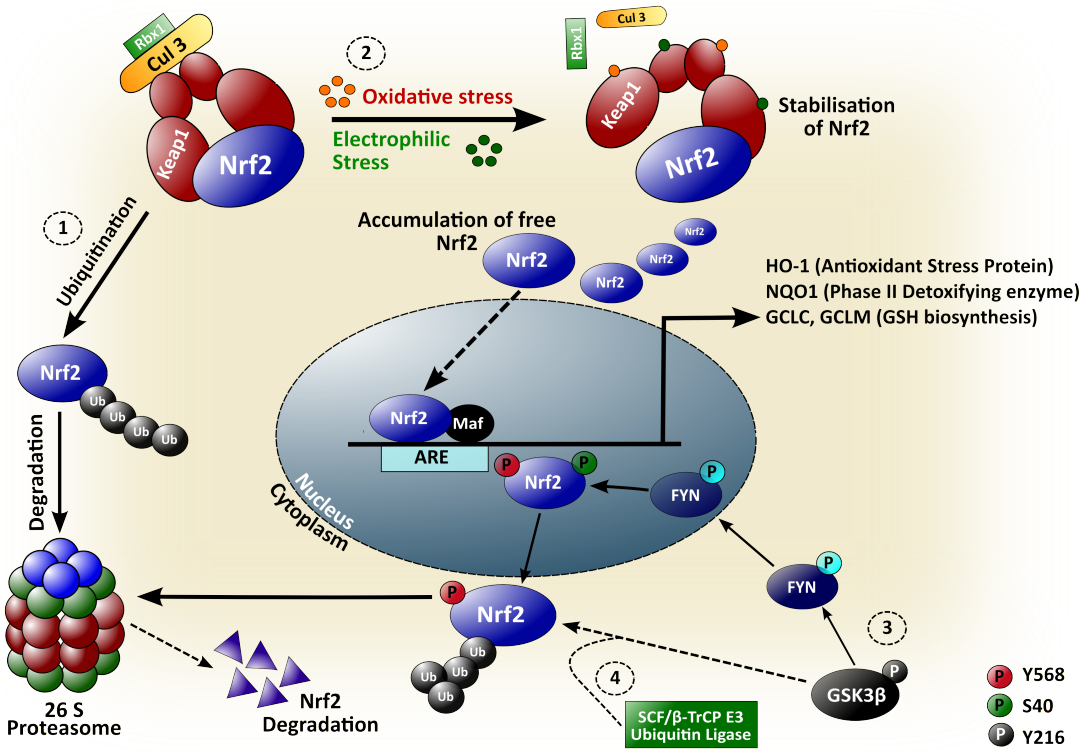

Figure 1.9. Cytoprotection afforded by the Nrf2/ARE pathway.
The redox sensitive transcription factor Nrf2 is tethered to its cytoplasmic repressor Keap1 under normal conditions, and (1) ubiquitinated following the recruitment of Cullin 3 and ring box 1 protein to Keap1 to form a ubquitination complex, marking Nrf2 for degradation by the 26S proteasome. (2) Under conditions of increased oxidative or electrophilic stress, redox sensitive cysteine residues on Keap1 are reduced, resulting in the conformational change of Keap1, breakdown of the ubiquitination complex and stabilization of Nrf2. Free Nrf2 translocates to the nucleus and binds to small Maf proteins and upregulates the transcription of genes containing an ARE in their promoter sequence. (3) The GSK3β-FYN axis mediates the phosphorylation of Nrf2 and its nuclear export. (4) SCF/β-TrCP negatively regulates Nrf2 by ubiquitin dependent proteasomal degradation of GSK3β phosphorylated proteins. *Abbreviations*: β-TrCP, β-transducin repeat containing protein; ARE, Antioxidant response element; GSK3β, glycogen synthase kinase 3β; Keap1, Kelch like associated protein 1; Nrf2, NF-E2 related factor 2; SCF, Skp, Cullin, F-box containing complex; SH, cysteine; Ub, ubiquitin.

Although non-enzymatic antioxidants (GSH, carotenoids and ascorbic acid) efficiently tackle ROS formation under normal physiological conditions, increased exposure to electrophilic, xenobiotic or oxidative stress results in the spatial modification of Keap1 protein (Taguchi *et al.*, 2011). Cysteine residues 613, 226, 273, 288 and 151 have been reported to act as redox sensitive thiol residues which influence the disruption of the ubiquitination machinery, stabilising Nrf2, and allowing for its nuclear translocation (McMahon *et al.*, 2010)(Zhang & Hannink, 2003; Motohashi & Yamamoto, 2004). Controversially, Baird *et al.* have recently

reported that Keap1 undergoes a conformational in which Cul3 does not dissociate, but Nrf2 is stabilised, preventing Nrf2 ubiquitination and its subsequent degradation. As the rate of Nrf2 degradation is decreased, "free" unbound Nrf2 in the cytosol is then able to translocate and accumulate in the nucleus, where it binds to small Maf proteins to increase the expression of phase II detoxifying and antioxidant genes (Figure 1.7) (Motohashi & Yamamoto, 2004; Alfieri *et al.*, 2011; Taguchi *et al.*, 2011).

Interestingly, in Keap1 KO mice, an increased nuclear accumulation of Nrf2 has been reported (Wakabayashi *et al.*, 2003). Surprisingly, Keap1 KO mice died before weaning, with post-mortem analysis revealing hyperkeratosis in the oesophagus and forestomach (Wakabayashi *et al.*, 2003). This data thus suggests that the constant activation of Nrf2 may not confer protection to the cellular system, and hence Keap1 plays a central role in the regulation of Nrf2 activity.

Interestingly, the presence of a Keap1 independent pathway promoting Nrf2 degradation has also been documented. As mentioned previously, Keap1 interacts with the DLG and ETGE motif present in the Neh2 domain of Nrf2. Under the presence of electrophilic stress or chemical inducers of the Keap1-Nrf2 pathway, Nrf2 escapes ubiquitination by Keap1, preventing its degradation. Furthermore, somatic mutations in either the ETGE or DLG motif allow Nrf2 to escape Keap1 regulated degradation. In 2004, McMahon *et al.* identified the importance of the Neh6 domain in regulating the turnover of Nrf2 in an redox-insensitive manner, albeit with an increased half life of 40 min compared to Keap1-mediated regulation (10 min in COS1 cells) (McMahon, *et al.,* 2004). In 2006, Salazar *et al.* demonstrated that glycogen synthase kinase 3β (GSK-3β), a Ser/Thr kinase, is responsible for the nuclear exclusion of Nrf2 in HEK293T cells (Salazar, *et al*, 2006). Furthermore, Rada *et al*. demonstrated similar increases in Nrf2 protein in cells treated with two well characterised Nrf2 inducers, tert-butylhydroquinone and sulforaphane, as well as the GSK-3β inhibitor SB216763 in mouse embryonic fibroblasts (MEFs) (Rada *et al.*, 2011). Interestingly, Rada *et al.* also demonstrated an increase in Nrf2 protein in both WT and Keap1$^{-/-}$ MEFs treated with the GSK-3β inhibitor SB216763, providing further evidence that elevation of Nrf2 protein upon GSK-3β inhibition is not dependent upon Keap1 (Rada *et al.*, 2011).

GSK-3β promotes proteasomal degradation of Nrf2 by recruiting SCF (Skp, Cullin, F-box containing complex)/ β-TrCP (β-transducin repeat containing protein) (Rada *et al.* 2011). The SCF/β-TrCP complex identifies and binds to GSK-3β phosphorylated target proteins and recruits the cullin-1 scaffold protein to form an E3 ligase complex (Figure 1.9). Therefore, β-TrCP acts as a scaffold protein required for the ubiquitination and proteasomal degradation of Nrf2, independent of Keap1 (Rada *et al.*, 2011). As discussed by Rada *et al.*, knockdown of β-TrCP in HEK293T cells by siRNA resulted in an increase in Nrf2 protein levels, thus

demonstrating the importance of β-TrCP in regulating Nrf2 protein levels (Rada *et al.*, 2011). Notably, both isoforms of β-TrCP (β-TrCP-1 and β-TrCP-2) are involved in regulating cellular Nrf2 protein levels (Rada *et al.*, 2011). Interestingly, Chowdry *et al.* have recently shown that mouse Nrf2 contains two binding sites for β-TrCP (Chowdhry *et al.*, 2013). The two β-TrCP binding domains identified in the Neh6 domain are: (1) between amino acids 329-342, containing a putative $DSGIS^{338}$ binding site, and (2) between amino acids 363-379, containing a putative $DSAPGS^{378}$ binding site. Chowdry *et al.* also reported that only the DSGIS motif is subject to phosphorylation by GSK-3β. However, β-TrCP is also able to identify the two non-phosphorylated domains, suggesting that GSK-3β may not play a key role in promoting degradation of Nrf2 (Chowdhry *et al.*, 2013).

1.4.2 Role of Nrf2 in cerebral stroke

Nrf2 plays a crucial role in the protection of the brain following stroke, as notably Nrf2 KO mice exhibit increased cerebral infarct volume, cerebrovascular permeability and neurological deficits following experimental stroke (Shih *et al.*, 2005; Shah *et al.*, 2007). Table 1.8 highlights studies examining the effects of cerebral ischaemia and reperfusion injury *in vivo* on the redox sensitive transcription factor Nrf2. Based on these highlighted studies, it is evident that Nrf2 serves as key redox sensitive transcription factor involved in the protection of the brain parenchyma following cerebral stroke. Nrf2 is described as a redox sensitive transcription factor due to the redox-sensing capabilities of Keap1. Multiple reactive cysteines on Keap1 are modified under conditions of increased redox or oxidative stress, stabilising Nrf2 and allowing for its binding to the ARE. Furthermore, cerebral ischaemia-reperfusion increases the generation of ROS, contributing to a state of oxidative stress experienced by the brain.

The upregulation of Nrf2 regulated phase II detoxifying and antioxidant stress proteins is involved in antioxidant protection. As cerebrovascular permeability is increased in Nrf2 KO mice (Shih *et al.*, 2005; Shah *et al.*, 2007), this provides further evidence that Nrf2 may also confer protection to BBB endothelial cells. Although Nrf2 mediated protection is observed in wild-type and not Nrf2 KO mice, time-dependent changes for Nrf2 protein expression in the BBB endothelium following ischaemia and reperfusion injury have not been reported. Thus, in the present project, temporal and spatial distribution of Nrf2 was quantified in rat brains *ex vivo* following cerebral ischaemia and reperfusion for 4 – 72h.

Table 1.8 Studies of Nrf2 in oxidative stress and cerebral ischemia reperfusion mode

Animal	*Model*	*Transcription Factor*	*Findings*	*Reference*
Mouse	Transient focal cerebral ischemia, MCAo 90 minutes Reperfusion 1hour and 24 hours	Nrf2	Nrf2 -/- mice show increased brain edema and neurological deficit compared to WT mice after 24h reperfusion. Neuron cortical cells in vitro exhibit increased Nrf2 nuclear translocation after treatment with t-BHQ (inducer of Nrf2) and attenuated cell death after t-BuOOH treatment (a free radical donor).	(Shah *et al.*, 2007)
Mouse	Mitochondrial ROS production via external stimulus	Nrf2	$Nrf2^{-/-}$ mice treated with 3-nitropropionic acid (inhibitor of Complex II) and succinate dehydrogenase characterised by increased mitochondrial ROS, concentration-dependent neurological deficits noted compared to +/+ and +/- mice, implicating mitochondrial ROS in neurodegenerative diseases. t-BHQ no effect in $Nrf2^{-/-}$ compared to +/- animals. Interesting that t-BHQ intake reduced body weight in $Nrf2^{-/-}$ mice.	(Shih *et al.*, 2003)
Rats and Mice	MCAO 90 minutes, Reperfusion 24h	Nrf2	Neuronal cells cultured from $Nrf2^{-/-}$ mice have low basal ARE activity which is abrogated upon treatment with t-BHQ. No difference noted in the infarct volume of animals treated with t-BHQ and vehicle after occlusion, however, post 24h reperfusion, significantly reduced infarct volume and neurological deficits observed in mice treated with t-BHQ. Dietary uptake of t-BHQ in $Nrf2^{-/-}$ and $Nrf2^{+/-}$ mice expected to reduce infarct volume and neurological deficits compared to $Nrf2^{-/-}$ animals.	(Shih *et al.*, 2005)
Mouse	pMACO	Nrf2	Post treatment of mice with CO resulted in reduced infarct size and dissociation of Nrf2 from Keap1. Peak in Nrf2 activity recorded at 6 h after 18h CO treatment, approaching basal levels 24 h post treatment. HO-1 induction in response to CO noted at 6 - 48h post treatment. No induction of Nrf2 observed in $Nrf2^{-/-}$ mice post treatment.	(Wang, B, *et al*, 2011)
Mouse	tMCAO (24h)	Nrf2	Upregulation of Nrf2 observed in ipsilateral hemisphere vs contralateral hemisphere. Nrf2 strongest in cortex of ipsilateral hemisphere. Very little or no signal detected in ischaemic core. Nrf2 expression co-localised with microglia and neurons in penumbra. Nrf2 expression in ipsilateral and contralateral hemispheres after tMCAO.	(Dang, J, et al, 2011)

Mouse	tMCAO (60 min) Reperfusion >2h	Nrf2	Decreased Keap1 expression following 2h reperfusion. Peak expression of Nrf2 observed at 8h reperfusion following tMCAO in peri-infarct regions. Expression of Keap1 and Nrf2 noted in predominantly in neurons. Peak expression of HO-1 observed at 72h reperfusion	(Tanaka, N, *et al*, 2010)
Rats	tMCAO 60 min, 24h reperfusion	Nrf2	Pre-treatment rats with p-hydroxybenzyl alcohol (HBA) reduced lesion volume in striatum and cortex following experimental stroke. Increased Nrf2 gene expression observed in hippocampus after stroke compared to vehicle (however expression markedly lower than sham animals). Increased nuclear localisation of Nrf2 in PC12 cells following 2h HBA treatment.	(Kam, KY, *et al*, 2011)

1.5 Nrf2 regulated defence enzymes and intracellular antioxidants

As mentioned previously, Nrf2 mediates protection via the upregulation of genes that contain an ARE sequence in their promoter, which are genes encoding phase II detoxifying and antioxidant stress proteins. This project has examined the expression of three Nrf2-linked genes following cerebral ischaemia and reperfusion injury in rats *in vivo*.

1.5.1 Heme oxygenase-1

The heme oxygenase (HO) pathway has been described as one of the most powerful and protective mechanisms against oxidative stress, identified in systemic organs such as the brain, lungs, kidneys, spleen, intestine and liver (Maines, 1988; Siow *et al.*, 1999b; Wu *et al.*, 2011b; Wegiel *et al.*, 2013) .

HO activity was initially charcterised by Tenhunen *et al.*, in 1968, as a distinct enzyme required for heme degradation in hepatic microsomes (Ryter *et al.*, 2006). HO catalyses the first and rate limiting step in the degradation of free heme to the open-chain tetrapyrrole biliverdin (Ryter *et al.*, 2006). Biliverdin is subsequently converted to bilirubin by the NAD(P)H dependent enzyme biliverdin reductase (Figure 1.10). Both biliverdin and bilirubin are potent chain breaking antioxidants (Forstermann, 2008). Furthermore, evidence indicates that bilirubin plays a pivotal role in disrupting the formation of NADPH oxidase, reducing the generation of superoxide (Kwak *et al.*, 1991). The breakdown of free heme by HO also generates the potent vasodilator carbon monoxide (CO) and Fe^{2+}. The accumulation and removal of iron is regulated by the HO system, as Ferris *et al.* have demonstrate increased iron uptake and cell death in primary mouse fibroblast deficient for HO-1 (Ferris *et al.*, 1999).

There are three isoforms of HO-1; HO-1, a rapidly inducible isoform of HO, HO-2, a constitutively expressed isoform of HO, and HO-3, a hemoprotein involved in regulating the function of heme proteins (Maines, 1997; McCoubrey *et al.*, 1997). HO-1 activity is increased in response to multiple stimuli and agents, such as heat shock, ischaemia, GSH depletion, radiation, hyperoxia, hypoxia and multiple disease states (Maines, 1997). Moreover, the promoter sequence of the HO-1 gene contains an ARE, allowing for gene transcription via the redox sensitive transcription factor Nrf2 (Alam *et al.*, 1999). However, transcriptional regulation of the HO-1 gene has also been documented to be regulated by nuclear factor kappa B (NF-κB), activating protein 1 (AP-1), AP-2, hypoxia inducible factor 1 alpha (HIF-1α) and cyclic AMP (cAMP) response element binding protein (CREB) (Lavrovsky *et al.*, 1993; Lavrovsky *et al.*, 1994; Lonze & Ginty, 2002), highlighting that HO-1 transcription is regulated by multiple transcription factors.

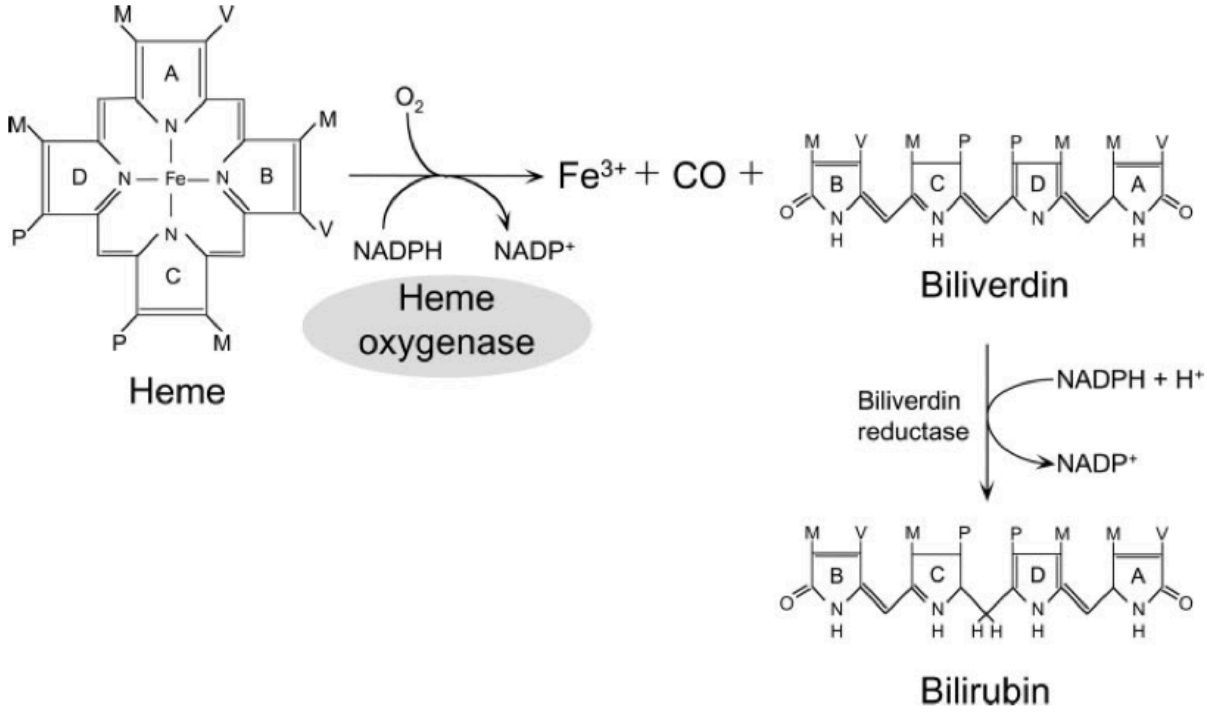

Figure 1.10 Schematic representation of the degradation of free heme by HO-1.
HO-1 catalyses the degradation of free heme to the antioxidants biliverdin and bilirubin. HO-1 cleaves heme between rings A and B, in the presence of NADPH, yielding equimolar concentration of biliverdin, CO and Fe^{3+}. Biliverdin is converted to bilirubin by biliverdin reductase. Both biliverdin and bilirubin are potent antioxidant species. Figure taken from Sikorski, et al. 2003.

Following stroke, HO-1 has been shown to mediate protection to the ischaemic brain. Panahian *et al.* were one of the first to show significant increases in neuroprotection in HO-1 transgenic mice subjected to 6h MCAo (Panahian, et al, 1997). HO-1 transgenic mice showed significant attenuation of cerebral infarct volume and oedema formation (Panahian, et al, 1997). Moreover, Chao *et al.* reported a reduction in lipid peroxidation and protein nitration, along with marked attenuation of infarct volume in following adenoviral overexpression of HO-1 in rats subjected to MCAo, providing further evidence of HO-1 mediated protection following cerebral ischaemia (Chao, et al, 2013). Further evidence indicates a reduction in HO-1 protein in Nrf2 KO mice subjected to MCAo, thus suggesting that HO-1 protein induction is mediated by Nrf2 (Zhao *et al.*, 2006). Further studies highlighting the role of HO-1 in protection of the ischaemic brain are summarised in Table 1.9.

Table 1.9 Cerebral ischaemia studies examining the role of HO-1 mediated protection

Species	*Model*	*HO-1 Model*	*Findings*	*Reference*
Mouse	3h tMCAo and 24 h reperfusion	Transgenic	Transgenic animals shows a marked attenuation of the infarct in comparison to non transgenic animals. Volume of edema was also reduced in transgenic animals. Marked increase in the expression of Bcl-2 also also observed in transgenic mice.	Panahian, N, et al, 1999
Mouse	Induction of cerebral damage by treatment with NMDA	Knockout	HO-1 $^{-/-}$ knockout animals demonstrated a significant increase in infarct volume compared to WT animals. Levels of NMDA and glutatmate receptor expression unaffected by HO-1 $^{-/-}$ model. In vitro neuronal culture studies demonstrate reduced viability in HO-1 $^{-/-}$.	Ahamad, A, et al, 2006
Mouse	*In vitro* cell culture of cortical astrocytes from postnatal mice	Knockout	HO-1 -/- has no effect upon expression of HO-2. HO-1 $^{-/-}$ astrocytes indicated reduced cell viability in response to dose dependent hemin treatment due to increased accumulation of hemin. Overexpression of HO-1 via adenovirus transfection ameliorated affects observed in HO-1 -/- cells.	Chen-Roetling, J, et al, 2005
Mouse	Intracerebral Haemorrhage	Knockout	Increased expression of HO-1 observed in microglial and endothelial cells, absent in HO-1 -/- mice.	Wang, J, et al, 2007

HO-1 is portrayed as a protective antioxidant enzyme, however, damaging effects of HO-1 have also been reported. Although, Péres-de-Puig et al. demonstrate an exacerbation of brain damage when HO activity was inhibited prior to permanent MCAo, activation of HO-1 activity following pMCAO also exacerbated cerebral damage (Perez-de-Puig *et al.*, 2013). Hence, this suggests that the protection afforded by HO-1 is dependent on its activation status, and time-window of expression. Interestingly, Sutherland et al. illustrated increased expression of both HO-1 and HO-2 protein in the rat brain after MCAo or hypoxia-ischaemic insult. Increased HO-1 protein was detected in neurons, glia, infiltrating macrophages and microglia in the infarct core after MCAo (Sutherland *et al.*, 2009). However, HO-2 increases were also defined to the vascular endothelium after hypoxia-ischemic insult (Sutherland *et al.*, 2009). This suggests that HO proteins are upregulated in specific cell type, and furthermore, in response to different stimuli.

Notably, reports have also shown the protective effect of HO-2 in the brain following neurodegenerative disease states. As reviewed by Parfenova et al. HO-2 is in the brain and its cerebral vessels, however, the pharmacological inhibition of HO-2 markedly increases oxidative stress induced damage following seizure, increased glutamate and other neurological disease states (Parfenova & Leffler, 2008). Basuroy et al. illustrated a marked increase in cell death of HO-2 deficient porcine cerebral endothelial cells subjected to oxidative stress following TNF-α treatment (Basuroy *et al.*, 2006). Furthermore, Chang et al. have also shown a reduction in HO activity in brains from HO-2 deficient animals subjected to traumatic brain injury, despite observing an increase in HO-1 protein expression (Chang *et al.*, 2003). Hence, these findings also illustrate a role for protection mediated by HO-2 in the brain, however, HO-2 expression is not regulated by Nrf2.

In view of the importance of HO-1 in protecting the brain against stroke-induced damage, the present project has examined the temporal and spatial distribution of HO-1 in ex vivo rat brain sections following experimental ischaemia and reperfusion injury. Furthermore, the effects of sulforaphane, a known natural Nrf2 inducer, on expression of HO-1 and other Nrf2 regulated enzymes were examined in rats pre-treated with the isothiocyanate prior to MCAo and reperfusion injury. The effects of sulforaphane pre-treatment was also assessed in an in vitro model of cerebral ischaemia using mouse derived brain endothelial cells subjected to oxygen-glucose deprivation.

1.5.2 NADP(H) Quinone Oxidoreductase 1

NAD(P)H: quinone oxidoreductase 1 (NQO1) is a homodimeric flavoprotein that primarily resides in the cytoplasm and uses either NADH or NADPH as reducing cofactors to catalyse the two electron obligate reduction of substrates such as quinone to hydroquinone (Figure 1.9)

(Ross *et al.*, 2000; Siegel *et al.*, 1998, Jaiswal 2000). Quinones are highly reactive molecules that may undergo a one-electron reduction to form an unstable semiquinone intermediate via the presence of enzymes such as xanthine oxidase. Reactive intermediate semiqunones are further utilised to produced hydroquinones, but produce superoxide as a by-product of such reactions. NQO1 by-passes the formation of such reactive intermediates, reducing the reactive quinone to a hydroquinone in a one-step two electron reduction (Ross *et al.*, 2000). By reducing quinones in such a manner, NQO1 promotes the phase II detoxification of quinones (Ross *et al.*, 2000). Furthermore NQO1 also catalyses the phase II conjugation of a range of substances, which includes quinone-imines, glutathionyl-substituted naphthoquinones, dichloro phenolindol phenol, methylene blue, azo and nitro compounds (Ross *et al.*, 2000).

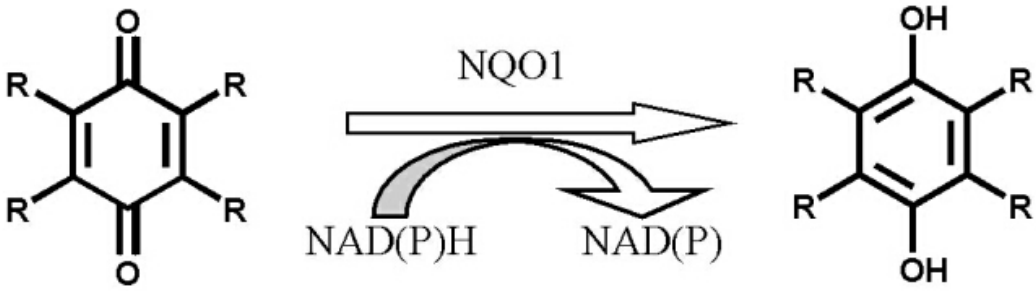

Figure 1.11 NQO1 mediated phase II detoxification of quinones to hydroquinones.

The promoter region of the NQO1 gene contains an ARE, allowing Nrf2 regulated mRNA transcription and protein expression (Lin *et al.*, 2011). Although it has been documented that NQO1 expression is regulated by aryl hydrocarbon receptor (AhR) and Nrf2, knockdown of Nrf2 in mouse aortic endothelial cells attenuates increases in NQO1 protein and mRNA expression following treatment wirh benzo(a)pyrene (BaP), a xenobiotic stimulant (Lin *et al.*, 2011). Bap is a well characterized inducer of AhR mediated protein expression, however, in the absence of Nrf2, BaP mediated expression of NQO1 is abrogated, suggesting that Nrf2 is key in regulating NQO1 protein expression (Lin *et al.*, 2011).

Stringer *et al.* have demonstrated the presence of NQO1 in the brain and central nervous system (Stringer *et al.*, 2004). Interestingly, the authors reported increased myelination of axons in NQO1 deficient mice, thus suggesting a role for NQO1 in regulation of myelination of the central nervous system (Stringer *et al.*, 2004). Lee *et al.* report a reduction in the basal levels of NQO1 and no induction following treatment of Nrf2 deficient primary cortical astrocytes treated with tert-butylhydroquinone (Lee *et al.*, 2003). He *et al.* also reported that basal

expression of NQO1 is absent in Nrf2 KO mice (He *et al.*, 2009), providing further evidence for Nrf2 mediated regulation of NQO1 expression.

Furthermore, in studies *in vivo* Seng *et al.* have demonstrated a role for NQO1 mediated protection in the brain (Seng *et al.*, 2009). The nuclear restricted protein in brain (NRP/B) is a nuclear matrix protein and has been identified as a co-factor for Nrf2, resulting in the induction of NQO1 (Seng *et al.*, 2009). NRP/B mutations, identified in primary human glioblastomas, have been shown to alter cellular localisation, reducing NRP/B interactions with Nrf2, and consequently reducing NQO1 expression in the brain (Seng *et al.*, 2009).

As discussed above for HO-1, this project examined the expression of NQO1 in rat brain sections *ex vivo* following cerebral ischaemia and reperfusion injury. Moreover, protein and mRNA expression of NQO1 were studied in an *in vitro* model of cerebral ischaemia using a mouse derived brain endothelial cell line.

1.5.3 Peroxiredoxin

Peroxiredoxins (Prx) are ubiquitously expressed non-heme peroxidase enzymes responsible for the catalysis and breakdown of H_2O_2 to H_2O, alkylhydroproxide to its corresponding alcohol and peroxynitrite to nitrite (Rhee *et al.*, 2001; Rhee *et al.*, 2005; Ishii *et al.*, 2012). Moreover, peroxiredoxins also control cytokine induced peroxide levels (Jin *et al.*, 2005). Prx were initially identified in yeast and mammals and reported to have a key role in protecting glutamate synthetase (Rhee *et al.*, 2001). The peroxidase activity of Prx's are reversible and effectively inactivated following protein modification by phosphorylation of tyrosine 194 (Woo *et al.*, 2010; Ishii *et al.*, 2012). There are six isoforms of Prx, divided into the three subtypes, which is dependent on the number of conserved cysteine residues directly involved in catalysis of H_2O_2: Prx I – IV contain of two catalytic cysteine residues, Prx V of two atypical cysteine residues, and Prx VI consists of one catalytic cysteine residue (Jin *et al.*, 2005). Although PrxV contains two cysteine residues, one of these cysteine residues is not conserved (Dayer *et al.*, 2008). Apart from their antioxidant functions, Prx have also been identified to serve as signalling molecules, with binding of Prx1 noted to the surface signal receptor toll-like receptor 4 (TLR4) (Ishii *et al.*, 2012). The oxidation status of Prxs may also be used as biomarker of oxidative stress. As reviewed by Poynton *et al.*, the catalytic cysteine residues of peroxiredoxin may be hyperoxidised and accumulate in the intracellular environment (Poynton & Hampton, 2013).

The promoter region of Prx, I, III (Miyamoto *et al.*, 2011) and VI (Chowdhury *et al.*, 2009) consists of the ARE, allowing for regulation by Nrf2. Kim *et al.* highlighted a reduction in Prx1 protein expression following the knockdown of Nrf2 in the human cancer cell line A549 following hypoxia and re-oxygenation (Kim *et al.*, 2007). Ishii *et al.* have also demonstrated a

reduction Prx1 protein expression and induction following the stimulation of peritoneal macrophages with oxidised LDLs (Ishii *et al.*, 2004). This provides further evidence that Nrf2 directly regulates Prx1 expression. The nuclear compartmentalisation of Prx1 has also been reported in HeLa cells, and illustrated to enhance NF-κB activity following treatment with H_2O_2 (Hansen *et al.*, 2007). However, cytoplasmic Prx1 is known to downregulate NF-kB activity following the elimination of peroxides (Kang *et al.*, 1998). Hence this demonstrates that the functions of Prx1 are also dependent on its cellular localisation.

Prxs are widely distributed among tissue, including the brain. Interestingly, a cell specific distribution of Prxs has been noted in the brain, with Prxs II – V expressed in neurons, Prx VI and I in astrocytes and microglia respectively (Jin *et al.*, 2005; Goemaere & Knoops, 2012). Although Prxs have been reported to protect the brain against ischaemia induced oxidative injury, a controversial role for Prxs following stroke was highlighted by Shichita *et al.* The authors suggested that the release of Prx from necrotic cerebral cells, 12h after ischaemia-reperfusion injury, promotes the expression of inflammatory cytokines on macrophages and increasing cell death (Shichita *et al.*, 2012a). Notably, Prx V and VI were demonstrated to increase IL-23 expression, while Prx I and II evoked less (Shichita *et al.*, 2012a). The release of Prxs from necrotic cerebral cells upregulate pro-inflammatory and cytokine responses following interactions with TLR4 and TLR2 (Shichita *et al.*, 2012b). Tao *et al.* however, show that increased expression of Prx1 *in vivo* significantly attenuated BBB permeability following transient MCAo and 24h reperfusion injury in mice (Tao *et al.*, 2013), thus suggesting a protective role for Prx1 following cerebral ischaemia and reperfusion injury.

1.5.4 Glutathione

Glutathione (GSH) is an intracellular tripeptide formed of glutamate, glycine and cysteine, and provides the first line of defence against increased ROS production. GSH directly scavenges ROS in a non-enzymatic manner, maintaining intracellular homeostasis (Meister & Anderson, 1983; Bannai & Tateishi, 1986; Backos *et al.*, 2012), and protects the brain to against oxidative injury (Dringen, 2000). As well as scavenging ROS, GSH aids the function of glutathione peroxidase (GPx) in reducing H_2O_2 and other peroxides (Schulz *et al.*, 2000; Lu, 2009; Backos *et al.*, 2012). Another function of GSH is to act as storage for glutamate and cysteine, which serves as an important cytoprotective mechanism in the brain, preventing cytotoxicity mediated by free glutamate and cysteine (Meister & Anderson, 1983; Backos *et al.*, 2012). The brain is reported to have high concentrations of GSH (Aoyama *et al.*, 2008; Shen *et al.*, 2011a), further highlighting a key role for GSH in protection of the brain against oxidant injury. GSH is also involved in the detoxification of numerous xenobiotics by serving as a cofactor for phase II detoxifying enzymes, resulting in the formation of water soluble GSH-drug conjugates

(O'Brien, 1988; Backos *et al.*, 2012). Although GSH is primarily cytosolic, it has been localised in the endoplasmic reticulum (ER) and nucleus (Chakravarthi *et al.*, 2006; Markovic *et al.*, 2007; Vivancos *et al.*, 2010).

GSH biosynthesis is dependent upon the formation of γ-glutamyl-L-cysteine from glutamate and cysteine via glutamate cysteine ligase (GCL), the rate-limiting enzyme in the formation of GSH. γ-glutamyl-L-cysteine reacts further with glycine via glutathione synthetase (GS) to generate GSH (Meister & Anderson, 1983; Krejsa *et al.*, 2010). GCL is a holoenzyme composed of a catalytic (GCLC) and modulatory domain (GCLM). Moreover, Nrf2, AP-1 and Nuclear Factor Kappa B (NF-κB) regulate the transcription of these subunits under oxidative stress conditions (Backos *et al.*, 2012; Aoyama *et al.*, 2008). The identification of the ARE in the promoter sequence of GCLC in HepG2 cells provides further evidence for the regulation of glutathione synthesis by Nrf2 (Mulcahy *et al.*, 1997).

In the presence of GPx, GSH is catalysed to form GSH disulfide (GSSG) or reduced GSH, which can be salvaged to restore GSH by glutathione reductase (GR) by utilising NADPH as an electron donor (Lu, 2009). Conditions of increased oxidative, electrophilic or xenobiotic stress result in the accumulation of GSSG due to the reduced availability of NADPH required for GR activity (Lu, 2009).

Shivakumar *et al.* demonstrated a 50-66% reduction in brain GSH levels in brains after 1h reperfusion-injury in rats subjected to 30 min MCAo (Shivakumar *et al.*, 1995). The authors also report an increase in malondialdehyde and ROS following the depletion of GSH after MCAo and reperfusion injury (Shivakumar *et al.*, 1995). Anderson *et al.* reported significant attenuation of infarct volume following the delivery of glutathione monoethyl ester, which increases intracellular glutathione content, prior to 2h MCAo and 24h reperfusion injury in rats (Anderson *et al.*, 2004). Interestingly, Paterson *et al.* highlight a decrease in neuronal GSH levels in humans that are either fasting, on low protein diet or on diets that may limit sulphur amino acid intake. This consequently reduces cysteine levels required for the biosynthesis of GSH, potentially linked to an increased susceptibility to stroke induced damage (Paterson & Juurlink, 1999). With regards to the cerebral endothelium, Hong *et al.* reported an increase in P-glycoprotein (Pgp) protein expression following the depletion of GSH in primary rat brain endothelial cells treated with buthionine sulfoximine (BSO) (Hong *et al.*, 2006a). Notably, Pgp is localised on the luminal surface of the cerebral endothelium and is involved in the transport of drugs (such as morphine and phenytoin) and lipids (Hong *et al.*, 2006a). As reviewed by Miller *et al.,* Pgp protein and mediated drug transport are increased after cerebral stroke (Miller *et al.*, 2008), suggesting an increased transport of blood-borne substances into the brain milieu following stroke. These findings thus establish a protective role for GSH in the ischaemic brain.

1.5.5 Other Nrf2 regulated proteins

Nrf2 has also been shown to regulate proteins that are involved in lipid and carbohydrate metabolism. Ludtmann *et al.* reported a role for Nrf2 in regulating mitochondrial oxidation of both short and long chain fatty acids. Oxidation of fatty acids were depressed in Nrf2 deficient mice but enhanced in wild-type animals (Ludtmann *et al.*, 2014).

Hence, regulation of this subset of genes by Nrf2 suggests that Nrf2 not only provides protection through upregulation of antioxidant genes, but also through regulating metabolic processes important for cell survival. Table 1.10 summarises proteins regulated by Nrf2.

Table 1.10 List of Nrf2 regulated proteins

Biochemical Function	***Gene/Protein Name***	***Reference***
Antioxidants	Heme-oxygenase 1	(Naughton *et al.*, 2002; MacLeod *et al.*, 2009)
	NADPH:Quinone oxidoreducatse 1	(MacLeod *et al.*, 2009)
	Gultamate cysteine ligase - catalytic domain	(MacLeod *et al.*, 2009)
	Glutamate cysteine ligase - modulatory domain	(MacLeod *et al.*, 2009)
	Gamma-glutamyltransferase1	(Agyeman *et al.*, 2012)
	Glutaredoxin 1	(Agyeman *et al.*, 2012)
	Glutaminase	(Agyeman *et al.*, 2012)
	Glutathione peroxidase 2	(Agyeman *et al.*, 2012)
	Glutathione peroxidase 4	(Agyeman *et al.*, 2012)
	Glutathione reductase	(Thimmulappa *et al.*, 2002)
	Glycine transporter	(MacLeod *et al.*, 2009; Agyeman *et al.*, 2012)
	Cystine/glutatamate transporter	(Agyeman *et al.*, 2012)

	Peroxiredoxin 1	(Reisman *et al.*, 2009)
	Peroxiredoxin 3	(Miyamoto *et al.*, 2011)
	Peroxiredoxin 5	(Miyamoto *et al.*, 2011)
	Peroxiredoxin 6	(Erttmann *et al.*, 2011)
	Thioredoxin	(MacLeod *et al.*, 2009)
	Thioredoxin reductase 1	(MacLeod *et al.*, 2009)
	Sulfiredoxin 1	(MacLeod *et al.*, 2009)
NADPH regeneration and carbohydrate metabolism	Malic Enzyme 1	(Wu *et al.*, 2011a; Agyeman *et al.*, 2012)
	Glucose-6-phosphate dehydrogenase	(Wu *et al.*, 2011a; Agyeman *et al.*, 2012)
	6-phosphogluconate dehydrogenase	(Wu *et al.*, 2011a; Agyeman *et al.*, 2012)
	Hexokinase domain containing 1	(Agyeman *et al.*, 2012)
	transaldolase	(Agyeman *et al.*, 2012)
	transketolase isoform 1	(Agyeman *et al.*, 2012)
	UDP-glucose dehydrogenase	(Agyeman *et al.*, 2012)
Lipid metabolism	Fatty acid desaturase 1	(Wu *et al.*, 2011a)
	Fatty acid desaturase 2	(Wu *et al.*, 2011a)
	Stearoyl-CoA desaturase 2	(Wu *et al.*, 2011a)
	acetyl CoA thioesterase 7	(Lee *et al.*, 2003)

	acetyl CoA thioesterase 8	(Lee *et al.*, 2003)
	acetyl CoA oxidase 1	(Lee *et al.*, 2003)
	acetyl CoA oxidase 2	(Lee *et al.*, 2003)
	carboxylesterase 1G	(Lee *et al.*, 2003)
	carboxylesterase 1H	(Lee *et al.*, 2003)
	Phospholipase A2	(Lee *et al.*, 2003)
Iron Metabolism	Ferritin	(MacLeod *et al.*, 2009)
	Ferrochelatase	(MacLeod *et al.*, 2009)

1.6 Activation of Nrf2 by dietary isothiocyanates

As mentioned previously, the redox sensitive transcription factor Nrf2 is activated following xenbiotic, oxidative or electrophilic stress. However, in the past decade, a number of studies have identified and focused on mediating Nrf2 activation by naturally occurring dietary compounds, some of which are listed in Table 1.11.

Table 1.11 Dietary activators of Nrf2

Dietary Nrf2 activators	*References*
AITC	(Ernst *et al.*, 2011; Wagner *et al.*, 2012; Hsu *et al.*, 2013)
Resveratrol	(Botelho *et al.*, 2009; Ren *et al.*, 2011; Clark *et al.*, 2012)
Epicatechin-3-gallate	(Shah *et al.*, 2010; Gomez-Guzman *et al.*, 2012)
Curcumin	(Yang *et al.*, 2009; Zhao *et al.*, 2010; Charoensuk *et al.*, 2011; Wu *et al.*, 2013)
Cinnamaldehyde	(Wondrak *et al.*, 2008; Chew *et al.*, 2010; Huang *et al.*, 2011)
Sulforaphane	(Dinkova-Kostova *et al.*, 2002; Zhao *et al.*, 2006; Hong *et al.*, 2010)
Plumbagin	(Son *et al.*, 2010)
Quercetin	(Miyamoto *et al.*, 2011; Murakami & Ohnishi, 2012)

Many studies have examined the potential therapeutic effects of these electrophilic compounds in the fight against caner, as well as treating cardiovascular complication, and neurological disease states. The electrophilic nature of these compounds suggests that they mediate Nrf2 activity following interaction with redox sensitive cysteine residues on Keap1. In this project, the affects the dietary Nrf2 inducer sulforaphane were examined. This section will briefly discuss (1) the isolation and discovery of sulforaphane, (2) its bioavailability and attainable levels *in vivo*, (3) the effects of sulforaphane on the Nrf2 defence pathway, and (4) its effects on treatment following cerebral ischaemia and reperfusion injury.

1.6.1 Sulforaphane

The dietary isothiocyanate sulforaphane, is derived from the glucosinolate glucoraphanin, an organosulfur compound present in brassica vegetables, such as broccoli, cauliflower, kale and Brussels sprouts (Stoewsand, 1995; James *et al.*, 2012). The enzyme myrosinase co-exists with the primary glucosinolate in brassica vegetables, however, it only catalyses the breakdown of glucoraphanin to the active isothiocynate sulforaphane, following mechanical activation (via chewing or during the preparation of food) (Ye *et al.*, 2002; Zhang & Tang, 2007). Moreover, the breakdown of glucosinolates is also partially catalysed by the gut flora containing enzymes that have similar activity to myrosinase (Ye *et al.*, 2002; Zhang & Tang, 2007). The role of

dietary isothiocyanates was initially demonstrated to reduce the effect of chemical carcinogenesis in animal models of cancer (Conaway *et al.*, 2002; Ye *et al.*, 2002).

The isothiocyanate sulforaphane (1-isothiocyanato-4-(methylsulfinyl)-butane) was isolated by Zhang *et al.* in the early 1990s using high performance liquid chromatography (Zhang *et al.*, 1992). Isothiocyanates are known inducers of Phase II detoxifying enzymes such as NQO1 and glutathione-S-tranferases (GST), along with xenobiotics and oxidative stimuli (Fahey *et al.*, 1997; Zhang & Tang, 2007). Interestingly, the structure of sulforaphane was isolated and resolved following the induction of NQO1 enzyme activity, as established by the prochaska assay, following the treatment of murine hepatoma Hepa 1c1c7 cells treated with broccoli extract (Prochaska & Santamaria, 1988; Zhang & Tang, 2007). Fahey *et al.* documented the isolation of 9 mg of sulforaphane extract from 640 g of fresh broccoli sprouts, although it was later shown that initial sulforaphane concentration was 10-fold higher in these extracts (Fahey *et al.*, 1997; Zhang & Tang, 2007). Zhang and colleagues also generated 40 different analogues of sulforaphane and assessed NQO1 enzyme activity by the prochaska assay to assess and determine the structure of sulforaphane found in broccoli extaracts. Sulforaphane isolated from broccoli has a chiral structure, possessing the R configuration and its inducer activity was matched by the synthetically derived (R,S)-sulforaphane isomer (Zhang & Tang, 2007). The induction of phase II enzymes was regarded as an important measure against carcinogenesis, and that the consumption of fruits and vegetables reduced the risk of cancer (Zhang & Tang, 2007).

Pharmacokinetic studies using sulforaphane have shown that once it is absorbed into cells, it conjugates to glutathione via glutathione-S-transferases (Basten *et al.*, 2002). It must be noted that the breakdown of the glucoraphanin yields both sulforaphane and sulforaphane nitrile (Matusheski & Jeffery, 2001; Basten *et al.*, 2002). However, Mathusheski *et al.* demonstrated that the nitrile form of sulforaphane is unable to induce GST and NQO1 activity *in vivo* in the liver, colonic mucosa and pancrease of Fisher 344 rats, and NQO1 enzyme activity *in vitro* in Hepa 1c1c7 cells (Matusheski & Jeffery, 2001). Hence, this suggests that the bioavailability of sulforaphane influences Nrf2-mediated protein expression and activity.

1.6.1.1 Bioavailability of sulforaphane

The bioavailability of sulforaphane is dependent upon multiple factors, including (1) the source of sulforaphane, (2) age and storage of broccoli and other cruciferous vegetables, (3) method of cooking and (4) the gut flora composition of individuals (Zhang & Tang, 2007; Vermeulen *et al.*, 2008). Fahey *et al.* were one of the first groups to identify an approximate 9-fold difference in the yield of sulforaphane from broccoli sold in local supermarket, including fresh and frozen

broccoli varieties, thus making it difficult to assume and define an initial concentration of glucoraphanin (Fahey *et al.*, 1997). The method of preparation and cooking of broccoli also influences the final levels of sulforaphane that is attained in systemic circulation. Healthy subjects were given fresh or steamed broccoli (200g) and notable increases in concentration of sulforaphane and its conjugates were observed in the urine of group subjects given fresh broccoli, 24h after administration (Conaway *et al.*, 2000). Moreover, the bioavailability of isothiocyanates was reported to be 3-fold greater in fresh broccoli compared to steamed broccoli (Conaway *et al.*, 2000). A similar trend was also observed by other studies (Vermeulen *et al.*, 2008), however, Vermeulen *et al.* also reported a delay in the systemic absorption of sulforaphane from cooked broccoli, with peak plasma levels attained after 6h, compared to 1.6h in subjects that consumed raw broccoli (Vermeulen *et al.*, 2008). Interestingly, 200g of raw broccoli serving consist of approximately 9.92µmol of glucoraphanin, whilst cooked broccoli comprises of 61.4 µmol glucoraphanin. These findings highlight the difference between cooking techniques, which may in turn have an effect on the pharmacokinetics and bioavailability of sulforaphane. Mukerjee *et al.* assessed cardioprotection in rats that were fed either steamed or cooked broccoli for 30 days prior to ischaemia-reperfusion injury in the heart and reported increased protection in rats fed steamed broccoli (Mukherjee *et al.*, 2010). The latter study clearly demonstrates the affect of high sulforaphane bioavailability on protective mechanisms *in vivo*.

As mentioned previously, sulforaphane is conjugated to glutathione in a reaction catalyzed by GST. There are three known families of GSTs, dependent upon cellular location; cytosolic, mitochondrial and microsomal (Gasper *et al.*, 2005). 7 classes of cytosolic GSTs have been identified, from which GSTM1-1 and GSTP1-1 are regarded as being important in the conjugation of sulforaphane to glutathione (Gasper *et al.*, 2005). Studies have established polymorphisms with the GSTM1 gene, resulting in the absence of a working gene product (Bhattacharjee *et al.*, 2013) with approximately 39% to 64% of various populations affected by homozygous null GSTM1 polymorphisms. Lin *et al.* demonstrated the lower prevalence of colorectal adenomas in GSTM1 positive human subjects compared to GSTM1 null subjects (Lin *et al.*, 1998). Controversially, Gasper *et al.* reported no significant differences in the bioavailability of sulforaphane and its conjugates between GSTM1 null and GSTM1 positive subjects, but suggest that GSTM1 positive subjects retain sulforaphane for increased durations, enhancing protective effects (Gasper *et al.*, 2005).

1.6.1.2 Effects of Sulforaphane on Nrf2-mediated responses

The activation of Nrf2 is in part dependent upon the modification of cysteine residues on the cytosolic Nrf2 repressor protein Keap1 (Chapple *et al.*, 2012). As mentioned previously, the

modification of cys151, cy273 and cys288 is critical for Nrf2 activation. The dietary isothiocyanate sulforaphane is able to conjugate to the mentioned cysteine residues, resulting in the conformational change of the Nrf2-Keap1 interaction, thereby reducing the rate of proteasomal mediated Nrf2 degradation, and promoting its nuclear translocation (Zhang & Hannink, 2003; Hong *et al.*, 2005; Chapple *et al.*, 2012).

It is well known that sulforaphane upregulates the activity of the phase II detoxifying enzyme NQO1, suggesting a mediated increase in NQO1 protein levels. An oligonucleotide microarray conducted by Thimmulappa *et al*. revealed significant increases in the transcripts of ARE-linked genes, which included NQO1, GST, glutathione-6-phosphate dehydrogenase (G6PDH) and γ-glutamylcysteine synthetase (GCS), following administration of 9 µmol sulforaphane/day for 1 week in wild type mice (Thimmulappa *et al.*, 2002). Sulforaphane treatment of Nrf2 KO mice had no effect on the expression of ARE-linked genes, suggesting that sulforaphane may selectively mediate the transcription of known ARE-linked genes via Nrf2.

1.6.1.3 Reported findings of sulforaphane treatment in experimental models of cerebral ischaemia and reperfusion injury

Sulforaphane studies have illustrated a decreasing risk in the prevalence of colorectal and lung cancer following increased consumption of this dietary isothiocyanate (Thimmulappa *et al.*, 2002). Although research has focused on targeting sulforaphane as a chemopreventative drug (Juge *et al.*, 2007), the ability of sulforaphane to mediate protection via the upregulation of phase II detoxifying enzymes and antioxidant stress proteins has become a prime focus for therapeutic strategies to combat cardiovascular and cerebrovascular diseases, including cerebral stroke.

Jing Zhao *et al.* were one of the first groups that employed sulforaphane post-treatment in a rodent model of cerebral ischaemia and reperfusion injury. Mice, subjected to 3h MCAo and 3 day reperfusion injury were treated with sulforaphane (5 mg/kg *i.p.*) 15 min after the induction of ischaemia and report significant attenuation of cerebral infarct volume (Zhao *et al.*, 2006). Zhao *et al.* were not able to define a mechanism underlying sulforaphane mediated a reduction in cerebral infarct volume, but reported an increase in HO-1 mRNA and protein expression in astrocytes and neurons following 24h sulforaphane treatment (Zhao *et al.*, 2006). Although this publication demonstrated the protective effects of sulforaphane against cerebral stroke, it does not confirm protection via the activation of the Nrf2 defence pathway.

Zhao *et al*. employed sulforaphane as an activator of Nrf2 in rodents subjected to intracerebral hemorrhage (ICH) following the injection of autologous blood (Zhao *et al.*, 2007b). Sulforaphane (5 mg/kg *i.p.*) was once again employed as a post-conditioning activator of Nrf2,

delivered to both rats and mice 30 min after the induction of ICH. Sulforaphane treatment reduced neurological deficits scores in rats following 10 days ICH, decreased leukocyte recruitment to the affected regions, and induced the mRNA expression of antioxidant and detoxifying enzymes, including NQO1, after 3h after sulforaphane treatment. Notably, in mice subjected to ICH, sulforaphane treatment was unable to reduce neurological deficits scores in Nrf2 KO mice, providing critical evidence that sulforaphane may mediate protection via the Nrf2 defence pathway following stroke (Zhao *et al.*, 2007b).

Another publication by Zhao *et al*. investigated the effects of sulforaphane treatment on the blood-brain barrier in mice subjected to traumatic brain injury following cortical impact by a pneumatic piston (Zhao *et al.*, 2007a). Sulforaphane enhanced the expression of HO-1 expression in blood brain barrier endothelial cells, attenuated the loss of tight junctional proteins and significantly reduced cerebrovascular permeability after traumatic brain injury (Zhao *et al.*, 2007a). Notably, sulforaphane treatment in Nrf2 KO mice did not attenuate cerebrovascular permeability, suggesting that sulforaphane mediates protection to the blood-brain barrier via Nrf2 (Zhao *et al.*, 2007a).

The studies highlighted in this section have employed sulforaphane as a post stroke therapeutic. With respect to the clinical setting, the time frame during which sulforaphane is administered post-stroke implies that patients would have to be in close proximity to a hospital to receive treatment. As mentioned previously, a high number of stroke patients are ineligible for treatment because of the restricted time frame in which rtPA has to be administered.

1.7 Pre-conditioning vs post-conditioning

From our current understanding of the published literature, stroke research focuses on upregulating protective mechanisms in the ischaemic penumbra, with the aim of limiting cell death and infarct volume and improving neurological outcomes. The failure of many clinical trials in stroke patients has prompted the use of other potential therapeutic drugs for the treatment of stroke.

Within a clinical environment, the low success rate of thrombolytic therapy using rtPA is due to the short time frame of efficacy after the onset of ischaemia. Moreover, the identification of ischaemic stroke may be delayed, as the symptoms of stroke may not coincide with its onset. This further delays the time frame in which efficacious treatment may be delivered (Dirnagl *et al.*, 1999; Dirnagl, 2012). Current stroke researchers are examining a new cohort of potential therapeutic drugs that may confer protection to the ischaemic brain, however, it remains to be elucidated whether pre- or post-conditioning confers greater protection.

Tables 1.12 and 1.13 highlight studies where dietary activators of the Nrf2 pathway were employed as post- or pre-conditioning agents in rodents to examine neuroprotection following cerebral ischaemia. Notably, both post- and pre-conditioning of rodents lead to a reduction in infarct volume. However, post-conditioning of rodents achieves approximately a 25 – 30% reduction in cerebral infarct volume, where as pre-conditioning therapy reduces infarct volume by approximately 60% (see Table 1.12). Zhao *et al.* used epicatechin, a dietary activator of the Nrf2 defence pathway, for neuroprotection against stroke. This study employed both pre- and post-conditioning of rodents and reported a greater reduction in cerebral damage in pre-conditioned animals (Shah *et al.*, 2010).

Table 1.12 Summary of *in vivo* studies post-conditioning methods to confer protection against cerebral ischaemia

Species	*Treatment agent*	*When treatment was administered*	*Finding*	*Reference*
Rats	Sulforaphane (5mg/kg)	15 min post ischaemia	• Post-treatment reduced infarct volume by approximately 30%	(Zhao *et al.*, 2006)
Mouse	Epicatechin	3.5h after MCAo (30mg/kg)	• Oral delivery of Epicatechin (30mg/kg) 3.5h after 90 min MCAo reduced infarct volume 25%	(Shah *et al.*, 2010)
Rats	Curcumin (300 mg/kg)	1h after 60 min MCAo	• Approximately 60% reduction in infarct volume in animals post-treated with curcumin	(Wu *et al.*, 2013)
Rats	Curcumin (100 – 500 mg/kg)	60 min after induction of MCAo	• Approximate 30% reduction in infarct volume observed in animals post treated with curcumin	(Zhao *et al.*, 2010)
Rats	Curcumin (50 – 100 mg/kg)	15 min after induction of MCAo	• Curcumin post-treatment reduced cerebral infarct area by 20%	(Yang *et al.*, 2009)
Mouse	Resveratrol (30 mg/kg)	3h after reperfusion injury (90 min MCAo and 24h reperfusion)	• Reveratrol post-treatment reduced cerebral infarct volume by approximately 55%	(Li *et al.*, 2012b)
Rats	Propofol (20 mg/kg)	60 min after MCAo (60 min MCAo and 4h reperfusion)	• Propofol post-treatment reduced cerebral infarct volume by 25%	(Wang *et al.*, 2011)

Table 1.13 Summary of *in vivo* studies using pre-conditioning strategies to confer protection against cerebral ischaemia

Species	***Treatment agent***	***When treatment was administered***	***Finding***	***Reference***
Mouse	Plumbagin (3 mg/kg)	24 or 6h prior to 60min MCAo and reperfusion	• Plumbagin pre-treatment reduced infarct volume by approximately 50%	(Son *et al.*, 2010)
Mouse	Epicatechin	90 min prior to 90 min MCAo and 24h reperfusion	• Epicatechin Pre-treatment decreased cerebral infarct volume by 50% • Epicatechin pre-treatment also dose dependently improved neurological deficit score (20 – 50% improvement)	(Shah *et al.*, 2010)
Rats	Curcumin (200mg/kg)	Injected over 3 days prior to 2h MCAo and 24h reperfusion	• Curcumin pre-treatment reduced infarct volume be approximately 60%	(Liu *et al.*, 2013b)
Rats	Sevoflurane	30 min prior to induction of cardiac arrest (transient global ischaemia)	• 60% increase in neuronal activity in sevoflurane pre-treated rats compared to control	(Payne *et al.*, 2005)

As the onset of cerebral ischaemia in human subjects cannot be predicted, clinical trials using pre-conditioning strategies are yet to be conducted. Pre-conditioning studies aim to induce protective mechanisms in the brain prior to the onset of an ischaemic insult. This results in the increased tolerance of brain tissue to the ischaemic insult (Dirnagl *et al.*, 2003), conferring greater protection to the brain and reducing the observed infarct volume (Figure 1.10). The concept of ischaemic preconditioning is illustrated in Figure 1.10. Preconditioning strategies have not only been limited to treatment of rodent models with pharmacological compounds, but has also explored mechanical techniques, where by brief period of ischaemia have been shown to reduced infarct volume upon induction of a prolonged period of ischaemia (Barone *et al.*, 1998; Stagliano *et al.*, 1999). These studies thus support that pre-conditioning of the brain may aid in reducing the observed neurological deficits and cerebral damage following stroke.

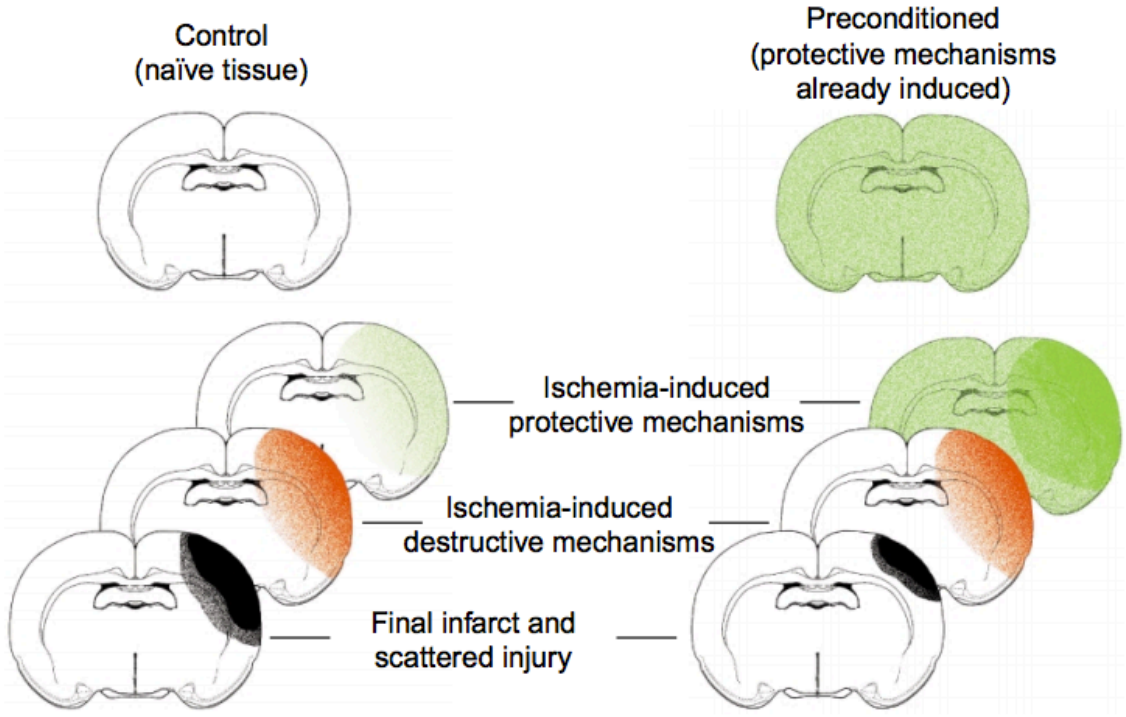

Figure 1.12 Concept of ischaemic preconditioning.
In vivo preconditioning of the brain spatially augments neuroprotective mechanisms. Upon the induction of ischaemic injury, neuroprotective mechanisms may be further enhanced, conferring greater protection to the pre-conditioned brain and resulting in the formation of smaller infarct regions. Figure taken from (Dirnagl *et al.* 1999).

Reviews by Dirnagl and Brathwaite have both identified the failures of clinical trials using drugs that have been validated in rodents to confer protection to the ischaemic brain (Dirnagl *et al.*, 1999; Brathwaite & Macdonald, 2013). Although, many clinical trials employ post-

conditioning methods to treat cerebral stroke patients, discrepancies exist between the clinical and research settings. Within the research environment, the severity of stroke and duration of occlusion can be controlled. Furthermore, researchers have unrestricted access to the rodent, allowing for the administration of potential therapeutic drugs within a defined time frame. However, such factors cannot be controlled in the clinical setting, as the duration of stroke and severity of occlusion is not uniform from patient to patient. Moreover, the requirement of imaging techniques to validate cerebral stroke further delays the time-frame during which beneficial drug treatment can be administered.

To further address the potential of pre-conditioning therapy for stroke, this project has investigated the effects of 1h sulforaphane pre-treatment in rodents subjected experimental ischaemia and reperfusion injury. This project aimed to examine whether upregulation of Nrf2 defences prior to the onset of stroke can protect the brain and cerebrovascular endothelium against the accompanying oxidative stress.

1.8 Aims and objectives

Stroke research has recently focused on targeting the Nrf2 defence pathway for protection of the neurovascular unit and the brain parenchyma, however the majority of studies have investigated upregulation of this pathway post-stroke. As mentioned previously, the number of cerebral stroke patients is expected to increase in the next decades, thus warranting the need for further research into therapeutic strategies to limit the neurological deficits associated with cerebral stroke. As highlighted in this chapter, the ability of naturally occurring dietary isothiocyanates and phytonutrients to activate the Nrf2 defence pathway provides a potential therapy for stroke treatment. The dietary isothiocyanate sulforaphane is one such Nrf2 activator and studies have reported increased protection of the brain after treatment. However, the incidence stroke is not a predictable event, and access to a hospital for treatment by rtPA is not available to the majority of stroke patients within the defined narrow therapeutic window.

The key objectives of this research project were to:

1. Develop a novel immunohistochemical technique to quantitate Nrf2 protein expression and localisation in *ex vivo* brain sections from rats subjected to experimental ischaemia and reperfusion injury.

2. Determine the temporal and spatial distribution of Nrf2 in *ex vivo* brain sections following cerebral ischaemia-reperfusion injury.

3. Investigate the time course of Nrf2 regulated antioxidant enzyme expression in *ex vivo* brain sections of rats following ischaemia and reperfusion injury.

4. Investigate the effects of sulforaphane pre-treatment ('preconditioning') on Nrf2 expression in rats subsequently subjected to cerebral ischaemia-reperfusion injury.

5. Determine whether upregulation of Nrf2 regulated antioxidant enzymes in the brain and cerebrovascular endothelium by sulforaphane pre-treatment is associated with reduced cerebrovascular permeability and neurological deficits in rats subjected to experimental stroke.

6. Examine the effects of sulforaphane on Nrf2 regulated antioxidant enzyme expression in mouse derived brain endothelial cells.

7. Establish an *in vitro* model of ischaemic injury in brain endothelial cells, and investigate whether sulforaphane pre-treatment protects the brain endothelium following ischaemia induced by oxygen-glucose deprivation.

Chapter 2 - Methods

Chapter 2 – Methods

2.1 Middle cerebral artery occlusion and reperfusion injury

Occlusion of the middle cerebral artery results in the reduction of cerebral blood flow, however the degree of damage is dependent upon the duration of ischemia. The middle cerebral artery occlusion (MCAo) model is highly a reproducible model of experimental stroke and hence, is used widely in stroke research. Furthermore, the MCAo technique achieves cerebral damage similar to that observed in stroke patients (see section 1.2). Section 2.1.2 describes how the MCAo procedure was conducted in male Sprague Dawaley rats. Furthermore, the brains were then used to elucidate the temporal and spatial distribution of Nrf2 and its downstream targets in the ischaemic brain.

2.1.1 Animals

Adult male Sprague Dawaley rats were purchased from Harlan Laboratories UK and were housed under control conditions of 12 h light/dark cycles. Before surgery, water and pellet chow (SDS, UK) were available *ad libitum*. Animals (3 – 6 months) that were used for surgery weighed 260 – 300g. All procedures were performed in accordance with the UK Animal (Scientific Procedures) Act 1986 and ethical review by the UK Home Office and King's College London, under Project Licence No. PPL70/6579. The rat model of middle cerebral artery occlusion (MCAo) and reperfusion injury technique was performed under the supervision of Dr Mike Modo, IOP, and Dr Alessio Alfieri, Cardiovascular Division, King's College London, UK.

2.1.2 Middle cerebral artery occlusion

The method used for the transient occlusion of the middle cerebral artery in rats is an adaptation of the method established by Dr Mike Modo, IOP, King's College London, UK (Modo *et al.*, 2000). The MCAo surgery was learnt under the supervision of Dr Alessio Alfieri (Cardiovascular Division, King's College London). However, due to time constraints and limitation of resources, the majority of the brains examined within in this thesis were provided by Dr Alessio Alfieri.

Rats were anaesthetized with isoflurane (4% for the induction of anesthesia, 30% O_2 and 70% nitrous oxide) and transferred to the operating table in a supine position. During the surgical procedure, anaesthesia was maintained using 2.5% isoflurane. A rectal probe was used to monitor the animal's core body temperature which was maintained at $36^{O}C$ using a heating mat.

To begin the MCAo procedure, an incision was made from the lower jaw to the cavicular, and the skin pulled away. Connective tissue was carefully removed and the strap muscle isolated to

expose the right common carotid artery (CCA). Exposure of the CCA was carefully conducted by blunt dissection to isolate the artery from surrounding vessels, nerves and connective tissue. A 4-0 suture (Ethicon) was then applied to the common carotid trunk, nearest to the cavicular (Figure 2.1), and the CCA was exposed and isolated further in the direction of the head until reaching the carotid artery bifurcation, allowing for the identification of the external and internal carotid artery. A small clip was used to clamp the external carotid artery, as close as possible to the point of the bifurcation, and an identical clip used to clamp the internal carotid artery. An arteriotomy was made on the common carotid artery, as indicated in Figure 2.1, and a 6-0 silicon coated filament (Docol Corp, Massachusetts, USA) inserted into the common carotid artery. The clip was removed from the internal carotid artery and the filament advanced approximately 18-20 mm to occlude the ostium of the middle cerebral artery (MCA) for 70 min. The clip at the bifurcation of the common carotid artery branching to the external carotid artery (as shown in Figure 2.1A) prevents the occluding filament from entering the external carotid artery and ensures movement of the filament into the internal carotid artery. Following insertion of the occluding filament, another suture was applied on the CCA at the arteriotomy position to secure the occluding filament in place, and the clip on the external carotid artery was removed and temporary stiches applied to the wound. After insertion of the occluding filament, the animal was allowed to recover from the anesthesia at $28^{O}C$ for the duration of the occlusion (70 min).

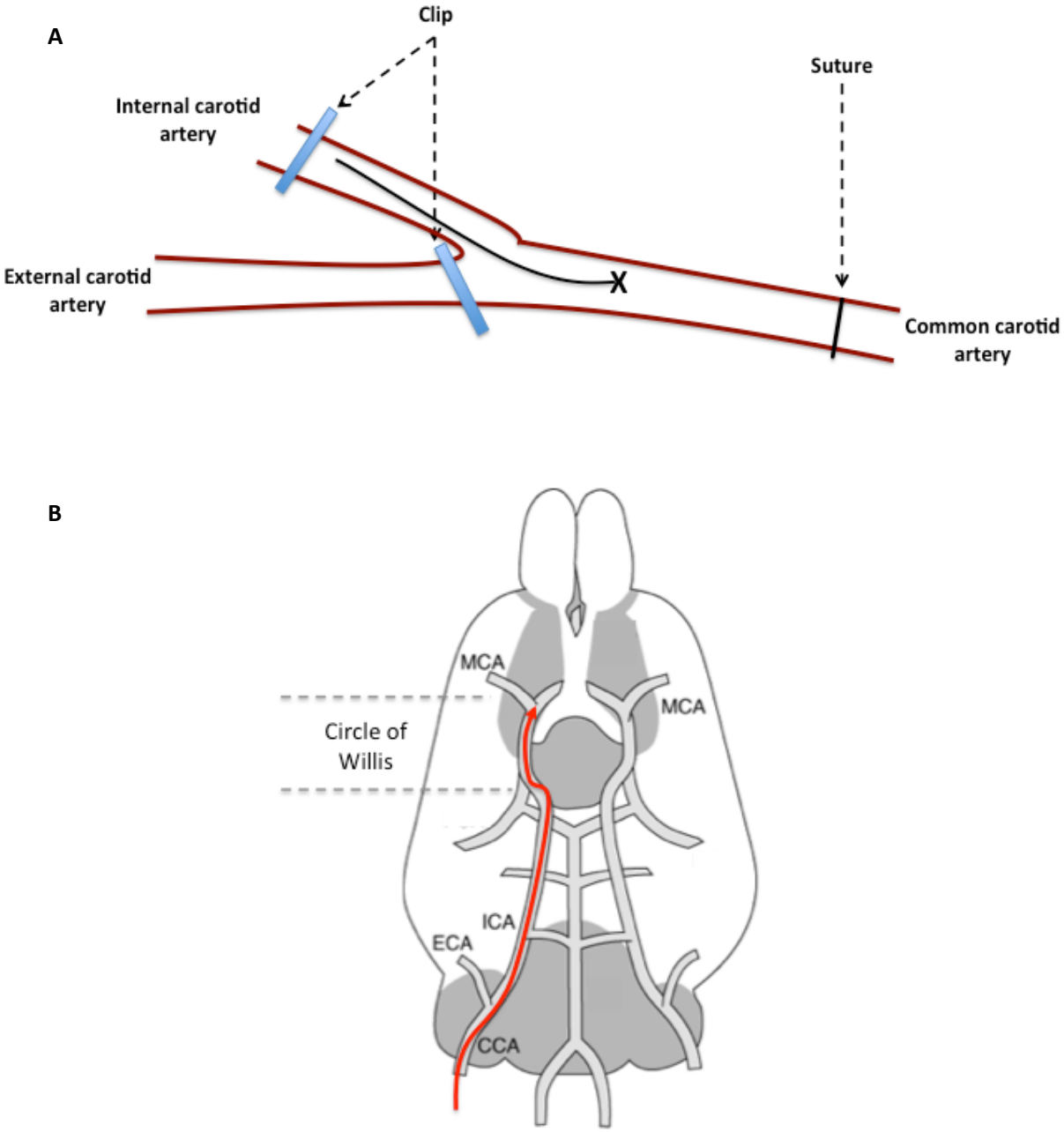

Figure 2.1 Insertion of filamentous wire into the common carotid artery to induce MCAo.
A, The filament is inserted into the common carotid artery at the incision made on the trunk of the carotid artery, marked by X. The clip is then removed from the internal carotid artery and the filament is advanced forward to occlude the middle cerebral artery, B. Abbreviations: CCA, Common carotid artery; ECA, External carotid artery; ICA, Internal carotid artery; MCA, Middle cerebral artery

2.1.3 Reperfusion following MCAo

To elicit reperfusion in the brain following 70 min ischaemia mediated by MCAo, 10 min before completion of the occlusion period, the animal was re-anaesthetized with isoflurane (4% for induction of anaesthesia, 30% O_2 and 70% nitrous oxide), transferred to the operating table in a supine position and anaesthesia maintained with 2.5 % isoflurane. The temporary stiches were removed and the wound opened to expose the common carotid artery trunk, allowing for the removal of the occluding filament and a ligature applied to prevent bleeding from arteriotomy in the common carotid. The wound was closed using a 4-0 suture and a topical analgesic (Emla Cream) applied to the surgical wound. Saline and glucose (1 mL) was subcutaneously administered to the animal to replenish the loss of fluid from the animal during surgery.

2.1.4 Perfusion and removal of rat brains

Brains were removed from the animals after defined time points of reperfusion (4h, 24h and 72h) and further processed for immunohistological or immunoblot analyses. Since gaseous anesthetics cause constriction of blood vessels resulting in poor perfusion, rats received an overdose of a barbiturate, pentobarbitone (120 mg/kg, i.p.). Once the animal had lost consciousness, the skin covering the thorax was removed and the sternum was lifted using flat forceps. The rib cage was cut down both sides to expose the thoracic cavity after which, the descending thoracic aorta was exposed and clamped using a curved heamostat, preventing the flow of perfusion reagents into the abdominal cavity. To facilitate perfusion, an incision was made at the apex of the heart, through which a cannula was inserted and clamped in the aorta, and another incision was made on the right atrium allowing for the release of the perfusate. The animal was initially perfused transcardially with cold saline to flush out the blood (25 ml/min) which was followed by perfusion with 4% paraformaldehyde (25 ml/min). Once the upper limbs of the animal had stiffened as a consequence of perfusion with 4% paraformaldehyde, the perfusion was stopped and the animal decapitated to allow for removal of the brain. Excised brains were placed in 4% paraformaldehyde for fixation overnight at $4^{O}C$, after which, brains were transferred to phosphate buffered saline (PBS) containing 30% sucrose and stored at $4^{O}C$ for subsequent sectioning to obtain 10µm thick coronal sections (see section 2.2.2).

2.15 Sulforaphane treatment of animals

To examine the effects of Nrf2 activation *in vivo*, rats were pre-treated with the dietary Nrf2 inducer sulforaphane (5 mg/kg i.p., dissolved in saline containing 1% corn oil; Sigma) (Dinkova-Kostova & Kostov, 2012) at 1 h before the 70 min period of MCAo, followed by 24 h reperfusion. Brains were perfused fixed and collected as described in section 2.1.4. Rats were also treated with sulforaphane (5 mg/kg in saline containing 1% corn oil) or vehicle (saline

containing 1% corn oil) for 1, 2, and 4 h and brains collected to examine the time course of Nrf2 activation by sulforaphane in naïve rats. Brains were removed as described in section 2.1.4 for analysis by quantitative immunohistochemistry (see section 2.2).

2.1.6 Collection and preparation of brains for western blotting

Brains from naïve rats treated for 1, 2 or 4 hours with vehicle (saline containing 1% corn oil) or sulforaphane (5 mg/kg, i.p.) were collected for analysis by immunoblotting. Rats received an overdose of pentobarbitone (120 mg/kg, ip) and brains were removed as previously described in Section 2.1.4, but without the saline and paraformaldehyde perfusion. After collection, brains were washed in cold saline, snap frozen in liquid nitrogen and stored at -80^{O}C until homogenisation. Collected brains were mechanically homogenized in 2mL SDS lysis buffer and centrifuged at 13,000 rpm for 15 min at 4^{O}C to separate supernatant containing the protein from tissue debris and fat. The supernatant was collected and stored at -20^{O}C. Relative protein concentration in tissue lysates were determined using the BCA assay (see section 2.3.12.1).

2.2 Analysis of protein expression in rat brains by quantitative immunohistochemistry

Standard immunohistochemistry protocols largely provide qualitative, or at best, semi-quantitative data regarding changes in expression of the protein of interest. To facilitate the direct quantification and cellular localisation of Nrf2 or antioxidant protein expression in brain tissue sections, we developed a technique utilising the properties of 3,3'-diaminobenzidine (DAB), which had previously been used to assess vessel permeability (Gauden *et al.*, 2007). The immunohistochemical technique described below is based on the biochemical properties of the DAB reaction with hydrogen peroxide to directly quantitate the protein content and spatial distribution of Nrf2 in rat brain sections.

2.2.1 Cryosectioning of rat brains

To increase the adherence and stability of brain sections on glass slides, superfrost plus microscope slides (Thermo Scientific) were quickly dipped in 10% formal saline and allowed to dry at room temperature. For sectioning, excised brains were removed from the 30% sucrose saline solution and the excess buffer gently removed by blotting using tissue paper. The cerebellum was removed from the brain using a sharp blade, after which, the brain was wrapped loosely in foil and frozen in dry ice prior to mounting on a cryostat chuck with cryo-embedding medium (Bright, UK). Approximately 1 mm of the rostral part of brain was removed prior to obtaining 10µm coronal brain sections at -24^{O}C using a freezing cryostat (OFT 5000, Bright, UK), with two coronal brain sections mounted per superfrost plus glass slide. Brain sections

were allowed to dry at room temperature for 24 hours and stored at -20^{O}C until required for staining and analysis by quantitative immunohistochemistry (See section 2.2.2) or immunofluorescence.

2.2.2 Staining and preparation of brain sections for quantitative immunohistochemistry

DAB-H_2O_2 may be utilised as substrates by endogenous peroxidases, which may result in background staining. Thus, endogenous peroxidase activity was quenched by incubating brain sections with the commercially available endogenous peroxidase-blocking reagent, Bloxall (Vector Laboratories Ltd, UK) for 10 min at room temperature (Stage 1, Figure 2.2).

For this immunohistochemical protocol, the avidin-biotin complex (ABC) method was employed to amplify and enhance the sensitivity of the DAB-H_2O_2 reaction. Biotin is required endogenously for many biological processes, however, in this adapted immunohistochemistry protocol, biotin is conjugated to either a secondary antibody, or a reporter enzyme (horseradish peroxidase; HRP) and forms a high affinity bond with avidin, a tetrameric protein that binds 4 biotin molecules, increasing the sensitivity and signal intensity upon addition of the substrates DAB and H_2O_2 (Figure 2.3) (Adams, 1992). Thus, endogenous avidin and biotin was quenched sequentially using respective avidin and biotin blocking solutions (Vector Laboratories Ltd, UK) for 15 min at room temperature (Stage 2, Figure 2.2).

For the identification of cerebral cell types and Nrf2, brain sections were further incubated with a cocktail of primary antibodies (Table 2.1) in 0.1% triton and 10% normal donkey serum in PBS for 16h at 4^{O}C (Stage 3, Figure 2.2). For the identification of astrocytic and endothelial structures, brain sections were incubated with fluorophores conjugated to antibodies (Table 2.2) in PBS at room temperature for 1 hour. To examine Nrf2 content by quantitative immunohistochemistry, brain sections were incubated with a goat anti-rabbit biotinylated secondary antibody in PBS for 30 min (Vector Laboratories, UK) and an additional 30 min with the avidin-biotin complex in PBS (Vector Laboratories, UK). The biotinylated secondary antibody and ABC reagents were used according to the manufacturer's instructions. Endogenous peroxides react with DAB to produce a brown coloured polymer, reducing the sensitivity and resulting in non-specific staining, thus endogenous peroxides were eliminated by incubating sections with 1mM ascorbic acid (Sigma Aldrich) in ddH_2O for 30 min.

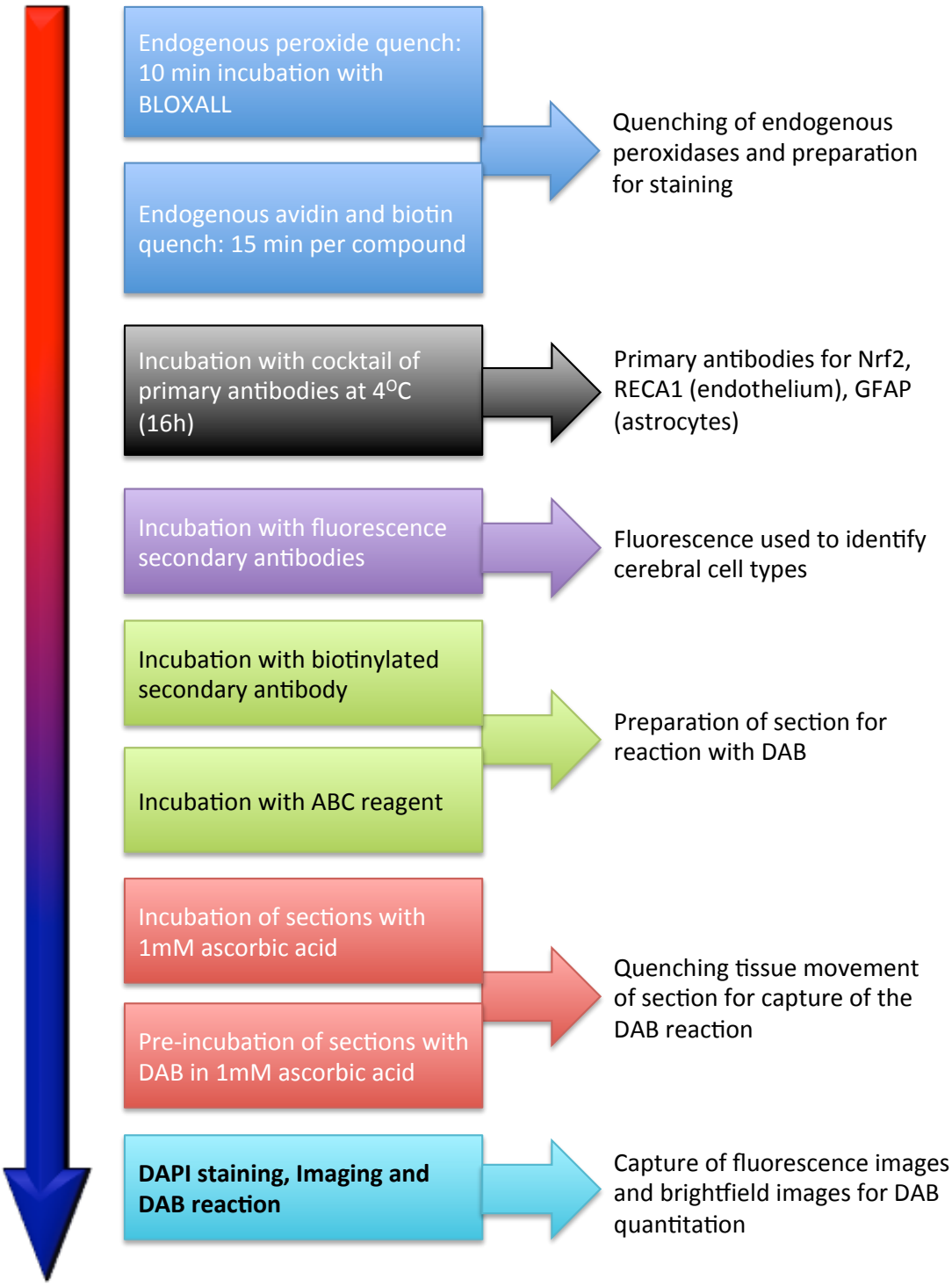

Figure 2.2 Flow diagram representing stage-wise preparation of *ex vivo* brain sections for the capture of brightfield images of the DAB reaction, required for quantitation of Nrf2 protein.

As DAB alone resulted in movement or detachment of the tissue, sections were incubated with DAB (Vector Laboratories Ltd, UK) in the presence of 1mM ascorbic acid, but in the absence of H_2O_2 to eliminate movement. For the identification of nuclear structures by fluorescence, brain sections were also incubated with 4',6-diamidino-2-phenylindole (DAPI, 2µg/ml; Roche) in ddH_2O for 5 min. Sections were hydrated in ddH_2O with 1mM ascorbic acid until required for image capture.

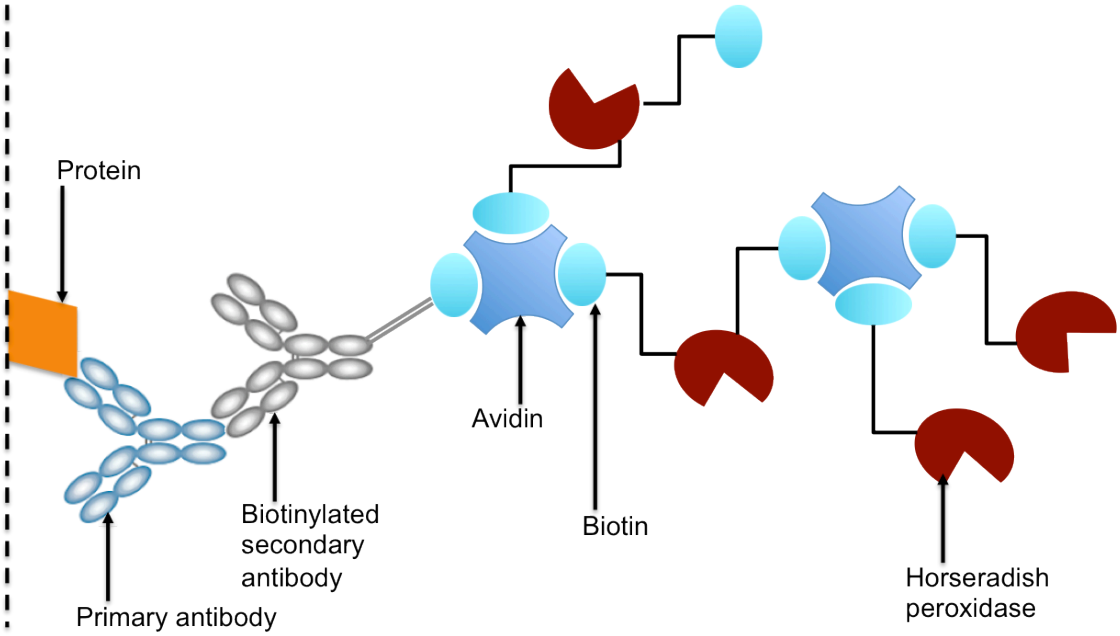

Figure 2.3 Schematic of immunohistochemical signal amplification by the avidin-biotin peroxidase complex.
Horseradish peroxidase conjugated to a complimentary secondary antibody results in low immunohistochemical signal intensity. The avidin-biotin peroxidase complex amplifies and increases sensitivity of a immunohistochemical stain in relation to the protein of interest by increasing the number of peroxidase active sites available to catalyse the immunohistochemical reaction.

Table 2.1 Primary antibody dilutions for immunofluorescence and DAB reaction studies

Primary Antibody	*Species*	*Diluent*	*Dilution*	*Manufacturer*	*Catalogue Number*
GFAP	Rabbit	0.1% triton PBS 10% serum	1:1000	DAKO	Z0333
GFAP	Goat	0.1% triton PBS 10% serum	1:100	Abcam	AB53554
RECA1	Mouse	0.1% triton PBS 10% serum	1:400	Abcam	AB9774
Nrf2	Rabbit	0.1% triton PBS 10% serum	1:100	Abcam	AB53019
Nrf2	Rabbit	0.1% triton PBS 10% serum	1:100	Abcam	AB31164
HO-1	Rabbit	0.1% triton PBS 10% serum	1:100	Abcam	AB31164
NQO1	Rabbit	0.1% triton PBS 10% serum	1:100	Abcam	AB31164
Prx1	Rabbit	0.1% triton PBS 10% serum	1:100	Abcam	AB

Abbreviations: GFAP, Glial fibrillary acidic protein; Nrf2, NF-E2 related factor 2; RECA1, Rat endothelial cell antigen 1

Table 2.2 Fluorescence secondary antibody dilutions for ex vivo brain sections studied by immunofluorescence and quantitative immunohistochemistry

Secondary Antibody	**Host Species**	**Target Species**	**Dilution**	**Manufacturer**	**Catalogue Number**
Cy5	Donkey	Goat	1:250	Abcam	AB6566
Alexa Fluor 488	Goat	Rabbit	1:500	Invitrogen	A-11008
Alexa Fluor 555	Donkey	Mouse	1:500	Invitrogen	A-31570

It must be noted that the identification of proteins in this immunohistochemical study is dependent upon antibody specificity. The specificity of the primary antibodies should be assessed in samples that are known not to contain the protein of interest. However, tissue from such genetically modified animals was not accessible to assess antibody specificity. Thus the use of antibodies was reliant upon (1) the provided data sheet of the antibodies from each respective manufacturer, (2) species cross reactivity. Negative control experiments demonstrated that the secondary fluorescent antibodies did not cross react with the tissue in the absence of complimentary primary antibodies (Appendix Figure 4).

2.2.3 Quantitative immunohistochemistry

The novel immunohistochemical technique developed and employed in this study is a further development of the assay developed within our laboratory, where horseradish peroxidase (HRP) was used as a fluid phase marker to estimate blood-brain barrier permeability following ischaemia-reperfusion injury in mice (Gauden *et al.*, 2007). The principle that HRP can be measured in tissue sections from the initial rate of 3,3'-diaminobenzidine (DAB) polymer formation has been extended to quantify HRP- conjugated antibodies in rat brain sections. The visualisation of the brown coloured DAB polymer occurs after the reaction of DAB with H_2O_2, in the presence of HRP (Equation 1).

$$\text{DAB} + \text{H}_2\text{O}_2 \longrightarrow \text{DAB percipitate product} + \text{H}_2\text{O}$$

Equation 1. Reaction of DAB with hydrogen peroxide in the presence of biotin peroxidase

2.2.4 Validation of quantitative immunohistochemistry technique using protein of known concentrations

Proof-of-principle experiments were conducted to establish that the relationship between HRP conjugated secondary to primary antibodies and a target protein is essentially linear. Bovine serum albumin (BSA, 2 mg/ml, Sigma, UK) was diluted in ddH_2O to obtain 0.15 µM, 0.075 µM and 0.0325 µM BSA solutions. Porcine gelatin (G2500, 0.25g, Sigma, UK) was added to 5 ml BSA aliquots and dissolved by gently warming. BSA-Gelatin was allowed to set at 4^{O}C overnight and then fixed in 4% paraformaldehyde for 24 h at 4^{O}C. BSA-gelatin blocks were transferred to PBS containing 30% sucrose until required for sectioning. Sections of 10µm thickness, were obtained from the gelatin blocks using a cryostat (OFT 5040, Bright, UK) and mounted on to superfrost plus glass microscope slides (Thermo Scientific, UK). The gelatin sections were treated and reacted in in the same manner as brain sections (see section 2.2.3 and 2.2.4).

BSA - gelatin sections were incubated with rabbit anti-BSA (Sigma) at 4^{O}C for 16 h, and then with a goat anti-rabbit biotinylated secondary antibody for 30 min at room temperature, followed by a further 30 min with the ABC reagent to amplify the 3,3'-diaminobenzidine (DAB) reaction product signal via the formation of the avidin and biotin complex. One section was taken from 4 replicate blocks for each albumin concentration.

2.2.5 Image capture, segmentation and calculation of initial rate of DAB polymer formation

Hydrated brain sections were placed in a specially designed microscope stage (Figure 2.4) attached to a Nikon Diaphot fluorescence microscope. Images of nuclei and GFAP staining were captured via a cooled CCD camera (ORCA-03G, Hamamatsu, Japan) controlled by a PC software package (ImageHopper, Samsara Research, Surrey). Water was removed and replaced with the DAB-H_2O_2 reaction mixture and images in brightfield were captured at 1 s^{-1} over 100 s. The methodology developed for calculating quantitative protein expression in tissue sections is discussed in Chapter 3.

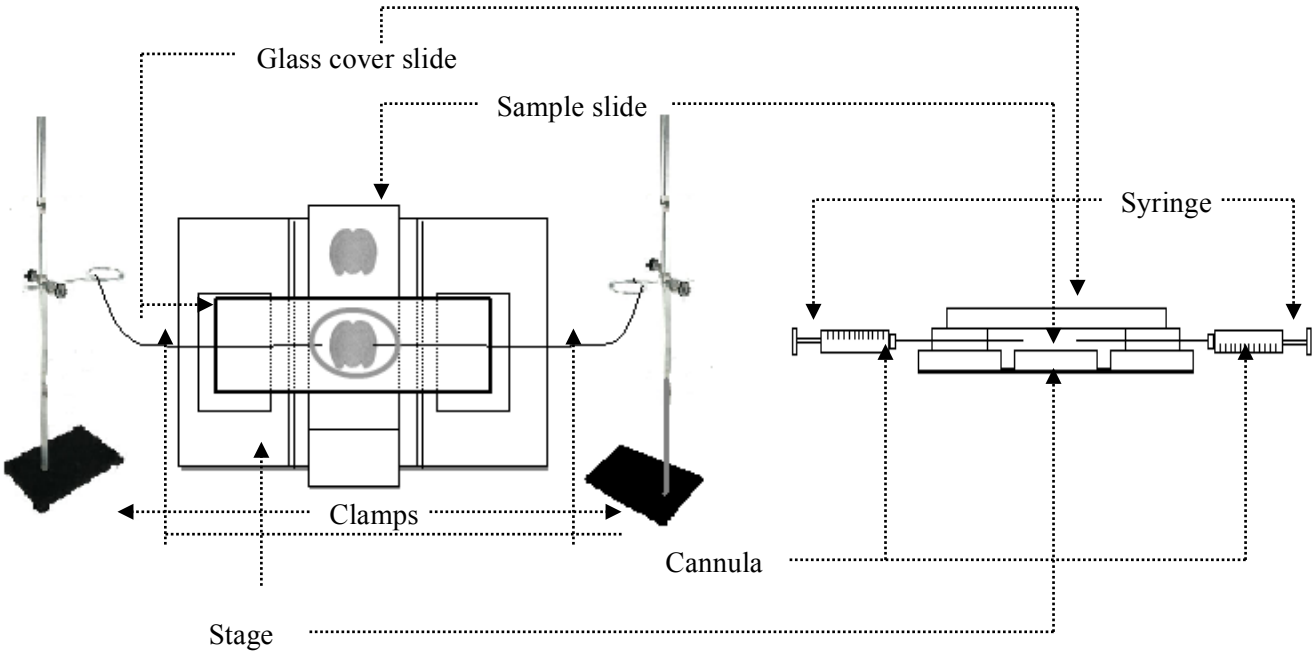

Figure 2.4 Schematic representation of the microscope stage designed to deliver the DAB reaction mix.
For the delivery of the DAB reaction mix to the section on the microscope stage, a special glass stage was designed to keep the section hydrated with ddH_2O during fluorescence imaging. The slide is positioned between the two cannulas and covered with another glass slide, holding the fluid over the section. Following capture of all fluorescent images, the ddH_2O was removed using the right hand side cannula, and the DAB reaction mix delivered through the left.

2.2.6 Quantification of fluorescence staining in brain sections

The protein expression of NQO1, HO-1 and Prx1 was assessed by immunofluorescence. Following the incubation of 10µm brain sections with primary antibodies (as described in Section 2.2.2), sections were incubated with donkey anti-rabbit alexa 488 to identify NQO1, HO-1 or Prx-1, and donkey anti-mouse alexa 555 to identify RECA-1 staining, for 1h at room temperature. Sections were then washed with water and left to dry at room temperature, before the application of a glass coverslip with vectashield mounting medium containing DAPI (Vector Laboratories Ltd) for nuclei identification. Stained brain sections were imaged with a cooled CCD camera (ORCA-03G, Hamamatsu, Japan) controlled by a PC software package (ImageHopper, Samsara Research, Surrey). Three random fields of view were captured from each brain section, and images captured in 32-bit format. Images were then analysed off-line using image J to quantify fluorescence intensity. Fluorescence intensity was quantified in the whole field of view by measuring the integrated density. Background fluorescence was measured in 3 different regions where tissue was absent in the same field of view, and corrected fluorescence intensity calculated using the following formula: integrated density – (area of the field of view X mean integrated density of background readings).

2.3 Assessment of protein induction in cerebrovascular endothelial cells

The analysis of brain sections by immunohistochemical and immunofluorescence techniques gave a detailed insight into the expression of Nrf2 and its linked downstream protein targets within different anatomical regions and cell types in the naïve and ischaemic rat brain, including the cerebrovascular endothelium. To complement the MCAo studies undertaken, the murine derived brain endothelial cell line bEnd.3 was used to better understand the mechanisms by which the brain microvascular endothelium is able to protect of the neurovascular unit following ischaemic damage.

2.3.1 Defrosting and cell culture of bEnd3

The mouse derived brain endothelial cell line, bEnd.3 was purchased from ATCC. Cells were defrosted rapidly at $37^{O}C$ and transferred to a T25 culture flask (25 mm^2) in Dulbecco's modified Eagle Medium (DMEM, Sigma-Aldrich) with phenol red, containing 4500 mg/L (25mM) glucose and supplemented with 10% fetal calf serum (FCS), 4mM L-glutamine, penicillin (100 U/ml) and streptomycin (100 µg/ml). Cells were maintained in a humidified 5% CO_2 incubator at $37^{O}C$. The medium was replaced 8 h after seeding and subsequently replaced every 48 h.

2.3.2 Subculture of bEnd3 cells in DMEM containing 25mM glucose

Confluent monolayers of bEnd.3 cells in T25 or T75 flasks were washed with warm sterile PBS to remove serum components that may affect trypsinisation. Cells were incubated with 1 – 1.5 ml trypsin/EDTA solution (0.1% trypsin and 0.02% EDTA, Sigma) at 37^{O}C for 2 min to detach cells. Trypsin/EDTA was inactivated in DMEM containing 10% FCS and split in a 1:3 ratio from a T25 to T75, 1:3 for cells in T75 flasks, or seeded into plates/coverslips for treatment. DMEM was changed every 48 h in the culture flasks or wells.

2.3.3 Freezing of bEnd3 cells

Confluent monolayers of bEnd.3 cells in T75 flasks were detached with trypsin/EDTA (PAA, UK) as described in Section 2.3.2. Cells were thoroughly re-suspended in DMEM and centrifuged at 1000 rpm for 5 min. The supernatant was aspirated and the resulting cell pellet and thoroughly suspended in 5% dimethlysulfoxide (DMSO) in DMEM (25mM Glucose, 10% FCS, 4mM L-Glutamine, penicillin (100 U/mL) and Streptomycin (100 µg/mL)). Cells were transferred to cryo-vials (1 ml/vial, 3 vials/T75 flask) and slowly frozen at -80^{O}C and then transferred to liquid nitrogen for long-term storage.

2.3.4 Culture and treatment of bEnd3 cells in DMEM containing 5.5mM glucose

Confluent bEnd.3 monolayers in T75 flasks, were sub-cultured as described in section 2.3.4, however, trypsin/EDTA was inactivated using phenol-red free DMEM containing 1000 mg/L (5.5 mM) glucose, supplemented with 10% fetal calf serum (FCS), 4mM L-glutamine, penicillin (100 U/ml) and streptomycin (100 µg/ml). Phenol-red free DMEM was changed every 48 hours and further sub-culture and experiments conducted using phenol-red free DMEM.

2.3.5 Treatment of bEnd3 cells with sulforaphane

Treatments were prepared in phenol-red free DMEM supplemented with 10% FCS. Confluent monolayers were treated with sulforaphane (0.1 – 10 µM, S4441, Sigma, UK), or 0.01% DMSO (vehicle) for 4, 8, 12 and 24 h at 37^{O}C.

2.3.6 Assessment of cell viability

Cytotoxic effects of sulforaphane was assessed by the tetrazolium salt 3-(4,5-dimethythiazol-2-yl)-2,5-diphenyltetrazolium (MTT) assay. The yellow tetrazolium salt is cleaved to form a cell impermeable purple formazan crystals following the interaction of MTT with mitochondrial dehydrogenase enzymes (Mosmann, 1983). The cleavage of MTT to form the puruple formazan crystals only occurs in metabolically active cells, thus the MTT assay provides a colourimetric based upon the development the cell impermeable dark purple formazan crystals (Mosmann,

1983). To determine whether sulforaphane had cytotoxic effects, bEnd.3 cells were seeded into a 96 well plate and treated in quadruplicate with sulforaphane (0.5 – 10 μM) in 200 μl DMEM supplemented with 10% FCS for 24 hours and incubated at 37 ^{O}C and 5% CO_2 (Figure 2.5). Hydrogen peroxide (0.5M, H_2O_2) served as a positive control and was added to the cells 30 min prior to incubation of cells with 10% MTT (0.5 mg/mL) solution (Figure 2.5).

After 24h treatment, bEnd.3 cells were incubated with 50 μL of 10% MTT (0.5 mg/mL) in DMEM supplemented with 10% FCS for two hours. Cells regularly checked using a light microscope for the formation of the purple coloured formazan crystals, after which 50 μL DMSO was added directly to each well and the plate gently agitated using a shaker for 10 min to ensure complete lysis of the cells. Absorbance (560 nm) was then measured using a microtitre plate spectrophotometer (Tecan, Switzerland) and data expressed as percentage change in absorbance units compared to untreated cells (control).

	1	2	3	4	5	6	7	8	9	10	11	12
A												
B												
C			Control	Vehicle (DMSO 0.01%)	0.5 μM SFN	1.0 μM SFN	2.5 μM SFN	5.0 μM SFN	10 μM SFN	0.5 M H2O2		
D												
E												
F												
G												
H												

Figure 2.5 Representative layout of bEnd.3 cells treatment in clear 96-well plates.
bEnd.3 cells were seeded in quadruplicate into clear 96 well plates, and upon reaching confluence, cells were treated with sulforaphane (SFN, 0.5 μM – 10 μM) or vehicle (0.01% DMSO) for 24 hours. DMEM was replaced in control wells. Cells were also treated with 0.5M H_2O_2 30 min before incubation with MTT to serve as a positive control for cell death.

2.3.7 Whole cell protein extraction

Cells cultured to confluence and treated with SFN (0.1 – 5μM) for 4 – 24h in 6 well plates were washed twice with non-sterile PBS at 4°C and proteins extracted by incubating cell monolayers with sodium-dodecyl sulphate (SDS) lysis buffer (50mM Tris base pH 6.8, 10% glycerol and

2% SDS) supplemented with 0.02% protease inhibitor cocktail (4-(2-aminoethyl) benzenesulfonyl fluoride, pepstain A, bestatin, E-64, leupeptin and aprotinin) on ice for 10 min. Protein concentration of collected protein extracted was determined by the BCA assay (see section 2.X) and stored at -20^{O}C until further analysis by immunoblotting.

2.3.8 Nuclear protein extraction

Cells were cultured in T75cm flasks until confluent and treated with sulforaphane (2.5 µM) for 1 – 4 h. Nuclear protein lysates were collected using a commercial nuclear extraction kit (Active Motif, USA) as per manufacturers instructions. Cells were washed once with cold PBS containing phophaste inhibitors (Active Motif, USA) and scrapped into a final volume of 3 ml buffer before being spun down at 500 rpm for 5 min. The resulting cell pellet was re-suspended and incubated in 500µl hypotonic buffer from the kit (Active Motif, USA) on ice for 15 min to rupture cell membranes. Next, 25 µl of detergent from the kit (Active Motif, USA) was added to the suspension and the solution vortexed at high speed for 10s, after which tubes were centrifuged at 13,000 rpm for 30s. Supernatants containing cytosolic extracts were collected into pre-chilled tubes and stored at -80^{O}C. Remaining cell pellets were re-suspended in 50µl complete lysis buffer from the kit (Active Motif, USA) and placed on a rocking platform for 30 min at 150 rpm. Tubes containing nuclear suspension were vortexted at high speed for 30 s and centrifuged at 13000 rpm for 10 min. Nuclear extracts in supernatants were collected into pre-chilled tubes and stored at-80^{O}C. Nrf2 protein content in the nuclear and cytoplasmic lysates were analysed by western blotting.

2.3.9 TransAM Assay for nuclear Nrf2 activity

Nuclear Nrf2 activity in bEnd.3 cells was also assessed and quantified using a commercially available ELISA kit (TransAM, Acive Motif, USA). Briefly, oligonucleotides containing the ARE sequence (5'-GTCACAGTGACTCAGCAGAATCTG-3'), to which active Nrf2 specifically binds, were supplied immobilised on an ELISA 96 well plate. Incubation of nuclear lysates in these ELISA plates and addition of a specific Nrf2 primary antibody allows for the binding activity of Nrf2 to the ARE sequence to be determined.

Nuclear lysates from bEnd.3 cells treated with either 2.5µM sulforaphane, or vehicle (0.01% DMSO) for, 1, 2 and 4 hours (see Section 2.3.7 for method of nuclear lysate collection) were processed on the same 96-well ELISA plate. Nuclear extracts (9 µg/well), diluted in the provided complete lysis buffer (10µL), were added in duplicate to the ELISA plate, alongwith 40µL of complete binding buffer. Two separate wells of the 96-well plate served as the blank (10 µL complete lysis buffer only) and a further two wells served as a positive control using the Nrf2 positive extracts provided in the TransAM kit.

After the incubation of samples for 1h at room temperature with mild agitation (150 rpm on an orbital shaker), the wells were washed with washing buffer (made as per manufacturers instructions) and incubated for a further 1h at room temperature with a specific Nrf2 primary antibody (1:100 dilution in provided antibody binding buffer, 100 µL/well), without agitation. Wells were then washed and incubated for a further 1h with the HRP-conjugated secondary antibody (1:1000 dilution in antibody binding buffer, 100 µL/well). Post antibody incubations, wells were washed with washing buffer and incubated with the provided developing solution (100 µL/well) for approximately 30 min until the solution colour turned dark blue, after which the reaction was then terminated with the addition of the provided stop solution (100 µL/well). Absorbance values were measured using a spectrophotometer (Surnise, Tecan) at 450 nm.

2.3.10 Knockdown of Nrf2 by short interfering RNA (siRNA)

To assess whether sulforaphane mediates the upregulation of phase II detoxifying and antioxidant enzymes in bEnd.3 cells via Nrf2 activation, siRNA transfection was employed to knockdown Nrf2. Short interfering RNA (siRNA) are short double stranded RNA molecules, which are approximately 20-25 base pairs in length. Once delivered to the mammalian cell, the long double stranded RNA is cleaved by the RNAse II enzyme Dicer, producing siRNA. These siRNA are then incorporated into the RNA-induced silencing complex (RISC), where they are unwound, resulting in the loss of the sense strand. The RISC is guided to the target mRNA transcript via the antisense strand, for endonucleolytic cleavage (Figure 2.6) (Dykxhoorn *et al.*, 2003).

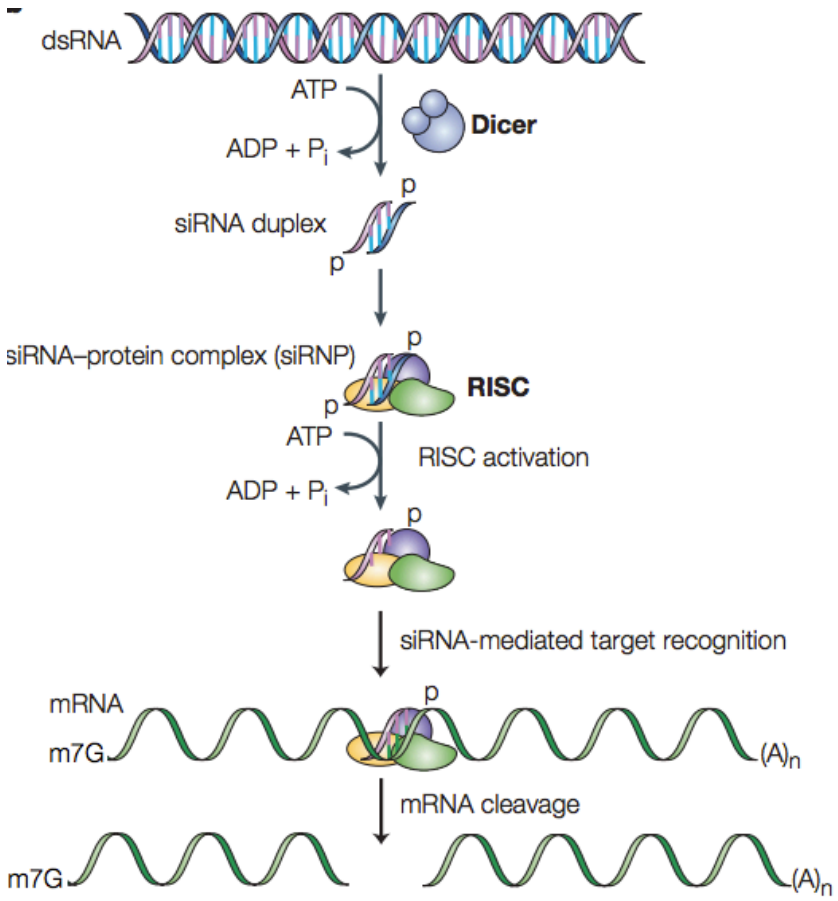

Figure 2.6 Gene silencing by short interfering RNA.
Exogenous short interfering RNA and endogenous micro RNA (miRNA) undergo the same process of maturation to obtain a single strand RNA that is complimentary to the mRNA of the target strand. The siRNA duplex is incorporated into the RNA induced silencing complex (RISC). Activation of the RISC results in the loss of the anti-sense strand from the duplex, allowing for siRNA-mediated target recognition and degradation of the target mRNA strand. Figure taken from (Dykxhoorn *et al.*, 2003).

siRNA transfection studies were performed in bEnd.3 cells seeded in 24-well plates at a density of 30,000 cells/well for 24h, after reaching approximately 50 – 60% confluency. 40 pmol of Nrf2 siRNA (Santa cruz Biotechnology, sc-37049) mixed with transfection reagent (Dharmafect 4, Thermo Scientific) in 100 µL OptiMEM medium (Gibco) was left to incubate at room temperature for 3 min. Notably, the Nrf2 siRNA mixture used was a pool of 3 neucleotide sequences. During this incubation period, cells were washed once with warm PBS and replaced with antibiotic free DMEM supplemented with 10% FCS and 4 mM L-glutamine. The siRNA transfection mixture was then added to each well (100 µL/well) in a drop-wise manner and the cells incubated for 24h at 37 ^{O}C prior to sulforaphane treatment.

2.3.11 Immunofluorescence localisation of Nrf2 in bEnd3 cells

Nrf2 is a major transcriptional regulator of phase II detoxifying and antioxidant stress genes that contain the antioxidant/electrophile response element (ARE/EpRE) in their promoter regions. Immunofluorescence was employed to assess nuclear localisation of Nrf2 in bEnd.3 cells after sulforaphane treatment. Cells were seeded on to glass coverslips in 24 well plates and when confluent, treated with sulforaphane (2.5µM, 1 – 4 h). Cells were then washed with cold PBS at 4°C and fixed in 4% paraformaldehyde for 10 min at room temperature. Fixed cells were incubated with 0.1% Triton in PBS at room temperature to permeabilise the cell membrane prior to incubation with a rabbit anti-Nrf2 primary antibody (1:100 dilution; 100µl/coverslip; SC-722, SantaCruz, USA) for 16h in PBS containing 10% donkey serum at 4^{O}C, followed by an anti-rabbit secondary antibody conjugated with Alexa-flour 488 (1:1000 dilution; Invitrogen) at room temperature for 1 h.. Coverslips were then removed from 24-well plates and allowed to dry briefly at room temperature. To identify nuclei, coverslips were mounted on to glass slides with mounting medium containing DAPI (Vectashield, Vector Laboratories, UK). Nrf2 specific fluorescence (excitation 499nm/ emission 519 nm) was visualized using a Nikon Diaphot microscope adapted for fluorescence (Nikon, Japan) and captured using a cooled CCD camera (ORCA-03G, Hamamatsu, Japan) controlled using PC software (ImageHopper, Samsara Research, Surrey, UK).

2.3.12 Quantitative immunohistochemistry for Nrf2 in bEnd.3 cells

The quantitative DAB-H_2O_2 immunohistochemical technique was also employed in bEnd.3 cells to, firstly validate the technique in cultured cells, and secondly to quantitate nuclear translocation of Nrf2 in bEnd.3 cells.

Cells were seeded on glass slides (Superfrost plus, Thermo Scientific, UK) and confluent monolayers, treated with sulforaphane (2.5 µM) or vehicle (0.01% DMSO) for 1, 2 and 4 hours. Cells were then washed with cold PBS at 4°C and fixed with 4% paraformaldehyde at room temperature for 10 minutes. Fixed cells were permeabilised with 0.1% triton in PBS for 10 min at room temperature and incubated with Bloxall, and avidin/biotin blocking reagents to quench endogenous peroxidase, avidin and biotin activity (see section 2.2.3). Cells were then incubated with a rabbit anti-Nrf2 primary antibody (ab53019, Abcam, UK) for 16h at 4^{O}C and a goat anti-rabbit biotinylated secondary antibody for 30 min at room temperature. Cells were then incubated with the avidin-biotin peroxidase complex (as described in section 2.2.3) for a further 30 min and counter stained with DAPI in PBS to identify nuclei (2 µg/ml; Roche). Cells were hydrated in PBS and images captured and processed as described in section 2.2.4.

2.3.13 Western blot analysis

2.3.13.1 Determination of protein concentration

The bicinchoninic acid (BCA) assay was employed to determine the protein concentration of total cell lysates. The BCA assay is a two-step colorimetric assay that relies upon, firstly the reduction of Cu^{2+} to Cu^{+} that is dependent upon the protein concentration and, secondly, the chelation of bicinchoninic acid with Cu^{+}, resulting in the formation of a purple coloured precipitate (Smith *et al.*, 1985). Absorbance of the BCA-Cu^{+} complex was measured at 562nm and protein concentrations determined in relation to absorbance values of known protein standards.

To generate the standard curve, bovine serum albumin (BSA, 0.1 – 2.0 mg/ml) was dissolved in double distilled H_2O (ddH_2O). BSA protein standards were added in duplicate to wells of a clear 96-well plate (5 µl per well), diluted with SDS lysis buffer (1:1 ratio) and incubated with 200µl combined BCA reagent (reagent A: reagent B 50:1) at $37^{O}C$ for 30 min, following which absorbance (562 nm) was measured using a microtitre plate reader (Spectramax 190, Molecular Devices). A standard curve was generated by expressing the mean optical density (OD) values obtained at 562nm relative to the known BSA concentrations (Figure 2.7). Standard curves with a correlation coefficient of $R^2 > 0.995$ were accepted and used to determined cellular protein concentration. BSA protein standards were used on all 96-well plates when determining the concentrations of cell protein samples. All samples were determined in duplicate (5µl per well) and diluted 1:1 with ddH_2O.

The protein concentration for nuclear lysates were also determined using the BCA assay, however, the reducing agents used in the lysis buffer for collection of nuclear lysates were more reactive with Cu^{2+}. Thus, for the nuclear protein assay, a small volume of lysate (3µl) was diluted in ddH_2O (1:5 ratio) prior to measurement of protein concentrations.

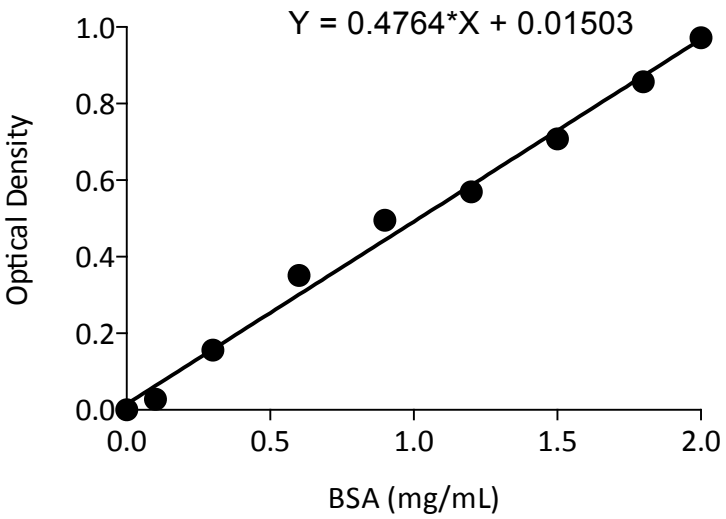

Figure 2.7 Representative BCA assay protein standard.
BSA protein standards (0.1-2.0 mg/ml) were added in duplicate to a 96 well plate well plate with 200µl of the BCA reagent. The plate was then incubated at 37^{O}C, following which, the absorbance (OD, 562 nm) was then measured on the spectra max plate reader.

2.3.13.2 Preparation of samples and SDS PAGE

Lysates were obtained to assess changes in protein expression following either sulforaphane treatment or OGD using poly-acrylamide gel electrophoresis (PAGE), allowing for the separation of proteins by molecular weight (MW) (Shapiro *et al.*, 1967). 10µg of protein was reduced by addition of 10% 2-Mercaptaethanol (2-ME) and 0.2% bromophenol blue (BPB, sample dye). Protein samples were denatured further by heating at 95^{O}C for 5 min before samples, along with a pre-stained protein ladder, were loaded in to designated lanes of a pre-set SDS-PAGE gels for separation by electrophoresis (Miniprotean 3, Biorad). The final concentration of acrylamide in the gels determines the degree of protein separation achieved. In this study 12% acrylamide gel were used which allows for adequate separation of proteins of MW 20 – 60 kDa; 10% gels for proteins of MW 60 – 100 kDa; and 8% gels for proteins of MW >100 kDa. For composition of PAGE see Appendix 2. Proteins were separated by SDS-PAGE at 150V for approximately 2h.

2.3.13.3 Transfer of separated proteins to membranes and immunoblotting

Separated proteins were then transferred onto a polyvinyldiene difluoride (PVDF) membrane (Millipore), pre-activated in 100% methanol and equilibrated in transfer buffer (see Appendix 3), using semi-dry electrophoretic transfer equipment (Biorad, USA) for 2 hours at 20V (Figure 2.8). The membrane was then blocked with PBS containing 5% skimmed milk powder and 0.1% Tween-20 at room temperature for 1 hour before incubation with primary antibody at 4^{O}C

overnight or at room temperature for 1 hour. Primary antibodies were diluted in PBS containing Tween-20 0.1% and 3% BSA. Subsequently membranes were incubated with HRP conjugated secondary antibody in PBS containing 0.1% Tween-20 and 3% skimmed milk powder for 1h at room temperature. Membranes were then subjected to washing with PBS containing 0.1% Tween-20 for 15 min once, followed by three 5-min washes, after the primary and secondary antibody incubations. For chemiluminescence detection of protein bands, the membrane was incubated with 1mL Enhanced Chemiluminescence (ECL) substrate solution (Milipore, UK) for 60 sec and bands visualised in a gel documentation system (G-Box, Syngene Ingenius Biosystems) with images captured using PC imaging software (Syngene 2D, Syngene Ingenius Biosystems), (Figure 2.9). Densitometric analysis of protein bands was conducted using PC analysis software (Image J, NIH, USA). Expression of α-tubulin served as a reference protein on each membrane analysed for expression of specific proteins in total cell lysates.

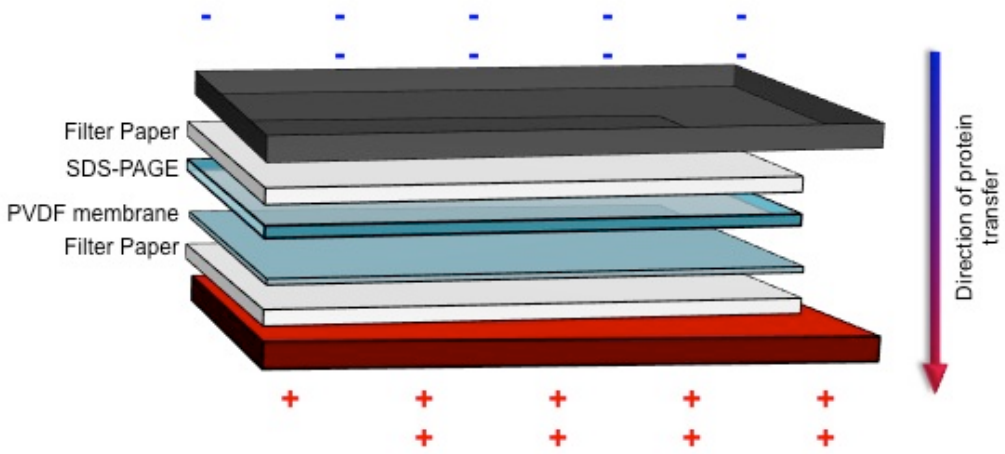

Figure 2.8 Semi-dry transfer of separated proteins from SDS-PAGE to PVDF membrane. Proteins separated on SDS-PAGE were then transferred onto a methanol activated PVDF membrane via semi-dry transfer. The gel was placed on top of the PVDF membrane and both placed between filter paper soaked in transfer buffer. Proteins transferred from the gel to the membrane in the direction of the arrow.

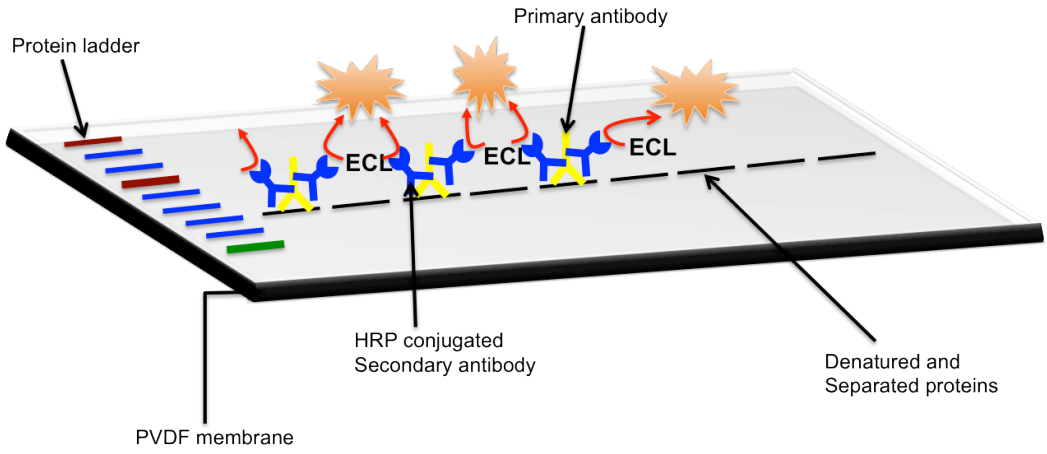

Figure 2.9 Detection of proteins on PVDF membrane using enhanced chemiluminescence. Separated proteins transferred onto PVDF membrane was incubated with a primary antibody targeting a protein of interest and subsequently with horseradish peroxidase (HRP) conjugated secondary antibody. HRP catalyses the reaction between chemiluminescent substrates to produce a luminescent signal.

Table 2.3 Primary antibody dilutions for immunoblotting bEnd.3 lysates

Primary Antibody	Species	Diluent	Dilution	Manufacturer	Catalogue Number
HO-1	Goat	3% BSA in PBS 0.1% Tween	1:500	Santacruz	SC-1797
NQO1	Goat	3% BSA in PBS 0.1% Tween	1:500	Santacruz	SC-16464
Nrf2	Rabbit	3% BSA in PBS 0.1% Tween	1:500	Santacruz	SC-722
α-Tubulin	Rat	3% BSA in PBS 0.1% Tween	1:5000	Millipore	MAB
Lamin A/C	Rabbit	3% BSA in PBS 0.1% Tween	1:500	Santacruz	SC-20681

Abbreviations: HO-1, Heme-Oxygenase 1; Nrf2, NF-E2 related factor 2; NQO1, NADP(H) Quinone oxidoreductase 1

2.3.14 Determination of glutathione in bEnd.3 cells

Intracellular glutathione provides the first line of defence against oxidative stress within the cellular environment. Furthermore, synthesis of intracellular GSH is modulated by enzymes regulated by the Nrf2/ARE signaling-pathway.. Thus in this project, we will determine whether sulforaphane treatment of bEnd.3 cells modulates total GSH content measured by assessing the level of GSH conjugation with O-phthadialdehyde (OPA), which emits a fluorescence signal measured at ex/em 340/420 nm (Senft *et al.*, 2000)

Confluent monolayers of bEnd.3 cells in 6 well plates were treated with 0.1-5 µM sulforaphane for 2, 4, 8, 12 and 24 h. Cells were then rapidly washed with cold PBS at 4°C and GSH precipitated and extracted by incubation with 6.5% trichloroacetic acid (TCA) for 10 min on ice. The supernatant containing GSH were collected and stored at -80^{O}C until analysis. The remaining cellular protein was determined following lysis with 0.5M NaOH at room temperature for 2 h and determination of protein content using the BCA assay (see section 2.3.7.1). Measured total GSH values were expressed relative to protein concentration.

To generate a standard curve for the GSH assay, serial dilutions of reduced GSH standards (0 – 0.15 nM, Sigma) in ddH_2O were added in triplicate (7.5 µl/well) to a black solid bottomed 96-well plates. Collected TCA samples were also added in triplicate (7.5 µl/well) to the same plate. Next, OPA (1 mg/ml) in methanol (15 µl/well) and phosphate/EDTA buffer (277.5 µl/well, KH_2PO_4 100mM, EDTA 10mM, pH 8.0) was added to each respective well and the plate incubated under dark conditions at room temperature for 25 min. Fluorescence of OPA (ex/em 340/420 nm) was measured using a fluorescence plate reader (Chameleon V, Hidex) and GSH concentrations calculated with reference to the GSH standard curve (Figure 2.10).

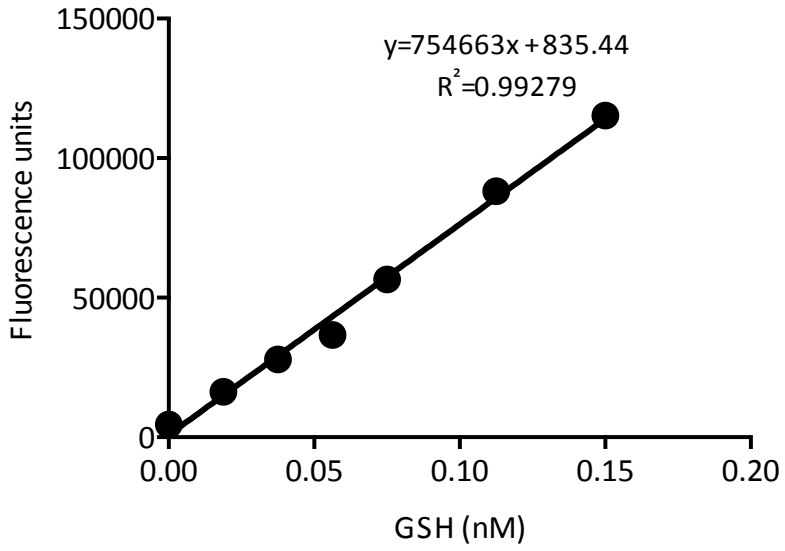

Figure 2.10 Representative GSH standard curve.
GSH standard curve was generated from fluorescence readings of GSH expressed relative to its known concentrations (0 – 0.15nM GSH). The equation derived from the standard curve was then used to calculate the concentration of GSH in samples run on the same plate as the standard curve.

2.3.15 Quantitative reverse transcription polymerase chain reaction (qRT-PCR)

Levels of mRNA for genes of interest in confluent bEnd.3 cells cultured in 6 well plates and treated for 4h with sulforaphane (2.5 μM) or vehicle (0.01% DMSO) were determined by quantitative reverse transcription polymerase chain reaction (qRT-PCR). Extraction of mRNA was performed using a commercially available kit (Nucleospin 96-RNA, Macherey-Nagel, Germany) as per the manufacturer's protocol.. Cells were then washed twice with cold PBS at 4°C and lysed using kit lysis buffer (RA1, Macherey-Nagel, Germany) on ice (260μL/well). Collected cell lysates were stored at -80°C until further processed for mRNA isolation.

2.3.15.1 Isolation of mRNA

Cell lysates were first diluted in a 1:1 ratio using kit RA4 buffer and transferred to the supplied 96-well spin column plate. The plate was centrifuged at 3700 rpm for 5 min at room temperature to allow for the separation of nucleotides from other cellular components. Nucleotides bound to a silica membrane in the spin columns were then desalted using kit RA3 wash buffer by centrifuging at 3700 rpm for 5 min at room temperature, after which, genomic DNA was removed following incubation of the columns with DNase for 15 min at room temperature. Columns were then washed successively with kit RA2 (5 min, 3700 rpm), RA3

(5min, 3700 rpm) and RA4 (10 min, 3700 rpm) buffers at room temperature. Silica membranes were finally incubated with 50µL DNase RNase free water for 2 min at room temperature, followed by centrifugation at 3700 rpm for a further 5 min to elute mRNA.

2.3.15.2 Assessment of RNA purity

The purity and concentration of mRNA samples were determined using the NanoDrop ND-1000 spectrophotometer (NanoDrop Technologies, USA), by measuring absorbance at 260nm (A_{260}). RNA concentration was determined on the assumption that 1 absorbance unit at A_{260} is equal to 40 ng/µL RNA. Purity of RNA, with respect to protein contaminants, was assessed following determination of the ratio of absorbance at 260nm and 280nm (A_{260}/A_{280}), where as contamination by ethanol and guanidine was determined using the ratio of absorbance at 260nm and 230nm (A_{260}/A_{230}). Absorbance ratios of approximately 2.0 suggested good purity of RNA isolated from cell extracts (Bustin *et al.*, 2009).

2.3.15.3 Reverse Transcription to obtain cDNA

The isolated RNA (1 µg) was then reverse transcribed to cDNA using the High Capacity RNA to complimentary DNA (cDNA) kit, as per manufacturer's instructions (Applied Biosystems, UK). A given amount of RNA was diluted in nuclease free water to obtain the final required concentration. 10µL of RNA was mixed with 9µL 2x RT buffer and 1µL 20x buffer mix and samples reverse transcribed using a thermal cycler (DNA Engine Tetrad 2 Peltier Thermal Cycler) for 60 min at 37^{O}C, followed by 5 min at 95^{O}C and held at 4^{O}C. Samples that underwent thermal cycling in the absence of the reverse transcription active enzyme served as the negative control. The generated cDNA was stored at -20^{O}C, until required for qRT-PCR.

2.3.15.4 Quantitative polymerase chain reaction

Real time polymerase chain reaction (RT-PCR) was used to amplify and assess cDNA using a SYBRGreen based PCR mix (Sinsi-Mic, SYBRgreen NO ROX, Bioline, UK). 10µL mastermix for PCR reactions consisted of 5µL Sensi-mix (SYBRgreen), 0.5µL primer against target gene (10µM stock of forward and reverse primers), 2µL nuclease-free water and 2µL cDNA. The CAS-1200 robot (Corbett Life Sciences, Australia) was used to aliquot and mix cDNA to the PCR reaction mix.

cDNA was amplified using the Rotor-Gene 6000 system (Qiagen, UK) using a 3-step program as follows; (1) samples were heated to 95^{O}C for 10 min, activating the polymerase enzyme, (2) samples were then subjected to 40 cycles of 95^{O}C, to separate standard, 57^{O}C for 15s to allow for primer annealing and 72^{O}C for 10s to allow for product amplification. Details of the primers

used are summarised in Table 2.5. The RotorGene software was used to obtain a product melt curve for each gene to confirm the presence of a single PCR product, and to ensure no primer-dimer formation. RotorGene software was also used to transform the absorbance values to a logarithmic scale, allowing for gene copy numbers to be obtained relative to the standard curve.

Copy numbes of target genes were adjusted relative to the geometric mean of 3 house-keeping reference genes; Beta-2-M (B2M), ribosomal protein L13a (RPL13A) and succinate dehydrogenase unit complex (SDHA). The stability of these reference genes was determined using GeNorm v1.2 software (http://medgen.ugent.be/~~jvdesomp/genorm/), which analyses and calculates a stability measure (M value) for reference genes by calculating the variation in reference gene expression compared to other reference genes. An M value of <1.5 was considered sufficient to be included in the final pairing analysis, after which GeNorm was used to derive a normalisation factor based on the geometric mean of the reference genes included (Vandesompele *et al.*, 2002). The expression of target genes (copy numbers) derived for each respective sample was then corrected by the corresponding normalisation factor, minising non-biologica variations between the samples.

Table 2.4 Primers used for q-RT-PCR

Target Gene		*Primer Sequence*
Nrf2	F	ACTCCCAGGTTGCCCACATTC
	R	CAGAGAGCTATTGAGGGACTGG
NQO1	F	CCTTTCCAGAATAAGAAGACCTTGC
	R	GAAGCCACAGAAACGCAGGA
HO-1	F	CAACATTGAGCTGTTTGAGGAG
	R	CTCTGACGAAGTGACGCCAT
Keap1	F	ATCTACGCAGTCGGGGGTTC
	R	CCCGCTCTGGCTCATATCTCTC
Bach1	F	CGGAAATCGAGAAGCTGCAAAG
	R	AAAAGGAAAGCGGGCAGTCG
GCLC	F	TACTGAATGGAGGCGATGTTCT
	R	GTCGGATGGTTGGGGTTTGT
GCLM	F	ACAATGACCCGAAAGAACTGCT
	R	GGGTGTGAGCTGGAGTTAAGA
SDHA	F	CAAAAACAGACCTGCGGCTT
	R	CTGGGTATTGAGTAGAAATTGCATC
B2M	F	GTCGCTTCAGTCGTCAGCA
	R	TTGAGGGGTTTTCTGGATAGCA
RPL13A	F	GAGGGGCAGGTTCTGGTATT
	R	CGGGAGGGGTTGGTATTCAT

Abbreviations: F, Forward; R, Reverse

2.4 Oxygen and glucose deprivation studies in bEnd.3 cells

To assess whether protection to the cerebrovascular endothelium can be conferred by activation of the Nrf2 defence pathway, following sulforaphane pre-treatment, an oxygen and glucose deprivation (OGD) protocol was employed in bEnd.3 cells to simulate experimental ischaemia and reperfusion injury *in vivo*.

2.4.1 Oxygen and glucose deprivation

Cells were seeded onto glass coverslips (one coverslip per 35mm petri dish) or 6 well plates and when confluent, the DMEM growth medium was replaced with glucose free DMEM (A14430, invitrogen, UK) supplemented with 10% FCS, 4mM L-glutamine, penicillin (100 U/ml) and streptomycin (100 µg/ml). Cells were placed in the modular incubator chamber (MIC-101, Billups-Rothenberg Inc., USA) which was purged with 5% CO_2, 95% nitrogen for 10 min, following which the chamber was placed in the incubator at $37^{O}C$ for 2, 6, 8, and 12 hours. Control experiments were also conducted by replacing the medium with 5.5mM glucose DMEM supplemented with 10% FCS. Cells were placed in the incubator (in air, 5% CO_2) at $37^{O}C$ for 2, 6, 8 and 12 hours. Cells seeded on coverslips were used to assess cell death after OGD (see section 2.3.13.1) and total protein lysates harvested for 6 well plates (see section 2.3.6) for analysis by immunoblotting (see section 2.3.10).

2.4.2 Assessment of cell death after oxygen and glucose deprivation

Cell death in bEnd.3 cells after OGD was assessed using a commercial apoptosis detection kit, by which cells are stained with annexin V conjugated with FITC and ethidium bromide homodimer III (PK-CA707-30017, PromoKine, Germany). Phosphatidylserine (PS) is a phospholipid expressed on the cytoplasmic leaflet of the plasma membrane, but upon apoptosis or necrosis, PS is exposed on the cell surface. Annexin V (member of the annexin family of proteins) binds directly to PS, thus annexin V conjugated to FITC enables for the fluorescent visualisaton of dead cells (Martin *et al.*, 1995; Vermes *et al.*, 1995). Ethidium bromide homodimer III emits a fluorescent signal upon intercalating with nucleic acids, but is unable to penetrate the membrane of living cells, thus, positive staining of cell nuclei indicates cell death (Koopman *et al.*, 1994). The nuclear stain DAPI was employed to stain the nuclei of all living and dead cells, and ratio calculated for the number of dead against living cells based upon the two respective nuclear stains.

After OGD, bEnd.3 cells cultured on coverslips were washed with twice kit 1X binding buffer (100 µL) and incubated with annexin V (1:20 dilution) and ethidium bromide homodimer III (1:20 dilution) in 1X binding buffer (30 µl per coverslip) in the dark for 15 min at room temperature. Cells were then washed with 1X binding buffer and incubated with DAPI in 1X

binding buffer (2 µg/mL, Sigma, UK) for 5 min at room temperature. Cells were viewed using a Nikon diaphot microscope (Nikon, Japan) adapted for fluorescence and images were captured using a cooled CCD camera (Hamamatsu, Japan) controlled by PC imaging software (Image Hopper version 2,Samsara Research, Surrey, UK).

2.4.3 Sulforaphane pre-treatment of bEnd.3 cells prior to OGD

To assess whether sulforaphane pre-treatment affects cell viability and antioxidant protein expression after OGD, confluent monolayers of bEnd.3 cells equilibrated in DMEM (5.5mM glucose) supplemented with 10% FCS, were pre-treated with either vehicle (0.001% DMSO) or SFN (2.5µM) for 12 h. DMEM was then replaced with glucose free DMEM (supplemented with 10% FCS) and cells deprived of oxygen for 2, 6, 8 and 12 h as described in section 2.4.1. Total cell protein lysates were collected for analysis by Immunoblotting (See section 2.3.10) and cell death was assessed as described in section 2.4.2.

2.5 Statistical analysis

All data presented in the thesis are a representative of a minimum of at least 3 experiments from independent bEnd.3 cell cultures or individual rats, unless otherwise stated. Data is expressed as mean ± standard error of the mean (S.E.M) unless otherwise stated. Statistical analysis was performed using either one-way or two-way analysis of variance (ANOVA) followed by Tukeys post-hoc test using Graphpad Prism 6.0 Software. $P<0.05$ were considered statistically significant and were labeled and defined within the corresponding figure legends.

Chapter 3 – Development of a novel immunohistochemical technique using 3,3'-Diaminobenzidine

Chapter 3 Development of a novel immunohistochemical technique using 3,3'-diaminobenzidine

3.1 Introduction

Immunohistochemistry was first reported in 1941, although the technique has existed since the 1930's. The first reported study using immunohistochemical techniques showed the use of conjugated fluorescent antibodies to detect the expression of proteins in tissues *ex vivo* (Coons & Kaplan, 1950). Graham and Karnovsky were the first to pioneer the use of 3'3-diaminobenzidine (DAB) for immunohistochemical analysis of horseradish peroxidase (HRP) absorption in the renal proximal tubule of mice (Graham & Karnovsky, 1966a). Interestingly, DAB was used in the assessment of glomerular permeability following extravasation of HRP (Graham & Karnovsky, 1966b).

Immunohistochemical methods, using DAB, have traditionally been employed for localization of protein and examining organ permeability in pathological conditions. Results acquired using this method only provide qualitative data on the localisation of proteins (Taylor & Levenson, 2006). Moreover, digital image acquisition enabled for semi-quantitation of DAB staining, based upon the intensity of DAB staining on a pixel by pixel basis (Montgomery *et al.*, 2008;Kirkeby & Thomsen, 2005;Matkowskyj *et al.*, 2000). Hitherto, protein measurement in tissues has relied on the immunoblotting of whole tissue homogenates. Although immunoblotting allows for the detection of global protein changes, cell specific changes cannot be discriminated.

The development of the DAB polymer stain is dependent upon a chemical reaction between DAB and H_2O_2, catalysed by HRP. Increased association of an HRP conjugated to a secondary antibody will increase the final intensity of the DAB staining. However, the increased presence of HRP also increases the rate of DAB polymer formation, which serves as an index of protein content present in the tissue. Therefore, calculation of the rate of DAB polymer development allows for true protein quantitation in *ex vivo* sections. Moreover, the application of immunofluorescence and quantitative immunohistochemical techniques simultaneously allows for: (1) the identification of cerebral cell types by fluorescence and (2) quantification of target protein in defined cell structures using digital masking.

As mentioned previously, an objective of this project was to characterise the temporal, spatial and cell specific distribution of the redox sensitive transcription factor Nrf2, following cerebral ischaemia and reperfusion injury in rats. Immunoblotting techniques are unable to provide sufficient resolution to address the objectives outlined in this project. However, the application of immunofluorescence and immunohistochemical staining simultaneously, allowed for the

quantitation of proteins in specific cerebral cell types as well as in different regions of the brain. Thus, this chapter describes the development of a quantitative immunohistochemical technique, using DAB to quantitate Nrf2 protein expression in *ex vivo* brain sections from rats.

3.2 Validation of the quantitative immunohistochemical technique

The immunohistochemical technique described in this chapter is a further advancement of the technique developed by Gauden *et al.*, where HRP was used as a fluid phase marker to determine BBB permeability following ischaemic stroke in mice (Gauden *et al.*, 2007). This quantitative immunohistochemical technique has been extended to quantify HRP conjugated secondary antibodies in *ex vivo* brain sections.

Proof-of principle experiments were conducted using known concentrations of bovine serum albumin (BSA), to establish the relationship between primary and conjugated HRP secondary antibodies (Figure 3.1). Production of the DAB polymer, following reaction with H_2O_2, results in the decrease of transmitted light that is able to pass through the tissue. Optical density is a measure of the changes in transmitted light that passes through a brain section or gelatin block section (10 μm), following production of the DAB polymer. Thus, calculating the initial rate of change in optical density provides information on the initial rate of DAB polymer formation.

Optical density curves were generated following capture of the DAB-H_2O_2 reaction in sections from gelatin blocks embedded with a known concentration of BSA (Figure 3.1A). An increase in the rate of the optical density curves is noted with increasing BSA concentration (Figure 3.1A). The initial portion of each optical density curve was then taken to signify the initial rate of DAB polymer formation. Calculation of the regression co-efficient for the linear portion of each optical density curve revealed a linear relation between the initial rate of DAB polymer development and increasing BSA concentration in gelatin blocks (Figure 3.1B).

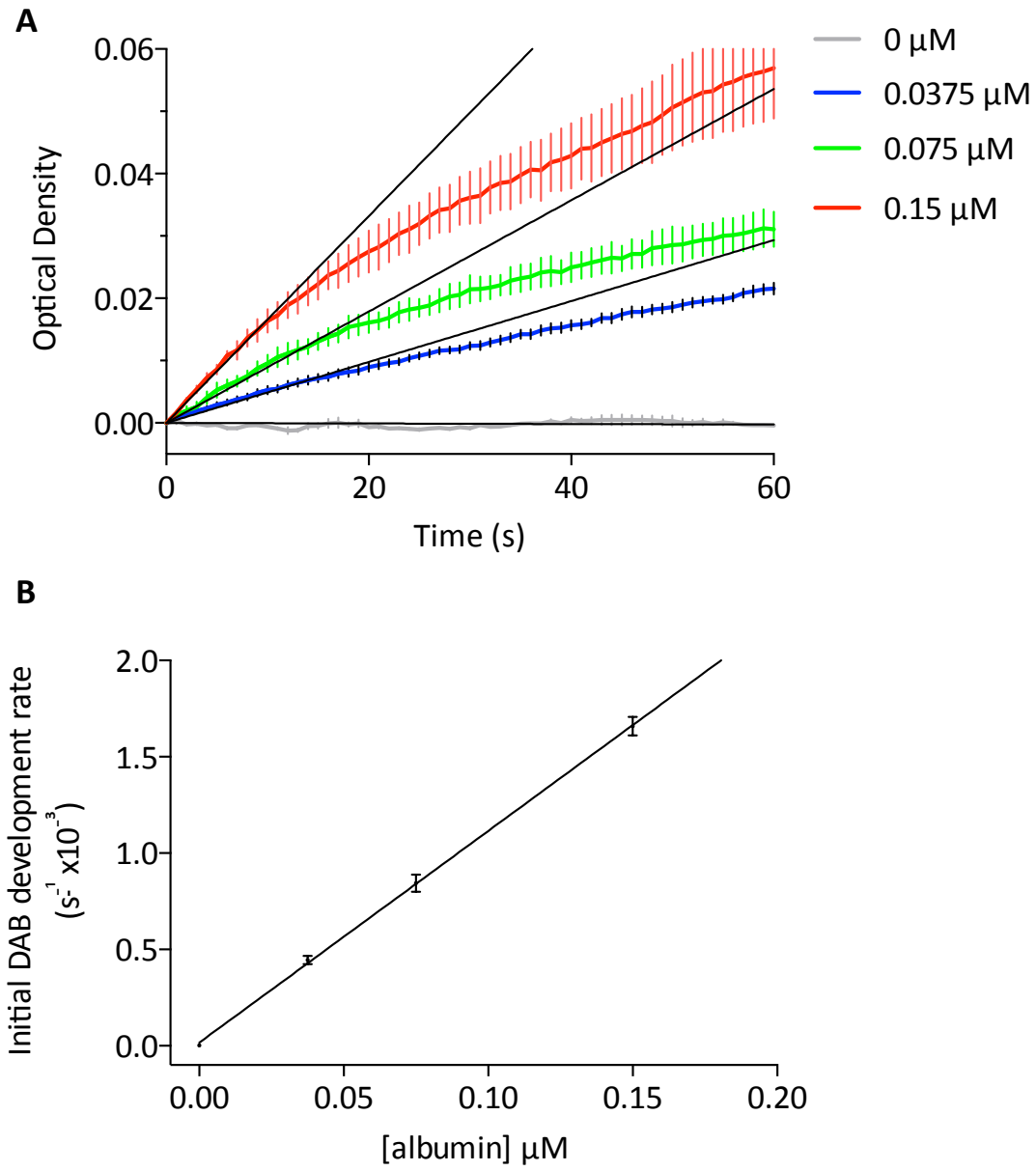

Figure 3.1 Linearity of 3'3-diaminobenzidine (DAB) polymer formation against known protein concentrations.
Frozen sections of 10µM thickness from porcine gelatin blocks containing a known concentration of bovine serum albumin (BSA, 0 – 0.15 µM) were incubated with an anti-BSA primary antibody and complimentary HRP conjugated biotinylated secondary antibody, and then treated with ABC solution. (A) Sequential images of the reaction with the DAB-hydrogen peroxide mixture were captured and analysed to determine the rate of change in optical density observed at each BSA concentration. Solid black lines represent the linear portion of each curve used to determine the initial rate of reaction. (B) The initial rate of optical density increase was linearly related to the BSA concentration. Data denote mean ± S.E.M, *n = 4*. Figure adapted from (Srivastava *et al.*, 2013).

3.3 Quantification of Nrf2 in *ex vivo* brain sections and segmentation

Proof-of-principle experiments in frozen gelatin blocks demonstrated the linear relationship between the initial rate of DAB polymer development and protein content. Thus, the quantitative immunohistochemical technique was employed to quantify the expression of Nrf2 in *ex* vivo rat brain sections. This quantitative immunohistochemical technique provides enhanced resolution with information on the temporal, spatial, and cell specific distribution of a protein of interest. To obtain such data following image acquisition of the DAB-H_2O_2 reaction, image processing was required to monitor Nrf2 levels present in the *ex vivo* brain section. Furthermore, image segmentation was also employed to determine the cellular and endothelial distribution of Nrf2 content.

3.3.1 Image processing to obtain quantifiable images

Following the preparation of rat brain sections for analysis by quantitative immunohistochemistry, brain sections were reacted with the DAB-H_2O_2 reaction mix, and images acquired every 1s over a 100s duration. Image processing was required to determine the levels of Nrf2 present in *ex vivo* brain sections following the generation of a DAB density map highlighting Nrf2 localisation, and its levels of expression (Figure 3.2D).

The DAB density map was generated by applying the Beer-Lambert's Law to the original image sequence (Figure 3.2A), i.e. taking the log ratio of the first image to subsequent images. This, generates a sequence of optical density images, whereby the development of bright regions over time reveal areas of high DAB polymer formation (Figure 3.2B). The optical densities through the stack for different regions (red square in Figure 3.2B) were corrected for residual, or background DAB-H_2O_2 reaction product development over the lumen of a cerebral microvessel, which was free of tissue (green square in Figure 3.2B). The time courses for DAB polymer development in the tissue (red line, Figure 3.2C) and the tissue-free region (blank, green line, Figure 3.2C) were subtracted to give the resulting net production of DAB polymer in the tissue (black line, Figure 3.2C). The linear portion of net DAB product development is demonstrated by the black dotted line (Figure 3.2C). A linear regression of the sequence of optical density images, which related to the linear portion of the DAB development curve, generated a spatial map for Nrf2 expression (Figure 3.2D). Bright regions indicate high levels of Nrf2, whereas dark regions indicate low levels of Nrf2. Furthermore, each individual pixel of the final Nrf2 spatial map coveys a value for the rate of DAB development that is used to quantify Nrf2 levels.

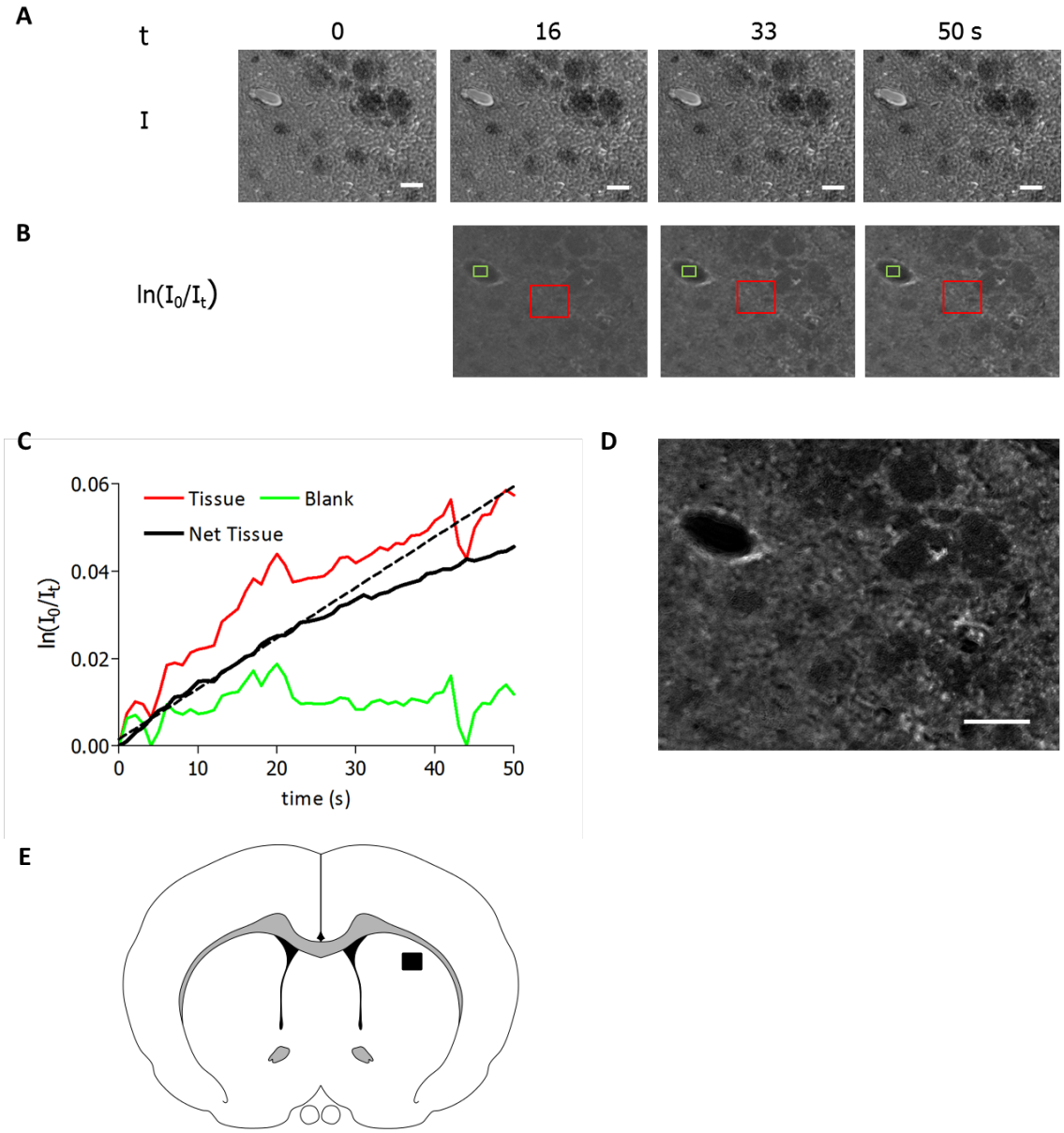

Figure 3.2 Method for calculating the spatial concentration of Nrf2.
Frozen brain sections (10 µm) were incubated with anti-Nrf2 primary antibody and a complimentary HRP conjugated secondary and treated with ABC solution. (A) Sequential images of the DAB-hydrogen peroxide reaction were acquired over 110 s. (B) The images in the stack were analysed using the Beer-Lambert Law to monitor the progression of DAB product development. (C) The net rate of DAB product development was calculated from the difference between the tissue (red square) and the background (green square). (D) The spatial localisation of Nrf2 was calculated on a pixel-by-pixel basis from the images in the stack selected from the initial linear reaction shown in (C). (E) Black square (■) in brain map represents the location of the acquired image. The scale bars denote 50µm. *Abbreviations:* I, image; I_0, Initial image; I_t; Image stack. Figure adapted from (Srivastava *et al.*, 2013).

3.3.2 Image segmentation to quantify cellular and endothelial Nrf2

Image segmentation was used to quantify Nrf2 levels in all cerebral cells and also the cerebral endothelium. Fluorescence images of cellular nuclei, stained by DAPI, and the cerebral endothelium, stained with anti-rat endothelial cell antigen 1 (RECA1) and complimentary fluorescent secondary antibody, were captured before reacting the brain section with DAB-H_2O_2. The captured fluorescence images were used to define the cellular distribution of Nrf2 levels and to generate a Nrf2 spatial map, (see Figure 3.2D). Furthermore, brain sections were also stained with glial fibrillary associated protein (GFAP), a marker of astrocytic processes.

To monitor the cellular distribution of Nrf2 in rat brains, the acquired fluorescence DAPI image (shown as blue in Figure 3.3A) was used to generate a digital mask (Figure 3.3C). This digital mask was superimposed on to the Nrf2 spatial map, shown in Figure 3.3B, to identify nuclear Nrf2 content (Figure 3.3D). Note, that warmer pseudo colours on the Nrf2 spatial map indicate high levels of Nrf2, whereas cooler pseudo colours show lower Nrf2 expression. The DAPI image was also used to define the cytoplasm for each identified nuclei. A 4μm ring was digitally drawn around each nuclei to define its cytoplasm, which was used to determine cytoplasmic Nrf2 content (Figure 3.3E). A 4μm ring was estimated to define the cytoplasm of each cell and hence selected to minimise overlap between adjacent cells. Nuclear segmentation was used to determine the nuclear to cytoplasmic distribution of Nrf2, with the sum of these components providing the total cellular Nrf2 content.

Endothelial Nrf2 content was determined in a similar manner using nuclear segmentation. Endothelial structures were segmented from the Nrf2 spatial map (Figure 3.4 A), using the respective fluorescence (RECA-1) image for the endothelium (Figure 3.4 B). A digital mask was generated and superimposed over the Nrf2 spatial map, highlighting the endothelial Nrf2 content (Figure 3.4 C).

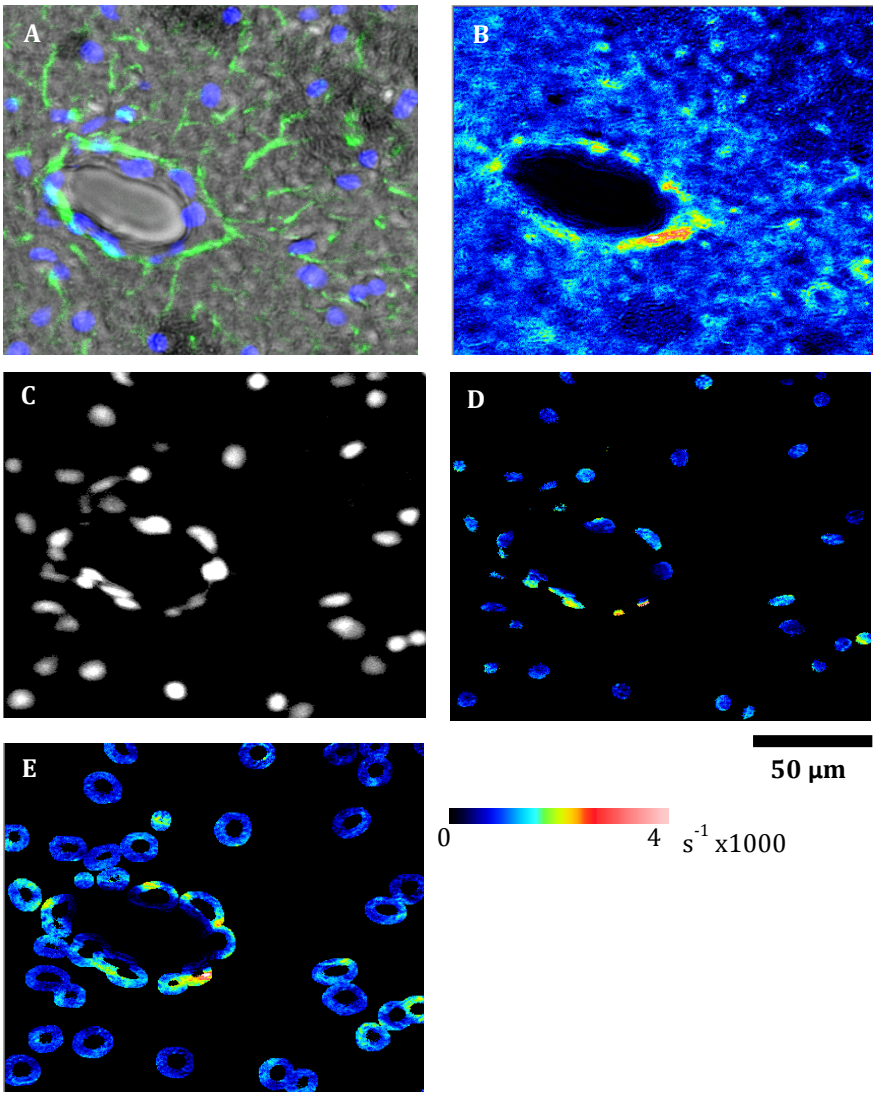

Figure 3.3 Segmentation to identify nuclear and cytoplasmic Nrf2 content of all cells in brain sections from rats.

(**A**) Composite image of the left-hand portion of the section in Fig. 3.2 A, with a fluorescence overlay of nuclei stained with DAPI (blue) and astrocytes with GFAP (green). (**B**) Nrf2 image is scaled to a pseudo colour map. (**C**) DAPI image of the nuclei was used to generate a mask that segmented the Nrf2 concentration in nuclei, as shown in panel (**D**). (**E**) Cytoplasm was taken to be a ring of 4 µm around each nucleus. The combined nucleus and its cytoplasm were taken to represent a cell. Figure taken from (Srivastava *et al.*, 2013).

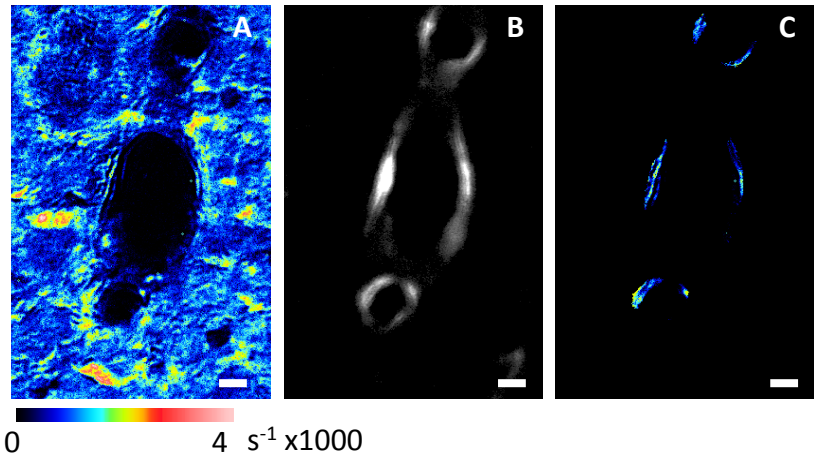

Figure 3.4 Segmentation to identify endothelial Nrf2 content in brain sections from rats. (**A**) Spatial map of Nrf2 distribution is scaled to pseudo colour map. (**B**) Fluorescence image of RECA1 was used to generate an endothelial mask. (**C**) Endothelial mask was superimposed on panel (**A**) to segment and show endothelial Nrf2 content. Scale bars represent 5µm.

3.4 Technical problems encountered during technique development

Although Sections 3.2 and 3.3 demonstrate a working technique and how cellular and endothelial Nrf2 contents were determined (shown in Chapter 4 and Chapter 5), a significant amount of time was required to resolve the technical difficulties encountered during development. This section describes the steps taken to resolve these issues.

3.4.1 Mounting of brain sections on glass slides

The success of this quantitative immunohistochemical technique was dependent on the stability of ex vivo brain sections on glass slides. The brain has a high fatty acid content, thus affecting the adherence of brain sections to glass slides. Brain sections from naïve and MCAo rats were obtained at a thickness of 10µm using a cryostat and mounted onto glass slides. Initially, brain sections were mounted onto uncoated glass slides and left to dry at room temperature for 24 h and then prepared for analysis by quantitative immunohistochemistry following incubation with primary antibodies overnight. However, this lead to the destabilization of brain sections with subsequent lifting off the glass slide. Poly-L-Lysine coating of glass slides increased stability of the section on the glass slides due to increased electrostatic coupling. Mounting of brain sections onto commercially available poly-l-lysine coated glass slides (Thermo Scientific) however failed to improve the adherence and stability of brain sections. Mounting brain sections on Superfrost Plus glass slides, which have a permanent positive charge, significantly improved the stability of sections and prevented them from lifting off during incubations.

3.4.2 Preservation of cerebrovascular endothelial staining in ex vivo brain sections for fluorescence identification during DAB

As mentioned previously in Section 3.3.2, fluorescence images of the endothelium were used to map endothelial distribution of Nrf2, following the generation of a digital endothelial mask. To generate a reliable endothelial mask, good staining of the endothelium is required, however, if fluorescence signal is weak, then the generated mask will not be fit for purpose. The cerebral endothelium was identified by fluorescence following staining of brain sections with a mouse RECA1 primary antibody and anti-mouse Alexa Flour 555 (red, Figure 3.5).

Cerebral vessels were identified under bright-field microscopy, combined with the circular arrangement of DAPI stained nuclei (Figure 3.5). Very little staining of the cerebral endothelium was observed in coronal rat brain sections that were mounted on to Superfrost Plus glass slides (Figure 3.5A). To improve endothelial staining, and prevent movement of the brain section, upon application of the DAB-H_2O_2 reaction mix (see Section 3.4.4), glass slides were pre-treated with formal saline prior to mounting of coronal brain sections. Although formalin pre-treatment of slides did not prevent movement of the brain section upon application of the

DAB-H_2O_2 reaction mix, endothelial staining was improved significantly (Figure 3.5B). Fluorescence images revealed greater endothelial staining around the vessel lumen, along with increased detection of the endothelium in the tissue specimens (Figure 3.5B).

3.4.3 De-stabilisation of ex vivo brain sections following hydrogen peroxide quench

Prior to incubation of brain sections with primary antibodies, sections were prepared for the DAB-H_2O_2 reaction by quenching endogenous peroxidase activity with 0.3% H_2O_2. The incubation of paraformaldehyde fixed coronal rat brain sections with 0.3% H_2O_2 resulted in effervescence, originating from the brain section, as shown in Figure 3.6. White arrows indicate the area of bubble formation within the captured field of view. Notably, the formation of bubbles affected the adherence of brain sections to the glass slide, reducing section stability and allowing the tissue section to lift off during subsequent incubations.

The H_2O_2 concentration was reduced 10-fold to 0.03%, however, following incubation with brain sections, bubbling was still observed (data not shown). As quenching of endogenous peroxidase activity with H_2O_2 destabilised brain sections, a commercially available endogenous peroxidase block (Bloxall, Vector Laboratories) was trialed. Incubation of brain sections with Bloxall did not cause the production of effervescence from the sections (data not shown). Moreover, the adherence of brain sections to the glass slide was not affected by subsequent incubations.

Figure 3.5 Detection of cerebral endothelial staining before and after formalin pre-treatment of slides.
Coronal brain sections (10μm) mounted on either (A) Superfrost Plus glass slides, or (B) formalin pre-treated Superfrost Plus glass slides. Brain sections adhered to both types of glass slides, as observed following bright-field microscopy (left panel). Sections were stained for nuclei with DAPI (blue, middle panel) and the cerebral endothelium with mouse anti-RECA1 primary and donkey-anti mouse Alexa Fluor 555 (red, right panel). Scale bar represents 10μm.

A – Superfrost plus glass slides

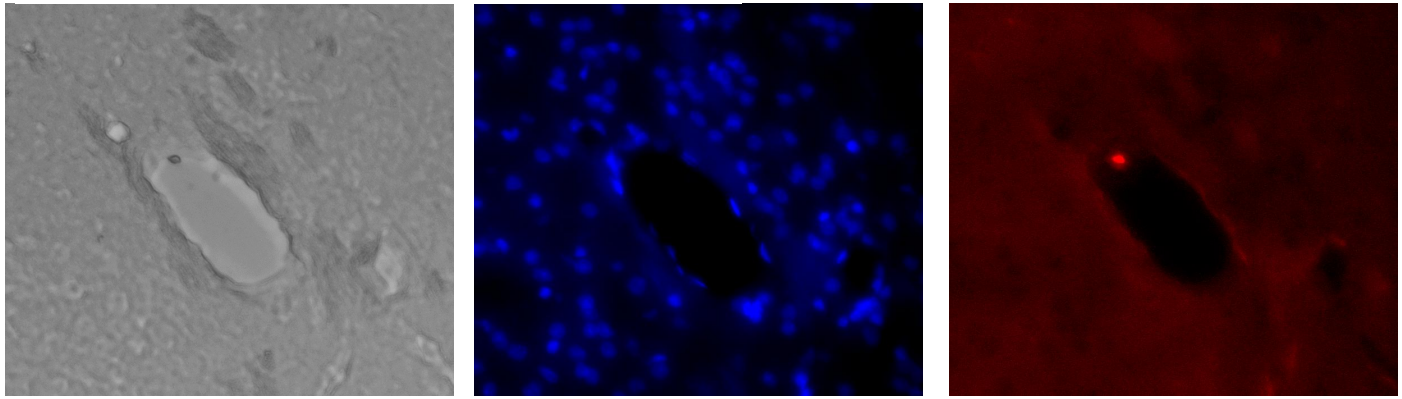

B – Formalin coated superfrost plus glass slides

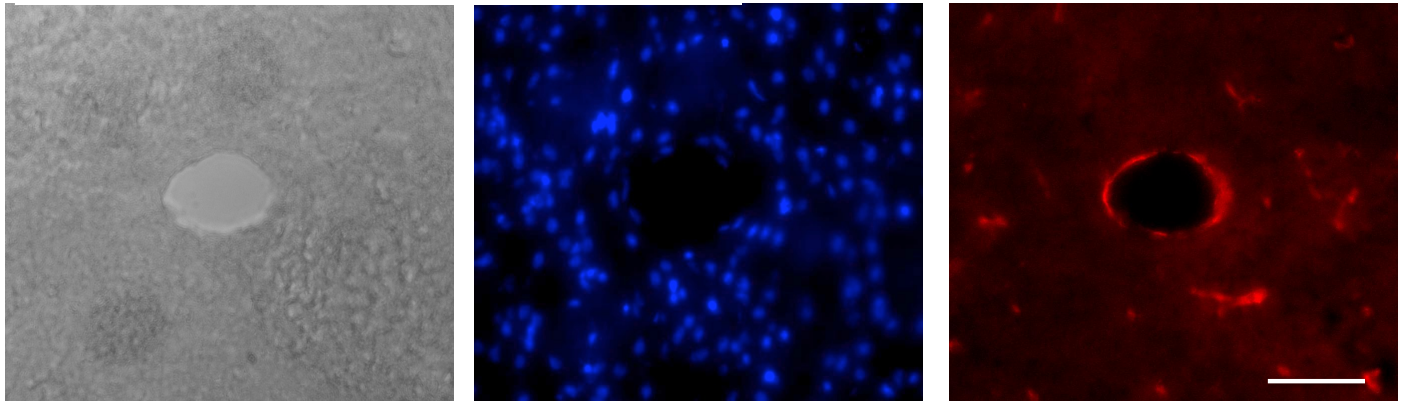

Brightfield **DAPI** **RECA1**

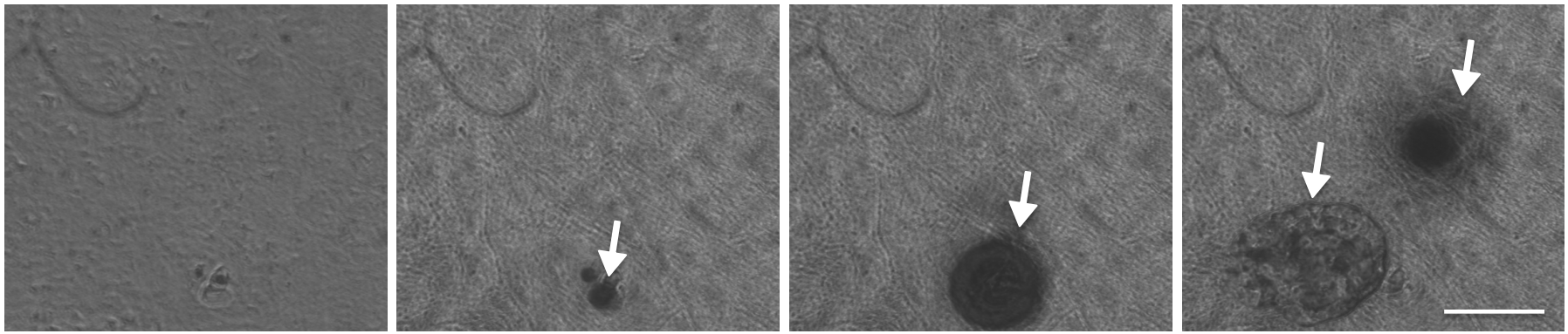

Figure 3.6 Effect of H2O2 quenching on paraformaldehyde fixed brain sections.
Coronal brain sections (10µm) were mounted on to superfrost plus glass slides, and prepared for the quantitative immunohistochemistry prior to primary antibody incubation. A brain section was placed on the microscope stage and brightfield images captured during incubation with 0.3% H_2O_2. White arrows show the formation of bubbles from the *ex vivo* brain section following incubation with 0.3% H_2O_2. Scale bar represents 10µm.

3.4.3 Movement of brain sections during capture of the DAB reaction

As mentioned previously, the quantitation of DAB immunohistochemistry is dependent on captured changes in optical density, resulting from production of the DAB polymer. Changes in optical density, caused by factors other than the production of the DAB polymer, will influence the result and mask possible findings related to protein levels in the *ex vivo* section.

After the capture of fluorescence images, *ex vivo* brain sections were reacted with the DAB-H_2O_2 reaction mix and a sequence of images captured. Analysis of the sequence of images revealed movement in the brain tissue upon application of the DAB-H_2O_2 reaction mix (Figure 3.7). Movement was observed immediately after application of the DAB-H_2O_2 reaction mix (Figure 3.7A) and continued for the duration of the capture (Figure 3.7B and C). The red line, shown in Figure 3.7, outlines the vessel lumen wall. With increasing time, the wall pulls away from the red outline indicating movement. Furthermore, the white arrows demonstrate movement observed in areas of the tissue further away from the lumen. This thus indicates that movement of the tissue is widespread and not localised to specific regions. Upon quantitative analysis of the optical density, the pseudo colour image of the resulting Nrf2 spatial map indicates warm colours around the vessel wall (Figure 3.7B).

This provides evidence that movement of the tissue influences the final quantitative analysis. As movement of the tissue was only observed upon application of the DAB-H_2O_2 reaction mix, the components of the commercially available reaction mixture were applied separately and images captured at 1s intervals for a total of 100s. This revealed that application of the DAB alone caused tissue movement (data not shown). Furthermore, pre-incubation of *ex vivo* brain sections with DAB alone prevented movement of the brain section following application of the DAB-H_2O_2 reaction mix. Although pre-incubation of brain tissue with DAB eliminated tissue movement, DAB was able to react with endogenous peroxides, allowing for the formation of the DAB-polymer.

3.4.4 Ascorbic acid quench of tissue prior to the capture of DAB reaction for quantitative analysis

Although movement of the brain section was eliminated, DAB pre-treatment resulted in partial staining of the tissue, masking DAB production upon application of the DAB-H_2O_2 reaction mix (data not shown). The brain consists of high levels of endogenous peroxides, which reacts with DAB, generating the brown coloured DAB polymer. Pre-treatment of brain sections with DAB, in the presence of 1mM ascorbic acid, eliminated movement and prevented partial

staining of the tissue (data not shown). This resulted in the acquisition of a sequence of images, quantifiable for Nrf2 in different sub-cellular compartments and cerebral cell types.

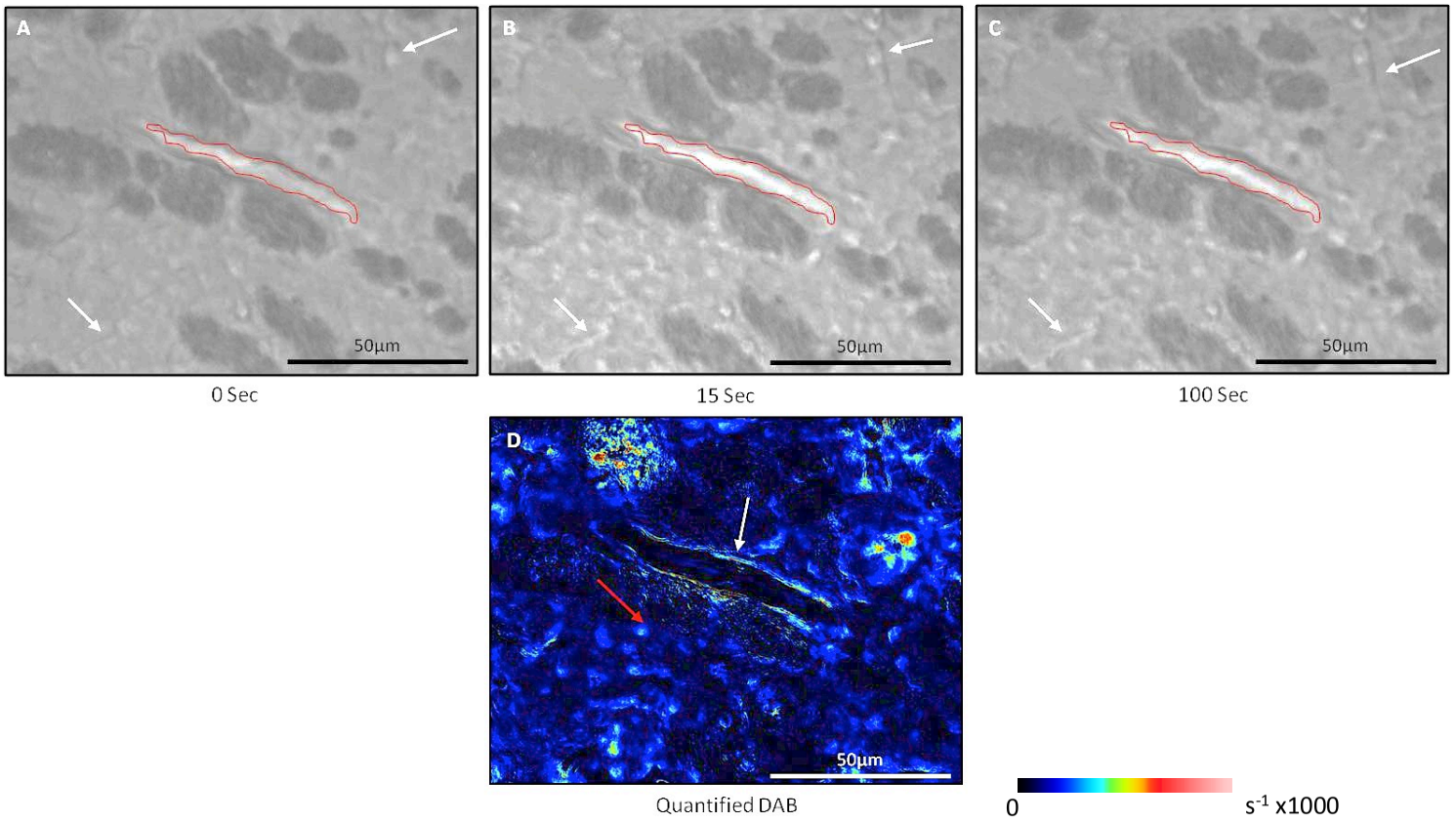

Figure 3.7 Movement of brain section during the capture of the DAB product development reaction.
The rate of DAB product development is calculated from the changes observed in optical density, however, upon application of the DAB reaction mix, movement of the tissue throughout the duration of capture masks the rate of DAB product development within the specified region. The lumen of the vessel captured in the field of view is outlined in red at the start of the reaction (A). After 15 s into the reaction (B), the vessel has expanded and further holes begin to appear, indicated by the white arrows. After 100 s after the application of the DAB reaction mix (C), the vessel is no longer in the same position as recorded in panel (A). Upon image processing, areas of movement are indicated by the bright coloured lines around the vessel, as indicated by the while arrow, where as the red arrow indicates area where no movement was detected and development of the DAB product recorded (D).

3.5 Discussion

Immunohistochemical techniques have primarily been used to provide qualitative data regarding protein expression in *ex vivo* tissue sections. Sophisticated imaging packages are only able to provide semi-quantitative data, based upon the intensity of staining, determined on a pixel-by-pixel basis. This chapter reviews the development of a quantitative immunohistochemical technique to provide true quantitation of protein levels in *ex vivo* brain sections. The validated quantitative immunohistochemical technique is employed in subsequent chapters to examine the temporal and spatial distribution of Nrf2 following ischaemia-reperfusion injury and sulforaphane treatment in rats.

3.5.1 Semi-quantitative versus true-quantitation

Immunohistochemistry using DAB is a widely employed technique for studying the expression of proteins in tissues (Graham & Karnovsky, 1966a). Immunohistochemical staining has been widely used as a qualitative research tool to examine the expression and cellular localisation of proteins. With the development of quantitative imaging packages, an increasing number of immunohistochemical stains are being quantified. However, such quantitation measures the intensity of staining on a pixel-by-pixel basis (Toyokuni *et al.*, 1997; Matkowskyj *et al.*, 2000). Although such information will inform the user of the variation in protein expression from one region to another, true protein content cannot be determined. Such immunohistochemical stains are used routinely in the clinical setting to detect proteins in tissue biopsies from patients, serving as biomarkers of disease states (Rizzardi *et al.*, 2012). Commonly used methods to semi-quantitate findings from immunohistochemical staining are (1) to either count the number of cells positive for the target protein (Tanaka *et al.*, 2011) and (2) to digitally quantitate the final DAB staining on a pixel-by pixel basis (Rizzardi *et al.*, 2012). Using both methods of quantitation, human error will affect the final result, in either counting the number of positive cells or in drawing the region of interest. Moreover, imaging software only detects regions of intense DAB staining, hence limiting quantification of the area where low levels of DAB staining are observed.

The production of the brown coloured DAB polymer is dependent upon a biochemical reaction between DAB and H_2O_2, catalysed by HRP (Nakane & Pierce, 1966). The number of catalytic sites available determines the intensity of DAB staining, whereby, the greater the number of catalytic sites, the greater the intensity of the stain. Based on this principle, our proof-of-principle experiments, using known concentrations of BSA in gelatine blocks, demonstrates and increasing rate of DAB polymer formation with increasing protein concentration. Furthermore, the present experiments in gelatine blocks established a linear relation between the protein

concentration and initial rate of DAB polymer formation (Figure 3.1). This finding validates that development of the DAB polymer provides a direct read-out of protein content, and thus can be used to quantitate protein levels in *ex vivo* tissue sections.

3.5.2 Advantages and disadvantages of the quantitative DAB technique

The quantitative immunohistochemical technique discussed in this chapter is an advancement of the technique reported by Gauden *et al*. Brain sections from mice subjected to experimental stroke were assessed for changes in cerebral microvascular permeability, following the injection of the fluid phase marker HRP (Gauden *et al.*, 2007). Within a research environment, the employment of such a technique will save on costs compared to magnetic resonance imagining (MRI). Furthermore, *ex vivo* brain sections from such animals may be used to assess both permeability, and the expression of target proteins by immunofluorescence, reducing the number of animals required for a particular study. However, considerable time is invested in sectioning, staining, reacting *ex vivo* sections with DAB-H_2O_2 and image processing. Hence the amount of time spent to obtain the final result may be out weighed by high throughput methods such as MRI.

The simultaneous application of immunofluorescence and quantitative immunohistochemistry protocols has allowed direct protein quantitation in the whole tissue, and specific cerebral cell types. Although immunoblotting protocols are able to show global changes in protein expression, sufficient resolution is not available to detect cell specific responses, highlighting the advantages of the DAB-H_2O_2 immunohistochemical technique.

Although true quantitation of protein content can be obtained using the quantitative immunohistochemical technique, only one section can be analysed at a time for a particular region of interest. Immunofluorescence staining and end-point immunohistochemistry allows for the detection and semi-quantitation of protein content in all regions of interest from one section. Thus, multiple sections are required for data analysis using the DAB-H_2O_2 immunohistochemical technique.

As mentioned previously, the cellular content of proteins was determined by summing the values of DAB polymer development in both nuclear and cytoplasmic compartments. The current analysis assumes that all cells lie in one plane; however, the true orientation of cerebral cells is unknown. Furthermore, it is evident from stained nuclei that some nuclei lie in close proximity to one another. In this instance, a drawn cytoplasmic ring may not accurately differentiate between nuclear and non-nuclear regions, as cytoplasmic regions from two cells may overlap. Therefore, it will be necessary to improve the analysis to detect true cell orientation and exclude overlapping cytoplasmic and nuclear regions.

This developed immunohistochemical technique allows the user to obtain quantitative data for a protein of interest. Moreover, with the application of appropriate cell markers, one is able to quantitate protein content in specific cell types. However, the preparation, staining and analysis of sections requires a significant amount of time, with section movement and/or loss of sections during antibody incubations and preparation of the DAB- H_2O_2 reaction resulting in loss of data. Therefore, this technique does not lend itself to a high-throughput for acquiring quantitative measurements of protein content. However, as mentioned previously, this technique provides valuable resolution to determine protein content in specified cell types along with measurements of total nuclear to cytosolic content of transcription factors and/or other protein shuttled between the nucleus and cytosol.

3.5.3 Movement of brain sections hindered the development of the technique

As discussed in this chapter, several technical difficulties were encountered during the development of the immunohistochemical technique. The high levels of polyunsaturated fats (PUFAs) in the brain affected adherence of coronal brain sections to plain glass slides. Thus, considerable time was invested in selecting the appropriate glass slide to mount brain sections. A major obstacle encountered during the development of this quantitative immunohistochemical technique was the movement of the brain sections upon treatment with the DAB- H_2O_2 reaction mix. Brain sections have a high fat content, which hinders their attachment to the glass slide. Although this problem was overcome with the use of Superfrost Plus glass slides, movement of brain sections was still observed, until DAB itself was identified as the major cause for tissue movement. Brains were excised from rats after transcardial perfusion with paraformaldehyde. The cause of this reaction remains to be elucidated, however, pre-incubation of sections with DAB, in the presence ascorbic acid, prevented movement of the section during capture of the DAB- H_2O_2 reaction.

3.5.3 Image processing

To quantify cellular content of a target protein of interest, this technique relies upon image processing to generate nuclear and cellular masks. The generation of any digital mask, whether nuclear or cellular, is dependent upon the clarity of the raw image captured. An intense fluorescence signal, for the desired cellular structure or compartment, ensures the generation of an accurate digital mask. Prior to formalin coating of Superfrost Plus glass slides, a weak fluorescence signal was acquired for endothelial staining (Figure 3.5A). Hence, to observe endothelial staining, the exposure time (over which the image was captured) was increased. However, the high exposure time also increased the background fluorescence captured. Under such circumstances, a clear digital mask could not be generated for analytical purposes, and hence such data sets were excluded from the study. Thus, the success of this technique is

critically dependent on the generation of digital masks for the purpose of protein quantitation in specific cerebral cell types and cellular structures. Failure to generate clear masks significantly limits data analysis.

3.6 Summary and conclusions

In summary, this chapter describes the development of a novel method for quantifying protein content in *ex vivo* tissue sections. For the purpose of this study, the quantitative immunohistochemical study, demonstrated in this chapter, was developed using brain sections, however, this technique is applicable to *ex vivo* sections from other tissues. Compared to immunoblotting protocols, this immunohistochemical technique provides the user with sufficient resolution to detect (1) cell specific protein content, (2) area(s) of protein expression and (3) quantitate protein levels expressed in given cells in the tissue specimen.

In following chapters, the quantitative immunohistochemical technique was employed to study Nrf2 protein content in brain sections from rats either subjected to MCAo and reperfusion injury (Chapter 4) and following pretreatment with dietary isothiocyanate sulforaphane (Chapter 5). Further experiments were also conducted in naïve rats treated with sulforaphane to monitor the time course of expression of Nrf2 and its target heme oxygenase-1 (Chapter 5). Furthermore, co-application of immunofluorescence and quantitative immunohistochemistry has enabled us to report on Nrf2 levels in the infarct core and peri-infarct regions of the stroke-affected hemisphere, noting that such spatial resolution cannot be obtained using immunoblotting techniques.

Hence, to conclude, we have developed the first truly quantitative immunohistochemical technique, to examine the temporal and spatial analysis of protein expression in *ex vivo* brain sections. This technique is not limited to the study of *ex vivo* brain sections, but may also be used to analyse protein expression in other *ex vivo* tissue specimens.

Chapter 4 – Nrf2 and ARE-linked protein expression in rat brains after MCAo injury

Chapter 4 Nrf2 and ARE-linked protein expression in rat brains after MCAo injury

4.1 Introduction

Brain damage following ischaemic stroke is the result of a series of pathophysiological mechanisms (Dirnagl *et al.*, 1999; Candelario-Jalil, 2009), including an excess production of ROS and RNS, with severe consequences for the viability of cells critical for brain function and cerebrovascular permeability (Alfieri *et al.*, 2011; Chen *et al.*, 2011; Fraser, 2011; Woodfin *et al.*, 2011). The brain is at an increased risk of oxidative damage due its high demand for oxygen, high metabolic activity, increased content of unsaturated fatty acids and low intracellular antioxidant capacity (Shohami *et al.*, 1997; Ozkul *et al.*, 2007; Ikonomidou & Kaindl, 2011).

The redox sensitive transcription factor Nrf2 orchestrates the expression of endogenous antioxidant defences against oxidative and nitrosative stress via the upregulation of phase II detoxifying enzymes and antioxidant stress proteins (Ishii *et al.*, 2000). Although activation of Nrf2 has been reported to attenuate brain damage and neurological deficits following stroke (Shah *et al.*, 2007; Yang *et al.*, 2009; Alfieri *et al.*, 2011; Kam *et al.*, 2011; Tanaka *et al.*, 2011), there are no reports that have quantified the temporal and spatial distribution of Nrf2 in nuclear and cytoplasmic compartments of cells in the ischaemic brain.

This chapter investigates the temporal and spatial distribution of Nrf2 in rat brains after MCAo and reperfusion injury, using the novel quantitative DAB immunohistochemical technique described in Chapter 3. In addition, Nrf2-linked antioxidant protein expression was investigated in *ex vivo* brain sections using immunofluorescence techniques.

4.2 Identification of contralateral and stroke-affected hemispheres in *ex vivo* rat brain sections

To assess the success of the transient MCAo surgery and identification of the stroke-affected hemisphere, protein expression of GFAP was assessed in 10µm brain sections from naïve animals (n=3) and animals subjected to 70 min MCAo followed by reperfusion for either 4h (n=3 animals), 24h (n=3) or 72h (n=3). GFAP expression is increased in astrocytes "activated" in neurodegenerative diseases and also in stroke.

Figure 4.1 (left panel, i) shows representative images of *ex vivo* brain sections stained for GFAP using the DAB-H_2O_2 staining method and captured using a digital camera (Nikon DXM-1200C). Captured images were used to generate pseudo colour maps highlighting the extent of damage following 70 min MCAo and 4 – 72h reperfusion injury (Figure 4.1, right panel, ii).

Low expression of GFAP is noted in naïve animals (Figure 4.1 A), however, increased GFAP staining is observed in *ex vivo* brain sections from animals subjected to 70 min MCAo and reperfusion injury (Figure 4.1 B – D). Moreover, GFAP staining is observed only in the right hand side hemisphere of the brain, thus identifying this as the stroke-affected hemisphere. After 4h reperfusion injury GFAP expression is varied throughout the stroke-affected hemisphere (Figure 4.1 Bi). Following 24h reperfusion injury a prominent upregulation of GFAP is visible in the right hemisphere (Figure 4.1 Ci), which is similar after 72 h reperfusion injury (Figure 4.1 Di). The pseudo colour maps for GFAP staining in *ex vivo* whole brain sections demonstrate a time dependent increase in GFAP protein expression following MCAo and reperfusion (Figure 4.1 B – Dii).

The stroke-affected hemisphere comprises of necrotic tissue, which forms the infarct core. Tissue at an increased risk of death upon reperfusion injury is defined as the peri-infarct region. GFAP is upregulated on astrocytes as a protective response to form a glial scar to prevent the volume of tissue damage from increasing. Due to the varied expression of GFAP after 4h reperfusion injury, the stroke core and peri-infarct regions could not be defined. GFAP expression may be the limiting factor in the identification of the peri-infarct and infarct core regions following 70 min MCAo and 4h reperfusion. The use of other immunohistochemical markers, such as microtubule-associated protein 2 (MAP2) may have allowed for delination of infarct core regions.

Fluorescence staining for GFAP in brain sections from animals subjected to 70 min MCAo and 24 h reperfusion injury revealed increased expression in a ring-like structure surrounding an area where little or no GFAP expression was detected (Figure 4.2). Thus, the infarct core was defined as an area where no GFAP expression was detected. Furthermore, peri-infarct regions were defined as areas where an increase in GFAP expression surrounded the infract core and cerebral cortex of the stroke-affected hemisphere.

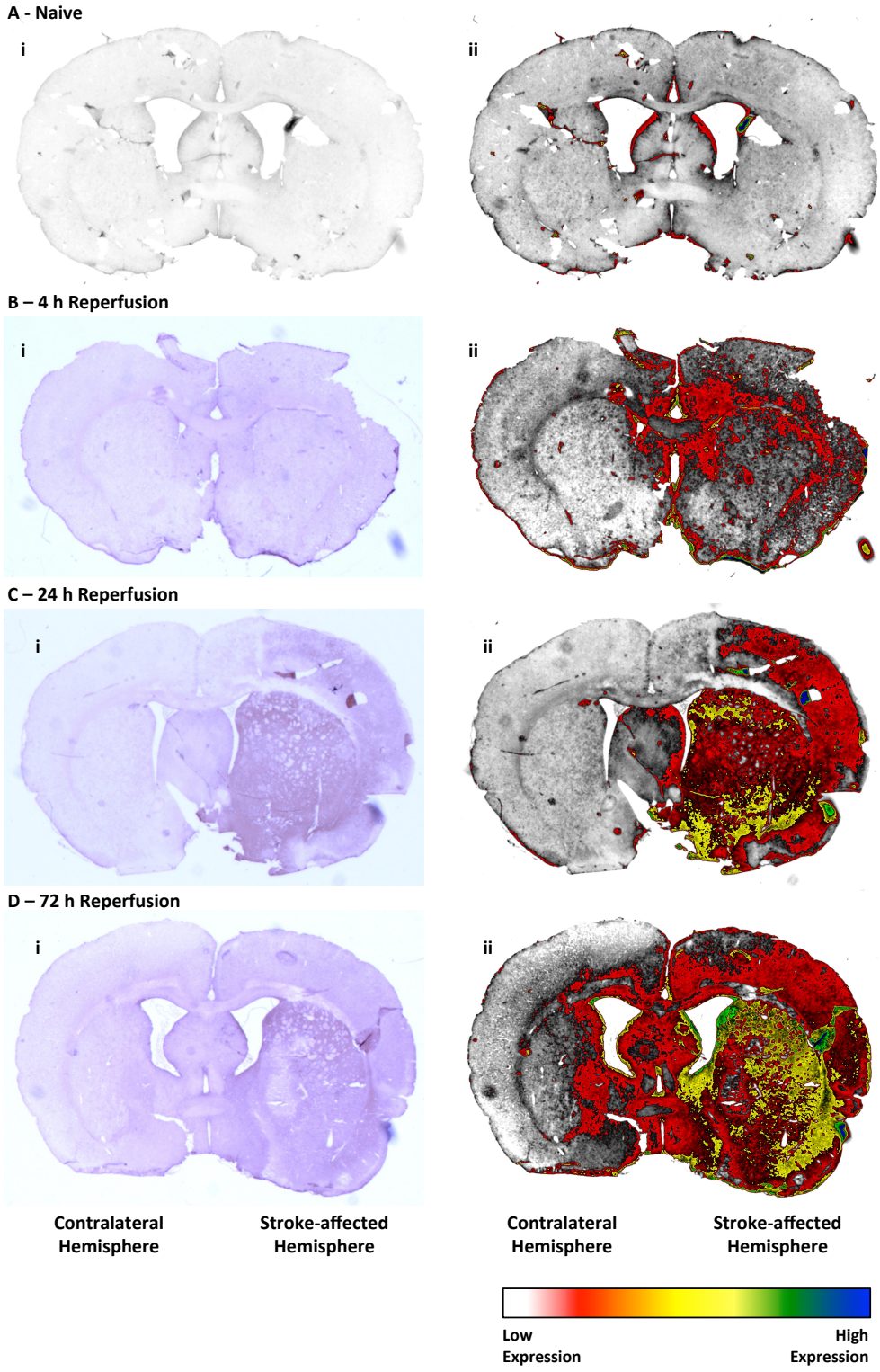

Figure 4.1 Identification of the stroke-affected hemisphere in ex vivo rat brain sections. Coronal brain sections (10 µm) were stained with anti-GFAP primary antibody and visualised by DAB immunohistochemistry. Representative photographs of DAB staining for GFAP in brain sections from (A) naïve rats and in rats subjected to 70 min MCAo and (B) 4h, (C) 24h and (D) 72h reperfusion injury (Left-hand panel, i). Pseudo colours maps from the captured DAB stained images showing the extent of damage following MCAo and reperfusion injury (right-hand panel, ii). Cooler colours designate areas of intense GFAP staining.

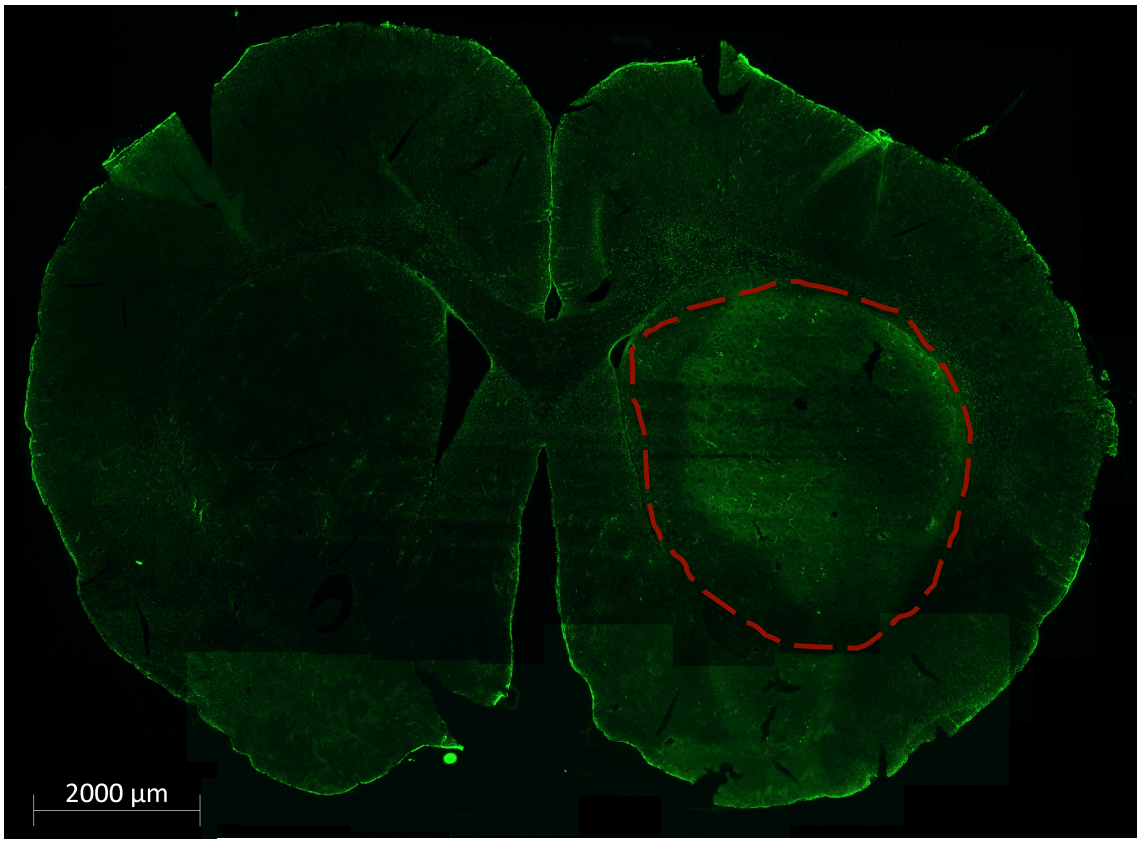

Figure 4.2 Identification of core and peri-infarct regions in the stroke-affected hemisphere after 70 min MCAo and 24h reperfusion injury.
Coronal brain sections (10µm) were stained with rabbit anti-GFAP primary antibody and donkey anti-rabbit Alexa-fluor 488 conjugated secondary antibody and visualised by fluorescence microscopy. Representative image of the whole brain generated by tiling captured images. The area of GFAP expression is observed in the right hemisphere. The red line indicates the region where an increase in GFAP is observed. Upregulated GFAP expression surrounds an area in the centre where no staining is detectable, which is defined as the infarct core in this study. Scale bar represents 2000 µm.

4.3 Temporal changes in nuclear to cytoplasmic ratio of Nrf2 following MCAo and reperfusion

Nrf2 protects of the brain against ischaemia-induced oxidative stress, however, to understand and define the temporal and cellular distribution of Nrf2 within the brain following MCAo and reperfusion injury, quantitative immunohistochemistry was employed to measure Nrf2 protein content in different cellular compartments (nuclear and cytoplasmic) as well as different cerebral cell types. Furthermore, based on the anatomical knowledge of the ischaemic brain depicted in Figure 4.2, the temporal and spatial distribution of Nrf2 was also defined in core and peri-infract regions of the stroke affected hemisphere and contralateral regions of ischaemic brain following MCAo and 4 – 72h reperfusion injury.

4.3.1 Time course of nuclear to cytoplasmic distribution of Nrf2 after ischaemia and reperfusion injury

Nrf2 translocates to the nucleus following increased oxidative or electrophilic stress, upregulating the expression of antioxidant proteins and phase II detoxifying enzymes (Ishii *et al.*, 2000; Ishii *et al.*, 2004). The distribution of Nrf2 between nuclear and cytoplasmic compartments was assessed in *ex vivo* brain sections from rats subjected to 70 min MCAo and reperfusion injury. Pseudo colours images of Nrf2 expression were generated using the quantitative immunohistochemical technique, where warmer pseudo colours indicate regions of high Nrf2 expression. Low expression of Nrf2 was detected in the naïve brain (Figure 4.3 A), however, following 70 min MCAo and reperfusion, a visual increase is noted after 4h reperfusion (Figure 4.3 B) with highest levels of Nrf2 protein expression observed after 24h reperfusion (Figure 4.3 C) compared to 72h reperfusion injury (Figure 4.3 D). The use of a digital nuclear mask generated from the complimentary DAPI image allowed us to determine the nuclear localisation of Nrf2. Compared to nuclei identified in naïve sections (Figure 4.3 B), increased nuclear localisation of Nrf2 was observed following MCAo and reperfusion injury (Figure 4.3 B-D), with a peak in nuclear Nrf2 content detected after 24h reperfusion injury (Figure 4.3 C). Furthermore, after 4h and 72h reperfusion injury, increased Nrf2 levels were detected in the cytoplasmic compartment, as indicated by the warmer pseudo colours surrounding the nuclei represented in purple (Figure 4.3 B and D). Staining for Nrf2 in cytoplasmic compartments was higher after 24h reperfusion compared to 4h and 72h reperfusion (Figure 4.3 C). Warmer pseudo colours detected in nuclear structures indicate greater nuclear Nrf2 content after 24h reperfusion injury.

Figure 4.3 Nuclear and cytoplasmic distribution of Nrf2 in the stroke-affected hemisphere following 70 min MCAo and reperfusion injury.
Coronal rat brain sections (10 µm) were incubated with rabbit anti-Nrf2 primary antibody and anti-rabbit biotinylated secondary antibody. Sections were reacted with DAB-H_2O_2 and images captured to quantify Nrf2 expression in *ex vivo* brain sections from (**A**) naïve animals and animals subjected to 70 min MCAo and (**B**) 4h, (**C**) 24h or (**D**) 72h reperfusion injury. Pseudo colour images were generated for Nrf2 expression in *ex vivo* brain sections following quantitative DAB (Left panels). Nuclear structures are represented in purple to highlight cytoplasmic distribution of Nrf2 (Center panels). A nuclear mask was generated using the respective DAPI stained image and superimposed on the pseudo colour image for Nrf2 demonstrating nuclear distributon of Nrf2 (Right panels). Scale bar represents 5µm. (**E**) Brain map showing the location of acquired images shown in **A**-**D**.

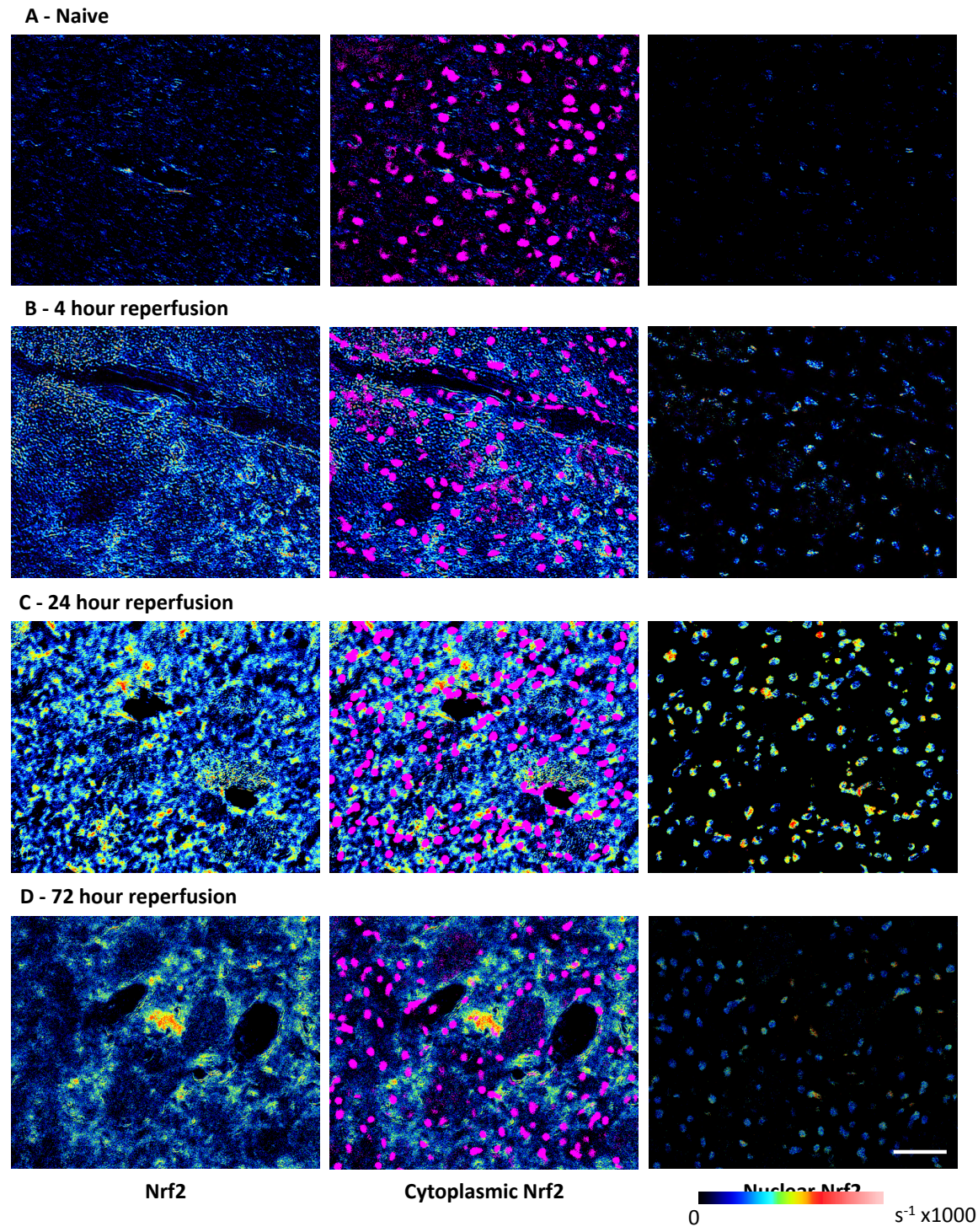
A - Naive
B - 4 hour reperfusion
C - 24 hour reperfusion
D - 72 hour reperfusion
Nrf2
Cytoplasmic Nrf2
0
s-1 x1000

E

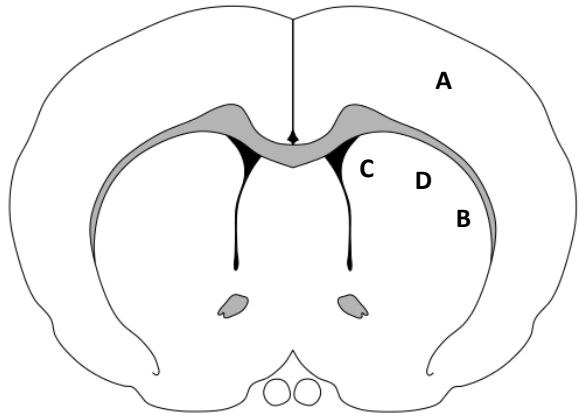
A
C
D
B

The nuclear to cytoplasmic ratio of Nrf2 was determined for each identified cell in brain sections from animals subjected to 70 min MCAo and reperfusion injury. Nuclear to cytoplasmic ratios greater than 1.0 indicate increased nuclear Nrf2 content, whereas values less than 1 indicate greater cytoplasmic Nrf2 content. After 4h reperfusion injury, no difference was observed between nuclear to cytoplasmic ratio of cells in the stroke-affected hemisphere and contralateral hemisphere (Figure 4.4 A), and furthermore, Nrf2 content was greater in cytoplasmic compartments (ratio < 1.0). Following 24h reperfusion injury, the nuclear to cytoplasmic ratio for Nrf2 was greater in the stroke-affected compared to the contralateral hemisphere (ratio >1.0), however, an increase in nuclear Nrf2 was noted in cells identified in both hemispheres (Figure 4.4 B). After 72h reperfusion injury, the nuclear to cytoplasmic ratio for Nrf2 was similar in cells in contralateral and stroke-affected hemispheres (Figure 4.4 C).

The mean nuclear to cytoplasmic ratio of Nrf2 was determined on a per cell and per animal basis (Figure 4.5). Although the trend of Nrf2 nuclear to cytoplasmic ratio was similar between the two analyses, no significance was noted on a per animal basis. Nuclear to cytoplasmic Nrf2 ratio was similar in contralateral (0.96 ± 0.09, n=3 animals) and stroke-affected hemispheres (0.95 ± 0.04, n=3 animals) after 4h reperfusion injury. Following 24h reperfusion injury, the mean nuclear to cytoplasmic ratio of Nrf2 increased compared to animals subjected to 4h reperfusion injury, with increased nuclear localisation in the stroke-affected hemisphere (1.08 ± 0.04, n=3 animals) compared to the contralateral hemisphere (1.01 ± 0.02, n=3 animals), however results were not statistically significant. After 72h reperfusion injury, no difference was noted in the nuclear to cytoplasmic ratio between contralateral (0.95 ± 0.05, n=3 animals) and stroke affected (0.96 ± 0.03, n=3 animals) hemispheres, and moreover, mean values were similar to those observed in brain sections from animals subjected to 4h reperfusion injury. Furthermore, no statistical significance was noted between the mean nuclear to cytoplasmic Nrf2 ratio for the control group (0.95 ± 0.01, n=5 animals) compared to any experimental group. As no difference was observed in Nrf2 nuclear to cytoplasmic ratios between sham and naïve rats (data not shown), the data was combined and shown as the control group.

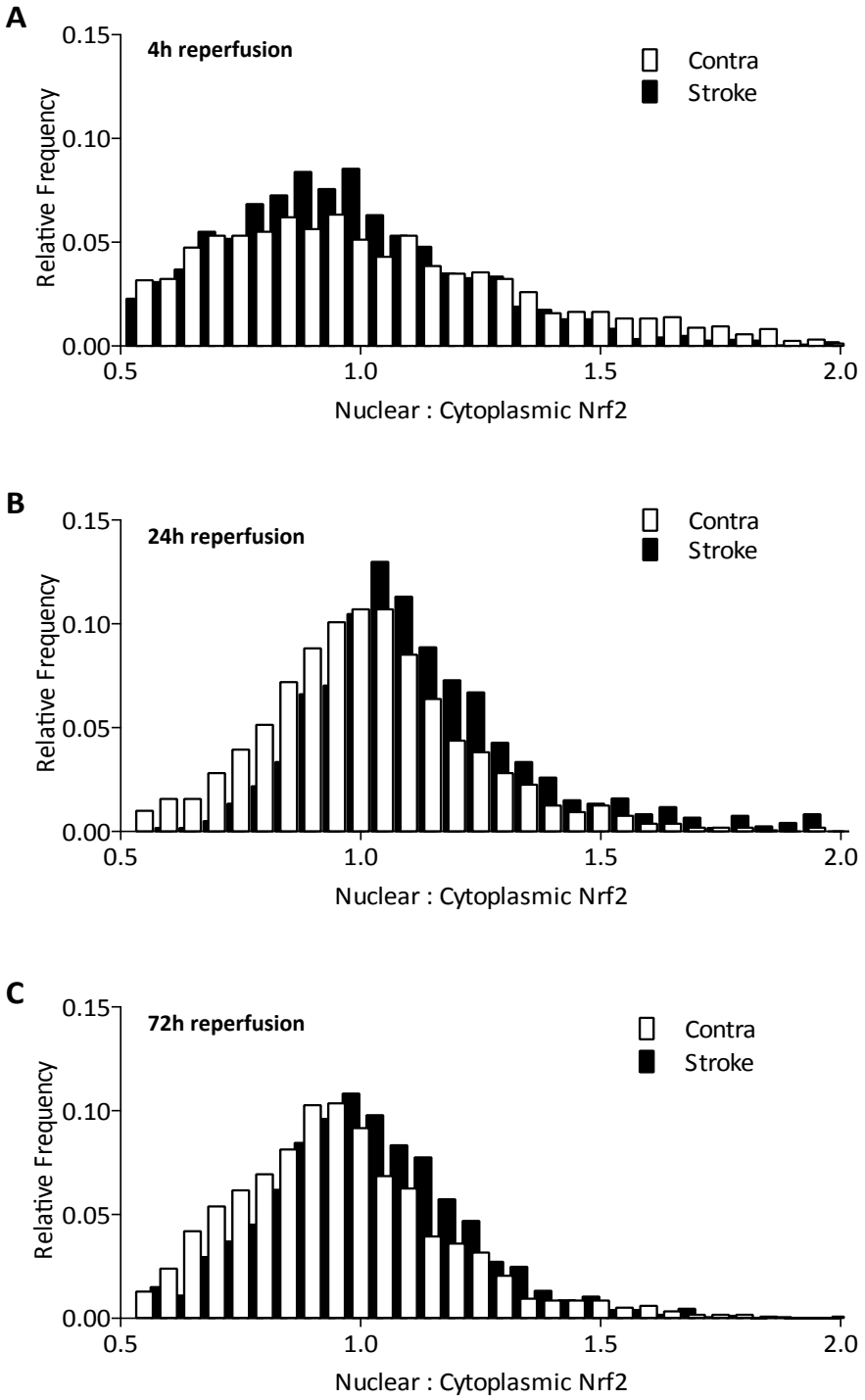

Figure 4.4 Temporal changes in nuclear to cytoplasmic distribution of Nrf2 in brain cells examined after 70 min MCAo and reperfusion injury.

The nuclear to cytoplasmic ratio of Nrf2 was determined for each respective cell defined by the nucleus and a 4μm ring taken to be its respective cytoplasm. Histograms show the nuclear to cytoplasmic ratio of the redox sensitive transcription Nrf2 in the contralateral (white) and stroke-affected (black) hemispheres after MCAo and (**A**) 4 hours reperfusion injury (1580 cells from contralateral and 2633 cells from the stroke-affected hemisphere) (**B**) 24 hours reperfusion injury (1675 cells from contralateral and 1194 cells from stroke-affected regions) and (**C**) 72 hours reperfusion injury (1168 cells from contralateral and 1725 cells from stroke-affected regions). Data attained from brain sections from n=3 animals per group, with sections obtained from the forebrain to midbrain of MCAo animals. The stroke bars represent cells counted in the peri-infarct, infarct core and cortex of the stroke-affected hemisphere.

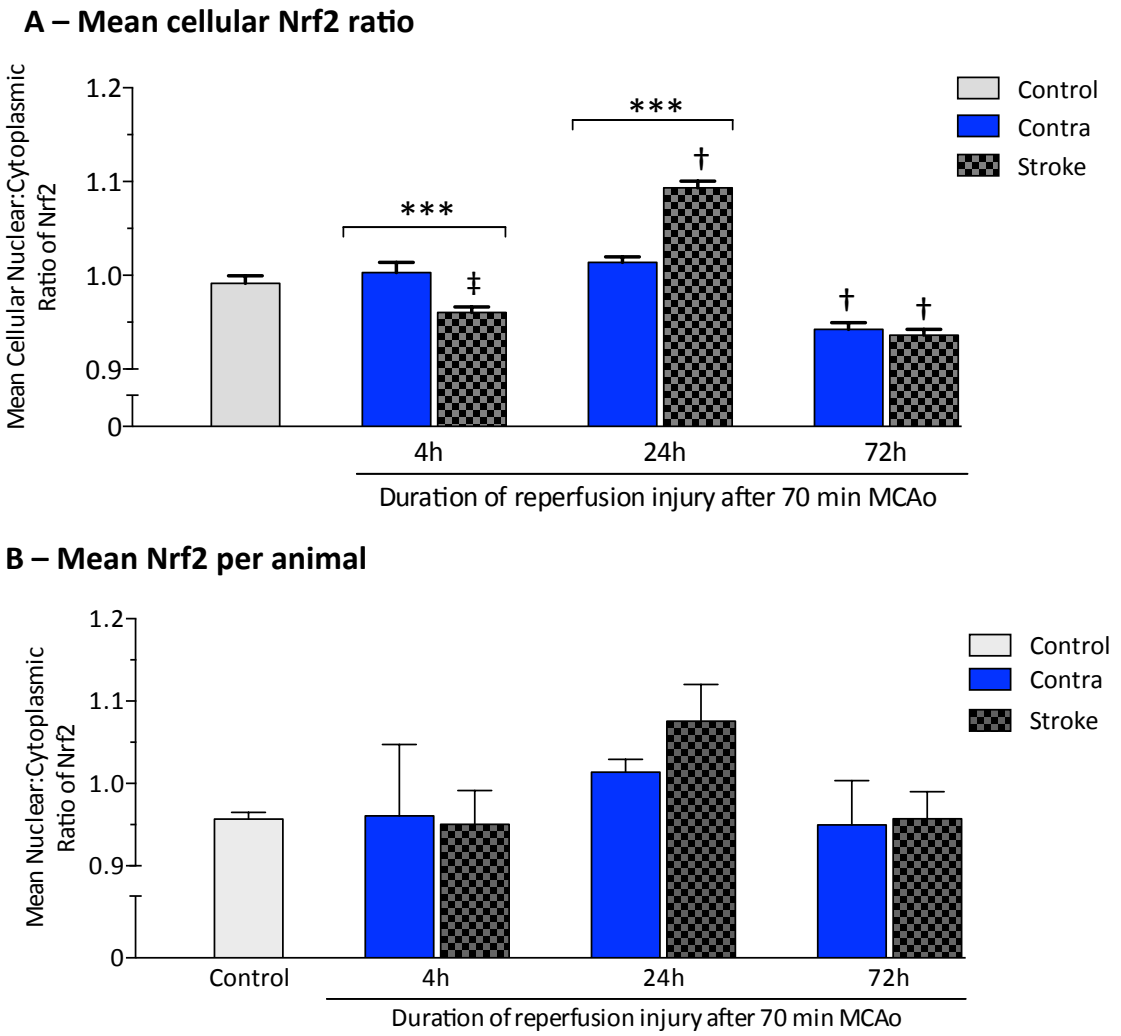

Figure 4.5. Summary of nuclear to cytoplasmic ratios of Nrf2 after MCAo and reperfusion.

Summary of mean cellular nuclear to cytoplasmic Nrf2 ratio in the control animals (n = 3199 cells) and in the contralateral, and stroke-affected hemisphere of animals subjected to 70 min MCAo and reperfusion injury for 4h (n = 1580 cells in contra, and 2633 in stroke-affected hemisphere), 24h (1194 cells in contra, and 1675 cells in stroke-affected hemisphere) or 72h (1168 cells in contra and 1725 cells in stroke-affected hemisphere). The mean ratio for nuclear to cytoplasmic Nrf2 was calculated on (**A**) a per cell basis or (**B**) per animal basis (n = 5 animals per control group, and n = 3 animals per experimental group). Data denote mean ± S.E.M, *** P<0.001, ‡ P<0.01 and † P<0.001 versus control brains. Coronal brain sections used for analysis were obtained from the forebrain to midbrain of MCAo animals. The stroke bars represent cells counted in the peri-infarct, infarct core and cortex of the stroke-affected hemisphere.

4.3.2 *Spatial distribution of Nrf2 protein content in contralateral, core and peri-infarct regions of the ischaemic rat brain*

Nuclear translocation of Nrf2 is critical in the upregulation of Nrf2-linked regulated antioxidant genes. Activation and stabilisation of Nrf2 is required for accumulation within the cell and nuclear translocation, The time course of Nrf2 activation and its cellular distribution within the brain was determined brain after MCAo and reperfusion injury.

The quantitative immunohistochemical technique was employed to quantify total cellular Nrf2 levels following determination of Nrf2 content in nuclear and cytoplasmic compartments. Based on GFAP staining of astrocytic activation after MCAo and reperfusion, cellular Nrf2 content was determined in peri-infarct and infarct core regions of the stroke-affected hemisphere from brains subjected to reperfusion for either 24 or 72h. Pseudo colour images were generated following the capture and quantitation of the DAB-H_2O_2 reaction to visually represent Nrf2 expression within the ischaemic rat brain (Figure 4.6). Warmer pseudo colours indicate higher expression of Nrf2. After 4h reperfusion, an increase in Nrf2 expression was observed in the stroke-affected hemisphere compared to contralateral regions (Figure 4.6 A). Following 24h reperfusion, Nrf2 expression was detected in peri-infarct and infarct core regions of the stroke-affected hemisphere, with a notable increase in Nrf2 expression observed in peri-infarct regions of the stroke-affected hemisphere compared to the infarct core and contralateral regions (Figure 4.6 B). Notably, staining for Nrf2 was greater in the contralateral region in sections from animals subjected to 70min MCAo and 24h reperfusion compared to animals subjected to 4 and 72h reperfusion (Figure 4.6 A and B). Furthermore, it was interesting to note that staining for Nrf2 protein remained elevated in peri-infarct regions compared to the infarct core after 72h reperfusion injury (Figure 4.6 C). Interestingly, a clear decrease in Nrf2 staining is observed in peri-infarct regions between 24h and 72h (Figure 4.6 B and C).

Figure 4.6 Distribution of Nrf2 in sub-anatomical regions of the ischaemic brain following MCAo and reperfusion injury.
10µm coronal brain sections from rats subjected to MCAo and reperfusion injury were incubated with rabbit anti-Nrf2 primary antibody and anti-rabbit biotinylated secondary antibody. Incubated sections were reacted with DAB-H_2O_2 and images captured to quantify Nrf2 expression in *ex vivo* brain sections. Pseudo colour images were generated to show Nrf2 expression in the contralateral hemisphere and stroke-affected hemisphere following (A) 70 min MCAo and 4h reperfusion injury and in the contralateral hemisphere and the peri-infarct and infarct core regions of the stroke-affected hemisphere following 70 min MCAo and (B) 24h and (C) 72h reperfusion injury. Scale bar represents 5µm. Brain maps show the location of acquired images from the contralateral hemisphere (■), stroke affected hemisphere (■), and peri-infarct (■) and infarct core (■) of the stroke affected hemispheres in rats subjected to 24h and 72h reperfusion after 70 min MCAo.

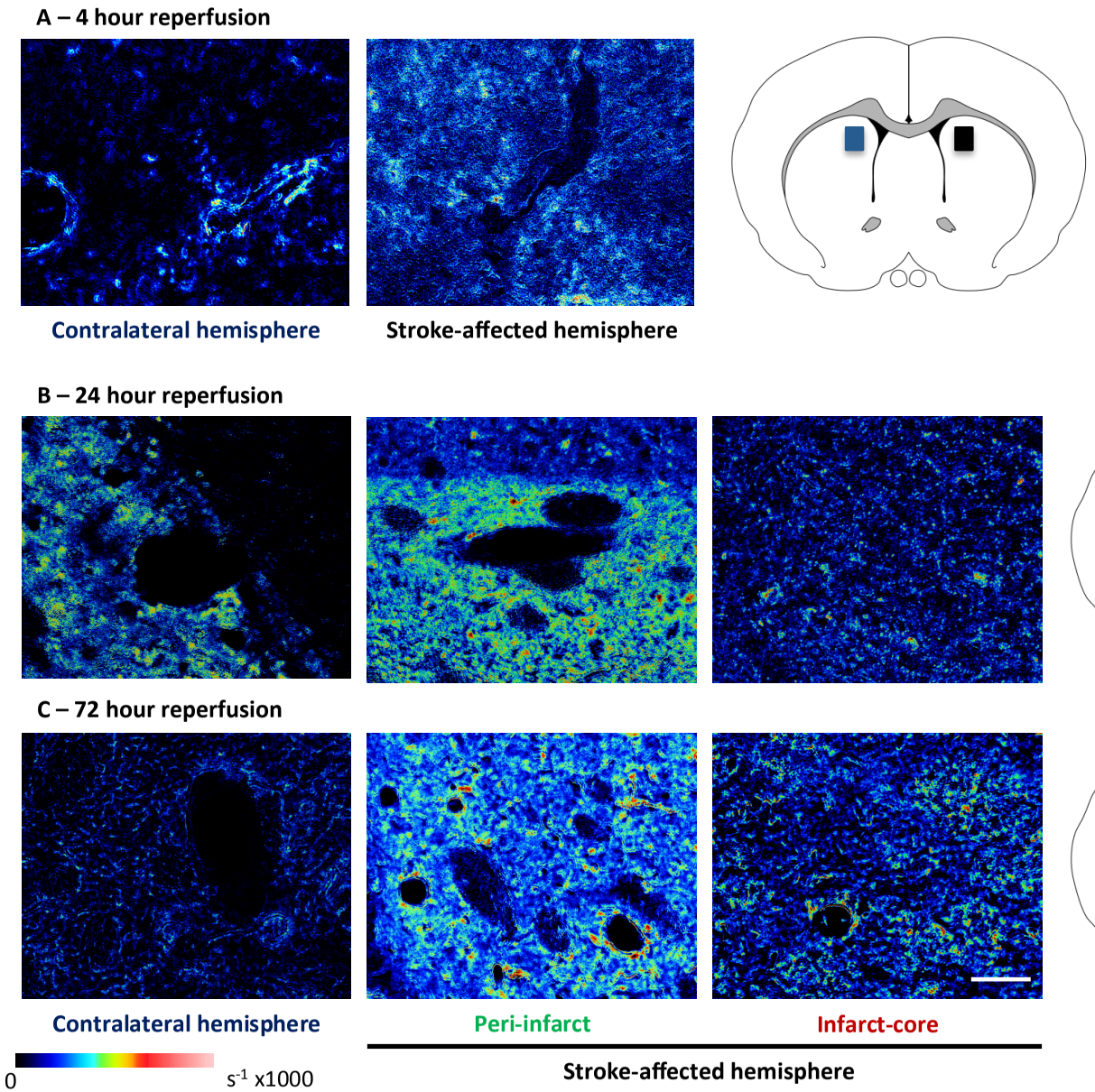
A – 4 hour reperfusion
Contralateral hemisphere
Stroke-affected hemisphere
B – 24 hour reperfusion
C – 72 hour reperfusion
Contralateral hemisphere
Peri-infarct
Infarct-core
Stroke-affected hemisphere
0
s-1 x1000

Total cellular Nrf2 content was determined by assessing Nrf2 localised in the nucleus, using a nuclear mask generated from the respective DAPI image, and a 10µm ring drawn around each nuclei to define its respective cytosol. The values for Nrf2 localised in each respective compartment were summed to give a value for total cellular Nrf2 content. Histograms were drawn showing the Nrf2 content in each identified cell in brain sections from animals subjected MCAo and reperfusion injury for 4h, 24h and 72h (Figure 4.7). After 4h reperfusion injury, a slight increase in cellular Nrf2 content was noted in cells resident in the stroke-affected compared to the contralateral hemisphere (Figure 4.7 A), however, following 24h reperfusion injury, a dramatic increase was observed in Nrf2 content in cells in stroke-affected regions. Moreover, Nrf2 content was greater in cells identified in the peri-infarct region compared to the infarct core. After 72h reperfusion, cellular Nrf2 content decreased in the infarct core to levels observed in the contralateral region (Figure 4.7 C). A notable decrease in cellular Nrf2 content in the peri-infarct region was also observed after 72h reperfusion compared to 24h, however, Nrf2 levels remained elevated in the peri-infarct regions compared to the infarct core and contralateral regions (Figure 4.7 C).

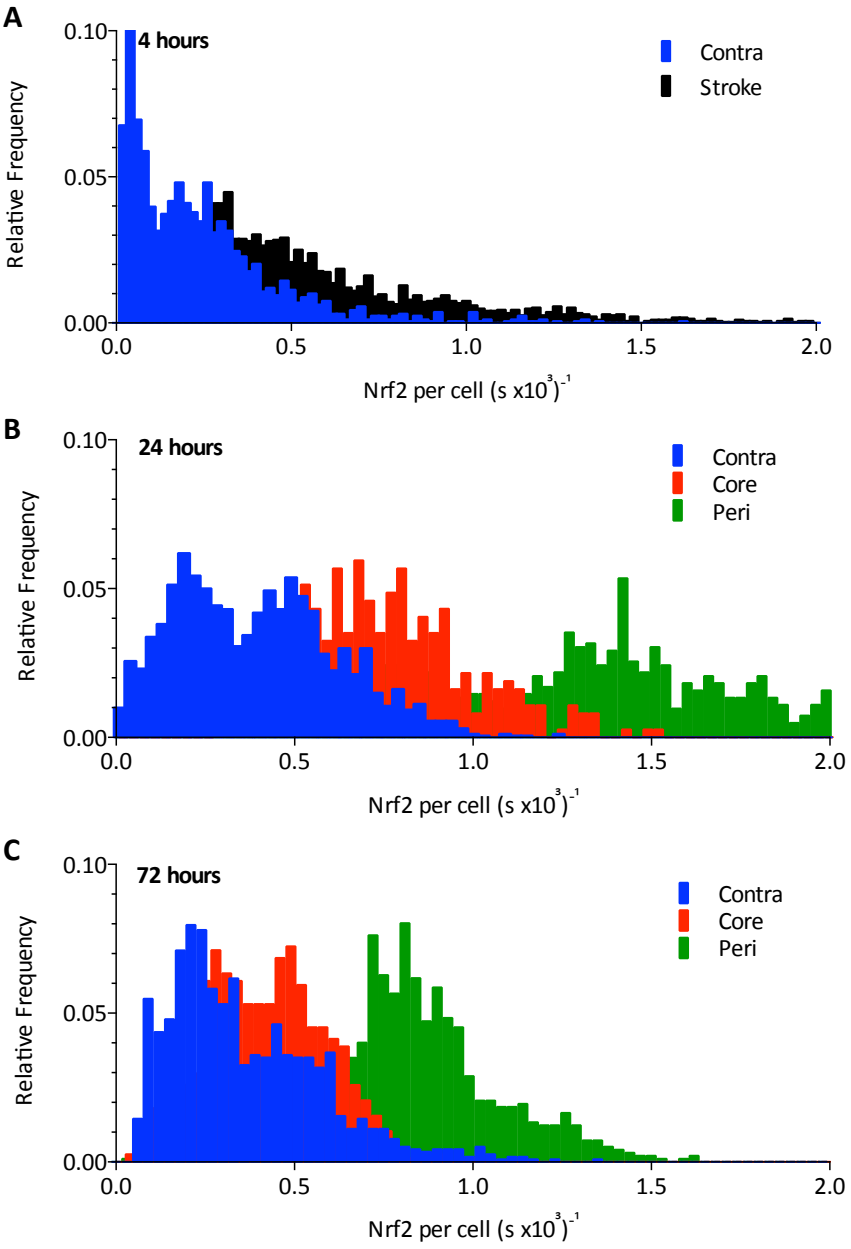

Figure 4.7 Total cellular distribution of Nrf2 content after 70 min MCAo and reperfusion injury.

The total cellular Nrf2 content was determined for each cell by summing of Nrf2 contents in nuclei and their respective cytoplasm. Histograms show the total Nrf2 content in each identified cell following 70 min MCAo and (**A**) 4h (1619 cells in contralateral and 2642 cells in stroke affected hemisphere), (**B**) 24h (1675 cells in contralateral, 924 cells in peri-infarct and 370 cells in infarct core), and (**C**) 72h reperfusion injury (1168 cells in contralateral, 943 cells in per-infarct and 622 cells in the infarct core). Total cellular Nrf2 content was measured in contralateral regions (blue) and in the stroke-affected hemisphere (black) following 4h reperfusion injury, and in peri-infarct (green) and infarct core (red) regions of the stroke-affected hemisphere following 24h and 72h reperfusion injury. The cells analysed are form cronoal section obtained from the forebrain to the midbrain of MCAo animals (n = 3 animals per experimental group).

The mean Nrf2 content was determined on a cellular and per animal basis. Although a similar trend is observed for both mean Nrf2 content after-both analyses, the observed standard error and the levels of significance are different between the two sets (Figure 4.9).

The mean Nrf2 content per cell in stroke and contralateral brain hemispheres for each individual animal subjected to 70 min MCAo and 4, 24, or 72h reperfusion injury was calculated. Following 4h reperfusion injury, cellular Nrf2 content in the contralateral hemisphere (0.21 ± 0.07 (s $x10^3)^{-1}$, n=3 animals) was similar to that observed in control brains (0.28 ± 0.08 (s $x10^3)^{-1}$, n=5 animals), however, a significant increase in Nrf2 content is observed in the stroke-affected hemisphere (0.51 ± 0.06 (s $x10^3)^{-1}$, n=3 animals) after 4h reperfusion (Figure 4.8 A and Figure 4.9 B, $P<0.001$). Notably, the significance of this trend is greater when mean cellular Nrf2 content was calculated ($P<0.001$, Figure 4.9 A).

After 24h reperfusion injury, total cellular Nrf2 content was significantly elevated in the peri-infarct region (1.35 ± 0.14 (s $x10^3)^{-1}$, n=3 animals) compared to the infarct core (0.68 ± 0.14 (s $x10^3)^{-1}$, n=3 animals, $P<0.01$) and contralateral regions (0.38 ± 0.13 (s $x10^3)^{-1}$, n=3 animals, $P<0.001$, Figure 4.7 B and Figure 4.9 B). Statistical analysis of mean cellular Nrf2 revealed the same level of statistical significance between all regions of the ischaemic brain following 24h reperfusion injury ($P<0.001$, Figure 4.9 A).

After 72h reperfusion injury (Figure 4.7 C and Figure 4.9 B), cellular Nrf2 content remained significantly elevated in the peri infarct region (0.85 ± 0.05 (s $x10^3)^{-1}$, n=3 animals) compared to the infarct core (0.41 ± 0.02 (s $x10^3)^{-1}$, $P<0.01$, n=3 animals) and contralateral (0.37 ± 0.06 (s $x10^3)^{-1}$, $P<0.01$, n=3 animals) brain regions. Cellular analysis yielded similar results, although statistical significance was greater between the two compared groups ($P<0.001$, Figure 4.9A). Furthermore, it is noteworthy that cellular Nrf2 content in the infarct core was similar to contralateral regions after 72h reperfusion (Figure 4.9).

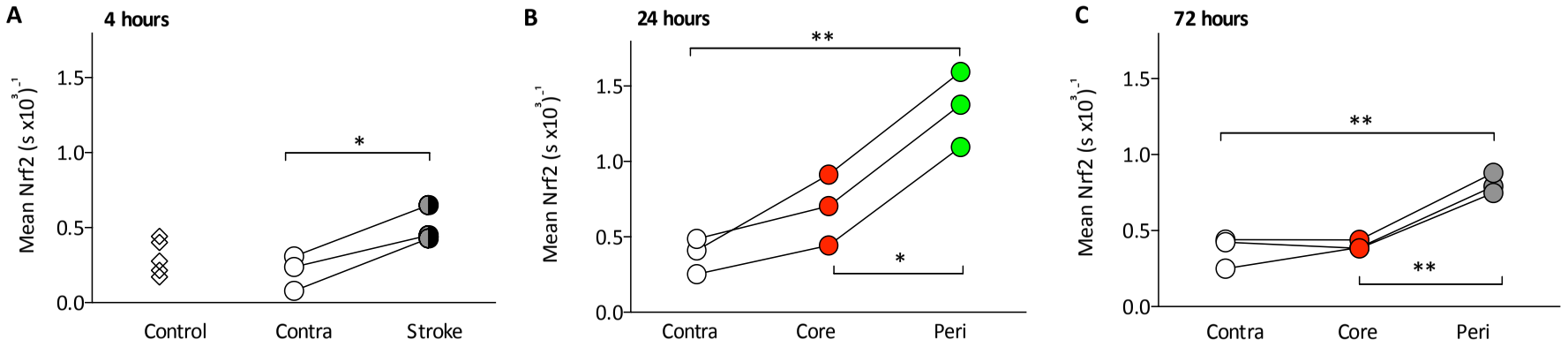

Figure 4.8 Temporal and spatial changes in total cellular Nrf2 content in brain cells following MCAo and reperfusion injury.
Total Nrf2 content was calculated on a cellular basis for stroke-affected and contralateral hemisphere in three sets of animals. Paired comparisons are shown for each animal subjected to 70 min MCAo and (A) 4h, (B) 24h and (C) 72h reperfusion injury. Additional data showing total cellular Nrf2 content in control animals not undergoing MCAo surgery is represented in (A) by diamonds. Data denote mean ± S.E.M., n=5 animals in control group and n=3 animals per MCAo experimental group * $p<0.05$, ** $p<0.01$.

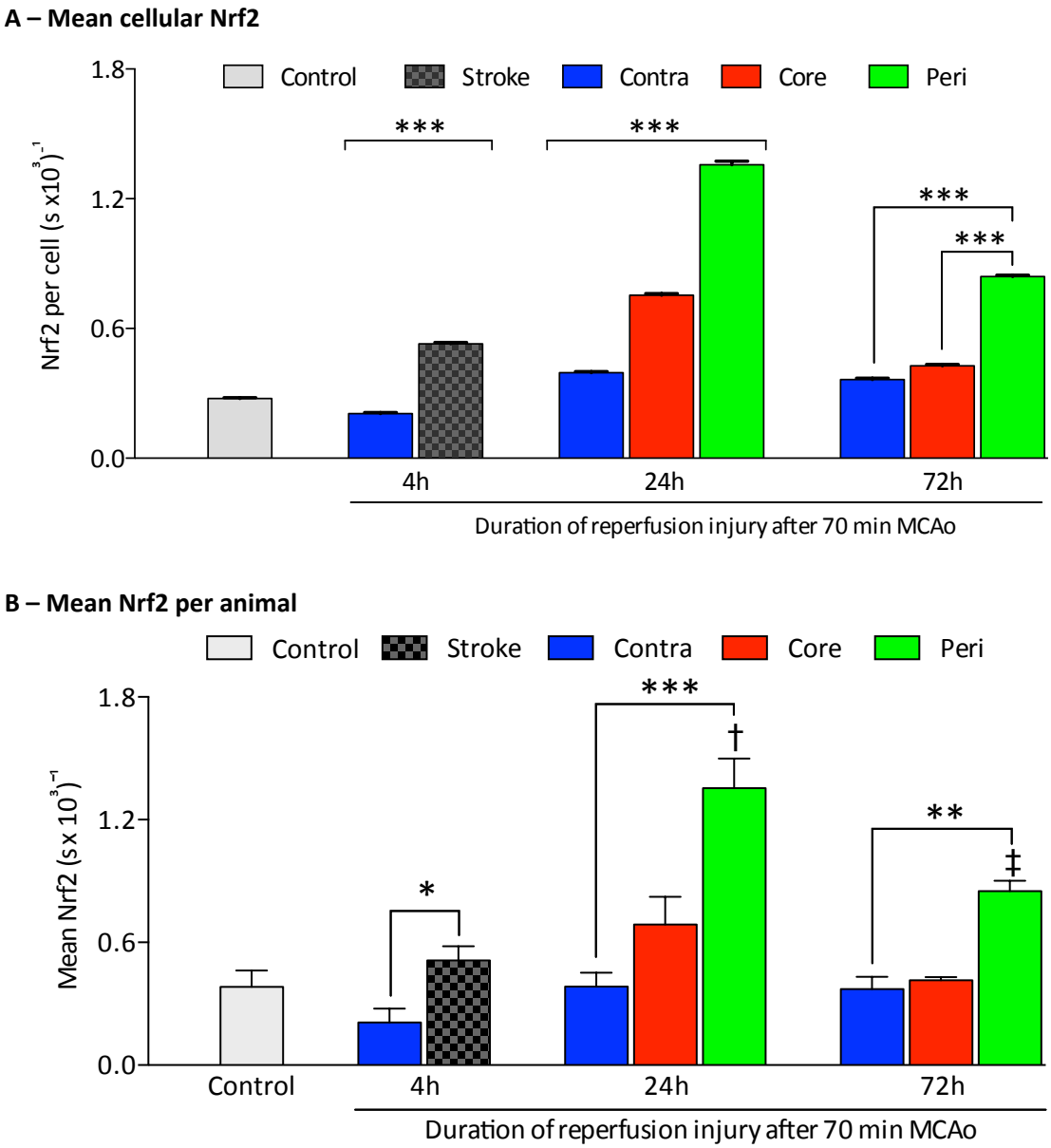

Figure 4.9 Summary of temporal and spatial changes in total cellular Nrf2 content in brain cells following MCAo and reperfusion injury.

Bar graphs show the summary of mean Nrf2 content, determined on a (**A**) per cell, or (**B**) per animal basis in control rats and in the contralateral, and stroke-affected regions of rats subjected to 70 min MCAo and reperfusion injury. (**A**) Mean Nrf2 content per cell from different brain regions was determined using 1500 – 3000 cells from 5 animals in the control group and 3 animals per experimental group. Data denote mean ± S.E.M., *** P<0.001. (**B**) Mean Nrf2 content per animal was determined from different brain regions. Data denote mean ± S.E.M., n=5 animals in control group and n=3 animals per MCAo experimental group * p<0.05, **p<0.01, *** p<0.001, † p<0.05 peri-infarct vs infarct core following 24h reperfusion injury, ‡ p<0.01 peri-infarct vs infarct core following 72h reperfusion injury. Coronal brain sections used for analysis were obtained from the forebrain to midbrain of MCAo animals. The stroke bars represent cells counted in the peri-infarct, infarct core and cortex of the stroke-affected hemisphere in animals subjected to 4h reperfusion after MCAo.

4.3.3 Endothelial specific distribution of Nrf2 following MCAo and reperfusion injury

Stroke research has focused on the role and importance of Nrf2 mediated protection in astrocytes and neurons, however, little is known regarding the expression of Nrf2 within the cerebrovascular endothelium and furthermore, the time course of Nrf2 expression in the endothelium following stroke. Low levels of Nrf2 were detected in the cerebrovascular endothelium of brain sections from naïve animals (Figure 4.10 A). However, in rats following 70 min MCAo and 4h reperfusion injury, an increase in endothelial Nrf2 expression was noted in both contralateral and stroke-affected regions (Figure 4.10 B). This increase in endothelial Nrf2 was greater in the stroke-affected regions following 24h reperfusion injury, and more so in peri-infarct regions compared to the infarct core (Figure 4.11 A). An increase is also noted in endothelial Nrf2 content in stroke-affected regions following 72h reperfusion injury (Figure 4.11 B).

Histograms demonstrate a trend for an increase in endothelial Nrf2 content, similar to that observed for all cerebral cells (Figure 4.12). The trend of endothelial Nrf2 content was similar between contralateral and stroke-affected hemisphere after 4h reperfusion injury (Figure 4.12 A). Notably, endothelial Nrf2 content was greater in the peri-infarct region of the stroke-affect hemisphere compared to the infarct core or contralateral regions (Figure 4.12 B and C).

Quantitation of endothelial Nrf2 content per RECA1 positive region revealed an increase in levels in the contralateral (0.63 ± 0.03) and stroke-affected hemisphere (1.03 ± 0.03) compared to control (0.18 ± 0.01) after 4h reperfusion injury (Figure 4.13 A). Endothelial Nrf2 content was greater in the peri-infarct (1.32 ± 0.02) and infarct core (0.80 ± 0.02) compared to contralateral regions (0.38 ± 0.01) after 24h reperfusion injury (Figure 4.13 A). Endothelial Nrf2 content decreased in all regions of the ischaemic brain after 72h reperfusion injury, however maintained a similar trend with increased endothelial Nrf2 content noted in the peri-infarct (0.70 ± 0.02) and infarct core (0.41 ± 0.01) compared to the contralateral region (0.30 ± 0.01, Figure 4.13). A similar trend for endothelial Nrf2 content was also noted following analysis on a per animal basis, however no significance was observed.

Figure 4.10 Endothelial distribution of Nrf2 in naïve animals and after 70 min MCAo and 4h reperfusion injury.

Endothelial distribution of Nrf2 was determined in *ex vivo* coronal brain sections (10 μm) from (A) naïve animals or after (B) 70 min MCAo and 4h reperfusion injury. Nrf2 content was determined using quantitative immunohistochemistry and pseudo colour images generated to show expression of Nrf2 in brains sections (Left panel). Fluorescence images of the endothelium were captured following staining with mouse anti-RECA1 primary antibody and donkey anti-mouse Alexa-fluor 555 (Middle panel). Captured fluorescence endothelial images were used to generate an endothelial mask, which was superimposed onto the Nrf2 image to show Nrf2 distribution in the cerebrovascular endothelium (Right panel). Scale bar represents 5μm. Black squares (■) in brain maps show the location of acquired images.

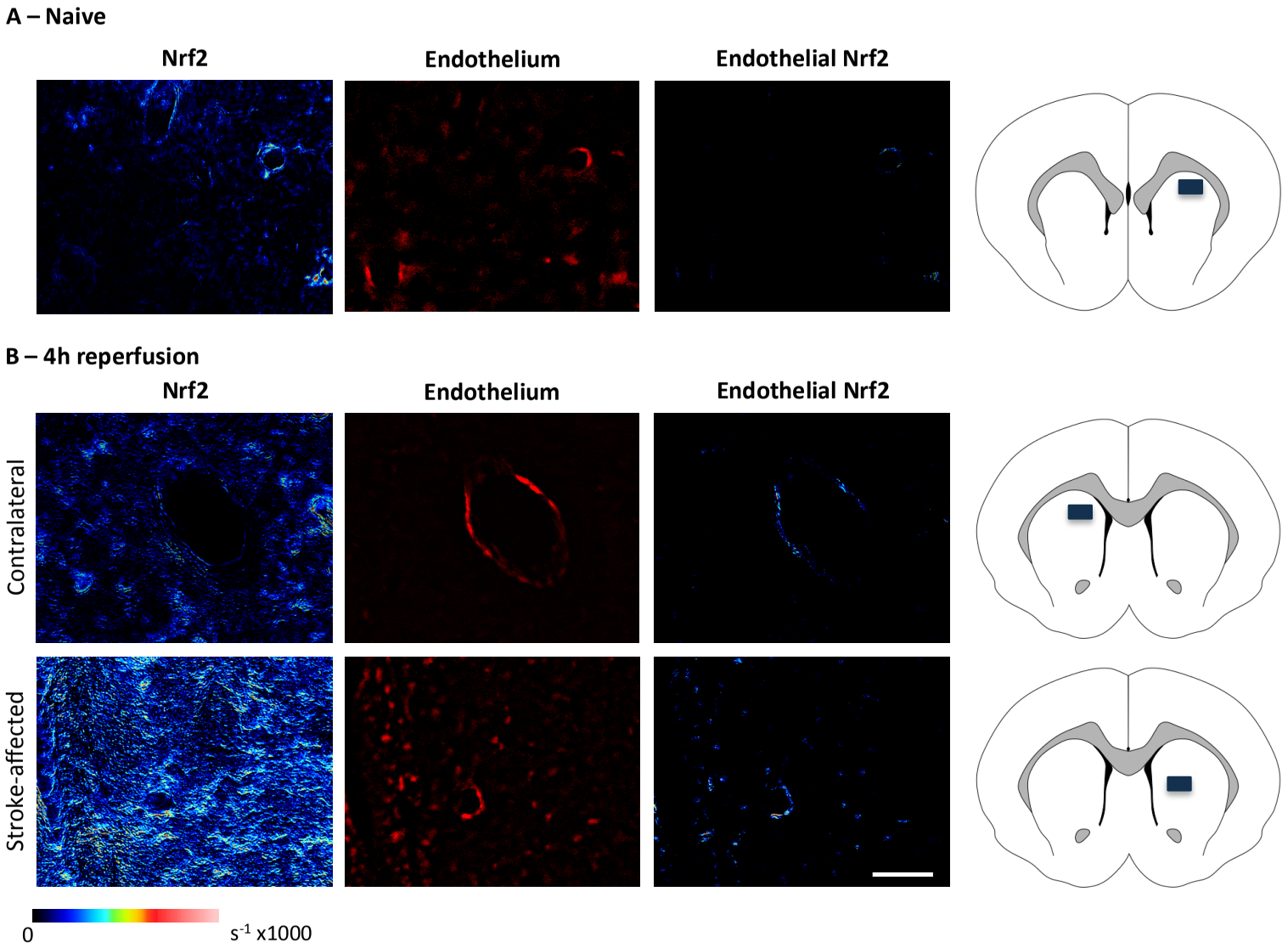
A – Naive
Nrf2
Endothelium
Endothelial Nrf2
B – 4h reperfusion
Nrf2
Endothelium
Endothelial Nrf2
Contralateral
Stroke-affected
0
s-1 x1000

Figure 4.11. Endothelial distribution of Nrf2 in animals subjected to 70 min MCAo and 24h or 72h reperfusion injury.

Endothelial distribution of Nrf2 was determined in 10µm *ex vivo* coronal brain sections from rats subjected to 70 min MCAo and (A) 24h or (B) 72h reperfusion injury. Nrf2 content was determined using quantitative immunohistochemistry and pseudo colour images generated to show expression of Nrf2 in brains sections (Left panel). Fluorescence images of the endothelium were captured following staining with mouse anti-RECA1 primary antibody and donkey anti-mouse Alexa-fluor 555 (Middle panel). Captured fluorescence endothelial images were used to generate an endothelial mask, which was superimposed onto the Nrf2 image to show Nrf2 distribution in the cerebrovascular endothelium (right panel). Scale bar represents 5µm. Black squares (■) in the brain maps show the location of acquired images. Note that panel A is shown on page 159, and panel B on page 160.

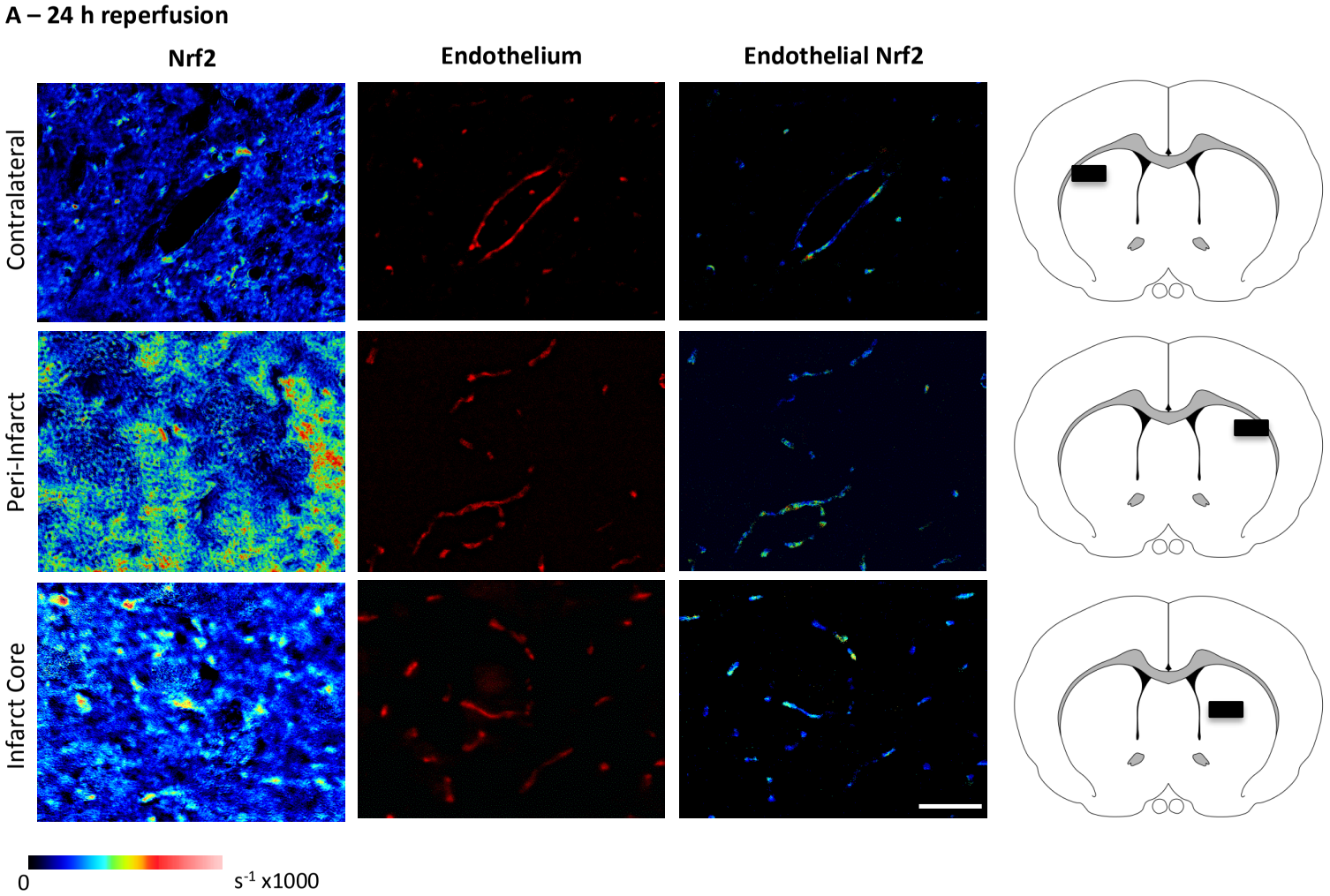
A – 24 h reperfusion
Nrf2
Endothelium
Endothelial Nrf2
Contralateral
Peri-Infarct
Infarct Core
0
s-1 x1000

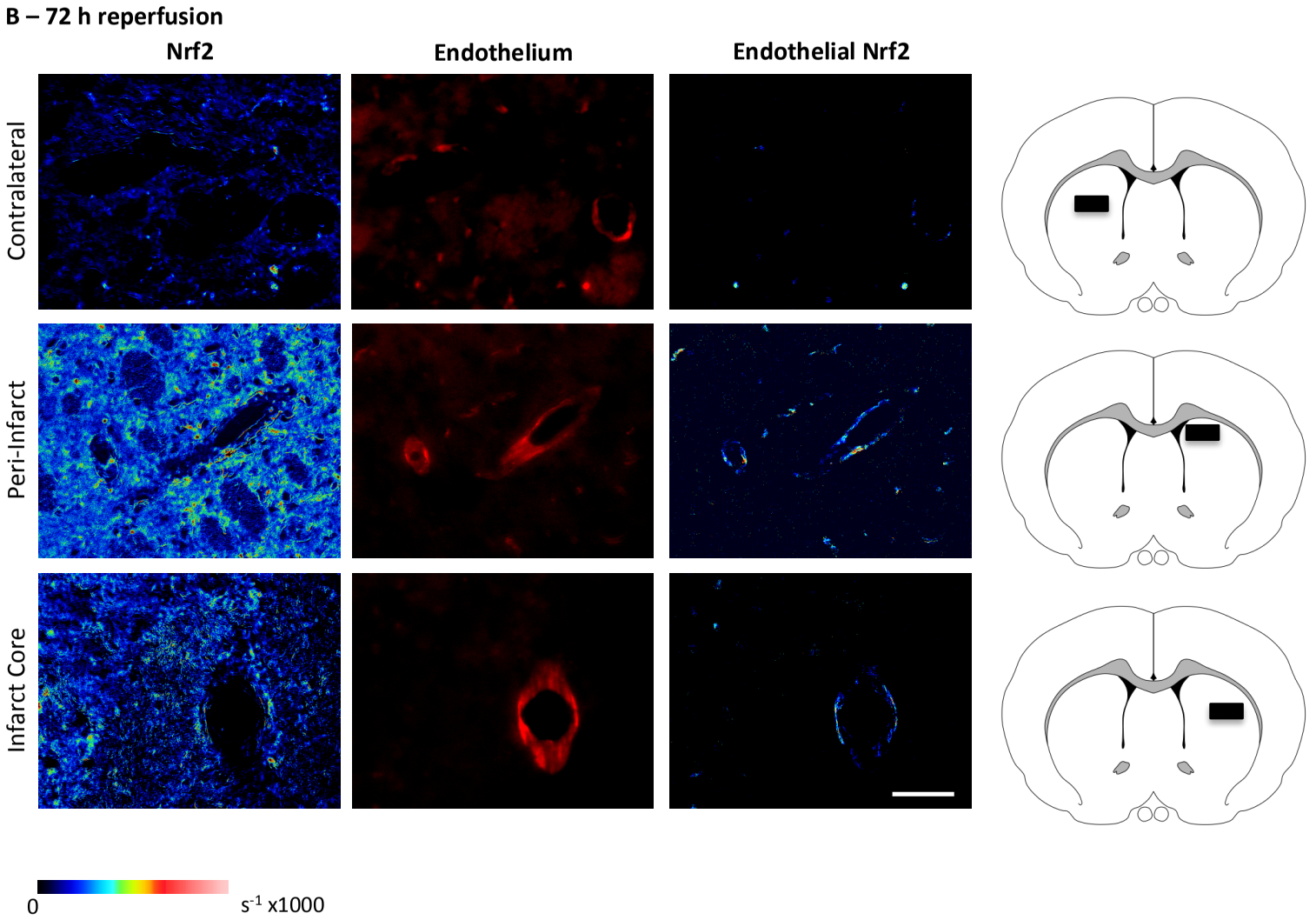
B – 72 h reperfusion
Nrf2
Endothelium
Endothelial Nrf2
Contralateral
Peri-Infarct
Infarct Core
0
s-1 x1000

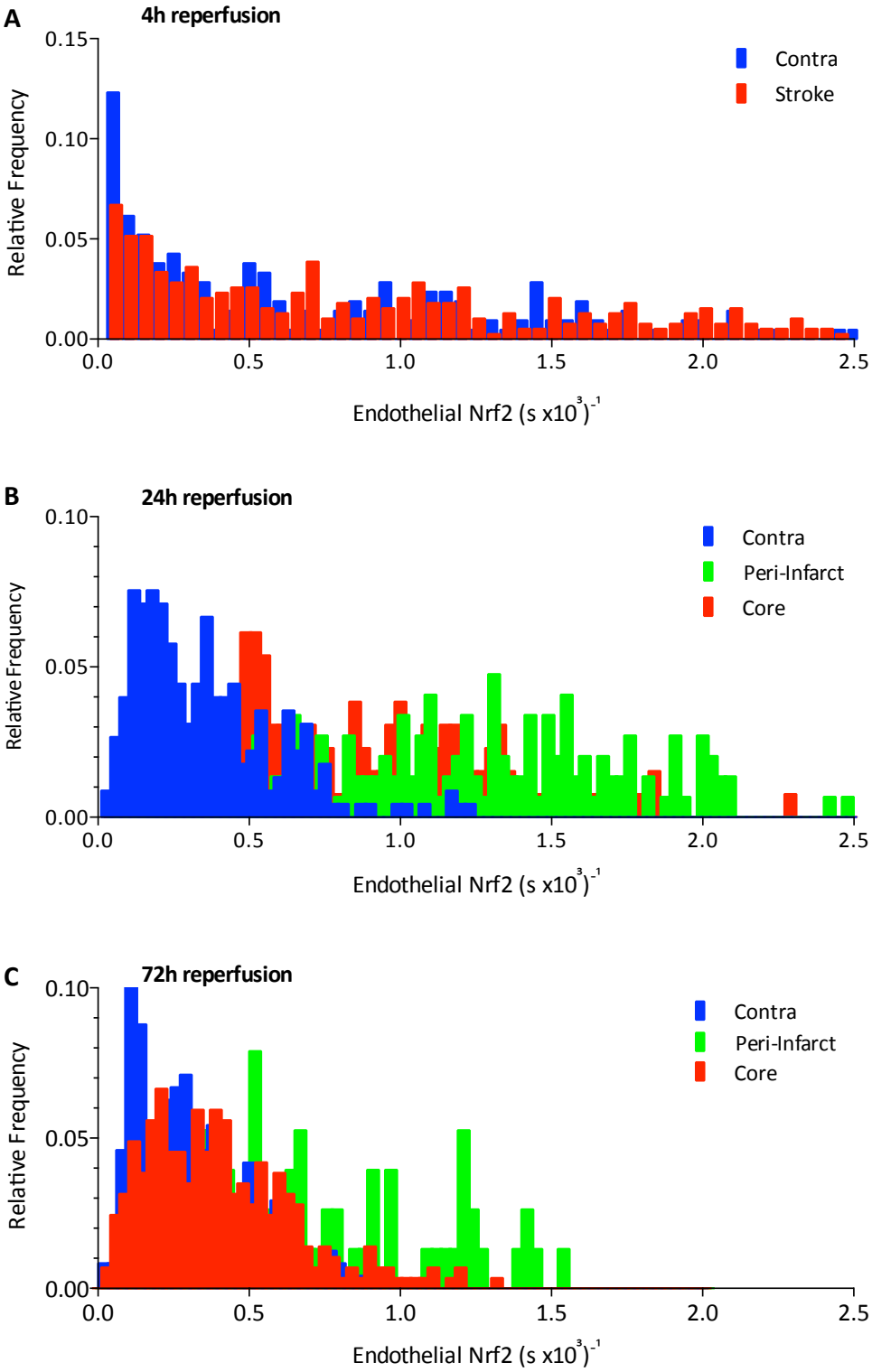

Figure 4.12 Temporal changes in endothelial Nrf2 content after MCAo and reperfusion injury.

Histograms show the Nrf2 content in endothelial positive structures, in stroke-affected regions and the contralateral hemisphere in animals subjected to 70 min MCAo and (A) 4h (n = 211 RECA1 positive regions in contra and 388 in stroke affected hemisphere), (B) 24h (255 RECA1 positive regions in contralateral, 130 in infarct core and 147 in peri-infarct regions) and (C) 72h reperfusion injury (239 RECA1 positive regions in contra, 296 in infarct core and 96 in peri).

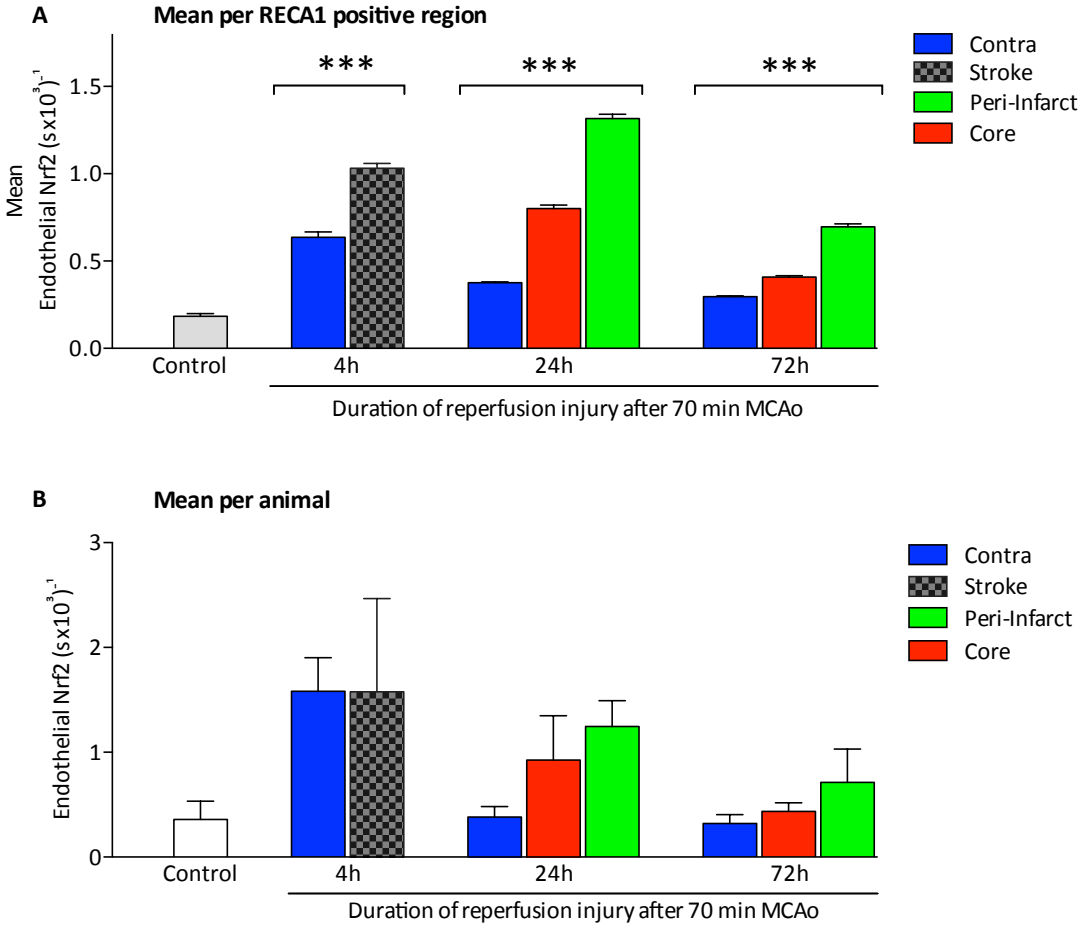

Figure 4.13 Summary of temporal changes in endothelial Nrf2 content after MCAo and reperfusion injury.

Bar graphs show the summary of mean endothelial Nrf2 content, determined (**A**) per RECA1 positive region, or (**B**) per animal in control rats and in the contralateral, and stroke-affected regions of rats subjected to 70 min MCAo and reperfusion injury. (**A**) Mean endothelial Nrf2 content from different brain regions was determined using 96 – 400 RECA1 positive regions from 5 animals in the control group and 3 animals per experimental group. Data denote mean ± S.E.M., *** $P<0.001$. Note that statistical significance is observed amongst all brain regions (contralateral, infarct core and peri infart) in animals subjected to 24h and 72h reperfusion, and between contralateral and stroke-affected hemisphere in animals subject to 4h repeffusion injury. (**B**) Mean endothelial Nrf2 content per animal was determined from different brain regions. Data denote mean ± S.E.M., n=5 animals in control group and n=3 animals per MCAo experimental group.

4.4 Induction of Nrf2-mediated proteins following MCAo and reperfusion injury

The time dependent expression of Nrf2 after MCAo and reperfusion injury was established in Section 4.3. As Nrf2 confers protection by upregulating the expression of antioxidant and phase II detoxifying enzyme, the expression of Nrf2-linked antioxidant proteins following MCAo and reperfusion injury in rat brains was assessed by immunofluorescence in *ex vivo* brains sections using basic fluorescence and confocal microscopy. Fluorescence studies of the expression of Nrf2 mediated proteins in *ex vivo* rat brain sections were done in collaboration with Dr Alessio Alfieri, King's College London.

4.4.1 Induction of HO-1 following MCAo and reperfusion injury

Rat brain sections (50µm) were examined for HO-1 expression following MCAo and reperfusion injury using confocal microscopy. An increase in HO-1 protein expression was detected in the stroke-affected hemisphere following MCAo and 24 or 72h reperfusion injury (Figure 4.14 A). Furthermore, following 24h reperfusion injury, HO-1 expression was observed surrounding the infarct core, as highlighted by co-staining with GFAP (Figure 4.14 A). Interestingly, HO-1 expression was detected in both peri-infarct and infarct core regions of the stroke-affected hemisphere after 72h reperfusion injury. Analysis of immunofluorescence intensity revealed a significant upregulation of HO-1 protein localised in peri-infarct regions after 24 and 72h reperfusion compared to the infact core and contralateral regions of the ischaemic brain. Though a general trend of greater HO-1 expression is also noted in the infarct core following 24 and 72h reperfusion injury, this increase was not significant (Figure 4.14 B).

Induction of HO-1 following MCAo and reperfusion injury was also assessed around identified cerebral microvessels and associated astrocytes by immunofluorescence staining. An increase in HO-1 induction was noted around cerebral microvessels identified within the peri-infarct region, after 70 min MCAo and 24h reperfusion injury (Figure 4.15 A). Brain sections were co-stained with cell markers for the endothelium by RECA1 and astrocytes by GFAP. Co-localisation was assessed following fluorescence intensity profiling, which is a measure of the fluorescence intensity for multiple channels recorded at any one pixel (Figure 4.15 B). HO-1 immunofluorescence co-localised predominantly with GFAP staining, indicating increased presence of HO-1 within astrocytes (Figure 4.15 B). Furthermore, co-localisation of HO-1 with astrocytes was significantly greater than in the cerebrovascular endothelium following 70 min MCAo and 4h ($P<0.01$) and 24h ($P<0.05$) reperfusion injury (Figure 4.15 C).

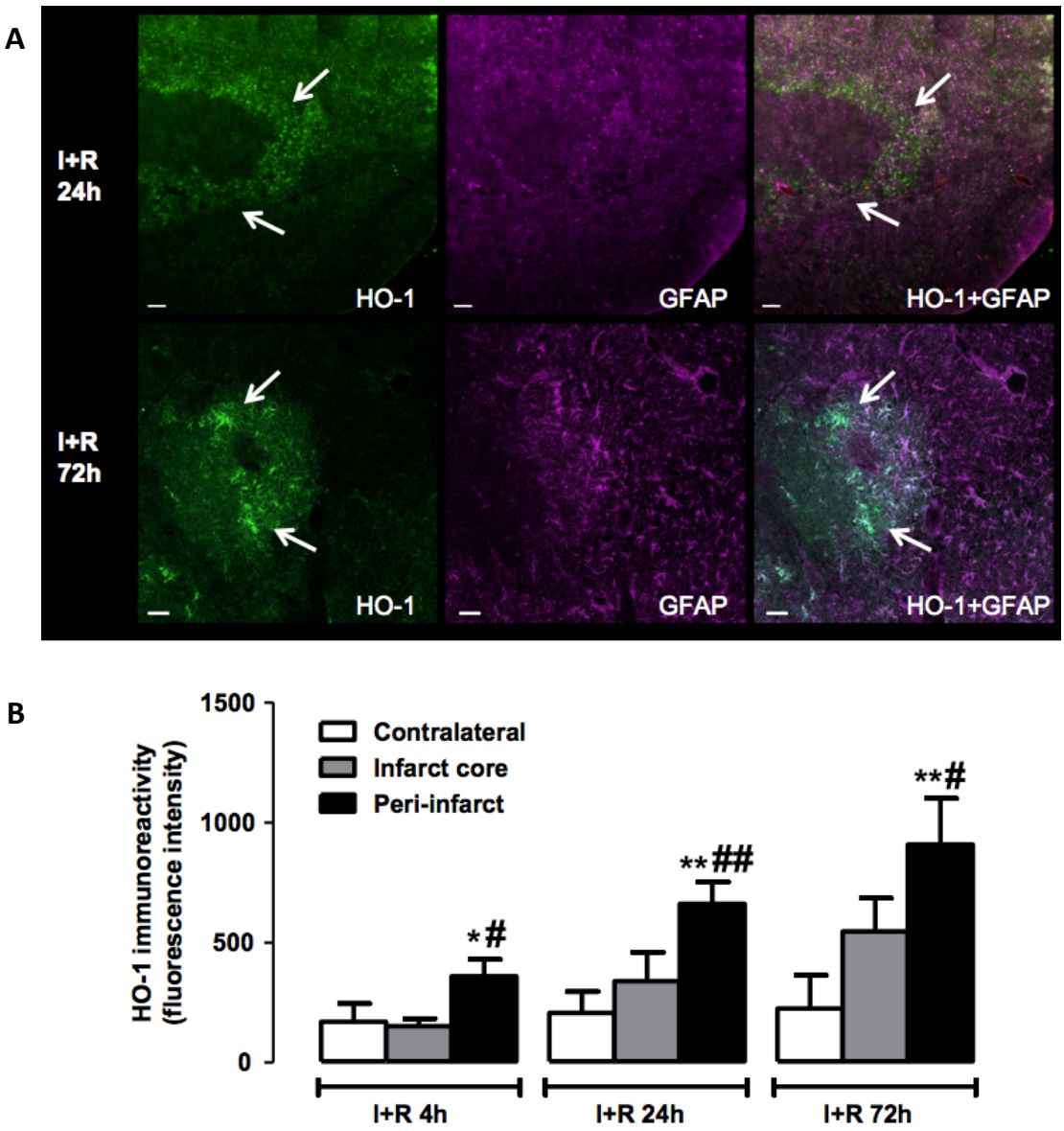

Figure 4.14 Induction of HO-1 following MCAo and reperfusion injury.
50µm coronal *ex vivo* brain sections from rats were incubated with anti-HO-1 primary antibody and donkey-anti rabbit 488 secondary antibody (green). Sections were also co-stained for GFAP (purple) to indicate area of stroke-affected damage. (A) Representative confocal images of HO-1 induction after 70 min MCAo and 24h (top panel, scale bar represents 200µm) or 72h reperfusion injury (bottom panel, scale bar represents 50 µm). White arrows indicate regions of HO-1 induction. (B) Temporal and spatial quantification of HO-1 fluorescence intensity in the contralateral hemisphere and infarct core and peri-infarct regions of the stroke affected hemisphere after 70 min MCAo and 4 – 72h reperfusion injury. Data denote mean ± S.E.M. * $P<0.05$ and ** $P<0.01$ versus contralateral hemisphere and # $P<0.05$ and ## $P<0.01$ versus infarct core. Figure taken from (Alfieri *et al.*, 2013).

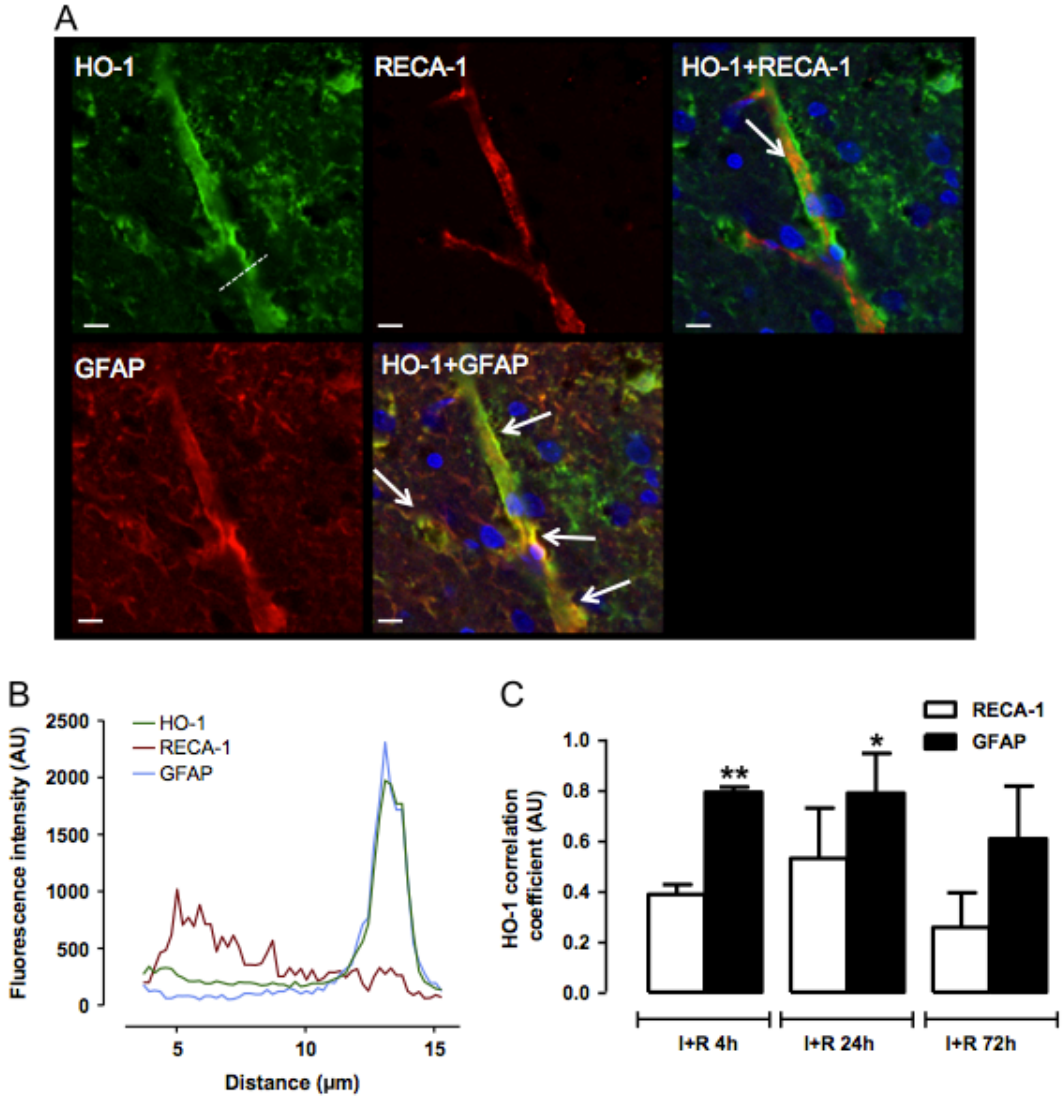

Figure 4.15 Expression of HO-1 in the neurovascular unit of peri-infarct cerebral microvessels after MCAo and reperfusion injury.
(A) Representative confocal images of cerebral vessels identified in peri-infarct regions of the ischaemic brain. Sections were co-stained for HO-1 (Green), the endothelial marker RECA1 (upper panel, red) and the astrocyte marker GFAP (lower panel, red). Merged images also show DAPI staining for nuclei (blue). White arrows indicate areas of HO-1 association with respective cell markers in merged images. Scale bar represents 10 µm. (B) Representative trace of fluorescence intensity profile across the identified cerebral microvessel in area indicated by dotted white line in (A). (C) Correlation coefficients of HO-1 fluorescence intensity in endothelium, identified by RECA1, and astrocytes, identified by GFAP. Data denote mean ± S.E.M. * $P<0.05$ and ** $P<0.01$. Figure taken from (Alfieri *et al.*, 2013).

4.4.2 Induction of Prx-1 expression following MCAo and reperfusion injury

The expression of Prx1, an Nrf2 regulated protein was assessed by immunofluorescence in 10μm coronal brain sections from rats subjected to 70 min MCAo and 24 h reperfusion injury. Expression of Prx1 was detected in brain sections from naïve rats, (Figure 4.16 A) with stronger staining for Prx1 detected in the stroke affected-hemisphere (Figure 4.16 C). A significant increase in Prx1 was also noted in the contralateral hemisphere compared to naïve rats ($P<0.001$, Figure 4.16 B). Quantification of fluorescence intensity for Prx1 revealed a significant increase in Prx1 in the contralateral and stroke-affected hemisphere compared to naïve ($P<0.001$, n=3 animals per experimental group). Although a slight increase in Prx1 expression is noted in the stroke-affected hemisphere, this trend in increase was not significantly increased in comparison to Prx1 levels detected in the contralateral hemisphere.

4.4.3 Induction of NQO1 in the rat brain after MCAo and reperfusion injury

Nuclear translocation of Nrf2 results in the upregulation of genes consisting of the ARE within its promoter region. In this chapter, the expression of HO-1 and Prx1 has been assessed following 70 min MCAo and reperfusion injury. NQO1 is a phase II detoxifying enzyme that is regulated by Nrf2, however little is known regarding its expression following ischaemia and reperfusion injury. Hence the expression of NQO1 expression was assessed by immunofluorescence in 10 μm coronal brain sections from naïve rats and after 70 min MCAo and 24h reperfusion injury.

Expression of NQO1 is detected in brain sections from naïve animals (Figure 4.17 A) and furthermore, similar levels of NQO1 fluorescence intensity is observed in the contralateral hemisphere of animals subjected to 70 min MCAo and 24h reperfusion injury (Figure 4.17 B). NQO1 expression is greater in the stroke-affected hemisphere (Figure 4.17 C) compared to the contralateral hemisphere and in naïve brains (Figure 4.17 A-C). Quantification of fluorescence intensity revealed a significant increase in NQO1 protein expression in the stroke-affected hemisphere compared to the contralateral hemisphere ($P<0.05$) and naïve rats ($P<0.01$, Figure 4.17 D).

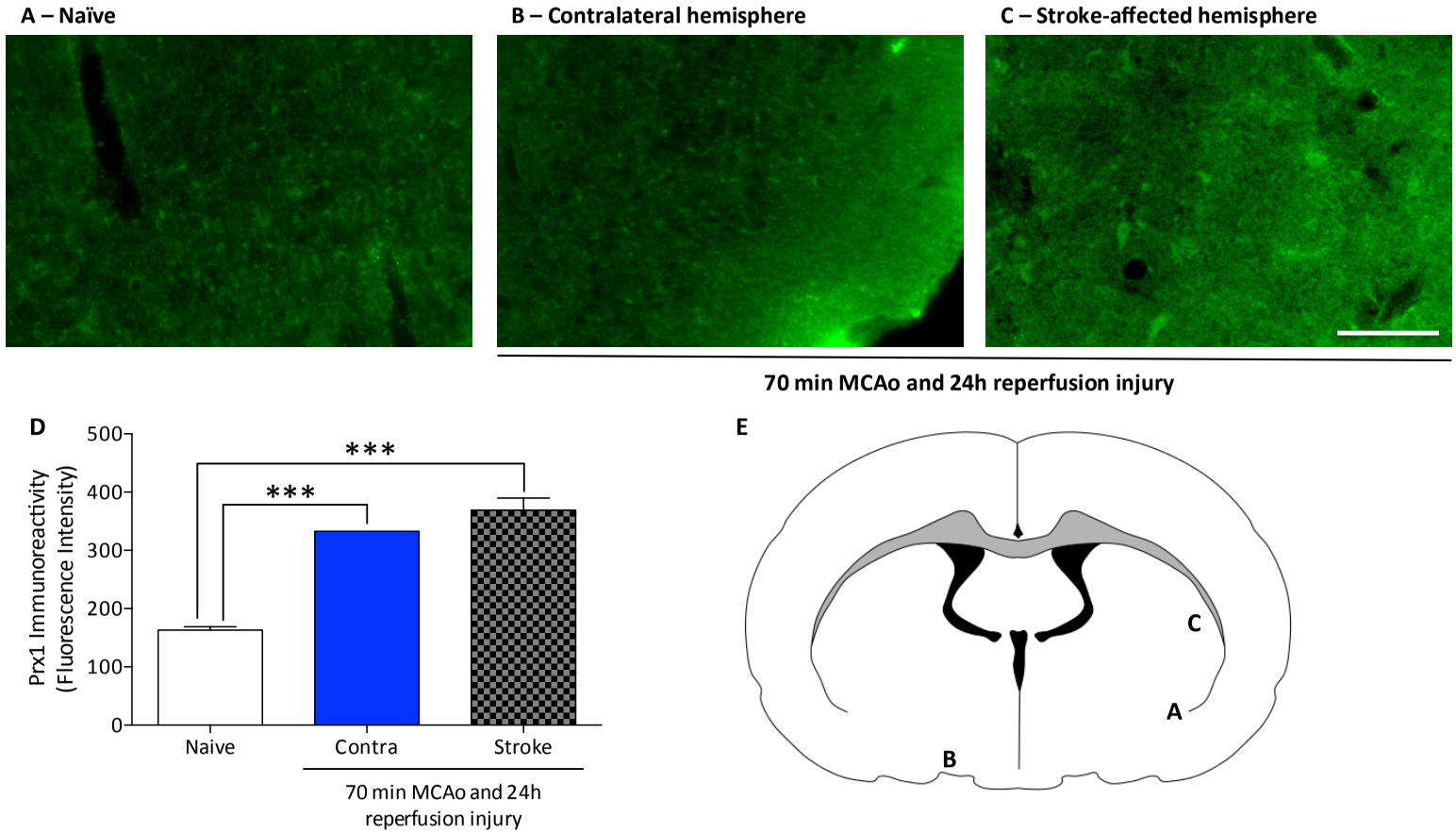

Figure 4.15 Induction of Prx1 in rat brains following 70 min MCAo and 24h reperfusion injury.
10µm coronal rat brain sections were stained with rabbit anti-Prx1 primary antibody and donkey anti-rabbit Alexa-Fluor 488 (green) and visualised by fluorescence microscopy. Representative images of Prx1 staining in brain sections from (A) naïve animals and (B) contralateral hemisphere and (C) stroke-affected hemisphere after 70 min MCAo and 24h reperfusion injury. Scale bar represents 50µm. (D) Fluorescence intensity for Prx1 was measured using image J following the capture of 32-bit grey scale images. Data denote mean ± S.E.M, ***P<0.001, n = 3 animals per experimental group, analysed by one-way ANOVA and Tukeys post-hoc test. (E) Brain map shows the location of acquired images.

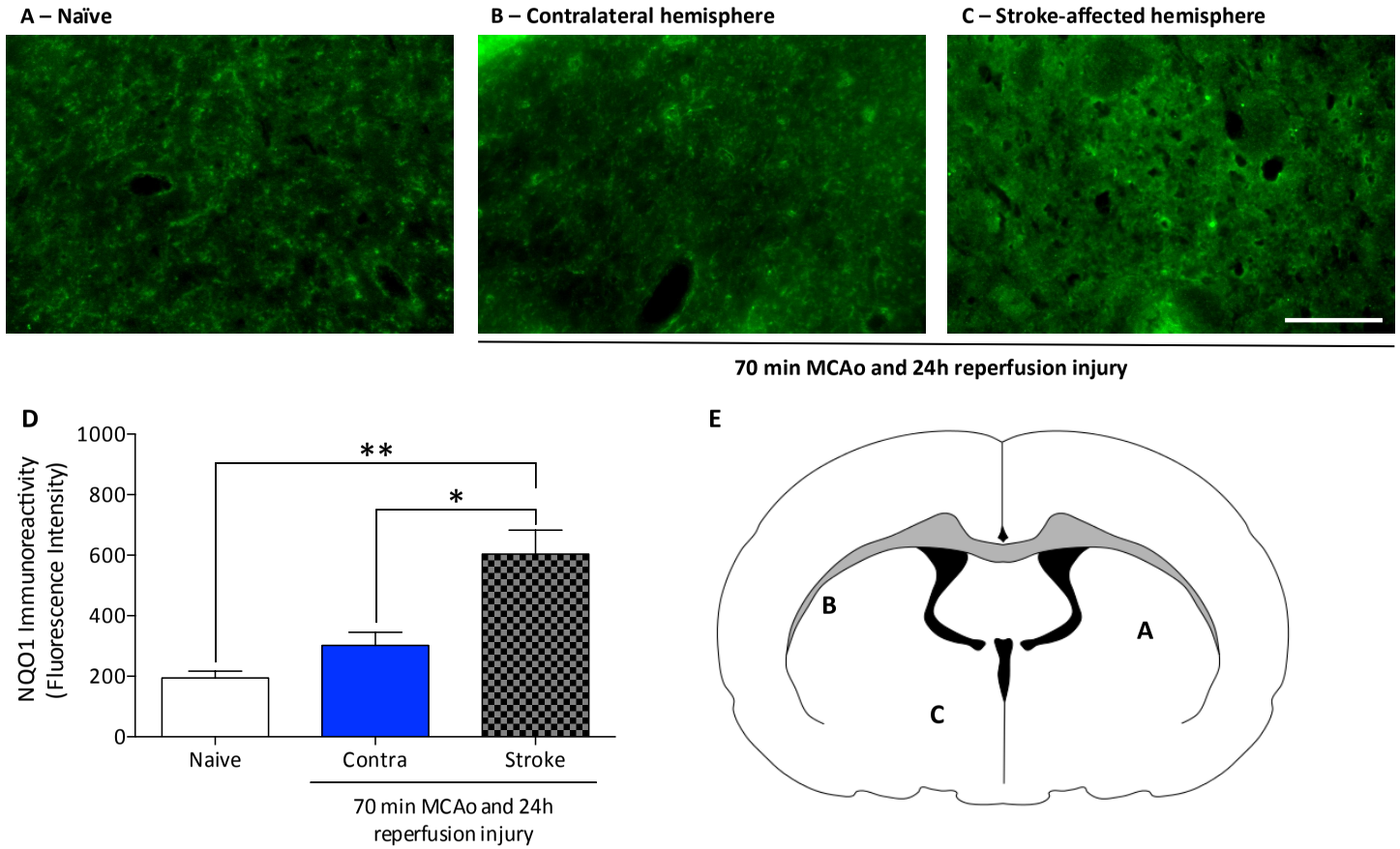

Figure 4.16 Induction of NQO1 in rat brains following 70 min MCAo and 24h reperfusion injury.

Coronal rat brain sections (10µm) were stained with rabbit anti-NQO1 primary antibody and donkey anti-rabbit Alexa-Fluor 488 (green) and visualised by fluorescence microscopy. Representative images of NQO1 staining in brain sections from (A) naïve rats and (B) contralateral hemisphere and (C) stroke-affected hemisphere after 70 min MCAo and 24h reperfusion injury. Scale bar represents 50µm. (D) Fluorescence intensity for NQO1 was measured using image J following the capture of 32-bit grey scale images. Data denote mean ± S.E.M, * $P<0.05$, ** $P<0.01$, n = 3 animals per experimental group, analysed by one-way ANOVA and Tukeys post-hoc test. (E) Brain map shows the location of acquired images.

4.5 Discussion

This chapter investigated the time and spatial distribution of the redox sensitive transcription factor Nrf2 in an experimental model of ischaemia and reperfusion injury in male Sprague Dwaley rats. A novel immunohistochemical technique (described in Chapter 3) has enabled (i) quantitation of Nrf2 in nuclear and cytoplasmic compartments of brain cells, and (ii) changes in the spatial distribution of Nrf2 content in brain cells and cerebral endothelium after ischaemia and reperfusion injury. Furthermore, Nrf2 mediated upregulation of antioxidant stress proteins after ischaemia and reperfusion injury was assessed using fluorescence and confocal microscopy.

4.5.1 The use of quantitative immunohistochemical and immunofluorescence techniques

Quantitative immunohistochemistry and immunofluorescence techniques have been employed to present the findings shown in this chapter. However, it must be stated that Nrf2 was only studied using the quantitative immunohistochemical technique; where as Nrf2-linked proteins were only studied using immunofluorescence. A disadvantage of the quantitative immunohistochemical technique is that only one brain section can be used to "quantify" protein content in one specific brain region at a time. The quantitative immunohistochemical technique however, provides sufficient resolution to observe and quantitate protein expression in different regions of the ischaemic brain and in different cerebral cells types. Western blots are unable to provide the same level of resolution and only convey information of global protein changes, thus demonstrating the advantages of the quantitative immunohistochemical technique. Furthermore, the ability of the immunohistochemical technique to distinguish protein content between nuclear and cytoplasmic compartments is advantageous in understanding the time-course of cellular distribution and allowing for detection of the nuclear accumulation of the redox sensitive transcription factor Nrf2 after ischaemia and reperfusion injury.

The quantitative immunohistochemical technique was also a viable method for studying the expression of Nrf2-mediated genes in *ex vivo* brain sections from rats. However, as described in chapter 3, section availability was limited due to the amount of tissue that was initially required to resolve the movement of brain sections observed during capture of the DAB-H_2O_2 reaction. Thus, immunofluorescence was adapted to observe the expression of Nrf2-linked proteins after stroke and furthermore, to undertake co-localisation studies to identify cerebral cell types responsible for the expression of Nrf2-linked proteins, as discussed further in Section 4.5.7.

4.5.2 Reproducibility of stroke damage following MCAo and reperfusion injury

The transient MCAo and reperfusion injury model of ischaemic stroke was employed in this study. Though the initial aims of the study were designed for a mouse model of stroke, our collaboration with Dr Mike Modo, IOP, King's College London, enabled us to undertake training in rats, providing our group with the necessary surgery expertise and the experience required to understand the skill required for the MCAo surgery. Access to the rat model of MCAo surgery also gave us the material required to troubleshoot the quantitative immunohistochemical protocol developed in chapter 3, and to design working protocols for immunofluorescence studies of Nrf2-linked proteins. It must be noted that the majority of rat brains used in this studied were provided by Dr Alessio Alfieri, Cardiovascular Division, King's College London. However, all experimental protocols were planned and discussed in detail with Dr Alfieri and the supervisory team.

4.5.3 MCAo surgery: Limitations and Reproducibility

The middle cerebral artery occlusion model is widely used in stroke research and is representative of occlusive stroke experienced by humans. Hence, the experimental stroke model employed in this study is dependent on the occlusion of the middle cerebral artery using an intraluminal silicon coated filament. Occlusion of blood flow, as detected by laser Doppler or a similar set-up, would inform the operator of the successful occlusion of the MCA. As no access to such equipment was available, the operator was dependent on (i) measuring the distance of filament advancement through the common carotid artery, and (ii) pushing the filament as far as possible until the occluding filament could not be advanced further. However, displacement of the intraluminal filament by the operator may result in the partial MCAo. Furthermore, variable length of the internal carotid artery, from animal to animal, will impact the final length required of the occluding filament.

Hence, as there were no means in place to assess reproducibility of MCAo in rats, reproducibility of the stroke model *in vivo* was assessed using two methods; (i) neurological behavioural assessment and (ii) staining for activated astrocytes, indicating the area of damage. Behaviour of each animal after MCAo surgery was measured on a global neurological scale to assess neurological function, which included righting reflex, spontaneous motility, horizontal bar test and grasping reflex. The behavioural assessment of animals after MCAo surgery was conducted by Dr Alessio Alfieri, Cardiovascular Division, King's College London. This data is presented in Appendix Figure 5 (Alfieri *et al.*, 2013).

Another technical limitation of this presented study is owed to availability of coronal brain sections for *ex vivo* analysis. As discussed in Chapter 3, a high percentage of material was used to successfully resolve the problem of tissue movement during the DAB-H_2O_2 reaction capture. This, however, limited the number of coronal 10µm brain sections available for analysis by, either quantitative DAB immunohistochemistry or immunofluorescence, for Nrf2 and its mediated proteins. Furthermore, no other stroke brains were available for sectioning and consequent analysis. Hence, to limit the effects of cerebral anatomical variations in studying Nrf2 protein expression following stroke, 10µm coronal brain sections from the forebrain were used from all stroke brains.

The study of Prx1 and NQO1 by fluorescence in 10µm brain section, however, was conducted in sections obtained beyond the mid-brain. As the extent of damage induced after MCAo and reperfusion injury, is not equal throughout the brain, this may affect the observed protein expression. The HO-1 data presented and discussed in this chapter was obtained from 50µm brain sections, analysed by Dr Alessio Alfieri, Cardiovascular Division, King's College London. Once again, the limited availability of matched-stroke brain sections inhibited the analysis of HO-1 protein in 10µm brain sections. However, employment of 50µm coronal brain sections allowed for confocal analysis to understand cell-specific HO-1 expression in greater depth.

4.5.4 Statistical analysis of summarised data

The summarised data, shown in this chapter, has been calculated as mean animal (n=3-5 animals per experimental group), and mean cellular Nrf2 ratio or content (n=200-3000 cells from 3 – 5 animals per experimental group). Mean Nrf2 ratio and content was calculated on a cellular basis, demonstrating the possibility of extracting protein data at a cellular level in *ex vivo* sections using the quantitative DAB-immunohistochemical technique. Although the trends for Nrf2 ratio and content were similar, statistical significance was lost on a per animal basis. Variations in results between animals following stroke maybe owed to, (i) the degree of ischaemic insult, (ii) the area of the brain used for analysis, and (iii) number of nuclei identified per section. In retrospect, on a per animals basis, this study was underpowered.

4.5.5 Expression of Nrf2 in the ischaemic brain

The present findings provide the first documentation of the temporal and spatial distribution of Nrf2 following experimental stroke in rodents. The redox sensitive transcription factor Nrf2 is important in protecting the brain parenchyma following stroke, as previous studies have shown that Nrf2 KO mice exhibit a significant increase in cerebral infarction volume compared to wild

type mice subjected to either transient occlusion of the MCA (Shah *et al.*, 2007; Wang *et al.*, 2012; Li *et al.*, 2013), or permanent occlusion (Shih *et al.*, 2005). Activation and nuclear accumulation of Nrf2 are required for the upregulation of endogenous antioxidant stress proteins and phase II detoxifying enzymes to restore redox homeostasis (Ishii *et al.*, 2000; Ishii *et al.*, 2004; Motohashi & Yamamoto, 2004; Alfieri *et al.*, 2011; Taguchi *et al.*, 2011).

From the presented data in this chapter, it is interesting to note a decrease in the nuclear to cytoplasmic distribution of Nrf2 in the stroke-affected hemisphere following 4h reperfusion injury (Figure 4.5), which suggests an increase Nrf2 protein synthesis upon reperfusion and greater cytoplasmic Nrf2 content (Figure 4.5). Kwak and colleagues have demonstrated the presence of an ARE in the promoter sequence of the Nrf2 gene following overexpression of Nrf2 in primary murine keratinocyte PE cells measuring Nrf2 promoter-luciferase reporter activity (Kwak *et al.*, 2002). Overexpression of a mutant form of Nrf2 protein in cells did not increase the Nrf2 promoter-luciferase reporter activity (Kwak *et al.*, 2002), confirming a role for Nrf2 in mediating an increase in Nrf2 protein.

The present study identified Nrf2 levels in cells identified with in the stroke-affected compared to the contralateral hemisphere after 24h reperfusion injury (Figure 4.5). After 72h reperfusion injury, a decrease in the nuclear Nrf2 content was observed with elevated levels in the cytoplasm, suggesting possible shuttling of Nrf2 from the nucleus. The mechanisms regulating the export of Nrf2 out of cellular nuclei following a stroke remains to be elucidated, however, the involvement of BACH1 in regulating nuclear translocation of Nrf2 may be speculated.

Nuclear to cytoplasmic Nrf2 ratio conveys information on the amount of Nrf2 present within the nucleus compared to its respective cytoplasm, but does not provide information on the total Nrf2 content within cerebral cells after ischaemia and reperfusion injury. Hence, nuclear and respective cytoplasmic contents for Nrf2 were summed, giving a value for total cellular Nrf2 content. Previous histological studies indicated an increased number of cells were positively stained for Nrf2 in the peri-infarct region of the stroke-affected hemisphere in mice subjected to 60 min transient MCAo and 8h reperfusion injury (Tanaka *et al.*, 2011). Moreover, immunofluorescence studies in rats subjected to 60 min MCAo and 24h reperfusion injury revealed an increase in Nrf2 staining in microglia, neurons and astrocytes in the peri-infarct region of the stroke-affected hemisphere (Dang *et al.*, 2012). Interestingly, neither study identified the presence of Nrf2 positive staining in cells within the infarct core (Tanaka *et al.*, 2011; Dang *et al.*, 2012). In this chapter, the presence of Nrf2 within the infarct core is shown, thus demonstrating the sensitivity of our novel immunohistochemical technique compared to previously used methods of detection. However, to further validate the Nrf2 antibody used in

this study, it would be important to stain sections from $Nrf2^{-/-}$ animals subjected to MCAo and reperfusion, to obviate non-specific antibody binding in the infarct core.

A significant increase in total cellular Nrf2 content was observed in both peri-infarct regions and infarct-core of the stroke-affected hemisphere after 24h reperfusion injury (Figure 4.7 B), which decreased after 72h reperfusion injury (Figure 4.7 C). These findings suggest that, compared to the infarct core, cells in the peri-infarct region have an elevated antioxidant capacity, enabling them to counteract the increased oxidative stress experienced after ischaemia and reperfusion injury. Notably, cellular Nrf2 content in the infarct core after 72h reperfusion injury was similar to levels observed in the contralateral hemisphere, however, peri-infract levels of Nrf2 remained elevated, albeit to a lesser extent than after 24h reperfusion (Figure 4.8 D). This suggests that, protective mechanisms maybe activated by Nrf2 at later time-points, to afford protection to the brain against reperfusion induced oxidative stress. Interestingly, a previous study highlighted a time-dependent increase in Nrf2 mRNA and protein, with peak expression noted after 24h in rats subjected to permanent MCAo (Yang *et al.*, 2009). The data presented by Yang and colleagues supports our findings of increased Nrf2 protein content in the rat brain following stroke, however, differences in the models of experimental stroke employed (permanent vs transient MCAo) may underlie varying mechanisms of Nrf2 activation.

4.5.6 Activation of Nrf2 in cerebrovascular endothelial cells

This chapter further focused on changes in endothelial specific Nrf2 levels following 70 min MCAo and reperfusion injury in rats. The DAB-H_2O_2 immunohistochemical technique was used to detect Nrf2 in the cerebrovascular endothelium of brains subjected to MCAo and reperfusion injury (Figure 4.9 and 4.10). Furthermore, the detection and increase in endothelial Nrf2 content within the stroke-affected hemisphere suggests Nrf2 is mediating protective responses in the cerebrovascular endothelium. Upon further resolution of the spatial distribution of endothelial Nrf2, elevated levels were observed in peri-infarct endothelium following 24 and 72h reperfusion (Figure 4.11). These finding further highlight in brain regions at an increased risk of death following reperfusion injury, Nrf2 is active in the endothelium to upregulate Nrf2-mediated defences, protecting the integrity of the blood brain barrier and the brain milleu. The cerebrovascular endothelium, a component of the blood-brain barrier, is required for protection of the neurovascular unit, brain parenchyma and maintaining an optimal environment for brain function (Abbott *et al.*, 2006; Alfieri *et al.*, 2011; Lehner *et al.*, 2011). Increased cerebrovascular permeability visualised after a stroke is due to the breakdown of the blood-brain barrier and cerebrovascular endothelial cell contraction following increased oxidative stress (Abbott *et al.*, 2006; Lehner *et al.*, 2011). Although, cerebrovascular permeability is increased

following stroke in Nrf2 knockout mice (Shih *et al.*, 2005; Shah *et al.*, 2007), there are limited reports documenting a key role for Nrf2 in the cerebrovascular endothelium, highlighting the need for current stroke-research to examine the importance antioxidant mechanisms for protection of the cerebrovascular endothelium. Previous studies have failed to validate the presence of Nrf2 within the cerebrovascular endothelium, however, immunofluorescence studies in an *en face* preparation of the mouse aortic arch revealed the presence of Nrf2 in endothelial cells *in vivo*. In this study, regions of laminar or "protective" flow were described as athero-protective, and regions of disturbed or "oscillatory" flow were described as being athero-prone (Dai *et al.*, 2007).

Although previous studies implicate Nrf2 mediated protection in the ischaemic brain, the present findings establish a time dependent activation and nuclear accumulation of Nrf2 after stroke. Thus the presented data gives a clear indication that Nrf2 mediated protection may only be afforded after 24h reperfusion injury, and not at earlier stages during reperfusion, necessary for the protection of the blood-brain barrier. Tanaka *et al* have shown the time course of the Nrf2 repressor protein, Keap1, in mice after MCAo and reperfusion injury (Tanaka *et al.*, 2011). A progressive decrease in the number of cells stained positively for Keap1, 2 – 24h after MCAo in peri-infarct and infarct core regions of the stroke-affected brain (Tanaka *et al.*, 2011). Interestingly, Tanaka *et al* highlight an increase in Nrf2 positively stained cells, 8h after reperfusion injury in peri-infarct regions (Tanaka *et al.*, 2011). As highlighted previously, our study shows a peak in Nrf2 protein content 24h after MCAo in rats. Thus suggesting that peak Nrf2 levels in the brain are attained between 8 – 24h after reperfusion injury

4.5.7 Upregulation of HO-1 in the ischaemic brain

As reported previously, Nrf2 regulates the expression of antioxidant stress proteins and phase II detoxifying enzymes. This chapter focused on the expression of HO-1, NQO1 and Prx1 after experimental ischaemia and reperfusion injury. The HO-1 data presented in this chapter obtained following the staining of 50µm coronal rat brain sections and analysed by confocal microscopy, allowed for in-depth analysis of cell-specific localisation of HO-1 by immunofluorescence. Although induction of HO-1 following stroke has been reported, the time course of its expression has not been investigated (Panahian *et al.*, 1999; Fu *et al.*, 2006; Satoh *et al.*, 2006; Saleem *et al.*, 2008; Chen *et al.*, 2012; Le *et al.*, 2013). HO-1 expression was increased in peri-infarct regions of the ischaemic brain, indicating activation of antioxidant defence mechanisms to increase protection afforded in tissues or cells at an increased risk of death upon reperfusion injury. Previous findings have provided important evidence for the role of HO-1 meditated protection following stroke. HO-1 transgenic mice, compared to wild type

mice, demonstrated significant reductions in cerebral damage following 6h or 24h permanent MCAo, highlighting the important of HO-1 mediated neurovascular protection in the ischemic brain (Panahian *et al.*, 1999). Moreover, Shah and colleagues demonstrated an increased cerebral infarct volume in HO-1 KO mice after permanent MCAo (Shah *et al.*, 2011). Furthermore, similar to the HO-1 findings in the present study, Moreira and colleagues reported increased HO-1 expression in ipsilateral hemisphere of Wistar and Goto-Kakizaki rats subjected to experimental ischaemia and reperfusion injury (Moreira *et al.*, 2007). Interestingly, Moreira's findings also showed increased HO-1 expression in ipsilateral astrocytes, and furthermore, reported increased astrocytic HO-1 around the lesion border (Moreira *et al.*, 2007), supporting our finding of HO-1 expression around the infarct core after 24h reperfusion injury. A similar increase in glial HO-1 expression following experimental ischaemia and reperfusion injury in SD rats has been reported by Matz and colleagues, (Matz *et al.*, 1997), supporting the findings presented in this chapter and suggesting an important role for astrocytes mediating protection to the ischaemic brain (Alfieri *et al.*, 2011). Geddes and colleagues provide more evidence of increased astrocyte and neuron specific HO-1 expression after 24h reperfusion injury in rats, and reported astrocyte specific HO-1 expression in the peri-infarct region (Geddes *et al.*, 1996), highlighting upregulation of antioxidant defence mechanisms in brain regions that are at an increased risk of death following ischaemia and reperfusion injury. It is interesting to note that HO-2 is not induced following experimental ischaemia and reperfusion injury (Geddes *et al.*, 1996; Sutherland *et al.*, 2009), which supports our published findings (Alfieri *et al.*, 2013) and further suggests that both HO-1 and HO-2 maybe regulated and activated independently to one another.

Confocal analysis of HO-1 expression around cerebral microvessls in peri-infarct regions after 24h reperfusion injury revealed HO-1 association with astrocytic processes enveloping cerebral endothelium (Figure 4.14). Though previous studies have not commented on HO-1 expression around cerebral microvessels following stroke, increased HO-1 has been reported around microvessels in naïve spontaneously hypertensive rats (Ruetzler *et al.*, 2001). Confocal analysis of brain sections from animals subjected to 72h reperfusion also showed increased HO-1 expressed in microglia within the infarct core (Alfieri *et al.*, 2013). Microglia are defined as the resident immune cells of the brain that are activated in response to the development of a neurodegenerative disease state (Nimmerjahn *et al.*, 2005). Furthermore, activated microglia scavenge damaged neurons (Gehrmann *et al.*, 1995), hence providing an explanation for the detection of microglia within the infarct core. Interestingly, following traumatic brain injury in rats, Liu and colleagues also reported a time-dependent increase in HO-1 positive microglia present within the lesion area, supporting our observation following MCAo and reperfusion

injury (Liu *et al.*, 2013a). The function of HO-1 positive microgila resident in the infarct core is unknown, however, in a model of liver ischaemia-reperfusion injury, HO-1 overexpressing macrophages attenuated apoptosis and conferred increased protection (Shen *et al.*, 2011b). Thus the findings presented in this chapter are consistent with data reported in the literature, indicating an upregulation of HO-1 in the brain after stroke.

4.5.8 Upregulation of Prx1 in the ischaemic brain

The antioxidant enzyme Prx1 functions to degrade hydroperoxides to water (Poynton & Hampton, 2013), and is regulated by Nrf2 (Schreibelt *et al.*, 2008; Hawkes *et al.*, 2013). The limited availability of 10µm coronal brain sections for immunofluorescence analysis prevented co-localisation studies for Prx1 with other cerebral cell-types, however, following 70 min MCAo and 24h reperfusion injury, increased Prx1 is observed in stroke affected regions of the ischaemic hemisphere, thus suggesting Prx1 may play a role in mediating protection to the ischaemic brain (Figure 4.15). Limited literature is available regarding the expression of Prx1 post-stroke, however a human study identified a 20-fold increase in Prx1 protein in blood samples of stroke patients (Dayon *et al.*, 2011). Furthermore, proteomic analysis of microdialysates from cerebral stroke patients revealed increased Prx1 expression in the infarct core compared to peri-infarct regions (Dayon *et al.*, 2011). Dayon *et al* have identified Prx1 as a potential biomarker post-ischaemia, however, Shichita and colleagues support and provide further evidence of upregulated Prx1 in the infarct core (Shichita *et al.*, 2012a). The release of Prxs from dying cells promoted activation of macrophages via toll like receptors 2 and 4 and upregulates pro-inflammatory responses, however, antibody mediated suppression of Prxs reduce IL-23 expression, providing evidence that Prxs mediating pro-inflammatory processes post-ischaemia (Shichita *et al.*, 2012a). Hence this data strongly suggests a paradoxical scenario for the role of Prx mediated protection in the ischaemic brain.

In vitro overexpression of Prx1 or Prx2 in neuronal cultures subjected to oxygen glucose deprivation and re-oxygenation attenuated increases in ROS generation, reduced OGD induced DNA-damage and neuronal cell death (Leak *et al.*, 2013). Moreover, Prx2 transgenic mice subjected to transient MCAo exhibited reduced infarct volume and increase neurological recovery (Gan *et al.*, 2012). Interestingly, the expression of Prx1 has been widely noted in the rat nervous system, with evident staining of Prx1 in astrocytic end feet of naïve rat brains (Mizusawa *et al.*, 2000). In this study, we were unable to study the expression of Prx1 in the cerebral endothelium due to the limited availability of sections. Previous studies have, however, reported Prx1 mediated protection against ROS, in rat brain endothelial cells (rBEC4) *in vitro*

(Schreibelt *et al.*, 2008). This therefore suggests that Prx1 may play a role in preserving the blood-brain barrier from oxidative stress induced damage.

Thus, published reports show a critical role for Prx mediated protection following stroke., however, warrants further research into the cerebral cell-types responsible for Prx expression, the time course of expression following ischaemia and sub types of Prx in the brain responsible for protection.

4.5.9 Upregulation of NQO1 in the ischaemic brain

Another Nrf2 regulated protein that was assessed following MCAo and 24h reperfusion injury was NQO1, a phase II detoxifying flavoenzyme that catalyzes the two-electron reduction of quinones to their hydroquinone form (Chen *et al.*, 2000; Nebert *et al.*, 2002; Siegel *et al.*, 2012). Co-localisation studies of NQO1 with different cerebral cell types was not possible during the course of this PhD due to the limited availability of 10µm coronal brain sections, however, a significant increase in NQO1 protein expression was detected in stroke-affected regions after 70 min MCAo and 24h reperfusion injury. Limited studies have assessed the time course of NQO1 expression following ischaemia and reperfusion injury *in vivo*, however, consistent with our findings, Kapinya and colleagues demonstrate increased NQO1 protein activity in neuronal cultures subjected to OGD and 24h re-oxygenation (Kapinya *et al.*, 2003). These authors also noted a biphasic response in NQO1 protein activity, with an increase noted at 1 and 24h re-oxygenation after OGD (Kapinya *et al.*, 2003), However, Kapniya *et al* also reported that inhibition of NQO1 activity *in vivo* decreased cerebral infarct volume following MCAo and reperfusion injury in mice (Kapinya *et al.*, 2003). Thus, the data goes against the central dogma of NQO1 being protective in stroke. However, the activation of NQO1 by inducers of Nrf2 have shown protective effects after MCAo and 24h reperfusion injury in mice (Wu *et al.*, 2013). To further underpin the protective effect of NQO1, Zafar and colleagues demonstrated protection of NQO1 overexpressing neuroblastoma cells against dopamine induced toxicity (Zafar *et al.*, 2006). Therefore, the data presented in this chapter and published findings suggest a biphasic mode of NQO1 activation, where earlier activation of NQO1 may be detrimental, and the later stages of activation confer protection following ischaemia-reperfusion injury.

4.5.10 Responses of the contralateral hemisphere in the ischaemic brain

The contralateral hemisphere is unilateral to the stroke-affected hemisphere and is not directly affected by surgical intervention. Although not significant, our Nrf2 analysis revealed alterations in the contralateral Nrf2 content over time. Nrf2 content was lower in the contralateral hemisphere compared to measured levels in control brains, but increased with

time. Moreover, our data also revealed a significant increase in Prx1 protein expression in contralateral brain regions from rats subjected to 70 min MCAo and 24h reperfusion injury. Diaschisis defines the remotes changes in the unilateral hemisphere that occurs due to brain lesions (Di Piero *et al.*, 1990; Reinecke *et al.*, 1999). The theory of diaschisis was founded by Von Monakow, and proposed that brain lesions are able to induce changes in blood flow, excitatory and inhibitory effects, which affect distant, unilateral brain regions (Feeney & Baron, 1986). Changes observed in the peri-infarct region and surrounding tissue cannot be classed as diaschisis, due to exposure to either partial occlusion or signaling depression arising from the lesion (Reinecke *et al.*, 1999). Positron emission tomography (PET) studies revealed reductions in cerebral blood flow, in the contralateral hemisphere of stroke patients, 7 – 14 days after cerebral infarction (Lagreze *et al.*, 1987).

In Wistar rats subjected to permanent MCAo, Reinecke *et al.,* showed increased excitability of contralateral regions of the brain 7 days after MCAo following electrophysiological measurements (Reinecke *et al.*, 1999). Takuwa *et al*., used laser-Doppler flowmetry and show decreased contralateral cerebral blood flow, 1 day after permanent MCAo in mice (Takuwa *et al.*, 2013). In another study by Clarkson *et al*., mitochondrial FAD-linked respiration, marked changes were observed in ipsilateral brain regions, both 1 and 3 days after hypoxia-ischaemic insult in male Wistar rat pups (Clarkson *et al.*, 2007). However, slight changes in mitochondrial respiration were recorded in the contralateral hemisphere, 3 days after insult (Clarkson *et al.*, 2007). Garbuzova-Davis *et al*., further demonstrated alterations in the integrity of the blood-brain barrier in the contralateral hemisphere of rats subjected to 60 min MCAo and 7 days reperfusion injury (Garbuzova-Davis *et al.*, 2013). They report an increase in permeability and increased recruitment of autophagosomes to the cerebral endothelium in the contralateral hemisphere 7 days after MCAo (Garbuzova-Davis *et al.*, 2013).

Thus, previous studies have highlighted changes in the contralateral hemisphere following stroke in the unilateral hemisphere. Furthermore, the demonstrated changes have been recorded days after the initial insult. Although our study does not cover an extensive time course, as depicted in the highlighted studies, we report changes in Nrf2 and its mediated proteins in the contralateral hemisphere, over 4 – 72h after ischaemia. Therefore, it is well established that metabolic and physiological changes occur in the contralateral hemisphere after stroke. To our knowledge, we are the first to report alterations in contralateral levels of Nrf2 and its mediated proteins, after stroke. This finding suggests that areas not directly affected by stroke in the brain also respond to the ischaemic insult following stroke. Hence, further investigation is required to understand why the contralateral hemisphere showed changes in the expression of Nrf2-linked proteins, and furthermore, whether these changes provide enchanced protection to the brain.

4.6 Summary and Conclusion

In summary, the data presented in this chapter employed immunofluorescence and quantitatve immunohistochemistry to assess the temporal and spatial distribution of Nrf2 and Nrf2 mediated ‘documentation of the temporal and spatial distribution of the redox sensitive transcription factor Nrf2 and identified increased Nuclear content of Nrf2 after 24h reperfusion, and elevated levels of cellular Nrf2 content in peri-infarct regions following 24 and 72h reperfusion injury. Furthermore, this chapter provides the first evidence of the temporal distribution of Nrf2 protein in the cerebrovascular endothelium and demonstrates elevated levels of endothelial Nrf2 in peri-infarct regions of the stroke-affected hemisphere after ischaemia-reperfusion injury.

Assessment of Nrf2-linked proteins in the brain after ischaemia and reperfusion injury revealed an increase in expression of HO-1, NQO1 and Prx1 in the stroke-affected hemisphere. Furthermore, this chapter demonstrates that HO-1 expression in cerebral cell types is dependent upon the time-frame of reperfusion injury.

In conclusion, the upregulation of Nrf2 and Nrf2-linked proteins following MCAo and reperfusion injury indicates an upregulation of Nrf2 driven protective mechanisms. However, the time-frame of Nrf2 activation and upregulation of Nrf2-linked proteins may occur at too late a time point to provide sufficient protection to the brain milieu immediately after reperfusion injury. Upregulation of Nrf2 in the brain and cerebrovascular endothelium prior to a stroke may aid in limiting cerebrovascular permeability and provide sufficient protection to the brain parenchyma.

Chapter 5 – Effects of Sulforaphane on naïve rat brains and pre-treatment prior to MCAo

Chapter 5 – Effects of sulforaphane on naïve rat brains and pre-treatment

5.1 Introduction

The redox sensitive transcription factor, Nrf2, is activated and in response to oxidative, electrophilic and xenobiotic stress, upregulates the expression of antioxidant stress proteins, and phase II detoxifying enzymes. The induction of Nrf2 may also be regulated by dietary isoflavones (Mann *et al.*, 2009; Siow & Mann, 2010; Zhai *et al.*, 2013) and isothiocyanates (Dinkova-Kostova & Kostov, 2012; Li *et al.*, 2012a).

Sulforaphane, found in cruciferous vegetables such as broccoli, brussels sprouts or kale, is a dietary isothiocyanate and electrophilic inducer of the Nrf2 defence pathway (Jazwa *et al.*, 2011; Cui *et al.*, 2012). Although previous studies have demonstrated the protective effects of sulforaphane in rodents following administration post-cerebral ischaemia (Zhao *et al.*, 2006), the effects of sulforaphane pre-treatment in a rodent model of cerebral ischaemia and reperfusion injury have not yet been investigated.

The findings presented in Chapter 4 documented the time course of Nrf2 expression following 70 min MCAo and reperfusion injury in rats. This chapter investigates the effects of sulforaphane pre-treatment, prior to ischaemia-reperfusion injury, on the expression of Nrf2 and Nrf2-linked proteins in contralateral, peri-infarct and infarct core regions of the ischaemic rat brain. However, prior to pre-treatment studies, the effects of sulforaphane on expression of Nrf2 and Nrf2-mediated proteins were assessed in naïve animals.

5.2 Effects of sulforaphane on the naïve rat brain

In this chapter, the time course of Nrf2 expression following sulforaphane treatment and its effect on Nrf2-mediated proteins was assessed in naïve rat brains *ex vivo* by quantitative immunohistochemistry, immunoblotting and immunofluorescence.

5.2.1 Sulforaphane mediated induction of Nrf2 in the naïve rat brain

The distribution of Nrf2 was assessed in *ex vivo* brain sections from naïve animals and animals administered sulforaphane (5mg/kg, *i.p.*) for 1, 2, 4 and 24h. Pseudo colour images were generated using the quantitative immunohistochemical technique, where warmer pseudo colours indicate regions of high Nrf2 expression. A significant increase in Nrf2 expression was observed in naïve rat brains 1h after SFN treatment (Figure 5.1 A), however, 2, 4 and 24h after sulforaphane treatment, a notable decrease in Nrf2 protein levels was observed (Figure 5.1 B-D). Mean cellular Nrf2 content revealed a significant increase after 1h sulforaphane administration (0.63 ± 0.14, n = 3 animals) compared to naïve (0.07 ± 0.01, n=3 animals.

P<0.01). Furthermore, Nrf2 content after 1h sulforaphane administration was significantly increased compared to 2h (0.21 ± 0.05, n=3 animals, P<0.05) or 4h after sulforaphane treatment (0.15 ± 0.05, n=3 animals, P<0.01). Though a trend in decreasing cellular Nrf2 content is noted up to 4h after sulforaphane, Nrf2 content increased, albeit non-significant, after 24h administration (0.39 ± 0.05, Figure 5.1 E).

To confirm our quantitative immunohistochemistry findings, immunoblotting experiments were conducted on whole brain homogenates from naïve rats treated with either 1% corn oil in saline (vehicle) or sulforaphane (5 mg/kg, *i.p.*) for 1, 2, 4 or 24h. Immunoblotting of brain homogenates for Nrf2 (Figure 5.2 A) and densitometric analysis relative to the loading control (Figure 5.2 B), ß-actin, revealed a similar trend in Nrf2 expression as to that observed in *ex vivo* brain sections by quantitative immunohistochemistry (Figure 5.1). Nrf2 protein content was increased markedly after 1h sulforaphane administration. Notably, a decreasing trend in cerebral Nrf2 content is observed over 2 – 4h after sulforaphane administration (Figure 5.2). Animals treated with the vehicle, 1% corn oil in saline, showed no change in cerebral Nrf2 content over 1 – 24 h. The immunoblot shown in Figure 5.2 is generated from one animal per experimental group, hence no statistical analysis was conducted.

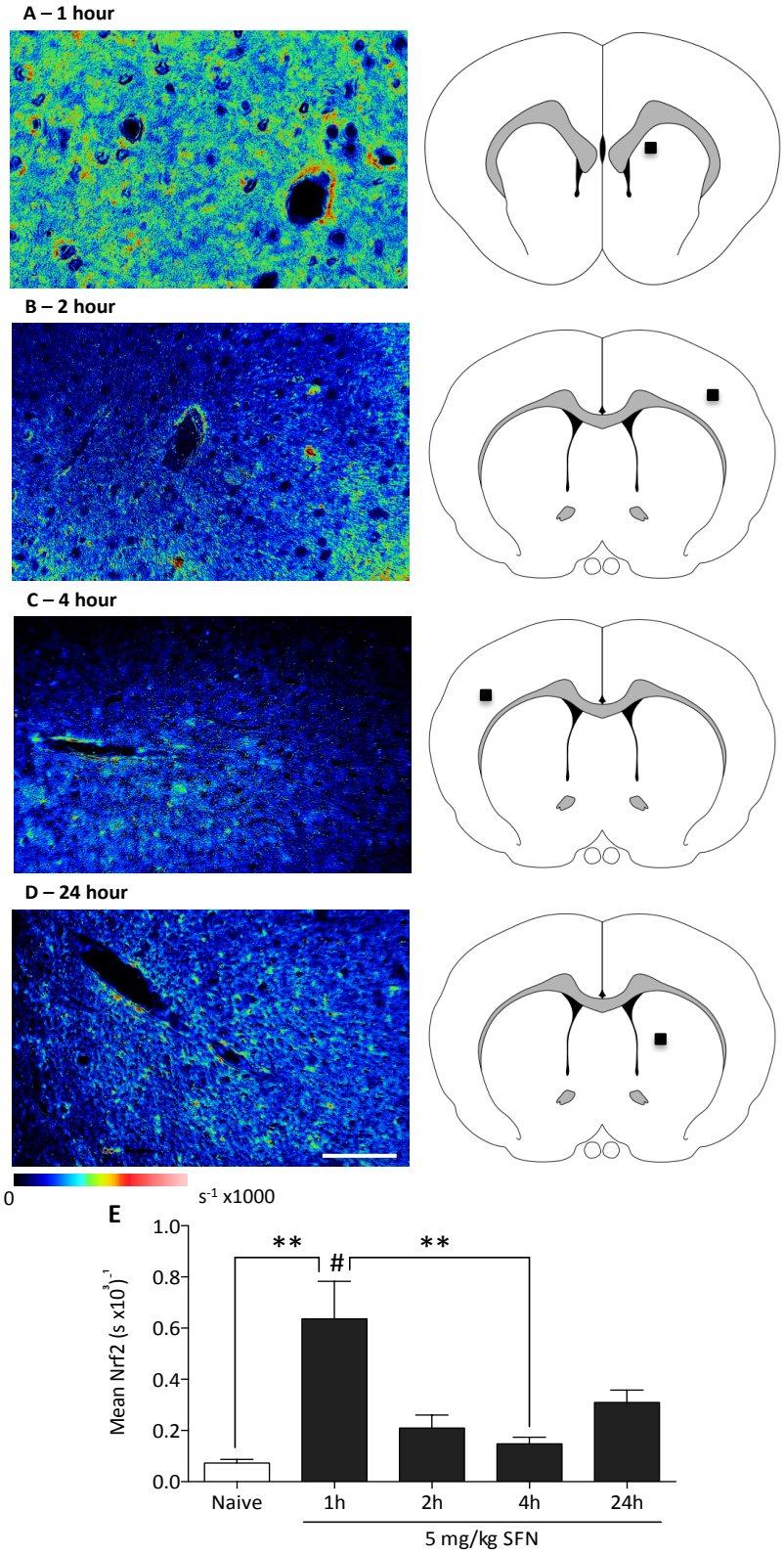

Figure 5.1 Induction of Nrf2 following sulforaphane administration in ex vivo brain sections from naïve animals.

Coronal brain sections (10µm) from naïve rats treated with sulforaphane (SFN) (5mg/kg , *i.p.*) were incubated with rabbit anti-Nrf2 primary antibody and anti-rabbit biotinylated secondary antibody. Sections were reacted with DAB-H_2O_2 and images captured to quantify Nrf2 content in *ex vivo* brain sections from animals treated with SFN for (A) 1h, (B) 2h, (C) 4h and (D) 24h. Black squares (■) in brain maps show the location of acquired images. (E) Summary of mean total cellular Nrf2 content in brain sections from naïve and sulforaphane treated animals. Data denote mean ± S.E.M, ** P<0.01 and # P<0.05 1h vs 2h SFN treatment, n=3 animals per experimental group. Scale bar represents 10µm.

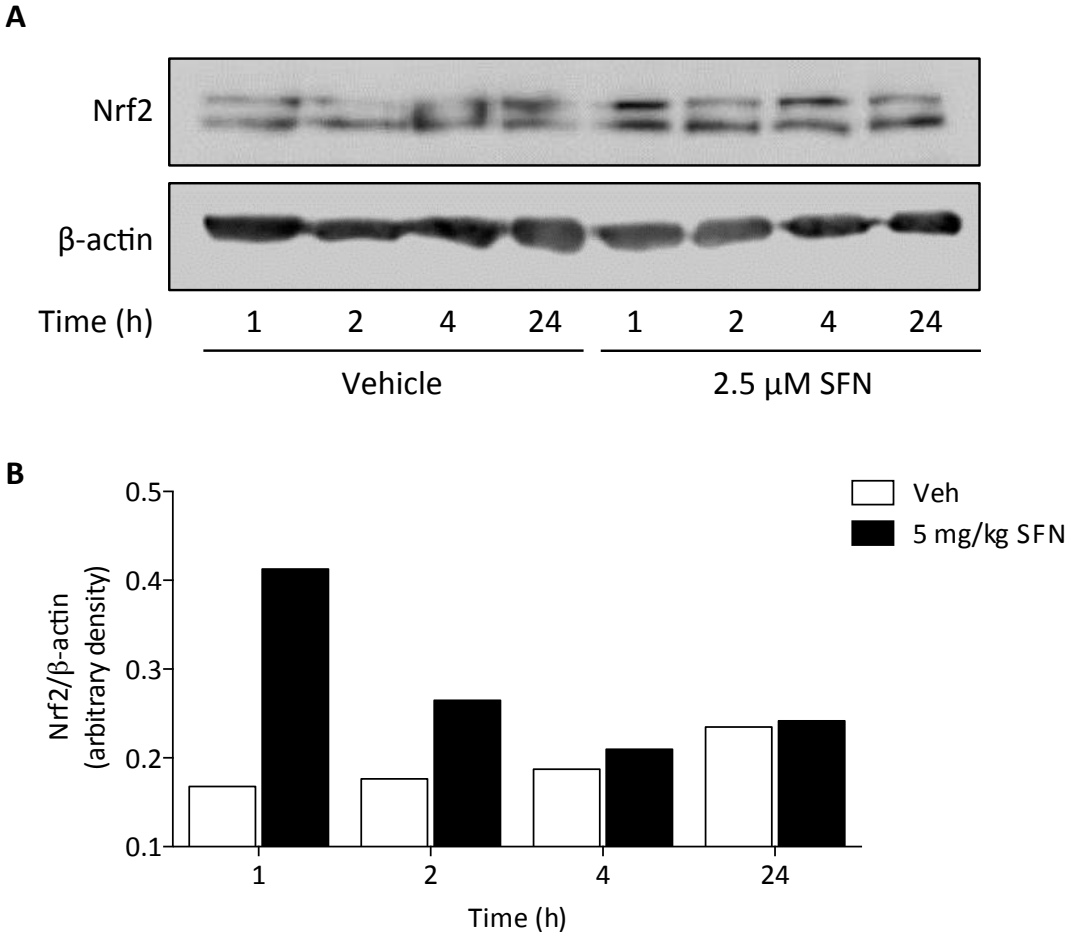

Figure 5.2 Sulforaphane (SFN)-mediated induction of Nrf2 in brain homogenates from naïve animals.

Brains from naïve rats treated with vehicle (1% corn oil in saline), or sulforaphane (SFN) (5mg/kg, *i.p.*) for 1, 2, 4 or 24h were homogenised to obtain whole brain lystaes. Collected lysates were separated on an 8% polyacrylamide gel, transferred onto PVDF membranes and (A) immunoblotted for Nrf2. ß-actin served as the loading control. (B) Densitometric analysis of Nrf2 expression relative to ß-actin. Data from 8 different animals treated with either vehicle or SFN.

5.2.2 Sulforaphane mediates the induction of Nrf2-mediated proteins in naïve brains

Analysis of *ex vivo* brain sections and immunoblotting of brain homogenates revealed an increase in cerebral Nrf2 content following sulforaphane treatment. Hence, the effect of sulforaphane treatment on Nrf2-linked proteins was assessed by either quantitative immunohistochemistry or immunofluorescence in brain sections from naïve rats administered sulforaphane (5mg/kg, *i.p.*) for 24h. The data shown in this section is from work done in collaboration with Keith Farell-Dillion, MSc student, Cardiovascular Division, King's College London.

HO-1 protein content was determined in 10µm brain sections from naïve and sulforaphane-treated rats using quantitative immunohistochemistry. Total cellular HO-1 content was determined following the addition of HO-1 in the nucleus and its respective cytoplasmic compartment. HO-1 expression was assessed (1) on a cellular basis (Figure 5.3 A), and (2) on a per animal basis for each per experimental group (Figure 5.3 B). Notably, as time was limited, the data for HO-1 in naive brains shown in Figure 5.3 was from 1 animal, whereas 3 animals were used per group of rats treated with sulforaphane.

A significant increase in the time-dependent protein expression of HO-1 was observed in brains 1 – 4h after sulforaphane treatment compared to cells in naïve brains ($P<0.05$ for 1h versus naïve and $P<0.001$ for 2 and 4h versus naïve, Figure 5.3A). Furthermore, a significant increase in HO-1 protein is observed 4h after treatment compared to 1 and 2h ($P<0.001$, Figure 5.3A). Although an increase in HO-1 protein is observed 2h after sulforaphane administration compared to 1h, this trend was not significant (Figure 5.3A). Although analysis of HO-1 protein expression revealed an increasing trend after sulforaphane administration, this trend was not significant (Figure 5.3B).

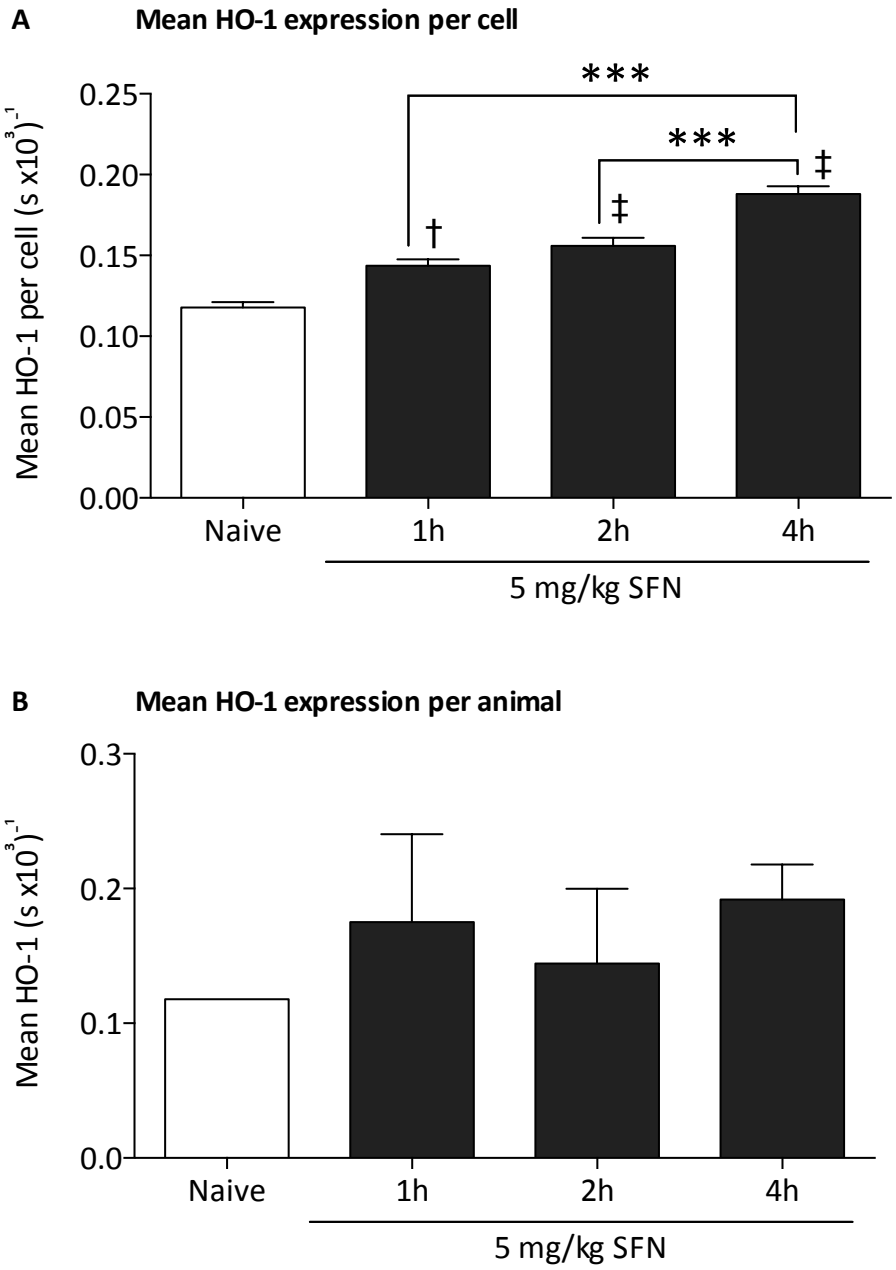

Figure 5.3 Quantification of HO-1 following sulforaphane treatment in naïve animals.
Coronal brain sections (10µm) from naïve and sulforaphane (1 – 4h, SFN 5 mg/kg, *i.p.)* treated animals were incubated with anti-heme oxygenase-1 (HO-1) primary antibody and expression assessed by quantitative immunohistochemistry. Sections were reacted with DAB-H_2O_2 and images captured to quantify HO-1 content in *ex vivo* brain sections from naïve and SFN treated rats. (**A**) Bar graph represents mean HO-1 protein content in all identified cells (cytoplasm and nuclear pair) determined from naïve (n = 176 cells) and 1h (632 cells), 2h (473 cells) and 4h (756 cells) sulforaphane treated rats. Data denote mean ± S.E.M. *** $P<0.001$, † $P<0.05$ vs naïve and ‡ $P<0.001$ vs naïve. Cells counted in this study were identified in the forebrain. (**B**) Bar graph represents mean HO-1 content determined from naïve (n=1 rat) and animals administered sulforaphane for 1 – 4h (n=3 animals per treatment group).

The limited availability of brain sections from naïve rats administered sulforaphane for 24h prevented analysis of Nrf2-linked enzymes by quantitative immunohistochemistry. Hence, immunofluorescence was used to examine the protein expression of HO-1 (Figure 5.4), NQO1 (Figure 5.5) and Prx1 (Figure 5.6). Significant increases in HO-1 ($P<0.05$) and Prx1 ($P<0.01$) protein was observed in brain 24h after sulforaphane administration. An increase in NQO1 protein expression was also noted, however, albeit this trend was not significant. Visual analysis of HO-1 and Prx1 fluorescence images suggests that 24h sulforaphane administration upregulates protein expression in the cerebral endothelium, identified by RECA1 immunostaining.

5.2.3 Sulforaphane treatment increases GFAP expression in the naïve rat brain

The astrocytic marker GFAP is a filamentous protein that is upregulated in response to increased oxidative stress following the introduction of a neurodegenerative state (Brahmachari *et al.*, 2006). To assess if GFAP expression is affected by sulforaphane treatment, GFAP levels were measured by immunofluorescence in naïve brain sections.

GFAP expression was below detection limits in the naïve rat brains (Figure 5.7 A). However, 1 – 4 h after sulforaphane administration, an increase in GFAP expression was observed by fluorescence microscopy (Figure 5.7 B – D). Fluorescent images for GFAP protein show increased staining in brain sections from animals treated with sulforaphane for 4h before sacrifice (Figure 5.7D).

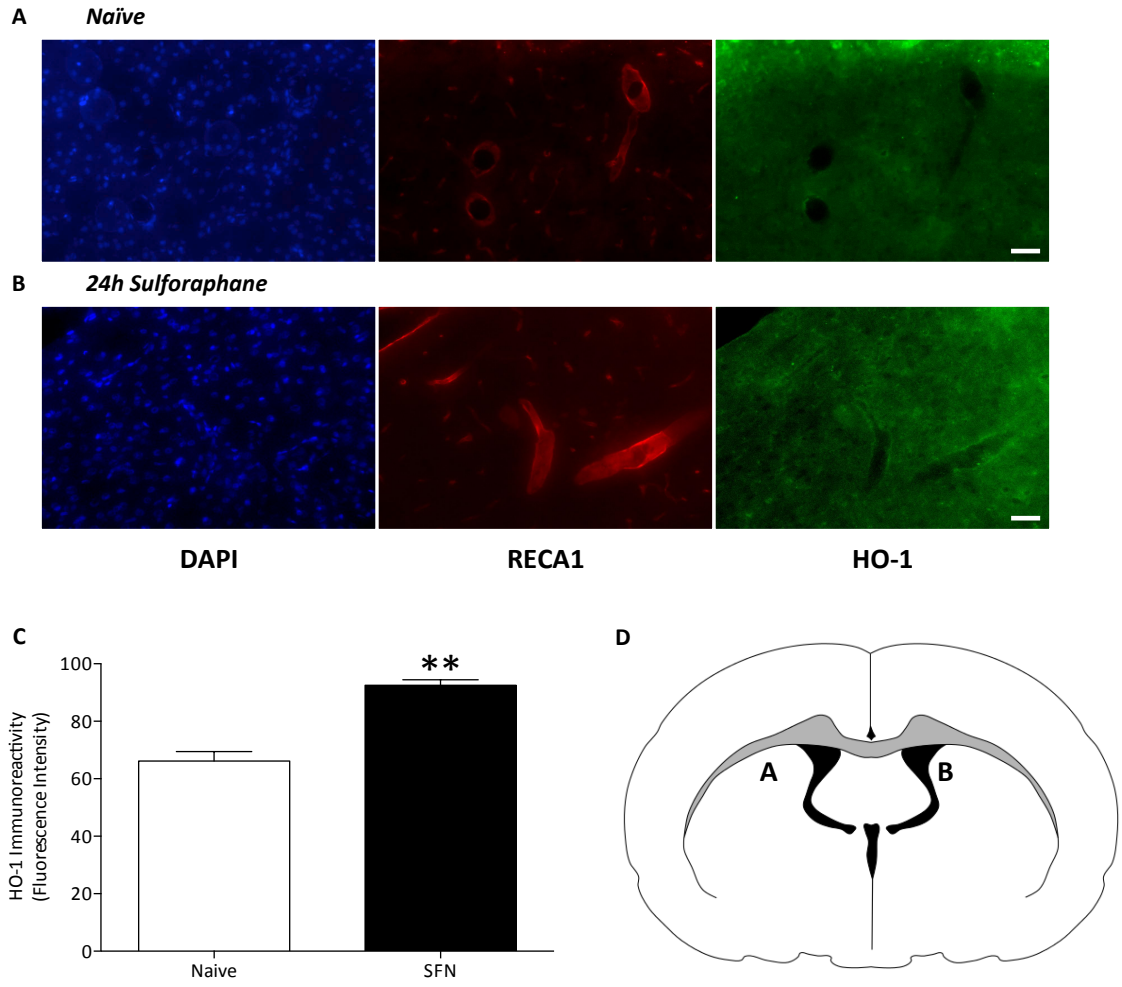

Figure 5.4 Induction of HO-1 following sulforaphane treatment in naïve animals.
10µm coronal brain sections from naïve and sulforaphane (24h, SFN, 5 mg/kg, *i.p.)* treated animals were incubated with anti-heme oxygenase-1 (HO-1) primary antibody and expression assessed by immunofluorescence. Representative immunofluorescence staining for DAPI for nuclei (blue), cerebral endothelium by RECA1 (red) and HO-1 staining (green) in (**A**) naive and (**B**) sulforaphane treated animals. Scale bar denote 5µm. (**C**) Fluorescence intensity for HO-1 was measured using image J. Three sections per animal were imaged, with 3 fields of view captured per section. Data denote mean ± S.E.M., n = 3 animals per group, ** $P < 0.01$ vs naïve. (D) Brain map shows the location of images in (A) and (B). Scale bar represents 5µm.

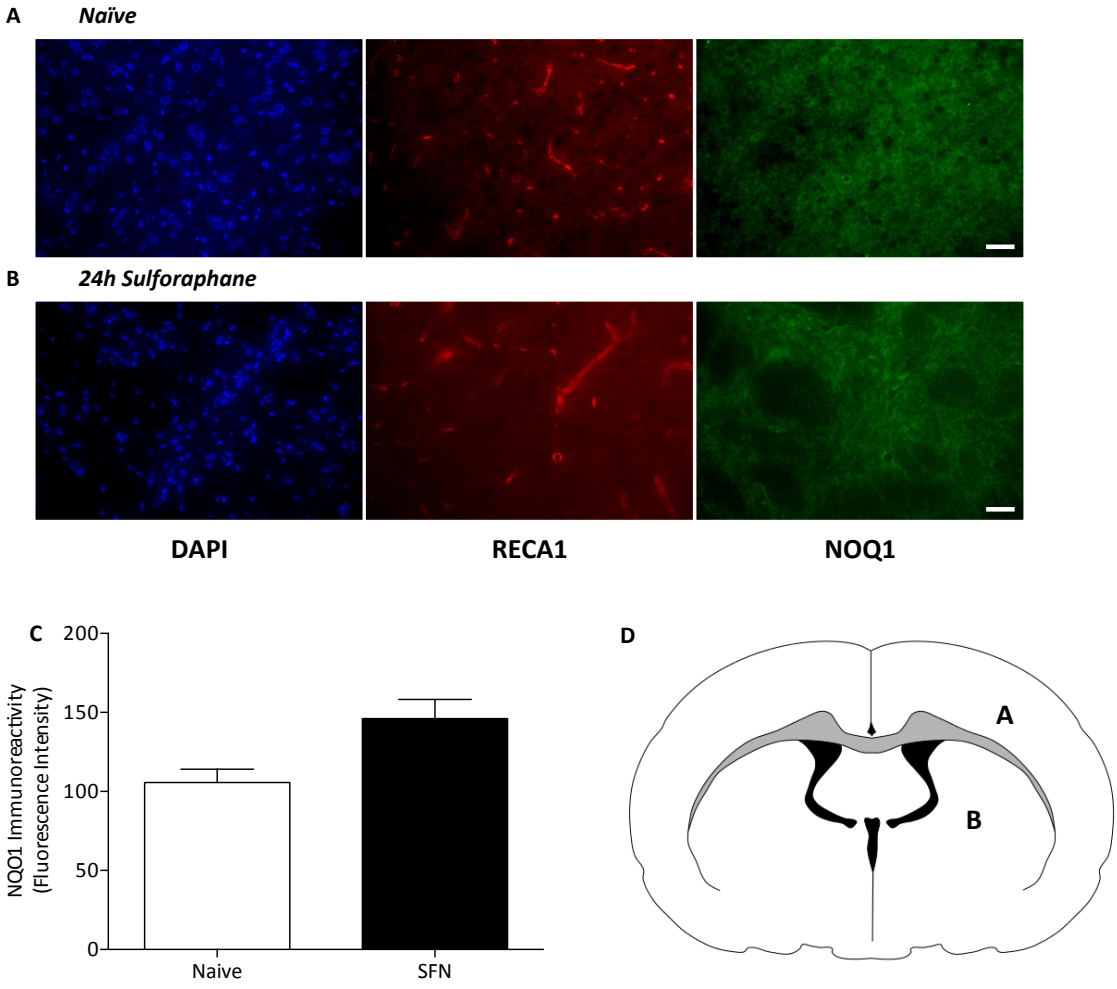

Figure 5.5 Induction of NQO1 following sulforaphane administration in naïve animals.
10µm coronal brain sections from naïve and sulforaphane (24h, SFN, 5 mg/kg, *i.p.)* treated animals were incubated with anti-NQO1 primary antibody and expression assessed by immunofluorescence. Representative immunofluorescence staining for DAPI staining nuclei (blue), cerebral endothelium by RECA1 (red) and NQO1 staining (green) in (A) naive and (B) sulforaphane treated animals. Scale bar denote 5µm. (C) Fluorescence intensity for NQO1 was measured using image J. Three sections per animal were imaged, with 3 fields of view captured per section. Data denote mean ± S.E.M., n = 3 animals per group. (D) Brain map shows the location of images in (A) and (B). Scale bar represents 5µm.

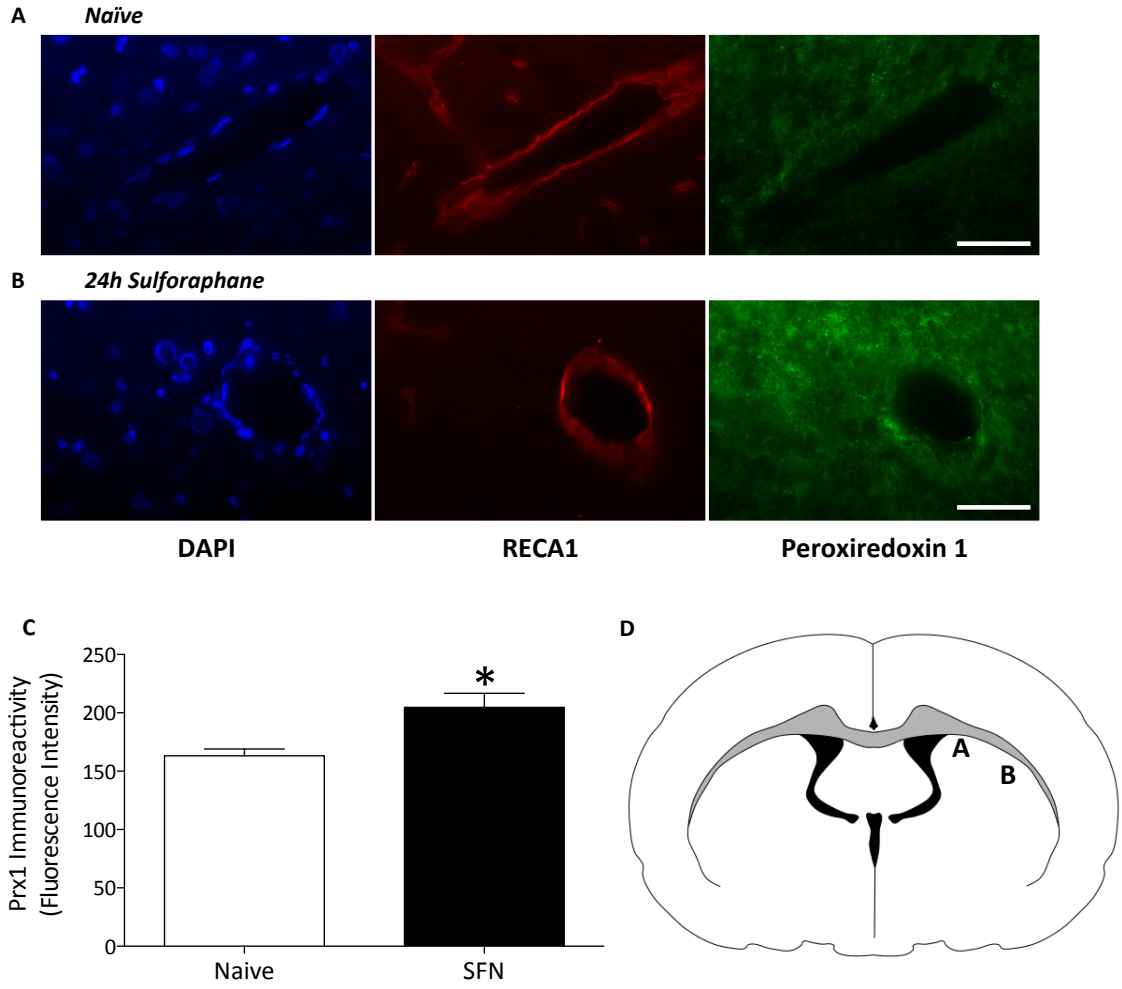

Figure 5.6 Induction of Prx1 after sulforaphane administration in naïve animals.
10µm coronal brain sections from naïve and sulforaphane (24h, SFN, 5 mg/kg, *i.p.)* treated animals were incubated with anti-peroxiredoxin 1 (Prx1) primary antibody and expression assessed by immunofluorescence. Representative immunofluorescence staining for DAPI for nuclei (blue), cerebral endothelium by RECA1 (red) and peroxiredoxin 1 staining (green) in (A) naive and (B) sulforaphane treated animals. Scale bar denote 5µm. (C) Fluorescence intensity for Prx1 was measured using image J. Three sections per animal were imaged, with 3 fields of view captured per section. Data denote mean ± S.E.M., n = 3 animals per group, * $P < 0.05$ vs naïve. (D) Brain map shows the location of images in (A) and (B). Scale bar represents 5µm.

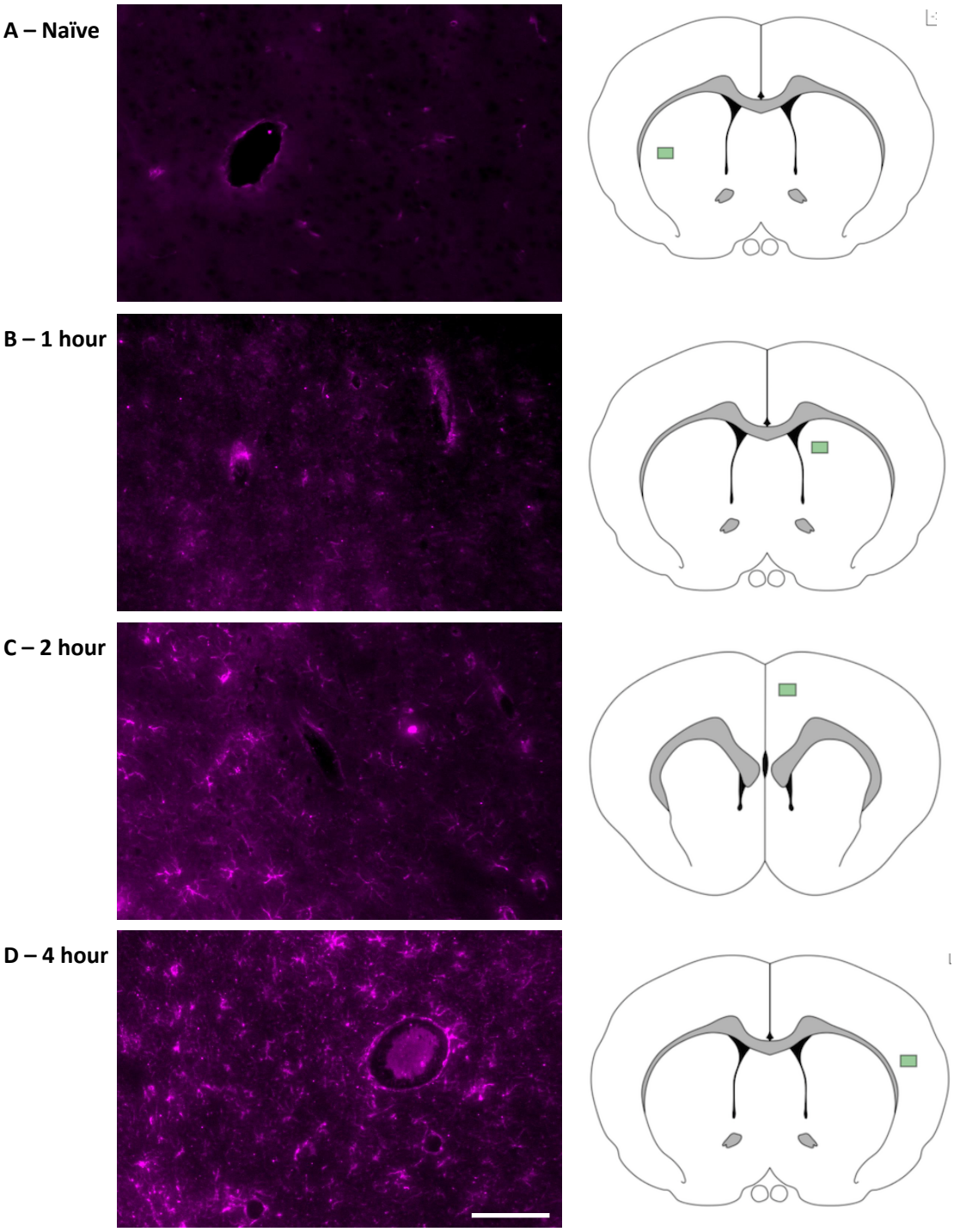

Figure 5.7 Sulforaphane treatment increases GFAP expression in the naïve rat brain.
GFAP expression was assessed in 10µm coronal brain sections from naïve and sulforaphane (SFN, 5mg/kg, *i.p.*) treated rats. Brain sections were incubated with a goat anti-GFAP primary antibody, and complementary donkey anti-goat Cy5 conjugated fluorescent secondary antibody. 32-bit grey scale fluorescence images were captured and pseudo coloured using Image J. Representative fluorescence images of GFAP expression in brain sections from (A) naïve rats and rats treated with SFN for (B) 1 hour, (C) 2 hour and (D) 4 hour. Green squares (■) in complimentary brain maps show the location of the captured image. Scale bar represents 10 µm.

5.3 Effects of sulforaphane pre-treatment on Nrf2 and Nrf2-linked protein expression after 24h reperfusion injury

Section 5.2 highlights the rapid induction of Nrf2 in the brain after sulforaphane administration in naïve rats, as well as demonstrating an increased presence of Nrf2-mediated antioxidant proteins. Studies have highlighted the protective effects of sulforaphane treatment post-ischaemia (Zhao *et al.*, 2006), but have failed to establish post-conditioning regimes as a valid therapeutic strategy to protect patients at a high risk of suffering from stroke. Hence, in this section, we investigated how 60 min sulforaphane pre-treatment, prior to 70 min MCAo and 24h reperfusion injury, affects the expression and cellular localisation of Nrf2 and Nrf2-mediated proteins. The effects of sulforaphane pre-treatment on Nrf2 following stroke were compared with the findings presented in Chapter 4, where rats were subjected to 70 min MCAo and 24h reperfusion only. It should be noted that the sulforaphane pre-treatment study was conducted after the control study (as discussed in Chapter 4). Although the findings in this chapter are compared directly with those reported in Chapter 4, in future experiment, both control and sulforaphane pre-treatment studies should be conducted simultaneously. These experiments were conducted in collaboration with Dr Alessio Alfieri, Cardiovascular Division, King's College London (Alfieri *et al.*, 2013; Srivastava *et al.*, 2013).

5.3.1 Sulforaphane pre-treatment reduces the nuclear to cytoplasmic ratio of Nrf2 protein after 24h reperfusion injury

As mentioned previously, Nrf2 translocates to the nucleus following increased oxidative or electrophilic stress to upregulate the expression of protective antioxidant stress proteins or phase II detoxifying enzymes. Administration of sulforaphane to naïve rats did not significantly alter the nuclear to cytoplasmic distribution of Nrf2 compared to control animals (Figure 5.8 A and C). After 70 min MCAo and 24h reperfusion injury in rats, an increase in nuclear to cytoplasmic distribution of Nrf2 was observed in the stroke-affected hemisphere, indicating increased nuclear accumulation of Nrf2 (Figure 5.8 C). However, in animals pre-treated with sulforaphane 60 min prior to MCAo and 24h reperfusion injury, a marked reduction in the nuclear to cytoplasmic distribution of Nrf2 was observed in both contralateral and stroke-affected hemispheres, compared to untreated animals ($P<0.001$, Figure 5.8 B and C). Although pre-treatment resulted in a significant increase in the nuclear to cytoplasmic distribution of Nrf2 in the stroke-affected hemisphere compared to the contralateral ($P<0.001$), cellular Nrf2 content was greater in the cytoplasmic compartment in both hemispheres of the ischaemic brain (ratio < 1.0, Figure 5.8 C).

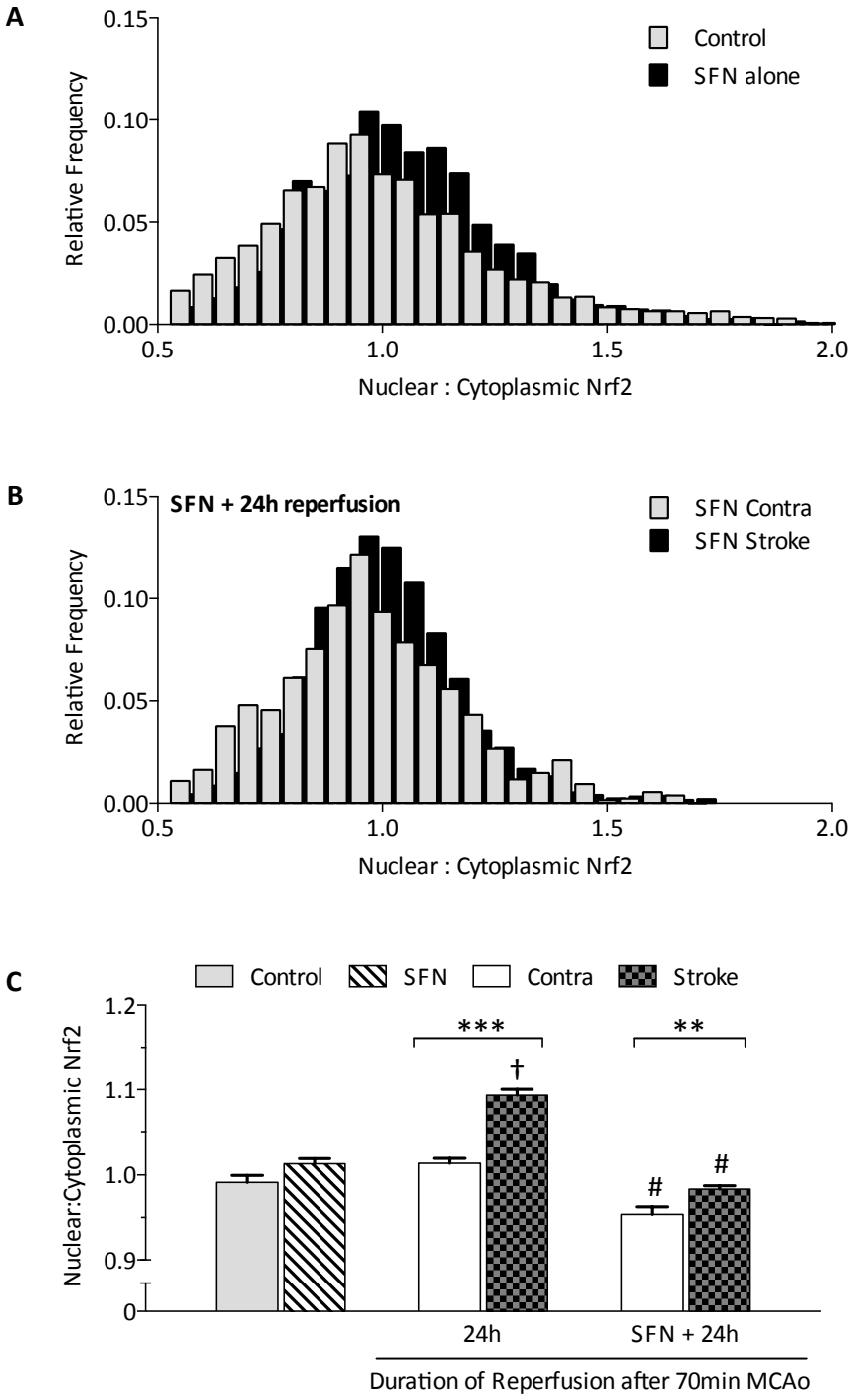

Figure 5.8 Nuclear to cytoplasmic distribution of Nrf2 after 1h sulforaphane pre-treatment prior to 70 min MCAo and 24h reperfusion injury.

The nuclear to cytoplasmic ratio of Nrf2 was determined for each respective cell defined by the nucleus and its 4μm ring taken to be its respective cytoplasm, irrespective of cell type. Cells counted in animals subjected to 70min MCAo and 24h reperfusion were identified in the forebrain, however, for SFN-pre-treated animals, cells counted were identified in the midbrain. Histograms show the nuclear to cytoplasmic ratio of Nrf2 in brain sections from (**A**) 3199 cells in control animals and 1869 cells in animals treated with sulforaphane (SFN, 5 mg/kg *i.p.*) for 24h, and (**B**) in the contralateral (1273 cells) and stroke-affected hemisphere (2420 cells) of pre-treated animals subjected to 70 min MCAo and 24h reperfusion injury. (**C**) Summary of mean cellular nuclear to cytoplasmic ratio of Nrf2. Data denote mean ± S.E.M., n=1273-3200 cells from 3 animals. ** P<0.01, *** P<0.001, † P<0.05 vs contralateral hemisphere, # P<0.001 vs matched hemisphere in animals not pre-treated with sulforaphane. Figure adapted from (Srivastava *et al.*, 2013).

5.3.2 *Sulforaphane pre-treatment reduces total cellular Nrf2 content after 24h reperfusion injury*

To investigate the effects of sulforaphane pre-treatment on cellular Nrf2 expression 70 min MCAo and 24h reperfusion, rats were pre-treated with sulforaphane (5 mg/kg, i.p.) for 1 hour before the start of 70 min MCAo duration. To understand Nrf2 cellular distribution, the sum of each nuclear and cytoplasmic pair was calculated to give a value for total cellular Nrf2. Furthermore, the spatial distribution of Nrf2 was also determined in the ischaemic brain of animals pre-treated with sulforaphane. Although the histogram does not clearly highlight a difference in Nrf2 protein spatial distribution (Figure 5.9 A), mean cellular Nrf2 values show a marked increase in cells within the peri-infarct region of the sulforaphane pre-treated ischaemic brain compared to the infarct core and contralateral brain regions ($P<0.001$, Figure 5.9 B). Furthermore, mean cellular Nrf2 content was also greater in the infarct core region compared to contralateral regions of the pre-treated brain ($P<0.001$, Figure 5.9 B). Moreover, a marked reduction of cellular Nrf2 was observed in all regions of the pre-treated ischaemic brain, compared to animals that were not pre-treated with sulforaphane, prior to 70 min MCAo and 24h reperfusion injury ($P<0.001$, Figure 5.9 B). Although analysis of Nrf2 content on a per-animals basis (Figure 5.9 C) showed the same trend as in Figure 5.8 B, no significance difference in Nrf2 content was observed between stroke-affected regions of the sulforaphane pre-treated ischaemic brain.

5.3.2 *Sulforaphane pre-treatment reduces endothelial Nrf2 content after 24h reperfusion injury*

Chapter 4 clearly demonstrated changes in endothelial Nrf2 content following ischaemia and reperfusion injury. Hence, endothelial distribution of Nrf2 in the sulforaphane pre-treated ischaemic brain was assessed using quantitative immunohistochemistry. The histogram shown in figure 5.9 illustrates an increase in endothelial Nrf2 with peri-infarct regions of the sulforaphane pre-treated ischaemic brain (Figure 5.10 A).

Calculation of the mean endothelial content interestingly reveals lower levels of Nrf2 in the infarct core region of the stroke-affected hemisphere compared with contralateral brain regions, although this trend is not significant (Figure 5.10 B). Mean endothelial Nrf2 levels were elevated in the peri-infarct region of the stroke-affected hemisphere compared to the infarct core and contralateral brain regions of sulforaphane pre-treated animals ($P<0.001$ Figure 5.10 B). Moreover, endothelial Nrf2 content was markedly reduced in all regions of the pre-treated ischaemic brain compared to animals that did not receive a sulforaphane (Figure 5.10 B).

Figure 5.9 Spatial distribution of Nrf2 in sulforaphane pre-treated animals subjected to 70 min MCAo and 24h reperfusion injury.

(**A**) Histogram shows the total Nrf2 content in each cell identified in the contralateral hemisphere (n = 1317 cells) and infarct core (1368 cells) and peri-infarct (1052 cells) regions of the stroke affected hemisphere of rats pre-treated with sulforaphane (SFN, 5 mg/kg *i.p.*) 1h prior to 70 min MCAo and 24h reperfusion. (**B**) Summary of mean total cellular Nrf2 content in cells from control animals, 24h sulforaphane (SFN) treated animals, and in contralateral and stroke affected regions from animals subjected to 70 min MCAo and 24h reperfusion injury ± SFN. Cells counted in animals subjected to 70min MCAo and 24h reperfusion were identified in the forebrain, however, for SFN-pre-treated animals, cells counted were identified in the midbrain. Data denote mean ± S.E.M, *** $P<0.001$ within experimental groups (contralateral vs core, contralateral vs peri and core vs peri) **C**) Mean Nrf2 determined per animal. Data denote mean ± S.E.M., *** $P<0.001$ and # $P<0.001$ vs complementary regions in animals subjected 70 min MCAo and 24h reperfusion injury.

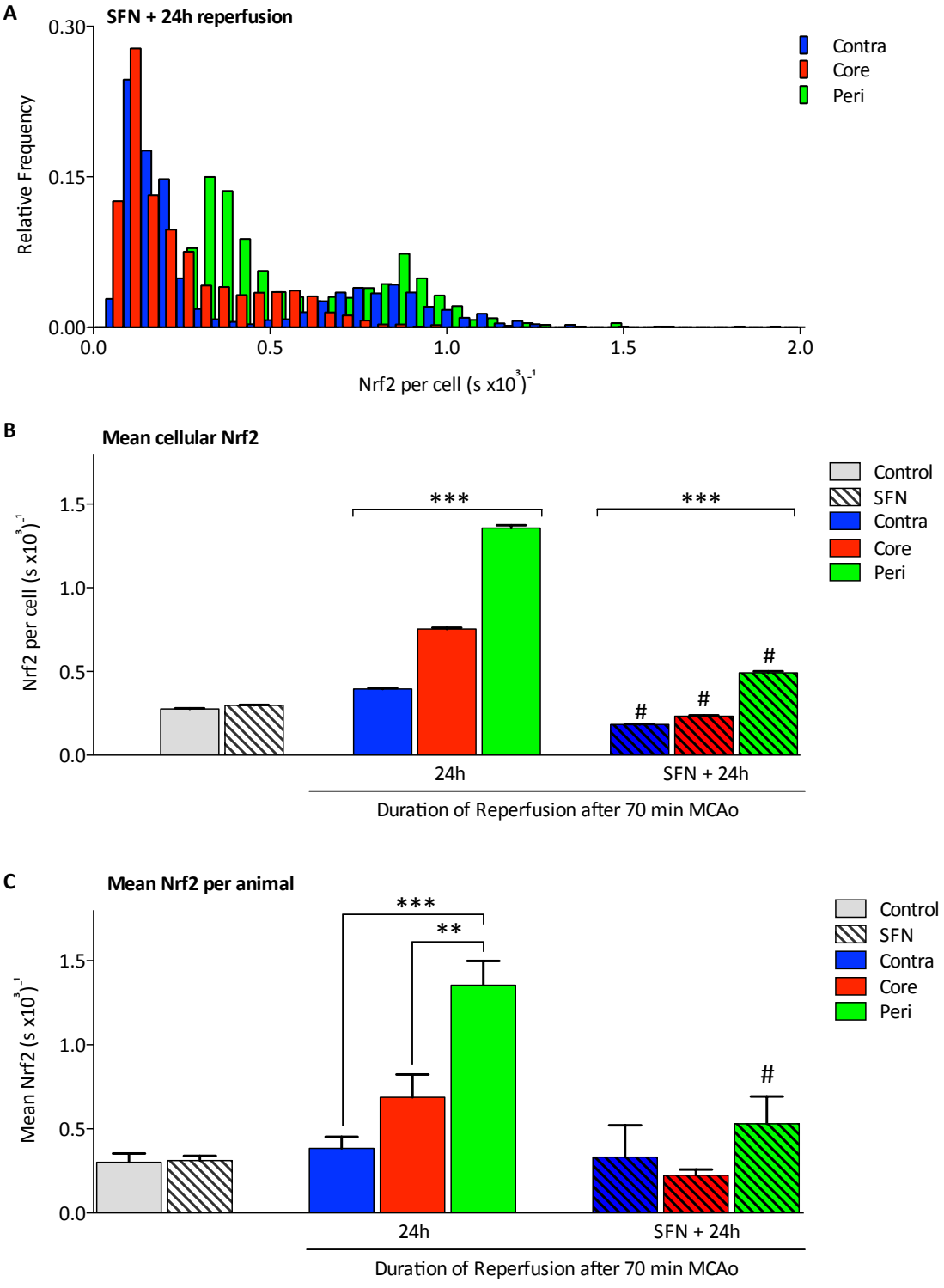
A
SFN + 24h reperfusion
Relative Frequency
0.30
0.15
0.00
0.0
0.5
1.0
1.5
2.0
Nrf2 per cell (s x10³)⁻¹
Contra
Core
Peri
B
Mean cellular Nrf2
Nrf2 per cell (s x10³)⁻¹
1.5
1.0
0.5
0.0
***
***
#
#
#
24h
SFN + 24h
Duration of Reperfusion after 70 min MCAo
Control
SFN
Contra
Core
Peri
C
Mean Nrf2 per animal
Mean Nrf2 (s x10³)⁻¹
1.5
1.0
0.5
0.0
***
**
#
24h
SFN + 24h
Duration of Reperfusion after 70 min MCAo
Control
SFN
Contra
Core
Peri

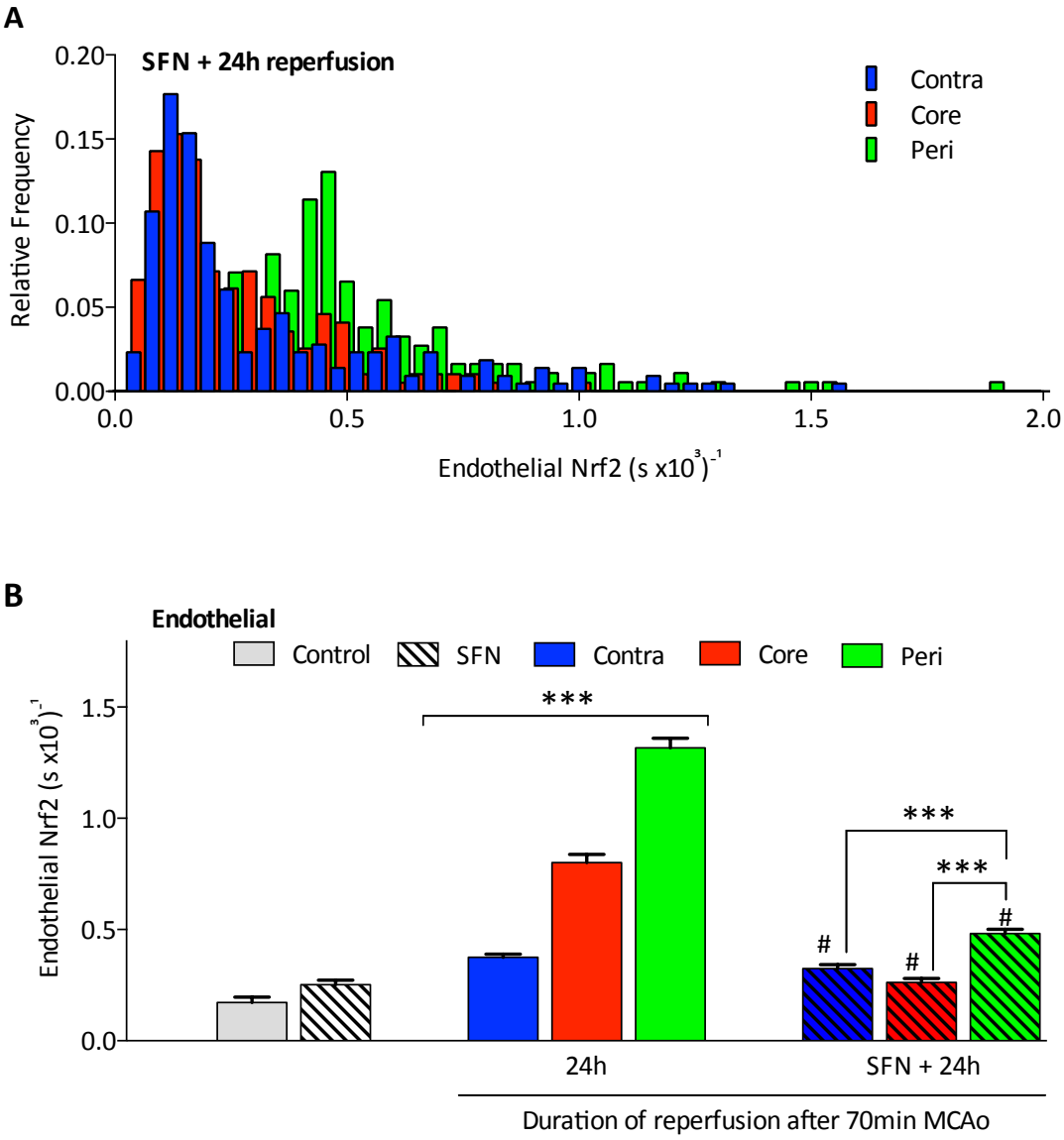

Figure 5.10 Effects of sulforaphane pre-treatment on endothelial Nrf2 content after MCAo and reperfusion injury.

Endothelial Nrf2 content was determined structures stained positive for RECA1. (**A**) Histogram shows the endothelial Nrf2 content in the contralateral hemisphere and infarct core and peri-infarct regions of the stroke-affected hemisphere. (**B**) Summary of mean endothelial Nrf2 content from control animals, 24h sulforaphane (SFN, 5 mg/kg *i.p.*) treated animals, and in contralateral and stroke affected regions from animals subjected to 70 min MCAo and 24h reperfusion injury ± SFN. Cells counted in animals subjected to 70min MCAo and 24h reperfusion were identified in the forebrain, however, for SFN-pre-treated animals, cells counted were identified in the midbrain. Data denote mean ± S.E.M., n= 5 animals in control group, and n=3 animals for each experimental group. *** $P<0.001$ within groups (contralateral vs core, contralateral vs peri, core vs peri), unless otherwise stated, and # $P<0.001$ vs complementary regions in animals subjected 70 min MCAo and 24h reperfusion.

5.4 Discussion

The dietary isothiocyanate, sulforaphane, is an inducer of the Nrf2 defense pathway. Previous studies have reported a role of sulforaphane-mediated protection in the brain post ischaemia and reperfusion injury. This chapter investigated how sulforaphane administration affects the expression of Nrf2 and Nrf2-mediated genes in the naïve brain, and furthermore, examined the impact of sulforaphane pre-treatment on Nrf2 expression after 70 min MCAo and 24h reperfusion injury. Currently, stroke research has focused on the upregulation of protective mechanisms post-ischaemia, however, destructive mechanisms are activated almost immediately after ischaemia. Thus, it was hypothesised that pre-conditioning will enhance basal protective mechanisms in the brain, conferring greater protection against ischaemia-reperfusion injury induced oxidative stress. The data presented in this chapter shows rapid induction in the expression of Nrf2 in the brain of naïve rats following SFN treatment. Moreover, 24h after sulforaphane administration, an increase is noted in expression of two Nrf2 mediated proteins, HO-1 and Prx1.

This chapter provides new evidence, highlighting marked attenuation of Nrf2 protein levels in cerebral cells and endothelium within all ischaemic brain regions in rats pre-treated with the Nrf2 inducer sulforaphane.

5.4.1 Sulforaphane rapidly induces Nrf2 expression in the naïve brain

The data presented in this chapter reveals a significant increase in Nrf2 protein expression within the brain of naïve rats following 1h of sulforaphane administration (Figure 5.2 and 5.2). Furthermore, a rapid decrease in Nrf2 expression was observed following 2h sulforaphane administration. These results are consistent with published findings from Jazwa *et al.* who demonstrated a similar response in striatal lysates of Nrf2 WT mice treated with a higher dose of sulforaphane (50 mg/kg, *i.p.*) (Jazwa *et al.*, 2011). Jazwa *et al.* also demonstrated that sulforaphane crosses the BBB, attaining peak concentrations in both striatal and ventral mid-brain tissue within 15 min of administration (Jazwa *et al.*, 2011). It is important to highlight that the dose of SFN used in Jazwa *et al.* studies with mice was 10-fold higher than the dose used in our current study. These findings suggest that lower concentrations of sulforaphane rapidly induce Nrf2 expression in the brains of naïve rodents.

Although sulforaphane increases Nrf2 expression in the rodent brain, Nrf2 *per se* does not affect the bioavailability of sulforaphane or its metabolites, (Clarke *et al.*, 2011). LC-MS/MS analysis of tissue revealed a dose dependent (5 – 20 µmoles) increase in accumulation of sulforaphane and its metabolites within brain, liver and plasma tissue from mice (Clarke *et al.*, 2011). Therefore, it is possible that the level of Nrf2 induction observed in naïve rodents is influenced

by the concentration of sulforaphane present within tissue. However, it remains to be elucidated whether sulforaphane or its metabolites induce Nrf2 expression.

5.4.2 Sulforaphane influences Nrf2-mediated protein expression in the naïve rat brain

Our study revealed increases in HO-1 and Prx1 expression in the naïve rat brain following sulforaphane administration. Furthermore, our findings provide the first evidence for increases in Prx1 protein expression in the naïve rat brain 24h after sulforaphane administration. Zhao *et al.* have shown that sulforaphane (5 mg/kg *i.p.*) increases HO-1 mRNA and protein expression in the naïve mouse brain after 24h (Zhao *et al.*, 2006). Furthermore, these authors identified increased localisation of HO-1 protein with cortical astrocytes and neurons (Zhao *et al.*, 2006). Our study further shows increased HO-1 expression in the cerebrovascular endothelium, 24h after sulforaphane administration in rats. This result is consistent with the findings of Zhao *et al*, who reported increased HO-1 expression in the cerebrovascular endothelium, 18h after sulforaphane treatment (50 mg/kg, *i.p.*) in mice (Zhao *et al.*, 2007a).

As discussed earlier in Chapter 4, the promoter region of the HO-1 gene contains multiple binding elements for various transcription factors. Hence, further experiments are required to confirm that the observed increase in HO-1 following sulforaphane administration is mediated via Nrf2 in Nrf2 KO mice or by silencing Nrf2 in rats using siRNA.

5.4.3 Sulforaphane pre-treatment effects Nrf2 expression after stroke

A marked attenuation of Nrf2 protein expression was observed in rats pre-treated with sulforaphane prior to 70 min MCAo and 24h reperfusion injury. As mentioned earlier, Nrf2 levels were elevated in cerebral cells 1h after sulforaphane administration in naïve rats (Figure 5.1 and 5.2). In Chapter 4, the time course of Nrf2 expression in cerebral cells was defined, revealing peak Nrf2 protein expression after 24h reperfusion injury with peak expression of Nrf2-mediated cytoprotective proteins attained 18 – 24h after reperfusion injury. The onset of destructive mechanisms following cerebral ischaemia occurs almost immediately (Endres *et al.*, 2008), and although reperfusion is described as a protective phenomenon, an increase in ROS generation is observed upon the re-introduction of blood-flow into the ischaemic vessel (Peters *et al.*, 1998). Therefore, the naïve brain may be "ill-equipped" to provide sufficient protection against ischaemia-reperfusion injury induced oxidative stress.

Zhao *et al.* demonstrated that sulforaphane treatment post ischaemia in mice reduced infarct volume, (Zhao *et al.*, 2006), however they did not investigate changes in cognitive function. Another study exploring intracerebral hemorrhage (ICH) as a model of cerebral stroke in mice, also highlights the protective effects of sulforaphane administration post-injury (Zhao *et al.*,

2007b). These authors reported a marked improvement in neurological scores and significant reductions in oxidative damage in mice post-treated with sulforaphane (Zhao *et al.*, 2007b).

Both studies showed the protective effects of sulforaphane when administered after injury, and moreover, the second study successfully highlighted that the protective effects of sulforaphane are likely to be conferred via the Nrf2-defence pathway (Zhao *et al.*, 2006; Zhao *et al.*, 2007b). However, theses studies imply that the protective effects of sulforaphane are only viable when administered in a short time frame (15 – 30 min) following the onset of ischaemia, although therapeutic stroke research has failed to comment on the outcomes of sulforaphane treatment if administered 6 – 24h after ischaemia. A clinical limitation of rtPA treatment in stroke patients is related to the short time-window of efficacy (< 3.5h after the onset of ischaemia), thus rendering a high percentage of patients ineligible for treatment by rtPA. Pre-conditioning strategies, to upregulate Nrf2 mediated cytoprotective enzymes, may provide an improved therapeutic method in limiting the neurological deficits observed after stroke in high-risk patients.

Sulforaphane pre-treatment resulted in the attenuation of Nrf2 protein expression in all regions of the ischaemic rat brain (contralateral and stroke-affected hemispheres). Furthermore, our study also highlighted significant improvements in neurological deficits in sulforaphane pre-treated rats (see Appendix Figure 5) (Alfieri *et al.*, 2013). It is well established that sulforaphane administration in rodents rapidly induces cellular Nrf2 expression after 1h, conferring increased protection. Although we demonstrated that Nrf2 protein content was similar to basal levels, 2h after sulforaphane administration, it is unclear how Nrf2 protein expression would be affected by ischaemia in pre-treated rat brains, thus warranting further investigation.

Quantitative immunhistochemistry for HO-1 revealed a time-dependent increase in protein expression 1 – 4h after sulforaphane administration in naïve rat brains. This data suggests that following sulforaphane pre-treatment, Nrf2-mediated proteins are upregulated earlier during reperfusion-induced injury. We further demonstrated increased area of HO-1 protein expression in the stroke-affected hemisphere of sulforaphane pre-treated rats (Alfieri *et al.*, 2013). Interestingly, the findings presented in this chapter also reports a decrease in Nrf2 protein expression in the brains of rats pre-treated with sulforaphane for 1h before 70 min MCAo and 24h reperfusion. However, in Figure 5.1, administration of sulforaphane *i.p.* (5 mg/kg) increased Nrf2 protein content in the brain after 1h, thus suggesting an increase in nuclear Nrf2 content. It is therefore possible that with this activation of Nrf2 at the time of induction of MCAo in sulforaphane pre-treated rats attenuates the later induction of Nrf2 observed in rats subjected to MCAo and reperfusion. These findings suggest that sulforaphane pre-treatment enhances the brain's antioxidant capacity, affording increased protection against ischaemia-reperfusion injury induced oxidative stress. However, further investigation is required to

understand the time-course of Nrf2 protein expression following MCAo in sulforaphane pre-treated animals.

In a different model of experimental stroke, Ping *et al* showed that pre-treatment of rat pups with sulforaphane (5 mg/kg *i.p.*), 30 min prior to 90 min hypoxia-ischaemia insult, attenuated cell death (Ping *et al.*, 2010). Ping *et al.* further demonstrated that sulforaphane pre-treatment increased Nrf2 and HO-1 protein expression after hypoxia-ischaemic insult (Ping *et al.*, 2010). Thus, although these authors have not shown the effects of sulforaphane in the naïve rat brains, the data confirms our findings.

The presented findings suggest that activation of Nrf2 pre-treatment by sulforaphane plays a key role in protecting against ischaemic brain injury. To validate whether sulforaphane pre-treatment protects the brain, infarct volume should be examined. Moreover, the early increase in antioxidant enzymes protein expression affords increased protection to the brain and may thereby limit the protein expression of Nrf2 after 24h reperfusion injury. However, to validate the current findings, the effects of sulforaphane pre-treatment need to be assessed in the absence of Nrf2.

5.4.4 Sulforaphane pre-treatment and the cerebral endothelium after stroke

As mentioned previously, the cerebrovascular endothelial cells and their tight junctions form a major part of the BBB. The loss of integrity of the blood-brain barrier is due to endothelial cell death, endothelial cell contraction and uncoupling of tight-junctional proteins. Mechanisms that underlie BBB breakdown remains to be elucidated, however, increased ROS generation and, oxidative stress has been shown to play a major role. Previous studies have demonstrated exacerbated infarct volumes following MCAo and reperfusion injury in Nrf2 KO mice (Shah *et al.*, 2007). This therefore suggests a key role for Nrf2 in protecting the BBB following stroke. Zhao *et al.* have shown that sulforaphane (5 mg/kg) treatment, post cortical brain injury in mice, attenuates the loss of tight-junctional proteins and moreover, decreases BBB permeability (Zhao *et al.*, 2007a). Zhao *et al.* further demonstrated an increase in HO-1 protein in the cerebrovascular endothelium 18h after sulforaphane treatment in mice (Zhao *et al.*, 2007a). Zhao *et al.* also reported that sulforaphane-mediated attenuation of cerebrovascular permeability is lost in the absence of Nrf2 (Zhao *et al.*, 2007a) and this suggests that upregulation of Nrf2 and Nrf2-mediated proteins could limit BBB breakdown.

The studies highlighted above demonstrate sulforaphane mediated protection post-cerebral injury. In the present study, treatment of rats with sulforaphane (5 mg/kg, *i.p.*) prior to 70 min MCAo and 24h reperfusion injury attenuated Nrf2 protein expression in the cerebrovascular endothelium. Furthermore, our findings also revealed a reduction in IgG macromolecular

protein leak in the stroke-affected hemisphere following sulforaphane pre-treatment (Alfieri *et al.*, 2013). Therefore, in contrast to post-injury treatment, sulforaphane pre-conditioning can also attenuate cerebral oedema formation. Moreover, this evidence suggests that sulforaphane pre-conditioning elevates antioxidant defence mechanisms in the endothelium, providing protection at an earlier stage during reperfusion injury and thereby limiting the need of later activation of Nrf2.

The fluorescence studies of Nrf2-mediated proteins suggest a trend of increased Prx-1 and HO-1 in the vascular endothelium 24h after sulforaphane administration. Moreover, as mentioned previously, quantitative immunohistochemistry studies revealed a time-dependent increase in HO-1 protein, 1 – 4 hours after sulforaphane treatment. Limited availability of brain sections from rats pre-treated with sulforaphane prior to 70 min MCAo and 24h reperfusion injury prevented the study of HO-1 protein expression by quantitative immunohistochemistry. However, fluorescence studies revealed increase HO-1 protein localised with the cerebral endothelium in the infarct core region of sulforaphane pre-treated rats subjected to stroke (Alfieri *et al.*, 2013). Although sulforaphane pre- or post-treatment of rodents subjected to experimental stroke shows an induction of Nrf2 and Nrf2 mediated targets, it remains yet to be elucidated whether pre-treatment confers greater protection that post-injury treatment.

5.4.5 Alternative mechanisms to sulforaphane-mediated protection in the brain

The expression of the astrocytic filamentous protein GFAP was used as a marker to demonstrate the presence of the stroke-affected hemisphere, and to determine the extent of damage. GFAP is expressed exclusively in astrocytes and is a key component of the astrocyte cytoskeleton (Middeldorp & Hol, 2011). Furthermore, the expression of GFAP is induced upon brain injury or the generation of a neurodegenerative state (Middeldorp & Hol, 2011). Notably, the absence of GFAP in mice resulted in morphological and functional changes of the BBB, coupled with increased cerebrovascular permeability (Liedtke *et al.*, 1996; Middeldorp & Hol, 2011). Moreover, Pekny *et al.* demonstrated the inability of primary astrocytes from GFAP KO mice to induce BBB properties in co-culture *in vitro* with bovine aortic endothelial cells (BAEC) (Pekny *et al.*, 1998). It is interesting to note the use of peripheral compared to cerebral endothelial cells in this study. However, it has been established that astrocytes can induce BBB properties in peripheral endothelial cells.

The studies highlighted above indicate the importance of GFAP in the function and regulation of BBB endothelial cells. Interestingly, our data revealed an increase in GFAP expression in the naïve rat brain, following sulforaphane administration. Although an increase was demonstrated 1-4h after sulforaphane treatment, further experiments would be needed to determine the time-dependent changes in GFAP expression, by either fluorescence or quantitative

immuhistochemistry. However this data provides evidence and suggest that the protective actions of sulforaphane may not only underlie the upregulation of the Nrf2 defence pathway but also mediates the expression of structural proteins, important to the integrity of the BBB. It remains unknown whether other dietary inducers of Nrf2 are able to upregulate GFAP expression in the naïve brain. In summary, sulforaphane treatment appears to attenuate cerebral infarct volume and limit BBB breakdown.

5.4.6 Limitations of experiments outlined in Chapter 5

The presented findings provide a strong indication that sulforaphane mediates protection via the Nrf2-defence pathway. However, it is well established that sulforaphane can influence other redox sensitive transcription factors, such as NF-kB and HIF-1α. Hence, to validate our findings, further experiments, in the absence of Nrf2, are required. *In vivo* experiment in rats, where Nrf2 is knocked-down by siRNA, will complement and validate our current results. However, the associated costs of conducting such experiment in rats is high, and furthermore, the use of siRNA reagents for Nrf2 knockdown could provide further stress of the cellular environment and thus influence the final data. Thus, to overcome such technical difficulties, Nrf2 KO and WT mice could be used to first characterise the model MCAo and reperfusion, and subsequently, this murine model can be utilized to investigate whether the effects of sulforaphane treatment *in vivo* are mediated by Nrf2.

Another limitation of the study presented in this chapter is the absence of vehicle treatment (1% corn oil in saline) in both naïve and pre-treated rats subjected to MCAo. The data shown in Figures 5.1 and 5.3 – 5.8 did not examine whether vehicle treatment has an effect on the protein expression of Nrf2 and its downstream targets. However, immunoblotting experiments showed no significant change in Nrf2 protein expression following treatment of naïve rats with vehicle (Figure 5.2). Though this data suggests that vehicle administration does not affect Nrf2 expression, the absence of brain tissue lysates from naïve rats questions the validity of the immunoblotting experiments.

Another technical limitation encountered was the limited availability of brain sections for analysis. Due to the latter inclusion of brain sections from rats treated with sulforaphane for 24h, and furthermore, sulforaphane pre-treated rats, limited access was available to meaningful brain sections. Thus, the brain sections used for analysis originated from the midbrain, introducing a possible anatomical variation on protein expression. Furthermore, the degree of damage experienced by the brain is not uniform throughout.

The rate of uptake and metabolism of sulforaphane varies between individuals. Although 5mg/kg sulforaphane is being delivered to each rat used in this study, our experimental design does not give us insights into the levels of sulforaphane attained in each individual brain.

5.5 Summary and conclusion

In summary, this chapter provides evidence for pre-treatment strategies for patients at a high risk of suffering from stroke using the dietary Nrf2 inducer sulforaphane. Destructive mechanisms, including oxidative stress, are launched almost immediately after the onset of ischeamia and reperfusion injury. Chapter 4 provided evidence showing the time-course for Nrf2 expression in the rat brain after ischaemia and reperfusion injury, with a peak in Nrf2 expression noted 24h after reperfusion injury. Activation of Nrf2 is required for the upregulation of Nrf2-defence proteins. Our study suggests that Nrf2 is upregulated 24h after ischaemia. Thus, it is possible that the late activation of Nrf2 may provide an explanation as to why antioxidant proteins fail to provide sufficient protection against the early onset of destructive mechanisms against stroke.

Sulforaphane administration in the naïve rat brain rapidly induced Nrf2 protein expression and hence, resulted in the upregulation of Nrf2-mediated protective proteins over a short time frame. Thus, the delivery of sulforaphane prior to stroke, increased antioxidant defence mechanisms and might confer greater protection against the early destructive mechanisms characteristic of stroke pathophysiology.

Thus, sulforaphane pre-treatment provides protection for the ischaemic brain by upregulating expression of Nrf2 and its downstream targets. Sulforaphane pre-treatment, also increased Nrf2-mediated protein expression in the cerebrovascular endothelium, limiting lesion progression and attenuating cerebral infarct volume after stroke. Based on our current findings, we propose that sulforaphane mediates protection to the ischaemic brain via the Nrf2-defence pathway. Hence, sulforaphane-preconditioning provides a potential therapeutic strategy applicable to patients at a high-risk of suffering from stroke and will aid in limiting cerebral infarct volume and associated neurological deficits.

Chapter 6 – In vitro studies of brain endothelium using bEnd.3 cells

Chapter 6 *In vitro* studies of the brain endothelium using the bEnd.3 cell line

6.1 Introduction

The cerebral endothelium is a part of the neurovascular unit, and an integral component of the blood-brain barrier (BBB) (Hawkins & Davis, 2005; Abbott *et al.*, 2006). As mentioned previously, the BBB is formed from a tight apposition of endothelial cells that are held together by tight junctional proteins (Klatzo, 1987; Greenwood, 1991; Bradbury, 1993). The endothelial barrier plays a critical role in protecting the brain parenchyma and maintains an optimal environment for brain function. BBB breakdown and associated increased vasogenic oedema, a consequence of endothelial cell contraction, following increased ROS generation, and disassembly of tight-junctional proteins (Klatzo, 1987; Greenwood, 1991; Bradbury & Deane, 1993; Hirase *et al.*, 1997; Juurlink & Sweeney, 1997). To date, various *in vitro* studies have examined the response of endothelial cells following oxygen and glucose deprivation (OGD) as an *in vitro* model of ischaemia and reperfusion injury (Xu *et al.*, 2000; Lee *et al.*, 2007; Bulbarelli *et al.*, 2012; Yang *et al.*, 2013). However, the effects of Nrf2-mediated protection in the endothelium *in vitro* have not been reported.

In vitro studies have also reported the effects of OGD in cultured astrocytes and neurons (Goldberg & Choi, 1993; Almeida *et al.*, 2002; Danilov *et al.*, 2009; Soane *et al.*, 2010; Qi *et al.*, 2012; Gu *et al.*, 2013). Moreover, Danilov *et al.* and Soane *et al.* investigated the role of sulforaphane-mediated protection following pre and post-treatment of astrocytes and neurons respectively (Danilov *et al.*, 2009; Soane *et al.*, 2010). However, the highlighted studies did not report or comment on the importance of the brain endothelium as an important component required for the protection of the brain parenchyma. Hence, to address the importance of increasing protection afforded by the brain endothelium, the murine derived transformed brain endothelial bEnd.3 cell line was used to examine the role of Nrf2 in vascular protection.

In vivo studies from our group have recently investigated the temporal and spatial distribution of Nrf2 in all cerebral cell types, including the cerebral endothelium, in rats subjected to MCAo and reperfusion injury (Alfieri *et al.*, 2013; Srivastava *et al.*, 2013). An increase in expression of Nrf2 and Nrf2-mediated proteins was observed in the cerebral endothelium of sulforaphane pre-treated rats subjected subsequently to MCAo and 24h reperfusion injury (Alfieri *et al.*, 2013). Sulforaphane pre-treatment significantly improved neurological deficits and also reduced cerebrovascular permeability in rats subjected to MCAo and reperfusion injury (Alfieri *et al.*, 2013). This finding suggests that sulforaphane pre-treatment prior to stroke, not only increased Nrf2-mediated defenses in astrocytes and neurons, but also in the cerebral endothelium.

In this chapter, the bEnd.3 cell line, was used to (1) establish an *in vitro* model of ischaemic injury, by subjected cells to OGD, (2) to investigate the effect of sulforaphane treatment on the

Nrf2-defence pathway in naïve bEnd.3 cells, and (3) to investigate whether sulforaphane pre-treatment protected cells against damage induced by OGD. Furthermore, the effects of OGD were examined in bEnd.3 cells adapted long-term (5 days) to physiological oxygen levels with the aim of establishing an improved model to study the blood brain barrier *in vitro*.

6.2 Characterisation of mouse brain endothelial cells

The mouse derived, immortalised brain endothelial cell line, bEnd.3, has been previously used as an *in vitro* model of the blood-brain barrier (BBB) (Zhang *et al.*, 2010; Watanabe *et al.*, 2013; Wuest *et al.*, 2013). Morphology of the brain endothelium is known to be different to the endothelial lining of other vascular beds. The brain endothelium does not have the typical copperstone morphology as observed in human umbilical vein endothelial cells (HUVECs), but are tightly packed (Figure 6.1 A).

eNOS protein expression was also determined and confirmed by immunoblotting in whole cell lysates from bEnd.3 cells (Figure 6.1 B), and by immunofluorescence (Figure 6.1 C), confirming endothelial characteristics of the bEnd.3 brain endothelial cell line.

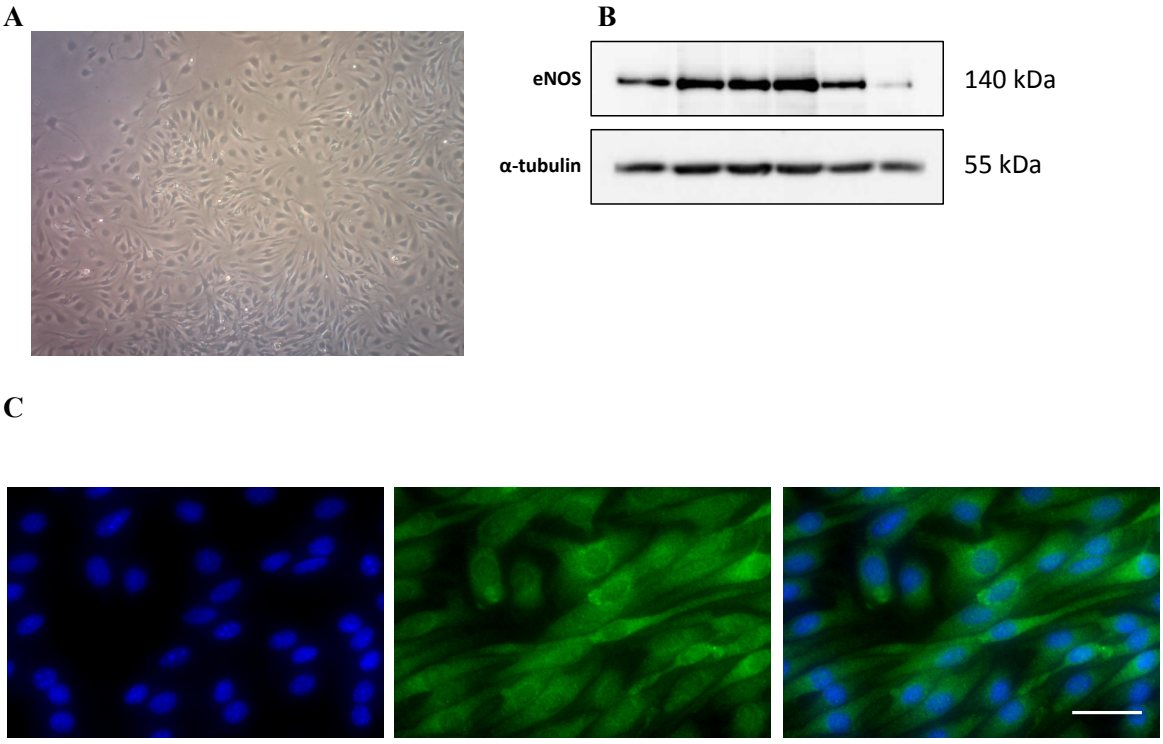

Figure 6.1 Characterisation of endothelial characteristics of the mouse derived brain endothelial cell line bEnd.3.

To characterize the endothelial properties of the mouse derived brain endothelial cell line bEnd.3, (A) Brightfield images of bEnd.3 cells in culture were captured to confirm brain endothelial morphology. (B) Total protein lysates from bEnd.3 cells were immunoblotted for eNOS, and alpha tubulin, which served as the loading control. (C) eNOS expression was also assessed by immunofluorescence. bEnd.3 cells were stained for Nuclei (DAPI, blue, left panel), eNOS (green, center panel). The right panel demonstrates a merge of both DAPI and eNOS. Scale bar represents 5 µm.

6.3 Oxygen-glucose deprivation responses in bEnd.3 mouse brain endothelial cells

As shown previously in this thesis, an experimental model of stroke was employed *in vivo* to assess the response and expression of Nrf2 and Nrf2-linked proteins after MCAo and reperfusion injury (Chapter 4) and sulforaphane pre-treatment (Chapter 5). *Ex vivo* analysis of rat brains revealed changes in the endothelial distribution of Nrf2 content, suggesting that Nrf2 may mediate protection to the cerebral endothelium after stroke. To compliment and corroborate our *ex vivo* findings, an *in vitro* model of cerebral ischaemia was established using bEnd.3 endothelial cells. Furthermore, the effects of sulforaphane treatment on the Nrf2 mediated signalling in bEnd.3 cells was studied. This section describes the establishment of an *in vitro* model of ischaemic damage in bEnd.3 cells and further demonstrates changes in Nrf2-linked protein expression following OGD.

6.3.1 Oxygen-glucose deprivation mediates time-dependent cell death in bEnd.3 cells

To replicate *in vivo* ischaemia-reperfusion injury *in vitro*, an *in vitro* model of ischaemic injury was established. Confluent monolayers of bEnd.3 cells, which were equilibrated in 10% FCS and 5.5 mM glucose, were deprived of oxygen and glucose for 2 – 12 h. Following OGD, cell death was assessed by staining cells with the ethidium bromide homodimer and annexin V (Figure 6.2). The membrane impermeable fluorescent dye, ethidium bromide, stains the nuclei of dying cells, whilst annexin V stains for phosphatidylserine, a phospholipid component that is expressed on the inner surface of the cell membrane (Siow *et al.*, 1999a). Upon cell death by apoptosis, phosphatidylserine is exposed on the cell surface, and thus is detected by annexin V.

A time-dependent increase in both annexin V staining and ethidium bromide homodimer was observed following OGD (Figure 6.2). Furthermore, the merged images demonstrate that not all ethidium bromide positive cells express phosphatidylserine (Figure 6.2), hence, visually this indicates that approximately 80 – 90% of cells are affected following longer exposure to OGD.

The number of nuclei stained positive for DAPI and ethidium bromide homodimer were counted for each respective field of view, and a ratio for dead vs living cells calculated (Figure 6.3). Ratios were calculated for cells subjected to OGD and time-matched controls. High ratio values indicated increased cell death following OGD. After 2h OGD, no difference was observed in the dead to live cell ratio compared to time-matched controls. However, a time dependent increase in cell death was observed over 6 to 12h (Figure 6.3). Notably, the cell death ratio was significantly greater compared to time-matched controls ($p<0.001$, Figure 6.3). No difference was observed in the ratio of dead versus living cells between time-matched controls.

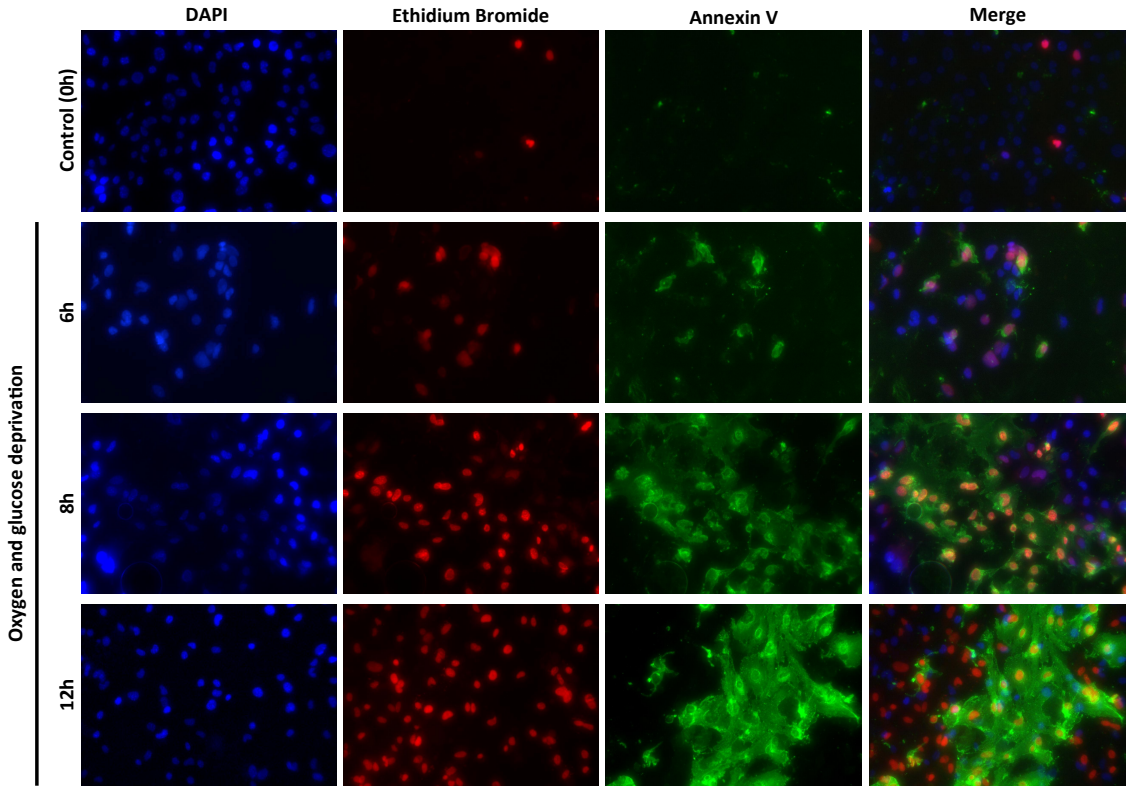

Figure 6.2 Oxygen and glucose deprivation mediates cell death in bEnd.3 cells.

Confluent monolayer of bEnd.3 cells, equilibrated in DMEM supplemented with 10% FCS and 5.5mM glucose, were subjected to oxygen and glucose deprivation for 2, 6, 8 and 12h. A Nikon diaphot microscope adapted for fluorescence was used to assess cell death using ethidium bromide homodimer (Red) to stain nuclei of dying cells, and annexin V to stain for phosphatidylserine (green). DAPI was used to stain all cell nuclei (blue). The final column shows a merge of each of the respective images captured. Orange coloured nuclei indicate co-localisation of ethidium bromide and DAPI staining, suggestive of cell death. Orange nuclei surrounded by annexin V staining indicate apoptotic cell death. Images are representative of experiments from n = 4 bEnd.3 cell cultures from passage 12 – 19.

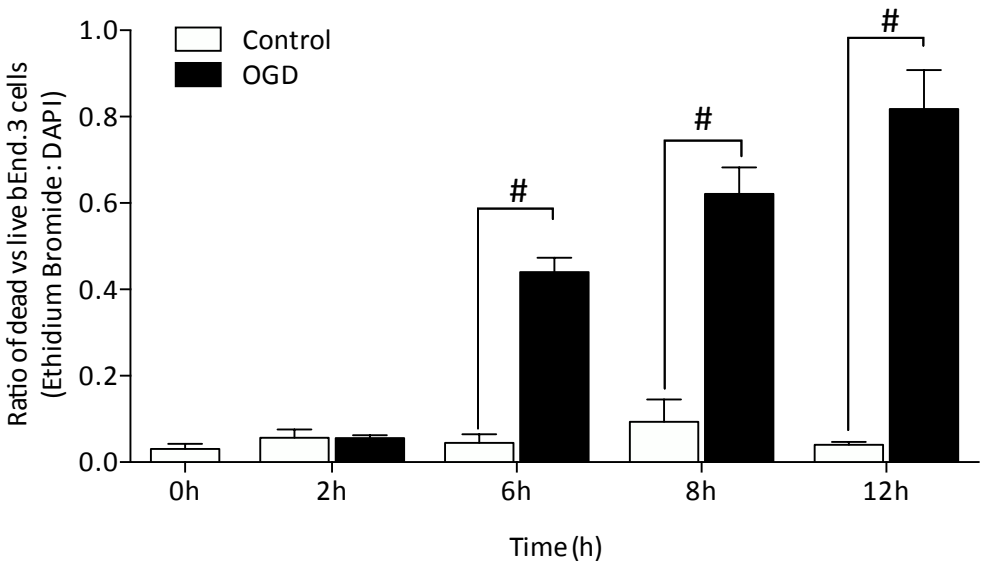

Figure 6.3 Effects of oxygen and glucose deprivation on bEnd.3 cell viability

Confluent monolayers of bEnd.3 cells, equilibrated in DMEM supplemented with 10% FCS and 5.5m M glucose, were subjected to oxygen and glucose deprivation for 2, 6, 8 and 12h. The ratio of dead cells (identified by ethidium bromide positive staining) to all cells in the field of view (DAPI positive staining) was determined. Data denotes mean ± S.E.M, and analysed by two-way ANOVA with Tukeys post-test. *n* = 3. # $P<0.0001$ against time matched controls, n = 3 independent bEnd.3 cultures, passage 12 – 19.

6.3.2 OGD increases HO-1 and NQO1 protein expression in bEnd.3 cells

Whole cell lysates from bEnd.3 cells subjected to OGD for 2 – 12h were analysed by immunoblotting for the expression of HO-1 and NQO1, two downstream protein targets of the redox sensitive transcription factor Nrf2 (Figure 6.4). A time-dependent increase in HO-1 expression was observed after OGD (Figure 6.4 A, upper panel). Densitometric analysis of HO-1, relative to the loading control α-tubulin (Figure 6.4 A, lower panel), revealed a significant increase in HO-1 protein expression after 12h OGD (Figure 6.4 B). Notably, HO-1 protein expression was similar in time-matched controls.

A time-dependent increase in NQO1 protein expression was also observed in bEnd.3 cells subjected to OGD for 2 – 12h (Figure 6.5 A). Furthermore, similar to HO-1 protein expression, no difference in NQO1 expression was observed in time-matched controls (Figure 6.4 A, middle panel). Densitometric analysis of NQO1 protein expression relative to α-tubulin, revealed a similar time course for OGD induced NQO1 expression, with peak levels observed after 12h OGD (Figure 6.4 C).

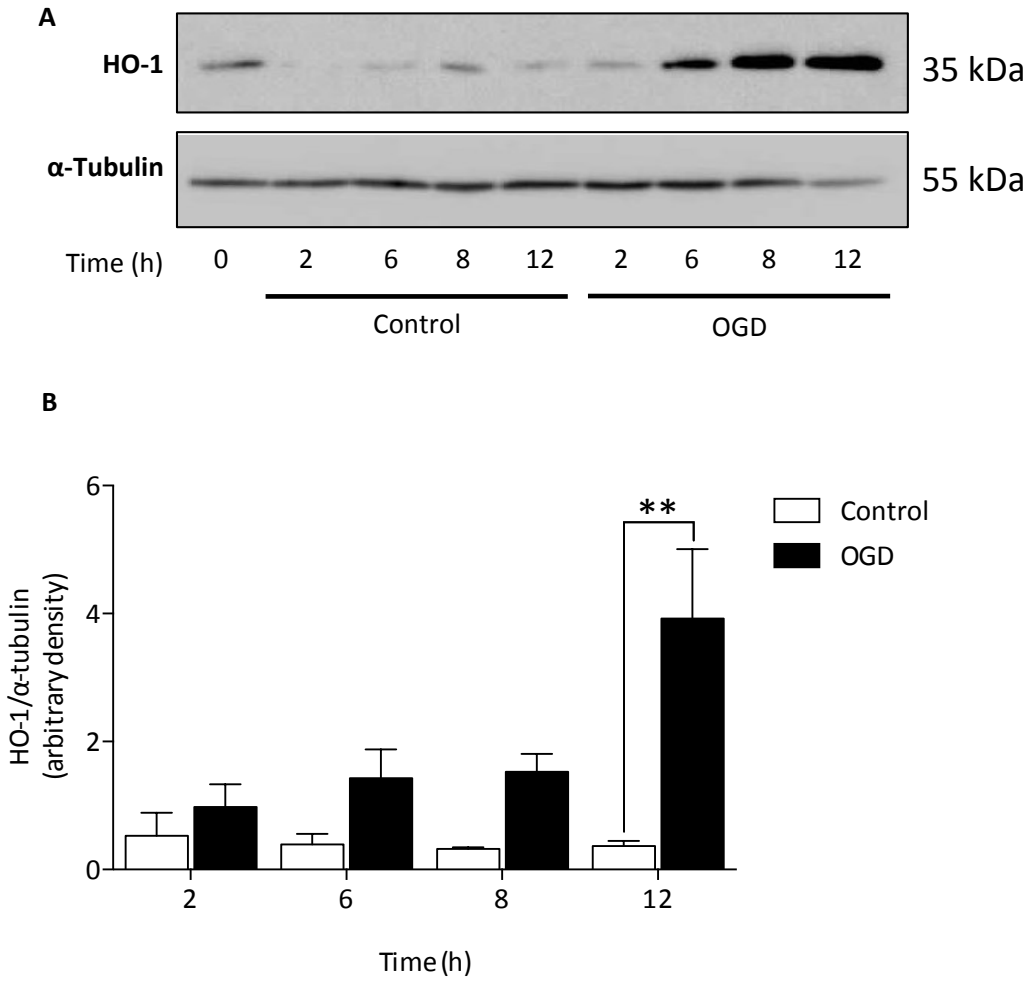

Figure 6.4 Oxygen and glucose deprivation induces HO-1 protein expression in bEnd.3 cells.

Confluent monolayers of bEnd.3 cells, equilibrated in DMEM supplemented with 10% FCS and 5.5mM glucose, were subjected to oxygen and glucose deprivation for 2, 6, 8 and 12 hours and whole cell lysates collected to examine HO-1 protein expression by immunoblotting. (**A**) Representative immunoblot for HO-1 protein expression. (**B**) Densitometric analysis relative to α-tubulin. Data denotes mean ± S.E.M, and were analysed by two-way ANOVA with Tukeys post-test. **P<0.01, *n = 3* bEnd.3 cell independent cultures (passage 12-18).

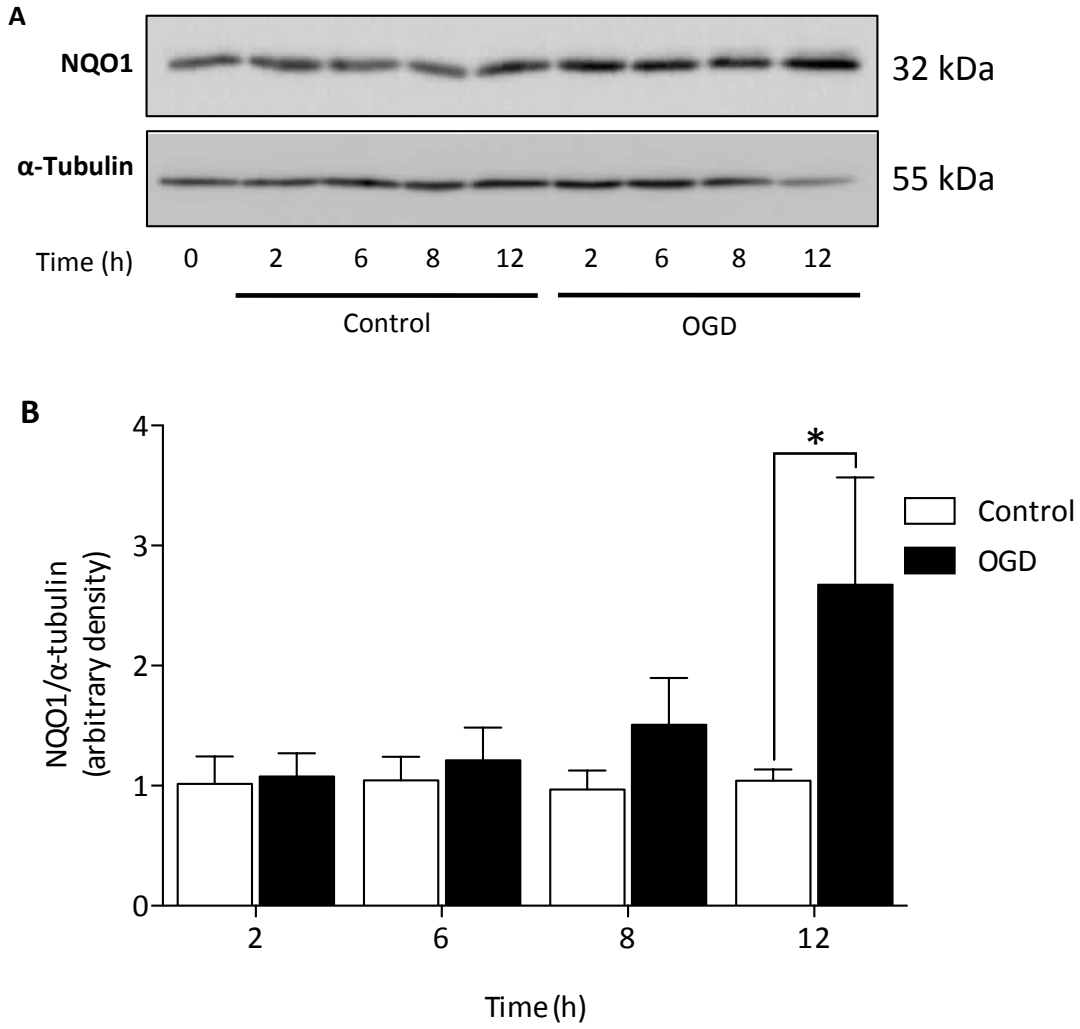

Figure 6.5 Oxygen and glucose deprivation induces NQO1 protein expression in bEnd.3 cells.

Confluent monolayers of bEnd.3 cells, equilibrated in DMEM supplemented with 10% FCS and 5.5m M glucose, were subjected to oxygen and glucose deprivation for 2, 6, 8 and 12 hours and whole cell lysates collected to examine NQO1 protein expression by immunoblotting. (**A**) Representative immunoblot for NQO1 protein expression. (**B**) Densitometric analysis of NQO1 expression relative to α-tubulin. Data denotes mean ± S.E.M, * P<0.05 analysed by two-way ANOVA and tukeys post-test, *n = 3* bEnd.3 cells independent cultures (passage 12-18).

6.4 Sulforaphane mediated responses in bEnd.3 cells

Chapter 5 established that pre-treatment of rats with sulforaphane enhanced Nrf2 protein levels prior to MCAo and 24h reperfusion injury. Furthermore, sulforaphane pre-treatment led to a reduction in lesion progression and cerebrovascular permeability following MCAo and 24h reperfusion injury (Alfieri *et al.*, 2013). As these findings provided clear evidence of a link between sulforaphane, Nrf2 and Nrf2-linked proteins in ischaemic brain damage *in vivo*, the effects of sulforaphane were also examined in bEnd.3 brain endothelial cells.

6.4.1 Effects of sulforaphane treatment on viability of bEnd.3 cells

The effect of sulforaphane treatment on bEnd.3 cell viability was assessed using the MTT assay. Confluent monolayers of bEnd.3 cells (passage 12-18) were treated with 0.5 to 10μM sulforaphane for 24h. Cells were also treated for 30 min with 0.5M H_2O_2, which served as a positive control for cell death. Sulforaphane treatment had no effect on bEnd.3 cell viability after 24h, compared to cells treated with 0.01% DMSO (vehicle), or medium (Figure 6.6). Notably, 30 min treatment with a high dose of H_2O_2 (0.5M) significantly reduced bEnd.3 cell viability, compared to control cells (Figure 6.6).

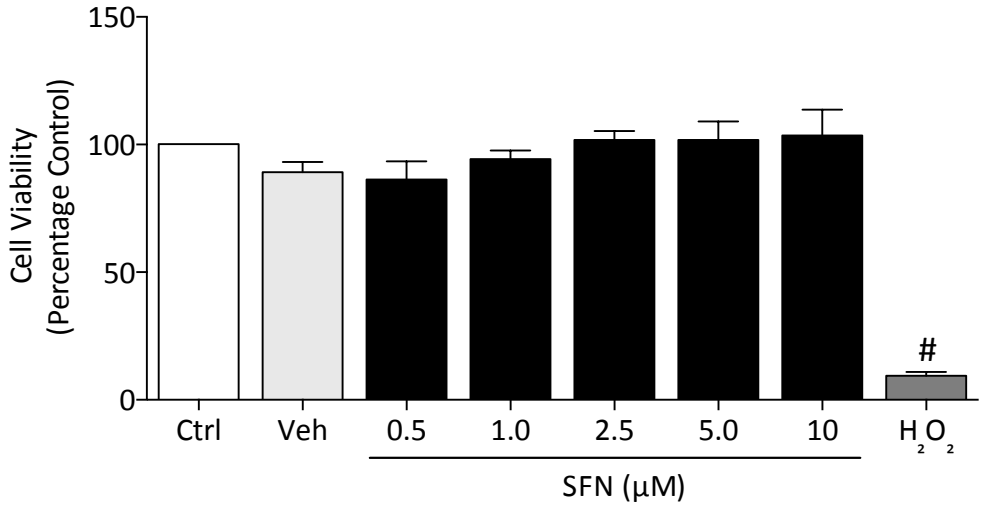

Figure 6.6 Effect of sulforaphane on bEnd.3 cell viability.

Confluent monolayers of bEnd.3 cells, equilibrated in DMEM supplemented with 10% FCS and 5.5m M glucose were treated with vehicle (0.01% DMSO), or 0.5, 1.0, 2.5, 5 and 10µM sulforaphane (SFN) for 24 hours. Cells were also treated with 0.5M H_2O_2, which served as a positive control for cell death. Cell viability assessed using the MTT assay and the percentage change in viability determined relative to vehicle. Data denote mean ± S.E.M, and were analysed by one-way ANOVA with Tukeys post-test *n = 4*, # P<0.001 vs control cells.

6.4.2 Effects of sulforaphane treatment on HO-1 protein expression in bEnd.3 cells

Concentration- and time-dependent effects of sulforaphane treatment on bEnd.3 cells were assessed by immunoblotting. Confluent monolayers of bEnd.3 cells (passage 12-20), equilibrated in DMEM containing 5.5mM glucose and supplemented with 10% FCS, were treated for 4 – 24h with either sulforaphane (0.5, 1.0 or 2.5μM) or 0.01% DMSO (vehicle). Whole cell lysates analysed for HO-1 protein expression by immunoblotting and densitometric analysis (Figure 6.7). Vehicle treatment had no effect on HO-1 expression in bEnd.3 cells over 4 – 24h, as demonstrated by immunoblotting (Figure 6.7 A) and densitometric analysis relative to the loading control, α-tubulin (Figure 6.7 B).

Sulforaphane treatment lead to concentration- and time-dependent increases in HO-1 protein expression, with peak HO-1 expression detected in cells treated with 2.5μM sulforaphane for 24h (Figure 6.7 A). Densitometric analysis, relative to α-tubulin revealed a significant increase in HO-1 protein expression in cells treated with 2.5μM sulforaphane compared to control, following 12h ($p<0.01$) and 24h ($p<0.001$). No significant increase in HO-1 protein expression was recorded after 4h sulforaphane treatment (Figure 6.7 B). Although an increase in HO-1 protein was noted after 8h treatment with 2.5μM sulforaphane this trend was not statistically significant.

A

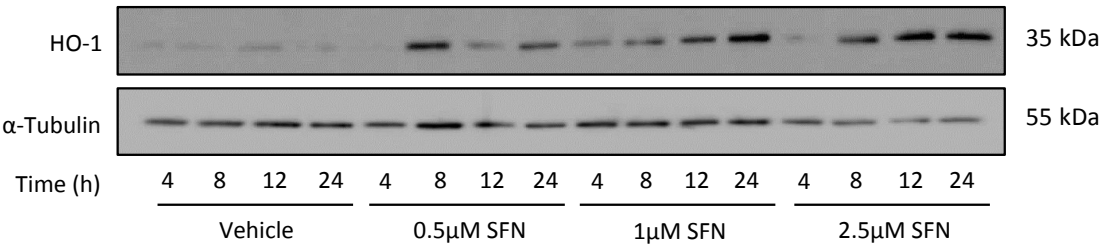

B

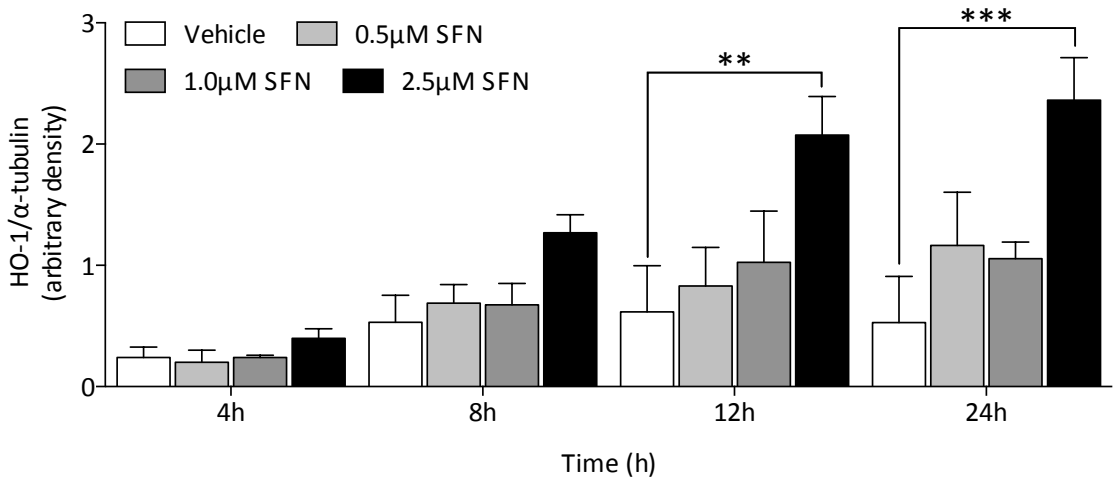

Figure 6.7 Time and concentration dependent effects of sulforaphane on HO-1 protein expression in bEnd.3 cells.

Confluent monolayers of bEnd.3 cells were equilibrated in DMEM (5.5mM glucose, 10% FCS) and treated for 4, 8, 12 and 24 h with 0.01% DMSO (vehicle) or 0.5μM, 1μM or 2.5μM sulforaphane (SFN). (**A**) Representative immunoblot of HO-1 protein expression (**B**) Densitometric analysis of HO-1 protein expression relative to α-tubulin. Data denote mean ± S.E.M, and were analysed by two-way ANOVA with Tukeys post test. ** $P < 0.01$, *** $P < 0.001$. n = 4 independent bEnd.3 cells cultures (passage 12 – 20).

6.4.3 Effects of sulforaphane treatment on NQO1 protein expression in bEnd.3 cells

Concentration- and time-dependent effects of sulforaphane treatment on NQO1 protein expression in bEnd.3 cells were assessed by immunoblotting. Confluent monolayers of bEnd.3 cells (passage 12-20), equilibrated in DMEM containing 5.5mM glucose and supplemented with 10% FCS, were treated for 4 – 24h with either sulforaphane (0.5, 1.0 or 2.5μM) or 0.01% DMSO (vehicle). bEnd.3 whole cell lysates were analysed for NQO1 protein expression immunoblotting (Figure 6.8). Treatment of bEnd.3 cells with vehicle had no effect on NQO1 protein expression over 4 – 24h (Figure 6.8 A and B).

Treatment of bEnd.3 cells with sulforaphane revealed concentration and time-dependent increases in NQO1 protein expression. NQO1 protein expression was greater in cells treated with 2.5μM SFN (Figure 6.8 A). Densitometric analysis, relative α-tubulin, revealed a significant increase in NQO1 protein expression in cells treated with 2.5μM sulforaphane for 8h ($p<0.01$), 12 ($p<0.001$) and 24h ($p<0.001$) compared to time-matched vehicle treated cells. No significant increase in NQO1 protein expression was observed after 4h sulforaphane treatment (Figure 6.8).

A

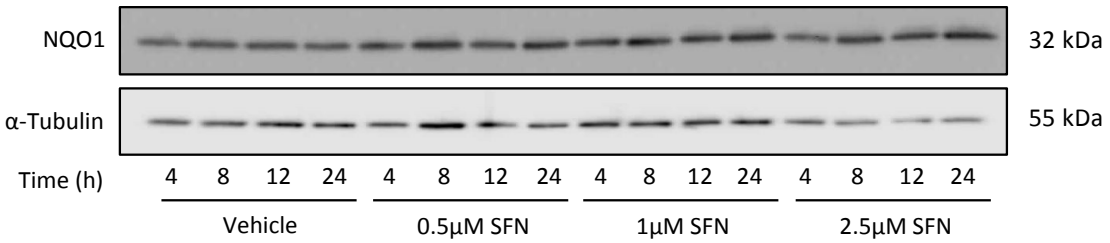

B

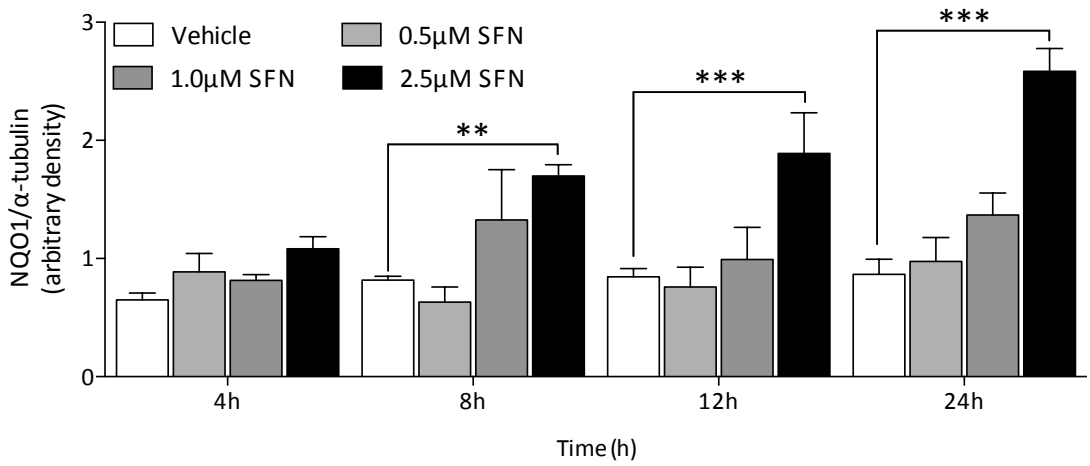

Figure 6.8 Time and concentration dependent effects of sulforaphane on NQO1 protein expression in bEnd.3 cells.

Confluent bEnd3 cell monolayers were equilibrated in DMEM (5.5mM glucose, 10% FCS) and treated for 4, 8, 12 and 24h with 0.001% DMSO (vehicle) or 0.5μM, 1μM or 2.5μM sulforaphane. (**A**) Representative immunoblot of NQO1 protein expression. (**B**) Densitometric analysis of NQO1 protein expression relative to α-tubulin. Data denote mean ± S.E.M, and analysed by two-way ANOVA with Tukeys post test. ** $P < 0.01$, *** $P < 0.001$. n = 3 independent bEnd.3 cultures (passage 12 – 20)

6.4.4 Effects of sulforaphane upon intracellular glutathione

Glutathione (GSH) is a key intracellular antioxidant protein, providing the cell with a first-line of defence against increased electrophilic or oxidative stress (Bannai & Tateishi, 1986). The effect of sulforaphane treatment on intracellular glutathione content was assessed in bEnd.3 cells using the OPA-assay. Confluent monolayers of bEnd.3 cells were treated for 2, 4, 8 and 24h with either 2.5µM sulforaphane, or 0.01% DMSO (vehicle). Intracellular GSH was extracted from bEnd.3 cells following treatment, and GSH content assessed by OPA-fluorescence. After 2h and 4h, no difference was observed in intracellular GSH content between sulforaphane and vehicle treated cells (Figure 6.9). After 8h treatment, intracellular GSH levels were increased in sulforaphane treated cells (76 ± nmol GSH/ mg protein) compared to vehicle treated cells (57.5 ± nmol GSH/ mg protein), although this trend was not significantly different (Figure 6.9). Following 24h treatment, GSH content remained elevated in sulforaphane treated cells (62.2 ± nmol GSH/ mg protein) compared to vehicle treated cells (45.6 ± nmol GSH/ mg protein), albeit the trend was not statistically significant.

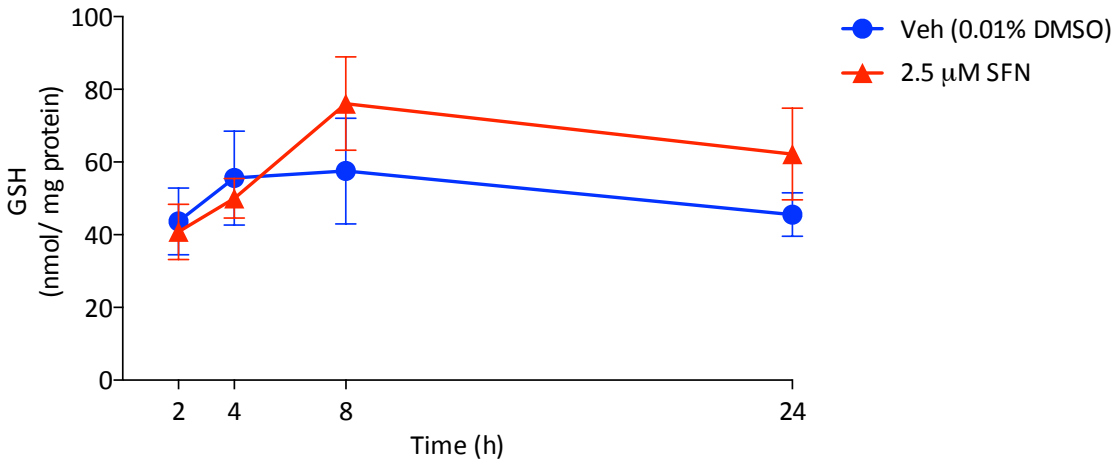

Figure 6.9 Effects of sulforaphane treatment on intracellular glutathione levels in bEnd.3 endothelial cells.

Confluent monolayers of bEnd3 cells, equilibrated in 5.5mM glucose DMEM were treated with either vehicle (DMSO 0.01%) or 1µM SFN or 2.5µM SFN for 2, 4, 8 and 24h. Glutathione (GSH) was extracted from whole cell lysates with 6.5% trichloroacetic acid and total cellular GSH levels measured by O-phthaldialdehyde (OPA) fluorescence and expressed per mg protein. Data denote mean ± S.E.M. n=3 independent bEnd.3 cell cultures (passage 12 – 20).

6.4.5 Effects of sulforaphane on mRNA expression of Nrf2 and Nrf2-linked genes

The redox sensitive transcription factor Nrf2 translocates to the nucleus to upregulate the expression of ARE responsive genes. As shown in Figures 6.7 and 6.8, sulforaphane upregulated NQO1 and HO-1 protein expression after 12 – 24h treatment. Moreover, findings in Chapter 5 established significant increases in cerebral Nrf2 protein levels 1h after sulforaphane treatment. To further examine the molecular actions of sulforaphane in brain endothelium, quantitative RT-PCR was employed to determine whether sulforaphane induced changes in mRNA levels of Nrf2 and Nrf2-associated genes in bEnd.3 brain endothelial cells. bEnd.3 cells were treated with sulforaphane for 4h prior to collection of cell lysates for mRNA analysis.

No significant differences in Nrf2 mRNA expression were observed after 4h treatment with 2.5μM sulforaphane compared to vehicle treated (0.01% DMSO) or control samples (Figure 6.10 A). However, a significant increase ($P<0.01$) was noted in mRNA expression of both NQO1 and HO-1 was noted after 4h sulforaphane treatment. Notably, no differences were observed in mRNA levels for NQO1 or HO-1 between vehicle treated and control cells (Figure 6.10 B – C).

The effect of sulforaphane treatment was also examined on two known regulators of Nrf2. Bach1 is known to bind to the ARE of the HO-1 gene and represses HO-1 protein expression (Hira *et al.*, 2007) (Figure 6.10 D). In this study, sulforaphane treatment significantly increased Bach1 mRNA expression at 4h compared to vehicle treated or control cells (Figure 6.10 D). Furthermore, mRNA expression of Keap1, a cytosolic repressor of Nrf2, was significantly increased in bEnd.3.cells treated with sulforaphane compared to vehicle treated or control cells (Figure 6.10 E). Notably, no differences were observed for either Bach1 and Keap1 mRNA levels between vehicle-treated and control cells.

The above data is also represented as fold-change respective to control in Appendix 6, and shows the same findings as that observed in Figure 6.10.

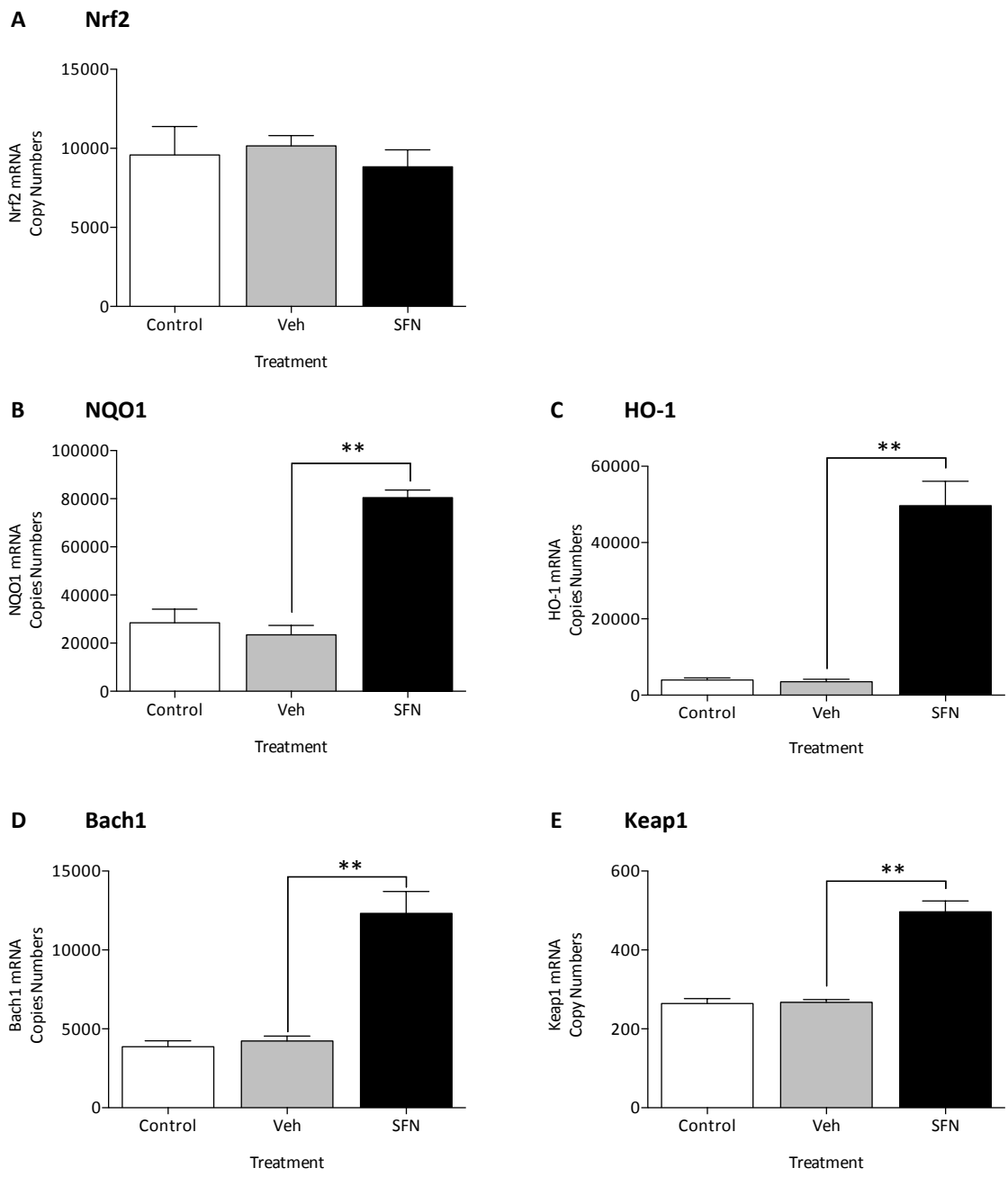

Figure 6.10 Effects of sulforaphane treatment on mRNA levels of Nrf2 regulated genes.

Confluent monolayers of bEnd.3 cells, equilibrated in DMEM supplemented with 10% FCS and 5.5m M glucose, were treated with either vehicle (0.01% DMSO) or 2.5µM sulforaphane (SFN) for 4h and RNA collected. qRT-PCR was employed to determine mRNA copy numbers for (A) Nrf2, (B) NQO1, (C) HO-1, (D) Bach1 and (E) Keap1 following normalization to three house keeping genes (SDHA, RPL13A and B2M). Data denote mean ± S.E.M., and were analysed by one-way ANOVA, ** $P<0.01$, n = 5 bEnd.3 cultures passage 10 – 19.

6.4.6 Sulforaphane induces nuclear translocation of Nrf2 in bEnd.3 cells

Administration of sulforaphane to naïve rats *in vivo* was followed by a rapid (1 – 2h) increase in cellular Nrf2 levels in *ex vivo* brain sections (see chapter 5). However, the cerebral cell types expressing increased Nrf2 content were not determined. As mentioned previously, a reduced cerebrovascular permeability following sulforaphane pre-treatment of rats subjected to MCAo suggests an increase in Nrf2-linked defences in the cerebral endothelium. Hence, Nrf2 expression was assessed in bEnd.3 cells following sulforaphane treatment *in vitro*.

bEnd.3 cells were treated for 1, 2 and 4 hours with either 0.01% DMSO (vehicle) or 2.5µM sulforaphane. Nuclear lysates were collected and analysed by immunoblotting for Nrf2 protein expression. No difference in Nrf2 protein expression was detected in nuclear lysates following vehicle treatment (Figure 6.11 A). Densitometric analysis of Nrf2, relative to the loading control Lamin A/C revealed no significant difference between 1 – 4h following vehicle treatment (Figure 6.11 B). Sulforaphane treatment increased nuclear Nrf2 content after 1h, which remained elevated after 2h and then decreased to levels similar to vehicle treated cells after 4h (Figure 6.11 A). Densitometric analysis revealed a decreasing trend in nuclear Nrf2 content after 1 – 4h after sulforaphane treatment, with Nrf2 content significantly lower in the nucleus after 4h sulforaphane treatment ($P<0.05$).

Furthermore, nuclear Nrf2 binding activity was assessed using an ELISA based Trans AM activity assay. Consistent with changes observed in nuclear Nrf2 protein levels, an increase in Nrf2 activity was observed over 1 – 4 hours in nuclear extracts from bEnd.3 cells treated with 2.5 µM sulforaphane (Figure 6.12). Notably a trend of increase in nuclear Nrf2 binding activity is observed after 1h sulforaphane treatment, albeit not significant. However, significant increases in Nrf2 binding activity were observed following 2h and 4h sulforaphane treatment ($P<0.05$).

A

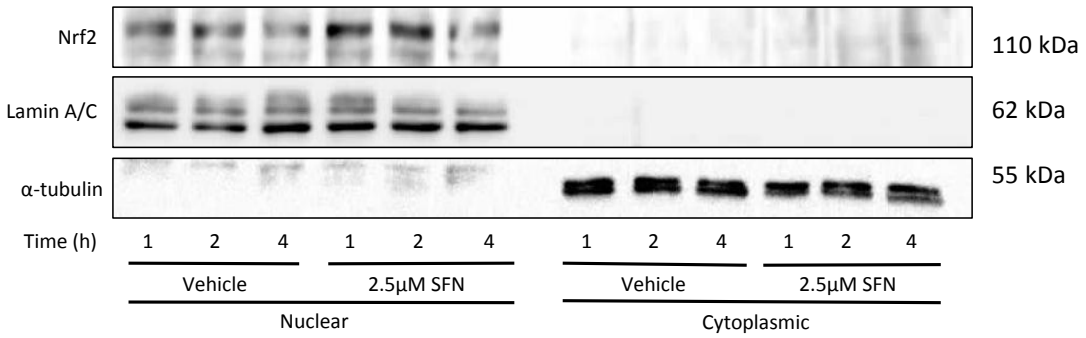

B

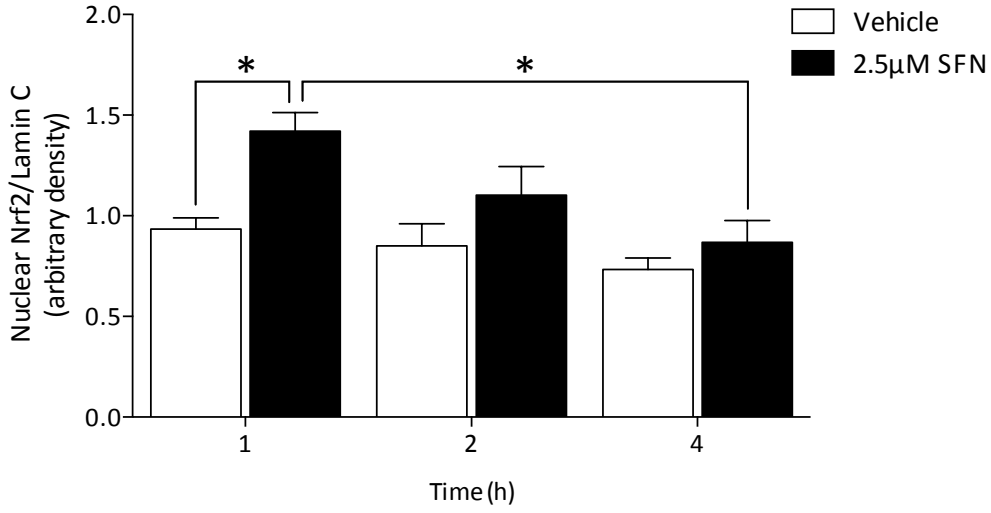

Figure 6.11 Time course of Nrf2 nuclear translocation in bEnd.3 cells following sulforaphane treatment.

Confluent monolayers of bEnd.3 cells in T75 flasks were equilibrated in DMEM (5.5mM glucose, 10% FCS) and treated for 1, 2 and 4 h with either 0.01% DMSO (vehicle), or 2.5μM sulforaphane. Nuclear and cytosolic fractions were extracted and analysed by immunoblotting. (**A**) Representative immunoblot for Nrf2 in nuclear and cytoplasmic extracts. Lamin A/C and α-tubulin served as the loading controls for the nuclear and cytoplasmic fractions respectively. (**B**) Densitometric analysis of nuclear Nrf2 relative to the loading control Lamin C. Data denote mean ± S.E.M, and were analysed by one-way ANOVA with Tukeys post-test. n = 4 independent bEnd.3 cell cultures (passage 10 – 19).

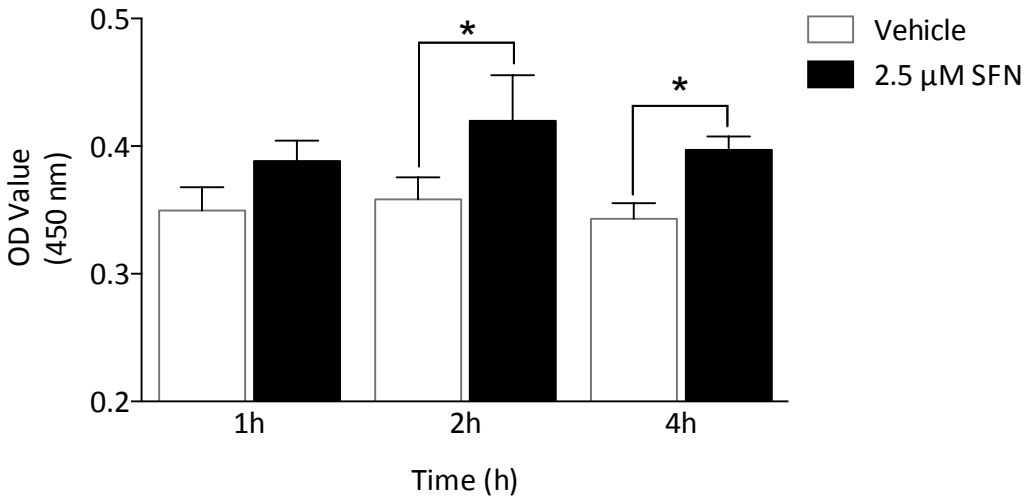

Figure 6.12 ARE-binding activity of nuclear Nrf2 in bEnd.3 cells following sulforaphane treatment.

Confluent monolayers of bEnd.3 cells equilibrated in DMEM supplemented with 5.5mM glucose and 10% FCS were treated with either 0.01% DMSO (vehicle) or 2.5µM sulforaphane (SFN) for 1, 2, or 4h. Nuclear extracts were collected using the commercially available Trans AM nuclear extraction kit and analysed for Nrf2 binding activity using an imobilised ARE oligo in an ELISA based assay. Nrf2 binding activity was assessed at 450 nm. Data denote mean ± S.E.M., and were analysed by two-way ANOVA with Bonferroni post-test. $P<0.05$, n=4 independent bEnd.3 cultures (passage 10 – 19).

6.5 Immunofluorescence and immunohistochemical localisation of Nrf2

Nrf2 expression and its cellular localisation was also assessed by immunofluorescence and quantitiative DAB-H_2O_2 immunohistochemistry following treatment of bEnd.3 cells with 2.5μM sulforaphane for 1, 2 and 4h. Following treatment, cells were fixed in paraformaldehyde and incubated with a primary rabbit anti-Nrf2 antibody and then either a secondary anti-rabbit Alexa fluor 488 antibody for fluorescence microscopy, or a biotinylated secondary antibody conjugated to HRP for quantitative immunohistochemistry.

Captured fluorescence images demonstrated an increase in nuclear Nrf2 fluorescence 1h after sulforaphane treatment (Figure 6.13), which subsequently declined over 2 – 4h (Figure 6.13). Quantitative immunohistochemistry in bEnd.3 cells corroborated our fluorescence findings of increased nuclear Nrf2 content after sulforaphane treatment. The histograms in Figure 6.14 represent the nuclear to cytoplasmic ratio of Nrf2 for each respective bEnd.3 cell identified. Sulforaphane increased Nrf2 maxiamlly after 2h compared to vehicle treated cells (Figure 6.14 A and B). Elevated nuclear to cytoplasmic ratios were maintained after 4h sulforaphane treatment (Figure 6.14 C). Mean nuclear to cytoplasmic ratio revealed a non-significant trend for increased nuclear localisation of Nrf2 following sulforaphane treatment, albeit this trend is not significant (Figure 6.15).

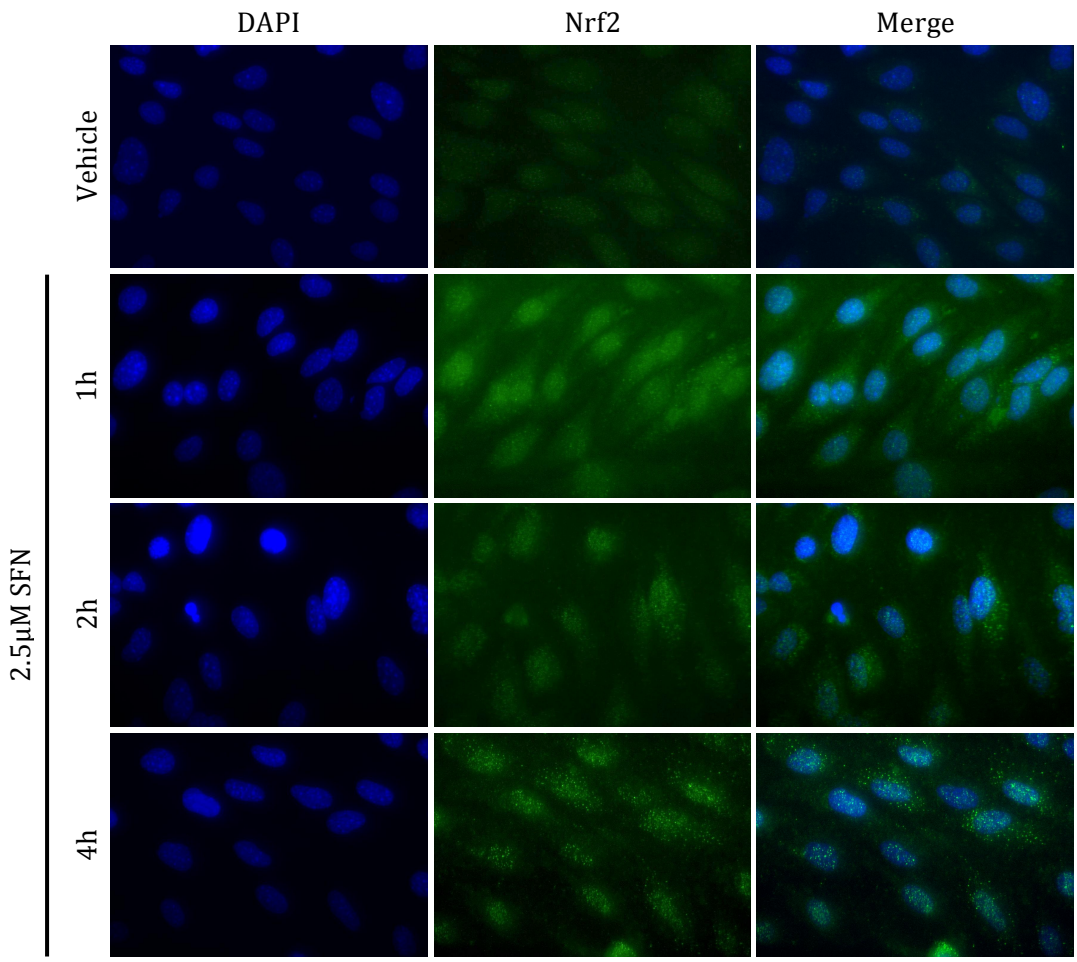

Figure 6.13 Sulforaphane induces nuclear translocation of Nrf2 in bEnd.3 cells.

Confluent monolayer of bEnd.3 were treated with 2.5µM SFN for 1 – 4h and protein expression of Nrf2 assessed by immunofluorescence following incubation of paraformaldehyde fixed cells with primary anti-Nrf2 antibody, and complimentary anti-rabbit Alexa Fluor 488 secondary antibody (green, center panel). DAPI was used to stain cell nuclei (blue, left panel). Right hand side panel shows a merge of the DAPI and Nrf2 channels.

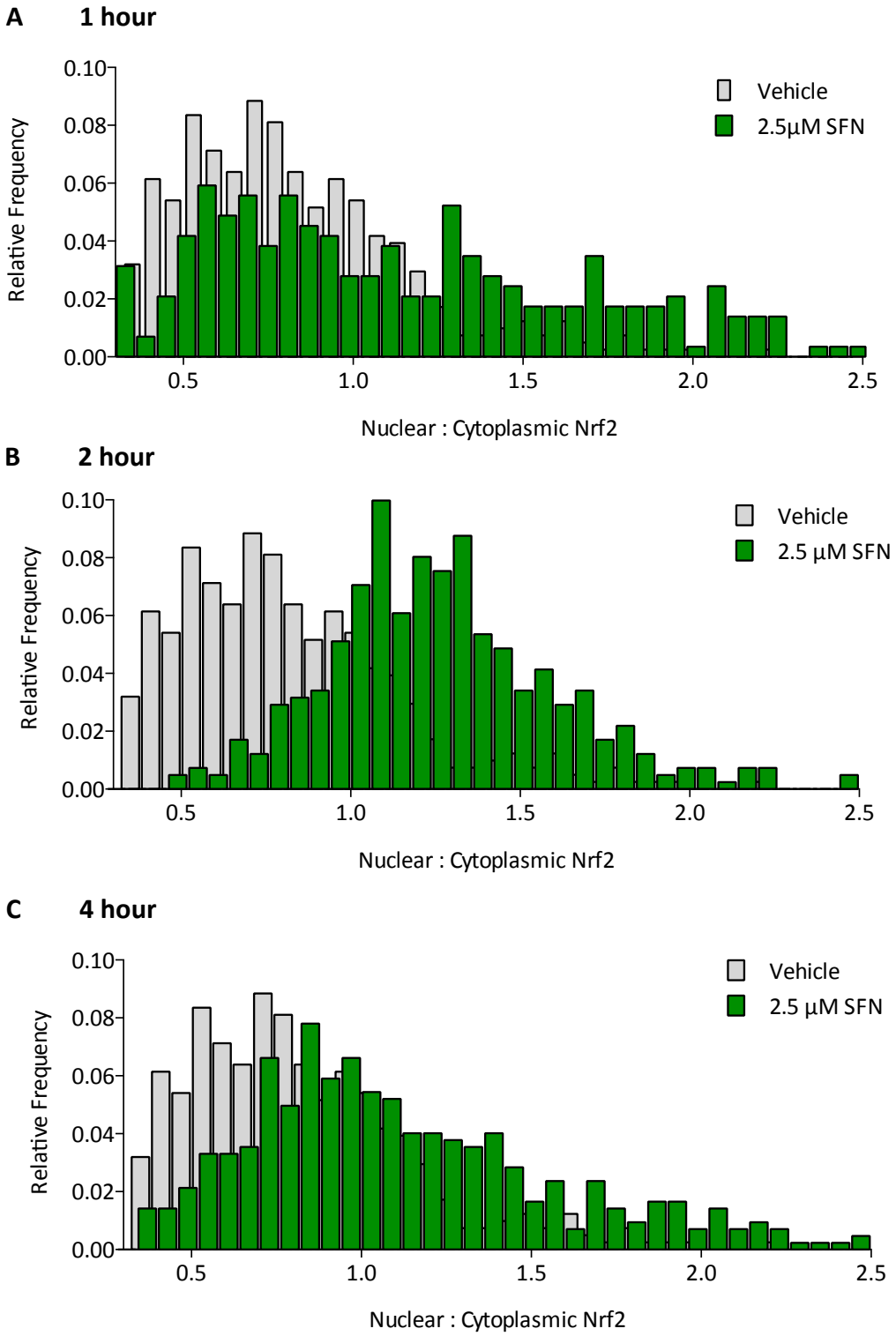

Figure 6.14 Histograms of Nrf2 nuclear to cytoplasmic ratio in sulforaphane treated bEnd.3 cells.

bEnd.3 cells were treated with 2.5µM sulforaphane (Green bars) compared to vehicle (0.01% DMSO, grey bars) for either (**A**) 1h, (**B**) 2h and (**C**) 4h and Nrf2 expression determined using quantitative immunohistochemistry. Histograms show the nuclear to cytoplasmic ratio of Nrf2 for each respective cell identified.

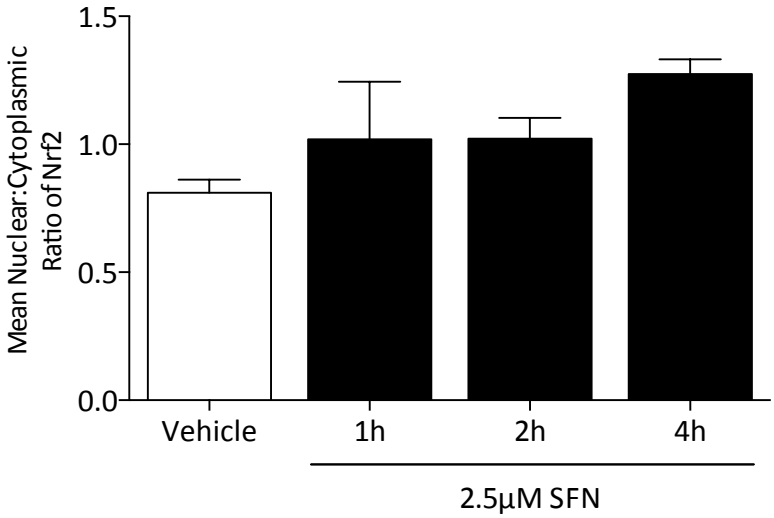

Figure 6.15 Mean nuclear to cytoplasmic Nrf2 ratio following sulforaphane treatment of bEnd.3 cells.

Mean nuclear to cytoplasmic ratio of Nrf2 content was determined for bEnd.3 cells treated with either vehicle (0.01% DMSO) or 2.5µM sulforaphane (SFN) for 1, 2 or 4h, and analysed by quantitative immunohistochemistry. Data denote mean ± S.E.M., and analysed by one-way ANOVA. n=4 independent bEnd.3 cell cultures, passage 10 – 15.

6.6 Sulforaphane mediates upregulation of HO-1 and NQO1 protein via Nrf2

The current findings in bEnd.3 cells suggest that sulforaphane mediates the upregulation of HO-1 and NQO1 via Nrf2. Hence to confirm the current findings, we sought to determine whether the observed upregulation is Nrf2 dependent. Nrf2 was knockdown in bEnd.3 cells following transfection with Nrf2 siRNA for 24h. bEnd.3 cell were then treated with 2.5 μM sulforaphane and collected whole cell lysates were immunoblotted for HO-1 (Figure 6.16) and NQO1 (Figure 6.17) protein expression.

As demonstrated in Figure 6.16, HO-1 protein expression increased significantly in control bEnd.3 cells treated with SFN, however, this increased was significantly abrogated in Nrf2 knockdown bEnd.3 cells, thus indicating HO-1 protein expression is mainly mediated by the Nrf2/Are pathway.

Sulforaphane treatment also increased NQO1 protein expression in control bEnd.3 cells after 24h treatment (Figure 6.17). However, a notable abrogation of NQO1 protein expression was observed in bEnd.3 cells knocked down for Nrf2 following sulforaphane treatment (Figure 6.17). Hence, this finding suggests that NQO1 protein expression following sulforaphane treatment is mediated via the Nrf2/Are pathway.

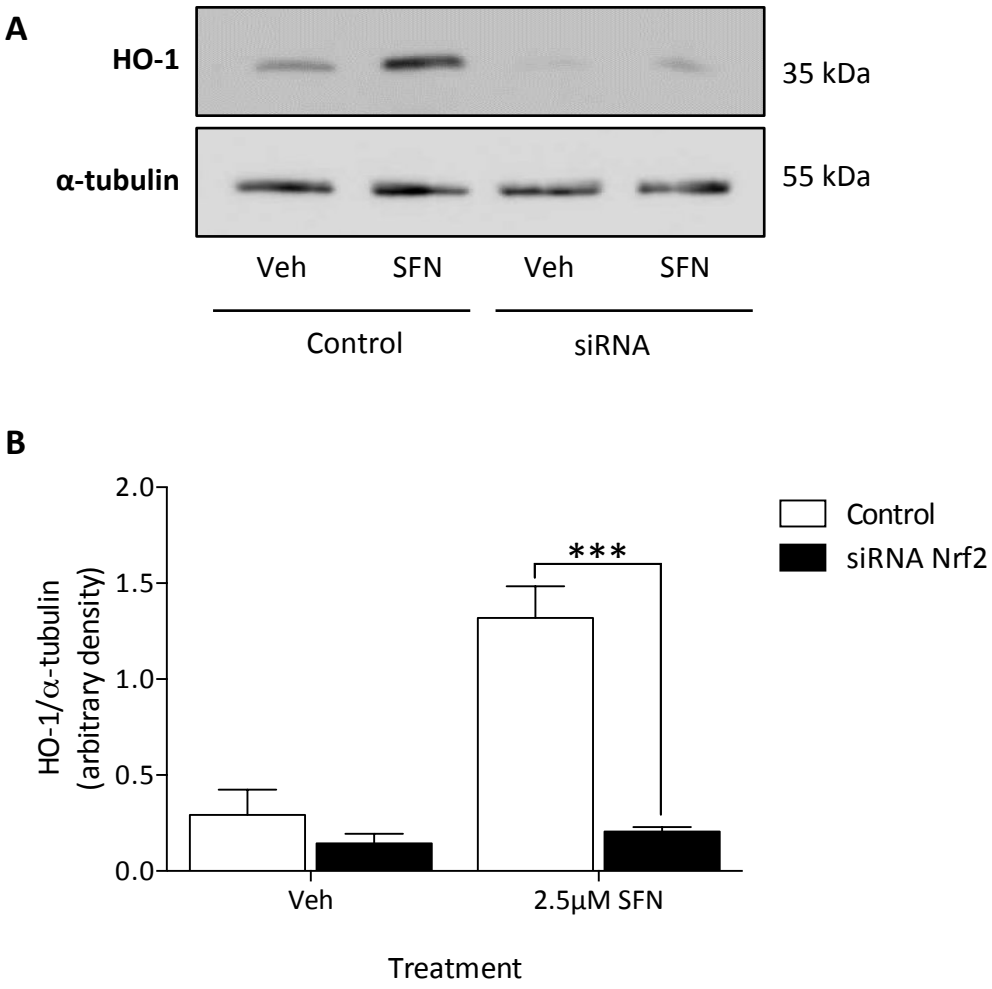

Figure 6.16 Effect of Nrf2 knockdown by siRNA on sulforaphane induced HO-1 protein expression in bEnd.3 cells.

bEnd.3 cells equi in DMEM supplemented with 10% FCS were transfected with Nrf2 siRNA for 24h, followed by treatment with either vehicle (0.01% DMSO) or 2.5 μM sulforaphane for 24h. Whole cell lysates were immunoblotted for HO-1 protein (**A**) and analysed by densitometry relative to the loading control α-tubulin (**B**). Data denote mean ± S.E.M., and were analysed by one-way ANOVA and Tukeys post-test *** P<0.001. n=3 independent bEnd.3 cultures (passage 10-15).

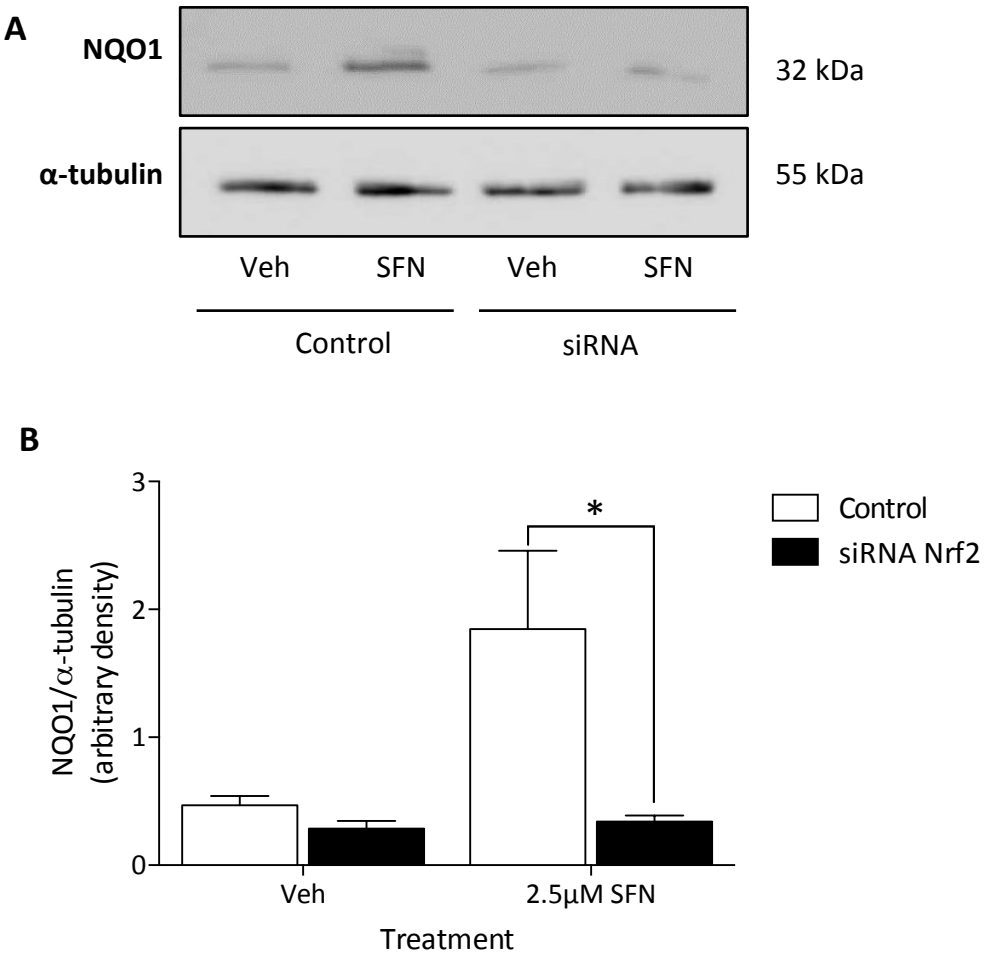

Figure 6.17 Effect of Nrf2 knockdown by siRNA on sulforaphane induced NQO1 protein expression in bEnd.3 cells.

bEnd.3 cells equilibrated in DMEM supplemented with 10% FCS were transfected with Nrf2 siRNA for 24h, followed by treatment with either vehicle (0.01% DMSO) or 2.5 μM sulforaphane for 24h. Whole cell lysates were immunoblotted for NQO1 protein (**A**) and analysed by densitometry relative to the loading control α-tubulin (**B**). Data denote mean ± S.E.M., and were analysed by one-way ANOVA and tukeys post-test, * $P<0.05$. n=3 independent bEnd.3 cell cultures (passage 10-15).

6.7 Sulforaphane pre-treatment and oxygen-glucose deprivation

The findings presented in this chapter revealed that treatment of bEnd.3 cells with sulforaphane lead to a trend for elevated intracellular GSH levels (Figure 6.9) and HO-1 and NQO1 protein and mRNA expression via the Nrf2-defence pathway. OGD experiments revealed a time-dependent increase in cell death following *in vitro* ischaemia and moreover, a time-dependent increase in HO-1 and NQO1 protein expression. Our *in vivo* experiments demonstrated an improvement in neurological function and attenuated cerebrovascular permeability in sulforaphane pretreated rats subjected to MCAo and reperfusion injury. Thus, we investigated the effects of sulforaphane pre-treatment in bEnd.3 cells subjected to OGD *in vitro*.

bEnd.3 cells were pre-treated with either vehicle (DMSO 0.01%) or 2.5μM sulforaphane for 12h, and then subjected to OGD for 2, 6, 8 and 12h. A ratio for dead versus living cells was determined after staining cells with ethidium bromide and DAPI to identify dead cells and all cell nuclei respectively. Vehicle and sulforaphane treatment did not affect the viability of bEnd.3 cells in time-matched experiments (Figure 6.18), consistent with cell viability findings determined using an MTT assay (Figure 6.6). In vehicle pretreated bEnd.3 cells, OGD resulted in a time-dependent increase in cell death (Figure 6.18), similar to findings shown in Figure 6.3. Notably, significant increases in cell death were only observed after 6h OGD compared to time-matched controls. Pre-treatment of bEnd.3 cells with sulforaphane (2.5μM) for 12h significantly reduced cell death following 6, 8 and 12 h OGD.

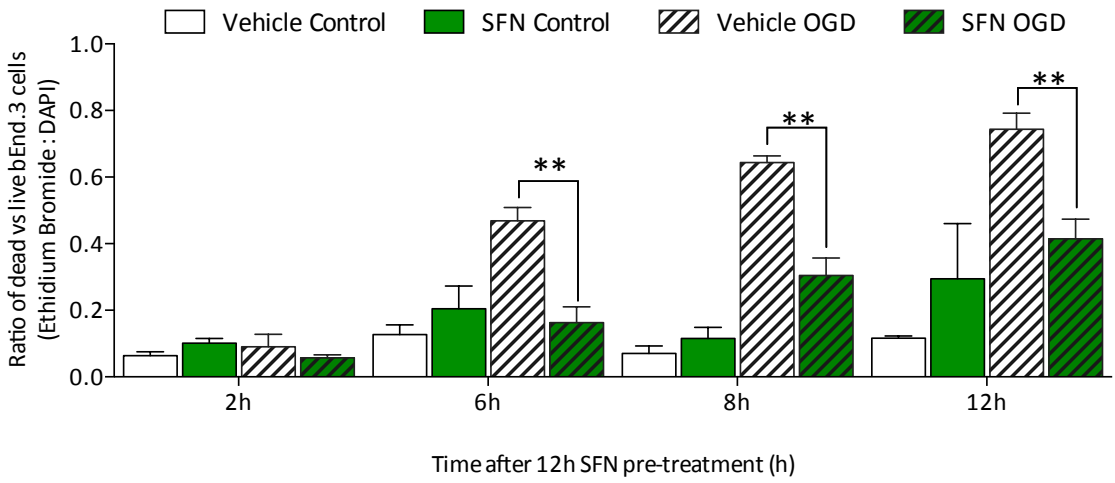

Figure 6.18 Cytoprotective effects of sulforaphane pre-treatment against oxygen and glucose deprivation induced bEnd.3 cell damage.

Confluent monolayers of bEnd.3 cells were pre-treated with vehicle (0.0001% DMSO) or 2.5µM sulforaphane for 12h and subjected to oxygen and glucose deprivation for 2, 6, 8 and 12h in the absence of sulforaphane. The ratio of dead cells (ethidium bromide positive staining) versus live cells (DAPI positive staining) was determined. Data denote mean ± S.E.M, and were analysed by two-way ANOVA with Tukeys post-test. ** $P<0.01$, n = 3 independent bEnd.3 cell cultures (passage 12 – 20).

6.8 Effects of OGD on bEnd.3 cells adapted to physiological oxygen levels

The *in vitro* experiments presented in this chapter were conducted in bEnd.3 endothelial cells cultured under ambient oxygen (21%) in standard 5% CO_2 incubators. *In vivo* endothelial cells in the brain are exposed to 3 – 7% oxygen, highlighting that the majority of *in vitro* studies with cultured are conducted under hyperoxic conditions. Thus, to assess whether brain endothelial cells are affected by changes in oxygen tension, the effects of OGD on bEnd.3 cell viability were re-examined in cells adapted to physiological oxygen levels (5%).

In bEnd.3 cells adapted to 5% O_2, OGD increased cell death after 2 h compared to control cells (Figure 6.19 A). Notably, the observed increase in cell death following 2 h OGD was greater in bEnd.3 cells adapted to 5% O_2 compared to cells cultured under 21% O_2 (Figure 6.19 B). To assess the effects of oxygen tension on Nrf2 mediated enzyme expression in bEnd.3 cells, HO-1 protein expression was measured in cells adapted for 5 days to either 5% or 21% O_2. bEnd.3 cells were treated with either 0.01% DMSO (vehicle), 2.5 µM SFN or 100 µM DEM for either 12 h or 24 h, and whole lysates immunoblotted for HO-1 expression. DEM served as a positive control for the induction of HO-1. No difference was observed in the induction of HO-1 in bEnd.3 cells cultured in 5% or 21% O_2 (Figure 6.20).

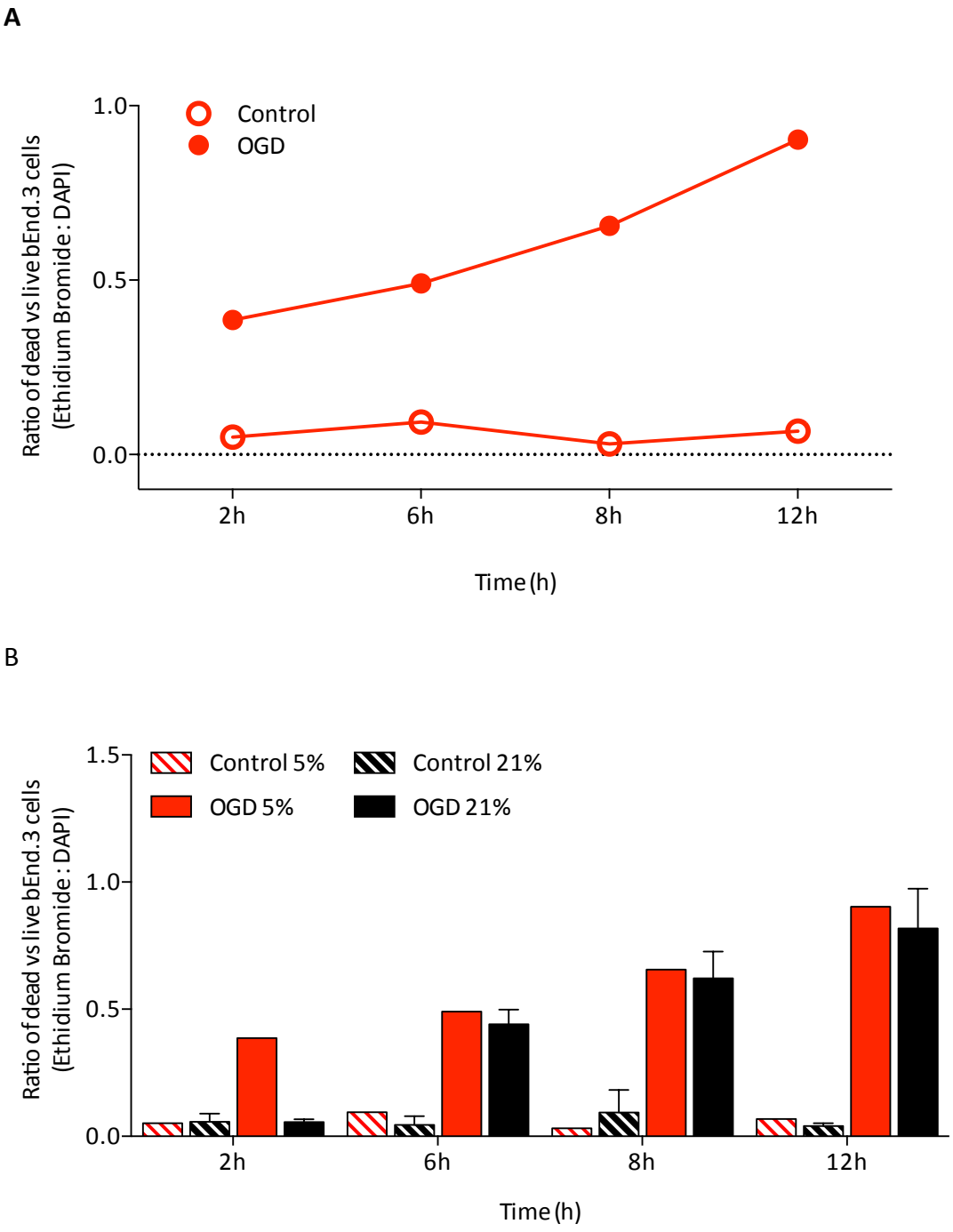

Figure 6.19 Effects of oxygen glucose deprivation on viability of bEnd.3 cells adapted long-term to physiological oxygen tension.

bEnd.3 cells were maintained in 5% oxygen for 5 days and then subjected to oxygen and glucose deprivation for 2, 6, 8 and 12 h under 5% oxygen. (**A**) The ratio of dead cells (ethidium bromide positive staining) to live cells (DAPI positive staining) was determined. Data denote mean ± S.E.M, n=2 independent bEnd.3 cell cultures (passage 15 – 18). (**B**) Comparison of cell death following OGD in bEnd.3 cells adapted under 5% O_2 (red bars) and 21% O_2 (black bars). Data for cell death in cell after OGD in cells cultured under 21% O_2 shown previously in Figure 6.3, n = 3 independent bEnd.3 cell cultures (passage 12 – 20).

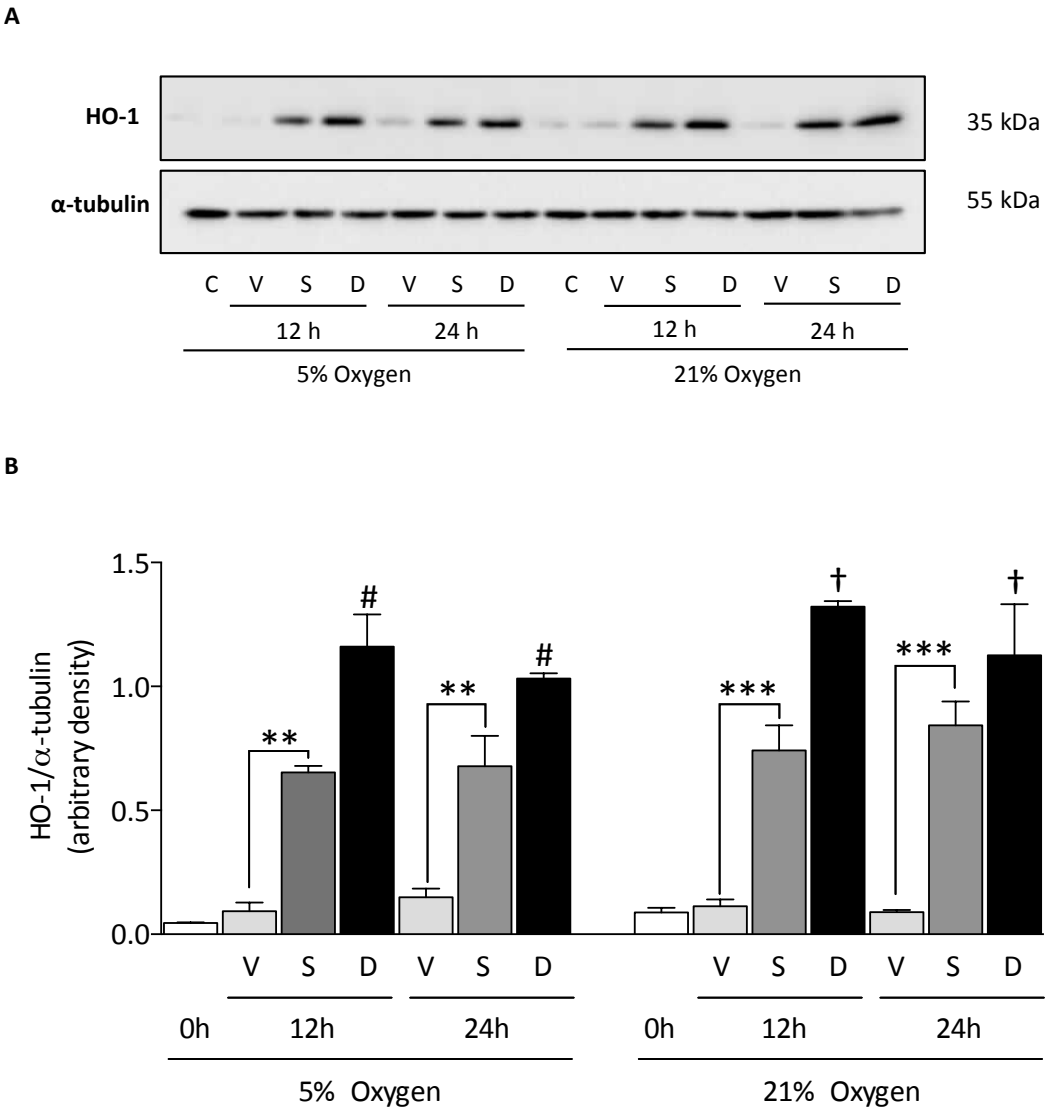

Figure 6.20 HO-1 protein expression in bEnd.3 cells adapted long-term to either 5% or 21% oxygen.

bEnd3 cells were adapted for 5 days to either 5% or 21% oxygen and then treated under the same oxygen tensions for 12 or 24h with either vehicle (V; DMSO 0.01%), 2.5µM SFN (S) or 100µM DEM (D). (**A**) Representative immunoblot for HO-1 protein expression relative to α-tubulin. (**B**) Densitometric analysis of HO-1 protein expression relative to α-tubulin. Data denote mean ± S.E.M. and were analysed by one-way ANOVA with Tukeys post-test. **P<0.01, ***P<0.001; #P<0.001 vs 0 h at 5% oxygen and † P<0.001 vs 0 h at 21% oxygen, n=3 independent bEnd.3 cell cultures (passage 15 – 20).

6.9 Discussion

The endothelium forms a major part of the BBB and plays a important role in protecting the brain parenchyma to maintain an optimal environment for brain function. *In vitro* stroke research has focused on increasing the protection afforded to neurons and astrocytes, but has failed to address the importance of the endothelium in protection of the brain following a stroke. The breakdown of the BBB, following ischaemia and reperfusion injury, occurs due to the uncoupling of endothelial tight junctions, increased endothelial cell contraction and cell death (Greenwood, 1991; Bradbury & Deane, 1993; Abbott *et al.*, 2006; Al Ahmad *et al.*, 2012). Changes in the blood-brain barrier, following cerebral ischaemia and reperfusion injury, results in the formation vasogenic oedema, giving rise to neurological deficits observed in stroke patients (Klatzo, 1987). Increased cerebrovascular permeability following stroke allows for components of the plasma to enter the brain parenchyma. Following BBB breakdown, the presence of albumin in the brain parenchyma results in increased ROS generation, mediating the activation of pro-inflammatory pathways (Ralay Ranaivo *et al.*, 2012). Furthermore, breakdown of the BBB enables transfer of proteins and ions into extracellular brain compartments, increasing oedema formation (Werner & Engelhard, 2007). These findings highlight the importance of protecting the cerebral endothelium following cerebral stroke.

In this chapter, the mouse-derived brain endothelial cell line bEnd.3 was used as an *in vitro* model of the BBB with the aim of modeling ischaemic injury *in vitro* using OGD. bEnd.3 cells exhibited a time-dependent increase in cell death following OGD, however, pre-treatment with the Nrf2 inducer sulforaphane decreased cell death. Sulforaphane treatment bEnd.3 endothelial cells resulted in increased nuclear translocation of Nrf2 and upregulation of its downstream targets HO-1 and NQO1 at both mRNA and protein levels. Furthermore, knockdown of Nrf2 abrogated protein expression of NQO1 and HO-1, providing strong evidence that sulforaphane may confer protection of brain endothelium via the Nrf2-defence pathway.

6.9.1 In vitro versus in vivo model of stroke

To further understand Nrf2 signaling in the brain endothelium, an *in vitro* model of the BBB was employed following the culture of the mouse derived brain endothelial cell line bEnd.3. Although OGD and re-oxygenation experiments *in vitro* would closely mimic our *in vivo* model of ischaemia and reperfusion injury, as discussed in chapters 3 – 5, time restraints in the current project did not allow for re-oxygenation experiments to be conducted. Thus the *in vitro* model of OGD employed in this chapter may illustrate pathways representative of permanent ischaemia models *in vivo*. Although *in vivo* models do not provide sufficient resolution to study cell specific responses, a single tissue culture model cannot account for paracrine interactions present *in vivo*. Therefore suggesting a need for *in vitro* models to closely mimic the *in vivo*

environment. In this study, the brain endothelium was examined alone, hence to improve on the current model, co-culture studies are required to understand whether the observed Nrf2 response are endothelial dependent, or influenced by other cerebral cell types, such as astrocytes. Nawashiro *et al*. demonstrated *in vivo* a role for GFAP, expressed on astrocytes, in modulation of BBB endothelial cells and increased BBB permeability in GFAP KO mice (Nawashiro *et al.*, 2000), thus supporting the rationale for co-culture models *in vitro*. Moreover, Yamagata *et al*. were able to induce BBB characteristics in bovine aortic endothelial cells following culture with astrocyte conditioned medium (Yamagata *et al.*, 1997). Arthur *et al*. also illustrated tight-junction formation *in vitro* in rat brain endothelium cultured in astrocyte conditioned medium (Arthur *et al.*, 1987). These studies thus provide strong evidence that paracrine interactions may influence intracellular signaling and may have increased similarities to the *in vivo* model.

To further elucidate Nrf2 signaling in the brain endothelium, an *in vitro* model of the BBB was employed mouse-derived brain endothelial cell line bEnd.3. Although OGD and re-oxygenation experiments *in vitro* would mimic our *in vivo* model of ischaemia and reperfusion injury, as discussed in Chapters 3 – 5, time restraints in the current project did not allow for re-oxygenation experiments to be conducted. Thus the *in vitro* model of OGD employed in this chapter may provide molecular insights of relevance to permanent ischaemia models *in vivo* (refs). Although *in vivo* models do not provide sufficient resolution to study cell specific responses, a single tissue culture model cannot account for paracrine interactions present *in vivo*. Therefore, the development of co-culture systems *in vitro* that mimic paracrine interactions at the BBB *in vivo* are warranted.

In this study, the brain endothelium was examined in isolation to gain insights into the role of Nrf2 in protection of endothelial cells against oxidative stress. Improvement of the current model involving co-culture studies are required to understand whether the observed Nrf2 responses are endothelial dependent or influenced by other cerebral cell types, such as astrocytes. Nawashiro *et al*. demonstrated *in vivo* an important role for GFAP, expressed on astrocytes, in regulating BBB permeability (Nawashiro *et al.*, 2000), thus supporting the rationale for co-culture models *in vitro*. Moreover, Yamagata *et al*. were able to induce BBB characteristics in bovine aortic endothelial cells following culture with astrocyte-conditioned medium (Yamagata *et al.*, 1997). Arthur *et al*. also illustrated tight-junction formation *in vitro* in rat brain endothelium cultured in astrocyte-conditioned medium (Arthur *et al.*, 1987). These studies thus provide strong evidence that paracrine interactions at the BBB influence intracellular signalling with similarities to *in vivo* conditions.

6.9.2 Cell culture oxygen tensions affect bEnd.3 cell death after OGD

In the present study, cell death after OGD was assessed fluorescently using the apoptotic marker annexin V for the detection of phosphatidylserine, which is expressed on the surface of cells undergoing apoptosis (Koopman *et al.*, 1994), and ethidium bromide, which stains the nuclei of dying cells. The increase in cell death after 6 h OGD is consistent with previously reported findings in bEnd.3 endothelial cells (Andjelkovic *et al.*, 2003; Xie *et al.*, 2012), primary bovine cerebral endothelial cells (Xu *et al.*, 2000), primary cortical rat astrocytes (Goldberg & Choi, 1993; Benavides *et al.*, 2005) and primary hippocampal mouse neurons (Soane *et al.*, 2010). However, the index of cell death used in the highlighted studies measured either the release of lactate dehydrogenase (LDH) or MTT activity. LDH catalyses the two-way conversion of pyruvate to lactate and back, however, LDH is present in the plasma following its release from dead cells. In comparison, the annexin V-ethidium bromide staining employed in the present study identifies cells under going apoptosis.

Notably, in most *in vitro* models of ischaemia, a minimum 6 h of OGD is required before the observation of significant cell death, irrespective of the cerebral cell type under investigation. In humans and rodents *in vivo,* cerebral cell death occurs within minutes following the induction of ischaemic injury (Dirnagl *et al.*, 1999; Kunz *et al.*, 2010), questioning whether current studies of ischaemia *in vitro* are of physiological relevance to an *in vivo* environment. Our preliminary studies of bEnd.3 cells subjected to OGD after adaptation in physiological O_2 (5% O_2 for 5 days) revealed a significant increase in bEnd.3 endothelial cell death 2 h after OGD (Figure 6.17) compared to bEnd.3 cells cultured under 21% O_2 (Figure 6.3). The majority of studies have not assessed the effects of OGD on cerebral cells adapted and cultured under physiological oxygen levels ranging between 5 – 7 %.

The majority of studies have using astrocytes, neurons, brain endothelium (Almeida *et al.*, 2002; Andjelkovic *et al.*, 2003; Griffin *et al.*, 2005; Soane *et al.*, 2010; Bulbarelli *et al.*, 2012) and cells from other vascular beds have characterised the intracellular redox environment in cells cultured under hyperoxic conditions, which is known to enhance Nrf2 mediated gene expression (Takahashi *et al.*, 1998; Cho *et al.*, 2002; Godman *et al.*, 2010). Some studies have highlighted increased survival and proliferation of neurons (Morrison *et al.*, 2000), larger neuronal mitochondrial networks (Tiede *et al.*, 2011), and differences in metabolism with increased uptake of glucose and increased activation of adenosine monophosphate activated kinase (AMPK) (Zhu *et al.*, 2012) in neurons cultured under physiological oxygen levels (~ 5%). Furthermore, Tiede *et al.* also show increased cell death in neurons adapted to physiological oxygen compared to those cultured under ambient air when treated with human immunodeficiency virus (HIV) (Tiede *et al.*, 2011). Albeit Tiede *et al.* use HIV and neurons to

demonstrate increased cell death, our findings are consistent to increased cell death after OGD in endothelial cells cultured under physiological O_2. Thus, the present finding provides novel evidence that cells cultured under physiological O_2 tension exhibit increased cell death at lower durations of OGD. Time constraints during the course of this project have not allowed us to determine the cause of increased cellular death in cells adapted to 5% O_2 following 2 h OGD.

Studies in cultured primary hippocampal neurons have shown that post-treatment of neurons with 0.5µM sulforaphane after 60 min OGD significantly reduced neuronal cell death 24 h after re-oxygenation (Soane *et al.*, 2010). Moreover, Soane *et al.* examined the effects of sulforaphane pre-treatment on hemin-induced neuronal cell death and reported a significant reduction in neuronal cell death in cells exposed to 10µM hemin (Soane *et al.*, 2010). Notably, increased free heme is observed in the brain after injury and contributes to oxidative injury. Pre-treatment of primary rat cortical astrocytes with 5µM sulforaphane protects against cell death induced by 4 h OGD and 48 h re-oxygenation (Danilov *et al.*, 2009). The cytoprotection afforded by sulforaphane pre-treatment in the present study corroborates previous reports and provides evidence for a therapeutic potential of sulforaphane as a pre-conditioning agent against stroke. Hence, further studies are warranted to monitor the concentration of sulforaphane and its metabolites reaching cerebral cells in the intact brain.

6.9.3 Sulforaphane affords cytoprotection of bEnd.3 cells

As mentioned previously, the dietary isothiocyanate sulforaphane is an electrophile and an inducer of the Nrf2 defence pathway (Wakabayashi *et al.*, 2004; Dinkova-Kostova & Kostov, 2012). Hence, sulforaphane may confer protection of cerebral cells via the Nrf2 defence pathway. The present study in bEnd.3 cells revealed a time- and concentration-dependent increase in HO-1 (Figure 6.4) and NQO1 (Figure 6.5) protein expression following sulforaphane treatment. Moreover, sulforaphane increased in mRNA expression of HO-1 and NQO1 in bEnd.3 cells. Although previous studies have shown that HO-1 expression is regulated by multiple transcription factors (Lavrovsky *et al.*, 1993; Ryter *et al.*, 2006), in bEnd.3 endothelial cells, sulforaphane induced HO-1 protein expression was attenuated in Nrf2 silenced cells (Figure 6.14). In 1998, Richmon *et al.* reported increased HO-1 protein expression in the rat brain 24 h after opening of the BBB following intracarotid administration of hyperosmotic mannitol (Richmon *et al.*, 1998). However, as highlighted previously, Panahian *et al.* illustrated a reduction in cerebral infarct volume and improved neurological outcome following stroke in HO-1 overexpressing animals (Panahian *et al.*, 1999). Although the expression of HO-1 was not assessed in the cerebrovascular endothelium in these two studies, the findings implicate an important role for HO-1 in protection of BBB endothelial cells. Interestingly, Bell *et al.* reported HO-1 induction restricted to astrocytes *in vitro* following OGD in mixed

astrocyte/neuron cultures (Bell *et al.*, 2011), suggesting that astrocytes are responsible for HO-1 induction in the brain. However, this hypothesis warrants further investigation to determine whether HO-1 expression is limited to astrocytes in astrocyte/endothelium co-culture models.

Sulforaphane induced NQO1 protein expression was also absent in Nrf2 silenced bEnd.3 cells (Figure 6.15), strongly suggesting that sulforaphane induces HO-1 and NQO1 exclusively via Nrf2. Interestingly, Gustafson *et al*. reported high levels of basal NQO1 activity in bEnd.3 endothelial cells compared to HUVEC (Gustafson *et al.*, 2003). This finding is also consistent with our observation of high levels of basal NQO1 protein expression in bEnd.3 cell lysates. The observed increase in NQO1 enzyme activity is consistent with previously reported findings in Hepa 1c1c7 hepatoma cells (Prochaska & Santamaria, 1988), mouse skin epidermis topically treated with sulforaphane (Dinkova-Kostova *et al.*, 2007), and astrocytes treated with 5µM sulforaphane (Danilov *et al.*, 2009). Moreover, Zhao *et al*. have shown a concentration-dependent increase in cerebral NQO1 activity 18 h after sulforaphane treatment *in vivo* (Zhao *et al.*, 2007a). Although Zhao *et al*. isolated cerebral microvessels from WT and Nrf2 KO mice, the authors did not report on either NQO1 activity or protein expression in these animals.

In this study, we examined the effects of sulforaphane treatment on intracellular GSH levels in bEnd.3 cells. GSH is a critical antioxidant protein that provides the first line of defense to increased oxidative stress. *In vivo,* Bragin *et al*. demonstrated elevated GSH levels in the penumbra compared to the core in rats subjected to MCAo and reperfusion injury (Bragin *et al.*, 2010). Furthermore, these authors also reported an increase in GSH levels in neurons compared to astrocytes in the penumbral region 24 h after 90 min MCAo (Bragin *et al.*, 2010). Our *in vitro* studies in bEnd.3 endothelial cells suggests that acute sulforaphane treatment may deplete intracellular GSH. However, 24 h after sulforaphane treatment, an increase in intracellular GSH content, albeit non-significant, was noted. Based on other studies in the literature, GSH may provide a role for protection of the cerebral endothelium (Sukumari-Ramesh *et al.*, 2010; Steele *et al.*, 2013). Furthermore, intracellular GSH is key in reducing and preventing apoptosis of human brain endothelial cells following challenge with methylglyoxal (Okouchi *et al.*, 2009). Kevil *et al*. demonstrated a significant reduction in protein expression of ICAM1 in mouse aortic endothelial cells treated with glutathione ethyl ester (GEE), known to increase intracellular GSH content (Kevil *et al.*, 2004). These studies illustrate that GSH may play a role in reducing endothelial cell permeability, leukocyte adhesion and preventing apoptosis. Although sulforaphane treatment of bEnd.3 did not lead to significant increases in GSH, it seems likely that sulforaphane may protect the neurovascular unit by modulating intracellular GSH levels (Alfieri *et al.,* 2011).

In both Chapters 5 and 6, sulforaphane was employed as a pre-treatment agent in both *in vivo* and *in vitro* models of stroke. Notably, the duration of pre-treatment in each model varied significantly. In Chapter 5, rats were only pre-treated with sulforaphane for 1 hour prior to the induction of ischaemic injury. However, the *in vitro* studies presented in this chapter employed 12h pre-conditioning. The results in naïve bEnd.3 cells (not exposed to OGD) reveal that HO-1 and NQO1 protein expression was increased significantly only 8h after sulforaphane treatment. These results are consistent with the findings of McMahon *et al.,* who reported that treatment of RL34 cells with sulforaphane only leads to an increase in NQO1 protein 8h after treatment (McMahon *et al.*, 2003). Moreover, nuclear fractions from bEnd.3 cells treated with sulforaphane revealed increased nuclear Nrf2 protein 1 – 4h after sulforaphane treatment. Following stress or the induction of Nrf2 using exogenous agents, Nrf2 accumulation and translocation to the nucleus requires at least 4h. Furthermore, mRNA has to be synthesised, processed and translated into protein, thus requiring at least 8 – 12h following induction of Nrf2 to increase metabolically active enzymes. Although 1h sulforaphane pre-treatment improved neurological outcome following MCAo and 24h reperfusion in rats (Chapter 5), *in vitro* results suggest further experiments should also be conducted with rats pre-treated for at least 12h prior to the induction of MCAo. Thus, the protection observed in animals pre-treated with sulforaphane for 1h may be further enhanced in animals pre-treated with sulforaphane for 12h.

6.9.4 Regulation of Nrf2 activity following sulforaphane treatment

Activation of Nrf2 following oxidative stress or by exogenous stimuli promotes nuclear translocation and upregulation of Nrf2 activity, leading to increased transcription of ARE responsive genes. Up-regulation of Nrf2 is regulated by feedback mechanisms to downregulate its activity. Two known regulators of Nrf2 activity are Keap1 and Bach1. Although the current study did not examine protein expression of these two regulators, qRT-PCR studies indicated a significant increase in Keap1 and Bach1 mRNA expression following sulforaphane treatment (Figure 6.10).

As mentioned in Chapter 1, Keap1 is a cytosolic repressor of Nrf2 that promotes Nrf2 degradation via the 26S proteasome following ubiquitination (Itoh *et al.*, 2003; Taguchi *et al.*, 2011; Niture *et al.*, 2013). Oxidation of cysteine residues on Keap1 results in disassembly of the ubiquitination complex, comprising cullin3 and ring box 1 protein, promoting nuclear translocation of Nrf2. Controversies currently exist as to whether Keap1 shuttles Nrf2 to the nucleus following disassembly of the ubiqutination complex (Nguyen *et al.*, 2005) or whether Nrf2 is stabilized following a conformational change of Keap1, promoting nuclear translocation of free Nrf2 (McWalter *et al.*, 2004; Kaspar *et al.*, 2009; Jain *et al.*, 2010a) . In Chapter 5, our *in vivo* data illustrated significant increases in Nrf2 protein in the brain following 1h sulforaphane

treatment (5 mg/kg, *i.p.*), which would suggest a decrease in the rate of Nrf2 ubiquitination and increased protein stabilization, resulting in increased accumulation within the cell. qRT-PCR analyses revealed no significant differences in Nrf2 mRNA levels 4 h after sulforaphane treatment compared with control or vehicle treated cells. Furthermore, these findings are consistent with the observed decrease in nuclear Nrf2 protein levels and reduction in total cell fluorescence for Nrf2 *in vitro*, and significant decrease in cerebral Nrf2 protein *in vivo* 4 h after sulforaphane treatment. Our findings do not provide sufficient resolution to distinguish between increased nuclear shuttling of Nrf2 or increased Nrf2 stabilization.

Notably, the immunoblotting data shown in Figure 6.11 suggests that Nrf2 is predominantly a nuclear protein, whilst limited cytoplasmic Nrf2 was identified. However, Figures 4.4 and 5.8 examined the levels of total cellular Nrf2 in the brain, identifying Nrf2 protein in both nuclear and cytoplasmic compartments. An increase in Nrf2 protein following stroke has been reported in the brain by immunohistochemical analysis (Tanaka *et al.*, 2011). Furthermore, the brightfield images presented by Tanaka *et al.* show increased staining in a cell within an intact brain section, but did not differentiate between nuclear and cytoplasmic Nrf2. Our immunohistochemical studies in Chapters 4 and 5 reported similar findings in ex vivo brain sections from male rats subjected to MCAo. Improved resolution obtained using the quantitative immunohistochemical technique allowed for the direct identification of Nrf2 protein in both nuclear and cytoplasmic compartments. Activation of Nrf2 results in a reduction of its ubiquitination and subsequent proteasomal degradation, which may allow for the identification of cytoplasmic Nrf2. Furthermore, this finding would suggest that the quantitative immunohistochemical technique may provide an improved sensitivity for the detection of proteins compared to traditional immunoblotting methods.

With respect to Keap1, 4h sulforaphane treatment significantly increased Keap1 mRNA expression in bEnd.3 cells, suggesting that decreased Nrf2 nuclear accumulation and cerebral protein content 2 – 4h after sulforaphane treatment may be due to increased Keap1 protein expression and/or activity. Further study is required to examine the time-dependent changes in Keap1 protein and its cellular localization after sulforaphane treatment. Interestingly, Sun *et al*. reported that Keap1 translocates to the nucleus to export Nrf2 for degradation (Sun *et al.*, 2007). These authors further reported that the nuclear Keap1-Nrf2 complex is unable to bind to the ARE (Sun *et al.*, 2007), suggesting that Nrf2 binds to the ARE independent of Keap1. Velichkova *et al*. demonstrated nuclear translocation of Keap1 protein in NIH 3T3 fibroblasts following treatment with diethylmaleate, however, mutation of the nuclear export signal on Keap1 increased the nuclear accumulation of both Nrf2 and Keap1 (Velichkova & Hasson, 2005). Sun *et al*. also reported that Keap1 shuttles between the nucleus and cytoplasm under physiological conditions and is independent of Nrf2 (Sun *et al.*, 2011). Although in the present

study, protein expression or cellular localization of Keap1 was not examined, our observation of increased Keap1 mRNA levels following sulforaphane treatment corroborates published findings. Furthermore, the observed increase in Keap1 mRNA may occur to promote nuclear export and increased degradation of Nrf2, providing a regulatory mechanism for Nrf2 activity following activation.

With respect to stroke, Tanaka *et al.* employed immunohistochemical analysis to demonstrate a decrease in Keap1 protein expression in *ex vivo* brain sections from mice subjected to MCAo and reperfusion injury (Tanaka *et al.*, 2011). This study however, this study did not specify the cerebral cell types responsible for the observed changes in Keap1 protein expression. Although we did not examine Keap1 and Nrf2 localisation following OGD in bEnd.3 cells, our *in vivo* findings of increased Nrf2 protein expression in rats brains following cerebral ischaemia and reperfusion injury (Chapter 4) corroborates findings reported by *Tanaka et al*. (2011). To further understand the mechanisms regulating Nrf2 levels after stroke and sulforaphane treatment, it would be important to determine parallel changes in Keap1 expression and its cellular localization.

Bach1 is known to inhibit Nrf2 activity by binding to the ARE following hetrodimerisation with small Maf proteins (Igarashi & Sun, 2006; Jyrkkanen *et al.*, 2011). In the presence of free heme, the Bach1-Maf complex is disassociated, allowing for Nrf2 binding to the ARE (Hira *et al.*, 2007). It is well established that Bach1 regulates cellular expression of HO-1 (Ferrando-Miguel *et al.*, 2003; Dohi *et al.*, 2006; Shan *et al.*, 2006; Sakoda *et al.*, 2008). Following an increase in HO-1 activity, increased iron and reduction in the levels of free heme allows for the formation of the Bach1-Maf inhibiting complex and its binding to the ARE, thereby preventing further transcription by Nrf2. As mentioned previously, our findings established a significant increase in Bach1 mRNA after 4 h sulforaphane treatment. Notably, Nrf2 mRNA levels were not significantly different between sulforaphane treated, vehicle-treated or control bEnd.3 cells. Furthermore, nuclear translocation studies of Nrf2 revealed a decrease following 4 h sulforaphane treatment. Although Bach1 protein levels were not assessed in the present study, our data suggest that Bach1 may also play a role in regulating Nrf2 nuclear accumulation and ARE binding activity in the brain endothelium. In this context, Jyrkkanen *et al.* have demonstrated a Nrf2-mediated increase in Bach1 mRNA in HUVEC overexpressing Nrf2 (Jyrkkanen *et al.*, 2011), suggesting that Nrf2 regulates Bach1 expression and activity. Jyrkkanen *et al*. also reported an ARE sequence in the Bach1 promoter region, with sequence homology between mouse and human Bach1 promoters (Jyrkkanen *et al.*, 2011). Although the present study has not examined Nrf2 binding to the promoter region of specific genes, our mRNA data for Bach1 is consistent with the findings reported by Jyrkkanen *et al*. (2011) and suggests that similar Nrf2 regulatory mechanism may exist in brain endothelium. Sakoda *et al*.

have reported an increase in brain HO-1 mRNA levels in Bach1 KO mice (Sakoda *et al.*, 2008), suggesting the presence of Bach1 in the rodent brain and its potential involvement in regulating Nrf2. Interestingly, MacLeod *et al.* have shown that Keap1 and Bach1 regulate Nrf2 activity via different mechanisms, as the knockdown of Bach1 did not confer protection to immortalised human keratinocyte HaCaT cells against a range of electrophilic stimuli and redox-cycling agents, although the knockdown of Bach1 significantly increased HO-1 gene expression (MacLeod *et al.*, 2009). Moreover, MacLeod *et al.* stated that the promoter region of HO-1 contains ARE-like sequences, enabling Bach1 binding (MacLeod *et al.*, 2009). Hence, it remains to be determined whether Bach1 plays a role in regulating other ARE-linked genes. With respect to stroke, Perez-de-Puig *et al.* reported a significant decrease in Bach1 protein expression in the mouse brain after 8 h permenant MCAo, which was associated with increased HO-1 protein and mRNA expression (Perez-de-Puig *et al.*, 2013). Although these findings are consistent with increased HO-1 and Nrf2 protein levels observed in ischaemic rat brain (see Chapter 4), it remains to be elucidated whether increased Bach1 activity after sulforaphane treatment affects its potential therapeutic benefits.

6.9.5 Is oxygen and/or glucose deprivation responsible for the upregulation of HO-1?

Examination of HO-1 protein expression in bEnd.3 cells subjected to oxygen and glucose deprivation revealed a time-dependent increase in HO-1 expression. In our model, we did not assess the upregulation of Nrf2 following OGD, however, there remains a possibility that the observed upregulation of HO-1 in the bEnd3 cells may occur as a result of oxygen and glucose deprivation. Appleton *et al.* (2003) reported a decrease in HO-1 protein content in extravillous trophoblast cells exposed for 24h to low oxygen (0.5%) and low glucose (0.2 mM) (Appleton *et al.*, 2003). Interestingly, Appleton *et al.* also reported a decrease in expression of HO-2, a constitutively expressed isoform of heme oxygenase, following exposure to lower levels of oxygen and glucose. This suggests that an increase in HO-1 protein expression may occur to compensate for the reduction in HO-2 protein levels. Furthermore, Chang *et al.* found increases in HO-1 mRNA following glucose deprivation for 12 – 24h in HepG2 cells (Chang *et al.*, 2002). Moreover, Takeda *et al.* reported an increase in HO-1 protein expression within 1.5h of glucose deprivation in cardiac fibroblasts (Takeda *et al.*, 2004). Thus, activation of HO-1 following OGD may be due to the deprivation of glucose from brain endothelial cells for a longer duration. It remains to be elucidated whether the observed changes in HO-1 protein levels are regulated by Nrf2 following OGD.

6.9.6 Summary and conclusions

In summary, the mouse-derived brain endothelial cell line bEnd.3 was used as an *in vitro* model of the brain endothelium. The effects of sulforaphane pre-treatment on bEnd.3 cell death

following OGD was further examined as an *in vitro* model of ischaemia. This chapter provides the first evidence that sulforaphane pre-treatment of bEnd.3 cells decreases cell death after OGD, highlighting that sulforaphane mediates protection of the brain endothelium. Notably, this chapter also reports the first experimental evidence that adaptation and culture of bEnd.3 cells under physiological oxygen tension increases cell death after shorter durations of OGD.

In conclusion, this chapter reports for the first evidence that sulforaphane pre-treatment provides protection to the cerebrovascular endothelium via the Nrf2 defence pathway, and hence may serve as a potential therapeutic intervention to limit the opening of the BBB following cerebal stroke. Moreover, to our knowledge, we also provide novel and primary evidence that the culture of cells under physiological tensions may provide greater relevance to the *in vivo* environment, and hence further experiments in primary rodent and human brain endothelial cells are warranted.

Chapter7 – General Discussion

Chapter 7 General Discussion

7.1 Summary of the project

The redox sensitive transcription factor Nrf2 orchestrates the expression of many antioxidant and phase II detoxifying enzymes, conferring protection against electrophilic, xenobiotic and oxidative stress following the induction of a pathophysiological disease state, such as cerebral ischaemia and reperfusion injury. Previous studies have highlighted the significance of Nrf2 mediated protection in the ischaemic brain, highlighting increased BBB breakdown, cerebrovascular permeability and increased neurological deficits in Nrf2 deficient animals.

This project reports the first quantitative measurements of the temporal and spatial distribution of Nrf2 following ischaemia and reperfusion injury in a rodent model of stroke, demonstrating peak expression of Nrf2 protein 24h after 70 min MCAo. Notably, 1h pre-treatment of rats with the dietary Nrf2 activator sulforaphane, reduced its expression 24h after 70 min MCAo and conferred increased protection to the brain following ischaemia and reperfusion injury.

Chapter 3 describes the development of a novel immunohistochemical technique using DAB, which allowed for true protein quantitation in *ex vivo* brain sections. Furthermore, whilst immunoblotting techniques only deliver information over a global scale, the immunohistochemical technique provides greater resolution to determine protein content in particular cell types, cellular compartments and different regions of the tissue.

In Chapter 4, the novel immunohistochemical technique was used to quantify nuclear accumulation of Nrf2 following cerebral ischaemia-reperfusion injury. Nrf2 was expressed differentially between the contralateral hemisphere and the infarct core and peri-infarct regions of the stroke-affected hemisphere. Nrf2 protein content was notably increased in all brain cells in the peri-infarct region of the ischaemic brain after 24h and 72h reperfusion injury. Chapter 4 further provides the first quantitative measures of endothelial Nrf2 expression and identifies a time-dependent increase in the spatial distribution of endothelial Nrf2 content. In parallel studies, immunofluorescence examination of *ex vivo* brain sections demonstrated a clear upregulation of the Nrf2-mediated antioxidant stress protein HO-1 after 24 - 72h reperfusion injury. HO-1 was predominantly expressed in astrocytes in the peri-infarct region of the stroke-affected hemisphere. Furthermore, following 24h reperfusion injury, increases were also identified in the protein expression of NQO1 and Prx1 in the stroke-affected hemisphere.

Chapter 5 examined the effects of pre-treating rats with the Nrf2 inducer sulforaphane on Nrf2 expression after stroke. DAB immunohistochemtry clearly demonstrated that sulforaphane pre-treatment markedly attenuated Nrf2 protein expression in all cells and the cerebrovascular

endothelium in the stroke-affected hemisphere after 24h reperfusion injury. Moreover, behavioural studies conducted by Dr Alessio Alfieri, Cardiovasular Division, KCL, confirmed significant improvements in neurological deficits after stroke in sulforaphane pre-treated animals. Notably, sulforaphane rapidly crossed the BBB and upregulated protein expression of Nrf2, HO-1, NQO1 and Prx1 in naïve rat brains.

As shown in Chapter 6, the mouse bEnd.3 endothelial cell line was employed to determine whether sulforaphane treatment conferred protection following *in vitro* experimental ischaemia. Pre-treatment of cells with sulforaphane for 12h prior to oxygen-glucose deprivation significantly reduced cell death. Further evaluation of the effects sulforaphane on naïve bEnd.3 cells revealed time- and dose-dependent increases in the protein and mRNA expression of HO-1 and NQO1, along with increased nuclear accumulation and ARE binding activity of Nrf2. siRNA knockdown of Nrf2 abrogated sulforaphane stimulated protein expression of HO-1 and NQO1. As sulforaphane treatment of bEnd.3 cells increased Keap1 and Bach1 mRNA, this may provide insights into the regulation Nrf2 activity following its activation.

Although data in Chapter 6 provides evidence that sulforaphane is a viable candidate to confer protection to cerebral endothelial cells, the current set of experiments were conducted in bEnd.3 cells cultured under ambient air (21% oxygen). Preliminary OGD experiments conducted using bEnd.3 cells cultured initially under physiological oxygen tensions (5%), revealed increased endothelial cell death following 2h OGD, a response absent in bEnd.3 cells cultured under ambient air. These findings demonstrate that cells cultured under ambient air may not be representative of the *in vivo* environment.

7.2 Protection of the blood-brain barrier by sulforaphane

This project provides novel insights into the time-course of Nrf2 protein expression in the brain after stroke, highlighting a significant delay in the activation and nuclear accumulation of Nrf2 post reperfusion injury. It is well established that under homeostatic conditions, the BBB protects the neurovascular unit and the brain parenchyma (Figure 7.1A), however, following the induction of cerebral ischaemia and reperfusion injury, we have breakdown of the BBB and increased cerebral cell death (Figure 7.1B). Notably, we demonstrated that pre-conditioning with the dietary Nrf2 inducer sulforaphane significantly improved neurological outcome following stroke. This suggests that cerebral damage and endothelial cell death following stroke was attenuated, allowing for the maintanaince of the integrity of the BBB (Figure 7.1C). However, further investigation is required to assess the effects of sulforaphane pre-treatment on BBB permeability to confirm this hypothesis.

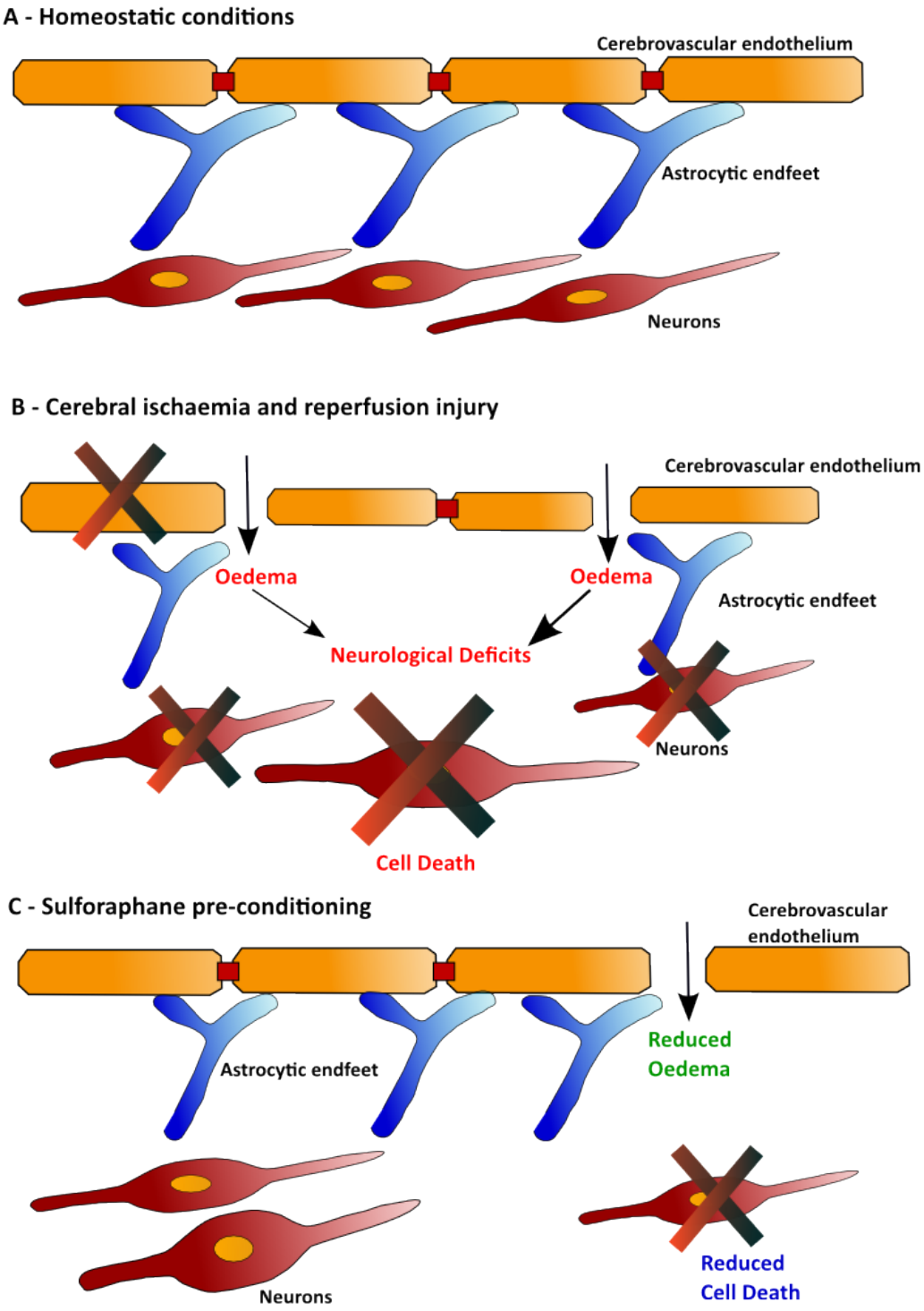

Figure 7.1 Effects of ischaemia-reperfusion injury on the neurovascular unit after stroke.

(**A**) Under normal conditions, a tight apposition of endothelial cells held together by tight-junctional complexes, form the BBB, which is supported by the presence of astrocytic endfeet and neurons. (**B**) Following cerebral ischaemia and reperfusion injury, the breakdown of the BBB, characterised by the loss of tight junctional complexes, endothelial cell contraction and cell death results in the formation of vasogenic oedema. This results in neuronal cell death and associated neurological deficits. (**C**) Sulforaphane pre-conditioning reduces breakdown of the BBB and confers increased protection to cerebral cells.

A major contributor to the pathophysiology of cerebral ischaemia is increased oxidative stress, resulting in increased formation of lipid peroxidation, protein carbonylation, and cell death (Figure 7.2). However, sulforaphane pre-conditioning increases Nrf2 activity and its mediated antioxidant and phase II detoxifying enzymes, increasing the capacity of cerebral cells, including the cerebrovascular endothelium, to counteract the increased oxidative stress exhibited during ischaemia-reperfusion injury (Figure 7.2).

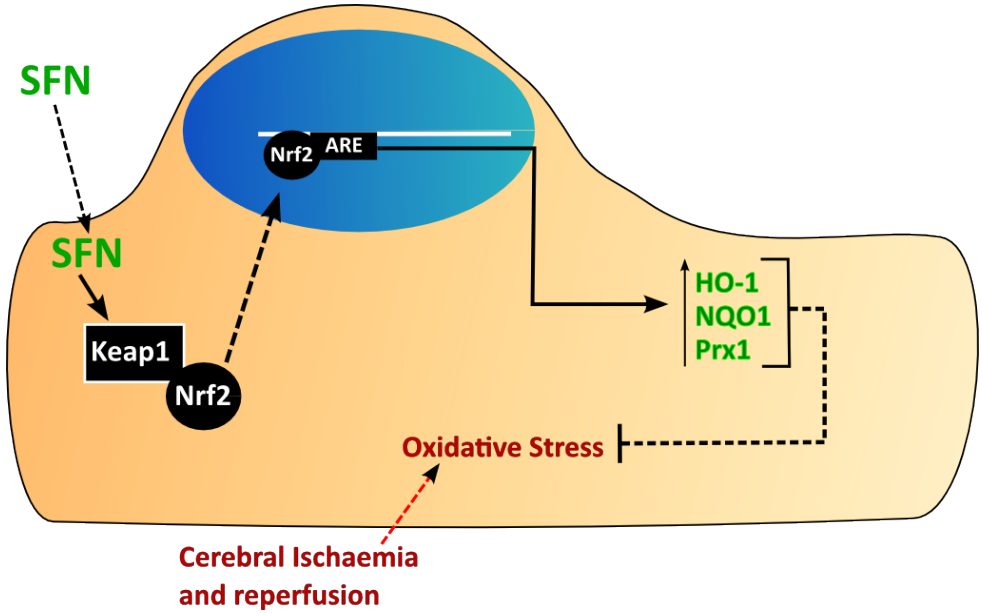

Figure 7.2 Schematic representation of Nrf2 activation by sulforaphane in cerebral cells.

Cerebral ischaemia and reperfusion injury increase oxidative stress within the cell, leading to cell damage and initiation of pro-apoptotic pathways. Pre-conditioning of the brain with sulforaphane (SFN) increases Nrf2 activation, and its nuclear translocation. This results in the upregulation of Nrf2 regulated targets, which include HO-1, NQO1 and Prx1. The upregulation of such antioxidant enzymes by pre-conditioning increases the cells capacity to counteract increased oxidative stress, protecting the cell from damage.

Hence, this study highlights sulforaphane as a potential therapeutic candidate for treatment of cerebral ischaemia and reperfusion injury. However, we delineate that pre-conditioning strategies will aid in attenuating the cerebral damage and neurological deficits experienced after a stroke, and aid in reducing the financial burden endured by heath services and affected communities.

7.3 Development of a novel immunohistochemical technique for *ex vivo* quantitation of protein expression

A major aspect of this project was the development of a novel immunohistochemical technique that could be employed for the quantitation of particular proteins in *ex vivo* tissue sections, allowing for the user to identify anatomical variations in protein expression. Protein quantitation was based on the initial rate of DAB polymer development, the product of a biochemical reaction between DAB and H_2O_2, which was catalysed by HRP conjugated to a secondary antibody. The concentration of HRP enzyme present to catalyse DAB polymer formation is related to the amount of protein present within tissue section. Furthermore, the concentration of the target protein with in tissue section will vary within different regions of the tissue.

Currently, studies employ the use of immunoblotting techniques to quantify changes in protein expression following the homogenisation of tissue, and separating extracted proteins by weight using SDS-PAGE. However, immunoblotting techniques are only able to confer information regarding the global changes in the proteins of interest, and furthermore, only provide a semi-quantitative measurement. However, the developed immunohistochemical technique allows for true protein quantitation in different anatomical regions of the tissue, and moreover, in different cell types, thus providing greater resolution compared to immunoblotting. An objective of this project was to quantify Nrf2 protein expression in the ischaemic brain, and furthermore, to examine Nrf2 expression in the cerebrovascular endothelium. The employment of our novel immunohistochemical technique allowed us to fulfil these objectives.

7.4 Cerebrovascular endothelium: required for protection of the brain parenchyma

There is a consensus that the upregulation of Nrf2 regulated defences following cerebral ischaemia affords protection to neurons and astrocytes in the brain. Neurons are integral to brain function, and astrocytes play a critical role in maintaining a homeostatic environment in the brain. The defined functions of these cells with in the brain milieu highlight the requirement for enhanced protection in neurodegenerative disease states. The cerebrovascular endothelium has however failed to receive the same amount of focus, raising the question “whether the cerebrovascular endothelium is important for brain function?”. As defined in Chapter 1, the cerebrovascular endothelium forms the BBB, and thus plays an important role in maintaining brain function and brain environment by regulating the flow of blood-borne substances to and from cerebral circulation. The loss of BBB integrity following cerebral stroke, or other neurodegenerative disease states, results in the formation of vasogenic oedema, which is associated with the observed neurological deficits. Hence, protection of the cerebral

endothelium is important for maintaining the integrity of the BBB and for protection of the brain parenchyma.

Activation of Nrf2 by a range of different stimuli results in a decrease in cerebral oedema formation, suggesting that increased protection of the cerebrovascular endothelium maintains integrity of the BBB (Zhao *et al.*, 2006; Yang *et al.*, 2009; Shah *et al.*, 2010; Son *et al.*, 2010; Ren *et al.*, 2011; Nada & Shah, 2012; Sumi *et al.*, 2013; Wang & Cui, 2013). Furthermore, the cerebral infarct volume, a measure of dead brain tissue, is also reduced following activation of Nrf2.

Although the global activation of Nrf2 confers protection, a reduction in cerebral oedema formation directly contributes to the observed reductions in cerebral infarct volume. In the present study, sulforaphane treatment of bEnd.3 cells *in vitro* increased the expression two Nrf2-linked proteins, HO-1 and NQO1 (Chapter 6). Furthermore, following *in vitro* ischaemia by OGD, a reduction in cell death is apparent in bEnd.3 cells pre-treated with sulforaphane. This data clearly illustrates that sulforaphane pre-treatment protects the brain endothelium *in vitro*. Zhao *et al.* demonstrated that 18h sulforaphane treatment of naïve mice increased HO-1 protein expression exclusively in the brain endothelium (Zhao *et al.*, 2007a), which is consistent with our observations for HO-1 expression in naïve rats treated with sulforaphane (Alfieri *et al.*, 2013).

Our sulforaphane pre-conditioning studies in rats *in vivo,* prior to MCAo and reperfusion injury also demonstrated increased HO-1 protein expression in the brain endothelium (Alfieri *et al.*, 2013). Although these *in vivo* findings suggest that sulforaphane mediated HO-1 protein increase in the brain endothelium is maintained after a stroke, we also reported that pre-conditioning improved neurological outcome and ameliorated lesion progression (Alfieri *et al.*, 2013).

Upon reperfusion injury in rats, Peters *et al.* observed a sudden increase in ROS generation (Peters *et al.*, 1998), which would directly affect the integrity of the BBB (Abbott *et al.*, 2006). As mentioned previously in Chapter 1, GSH provides the “first-line” of cellular defence against increased oxidative or electrophilic stress. Agarwal *et al.* demonstrated an increase in BBB permeability in rats treated with diethyl malate (DEM), an electrophile known to deplete intracellular GSH (Agarwal & Shukla, 1999). *In vitro* studies using bovine brain endothelial cells have associated a depletion of intracellular GSH levels to increase cerebrovascular permeability following 24 – 48h hypoxia (Plateel *et al.*, 1995). In the present studies with bEnd.3 cells, sulforaphane treatment evoked a trend for increased intracellular GSH content. It is thus conceivable that the maintenance of intracellular GSH levels in BBB may limit IgG

permeability and attenuate lesion progression following MCAo and reperfusion injury (Alfieri *et al.*, 2013).

Hence, the present *in vitro* findings provide insights into the possible mechanisms of action by which sulforaphane confers protection to the BBB endothelium *in vivo*. These data highlight that protection of the endothelium will protect the brain parenchyma, and further studies are warranted to explore therapeutic strategies to protect the BBB in neurodegenerative disease states.

7.5 Expression of Nrf2 in the ischaemic penumbra

Current stroke research focuses on increasing the protection afforded to the ischaemic penumbra in experimental models of stroke, with an aim to identify treatment regimes for the clinical setting. In 1981, Astrup *et al.* stated that the discovery of the ischaemic penumbra may be valuable for experimental research and also in the clinical setting (Astrup *et al.*, 1981). As described in Chapter 1, the penumbra is defined by changes in cerebral blood-flow, however, in ischaemia-reperfusion injury, the ischaemic penumbra is developed further by other pathophysiological processes.

7.5.1 Expression of Nrf2 and its mediated proteins in the ischaemic brain

Initiation of reperfusion increases the progression and formation of the ischaemic penumbra. However, as time elaspses after a stroke, the volume of penumbral tissue decreases, signifying increased cell death. The penumbra is defined by a deficit in blood perfusion to the tissue and increased oxygen extraction (Robertson *et al.*, 2011). In this study, the penumbral region in the infarcted brain could not be defined, however, with fluorescence imaging, we were able to define peri-infarct regions. Profiling studies examining the expression of Nrf2 within the ischaemic brain revealed differences in Nrf2 protein expression between the infarct core and penumbral regions of the brain. However, in our study, it is interesting to note that after 72h reperfusion, Nrf2 protein levels remained elevated in the peri-infarct regions, albeit, less than levels observed following 24h reperfusion injury. Based on this finding, it is conceivable that Nrf2 remains active in the peri-infarct regions to increase the antioxidant capacity of cells in the brain following stroke. Dirnagl *et al.* have suggested that the region of the ischaemic penumbra develops further due to depolarisation signals radiating from the ischaemic core, which is known to increase oxidative stress (Dirnagl *et al.*, 1999), and this may explain the observed increases observed for Nrf2 in the peri-infarct regions.

7.5.2 Sulforaphane pre-treatment may reduce cerebral ischaemia-reperfusion induced damage

As mentioned in Section 7.5.1, the penumbral region develops with increasing duration of injury and inadequate therapy to initiate protective mechanisms at an earlier time frame. In the present study, a significant attenuation of Nrf2 protein levels was observed in animals pre-treated with sulforaphane prior to 70 min MCAo and 24h reperfusion. DAB immunohistochemical analysis for Nrf2 levels in the sulforaphane pre-treated brain was only examined after 24h reperfusion injury. However, we speculate that the volume of infarcted tissue is reduced in rats pre-treated with sulforaphane. A possible mechanism may be due to the increased expression of HO-1 noted in the cerebrovascular endothelium 24h after sulforaphane administration *in vivo*, consistent with previously reported findings (Zhao *et al.*, 2007a). Furthermore, the present *in vitro* studies demonstrated a reduction in cell death in brain endothelial cells subjected to OGD following 12h sulforaphane pre-treatment. Increased endothelial HO-1 content may also enhance the capacity of the BBB to counteract increased oxidative stress following reperfusion injury, leading to reduced BBB permeability and formation of the infarct core.

7.6 Pre-conditioning versus post-conditioning therapeutic strategies

In the current clinical setting, treatment of stroke patients is dependent upon post-conditioning strategies using rtPA. However, the efficacy of post-conditioning treatment protocols are limited by a defined period in which the pharmacological intervention must be administered. In reality, most cerebral ischaemia patients are ineligible for treatment by rtPA due to limited access to an equipped hospital within the defined time-window of 4.5h.

Many studies have targeted the Nrf2-defence pathway to mediate protection to the ischaemic brain. However, as highlighted in Chapter 1, the majority of these *in vivo* models of cerebral ischaemia and reperfusion injury use Nrf2 activators post-ischaemic injury. Notably, Nrf2 activators are administered within minutes of either the induction of ischaemia or reperfusion injury. Clinicians prefer the development of novel drugs that may be administered to the patient as soon as cerebral ischaemia is identified, forcing research into post-stroke therapeutic methods. However, rodent models of stroke cannot be directly compared to human stroke, as the laboratory-based researcher has complete control over the duration of ischaemia, and commencement of reperfusion injury. Although studies conducted by Zhao *et al.* reported that sulforaphane administration 15 min post the induction of ischaemia in mice is protective (Zhao *et al.*, 2006), the likelihood that a clinical patient will be able to receive treatment within the

same time window is unlikely. This point raises the questions whether post-conditioning strategies are suitable for application within the clinical setting.

In the present project, pre-treatment of rats with the Nrf2 activator sulforaphane improved neurological outcomes after stroke (Appendix 5). Furthermore, pre-conditioning studies highlighted in Chapter 1 (Table 1.10) also demonstrate greater protection and reduced cerebral infarct volume compared to studies that employed post-conditioning methods. This provides a clear indication that pre-conditioning therapeutic strategies may confer increased protection to the brain against ischaemia-reperfusion injury induced damage. With regards to the Nrf2-defence pathway examined in this project, sulforaphane was able to increase Nrf2 protein levels in the naïve rat brain within 1h of administration. This suggests that sulforaphane treatment results in an increase of the brain's antioxidant capacity, affording greater protection to the brain during and after ischaemia. Notably, in the present study, rats were only pre-treated or "pre-conditioned" with sulforaphane for 1h prior to MCAo, hence it remains to be examined whether longer duration of pre-treatment with of sulforaphane could confer enhanced protection to the ischaemic brain.

A recent review published by the stroke treatment academic industry roundtable (STAIR) states that research should focus on the development of improved thrombolytic therapies that may be administered within 4.5h after the onset of ischaemia (Albers *et al.*, 2011). Although the aim to restore cerebral blood flow within this defined time window may provide efficacious results, the question remains whether patients will be able to access such therapies within this period. Sulforaphane and other Nrf2 activators are unable to induce thromobolytic actions within the ischaemic core. However, such compounds are able to confer protection to the brain via upregulation of endogenous defences. The present studies established that sulforaphane is able to cross the blood-brain barrier following an intraperitoneal injection *in vivo* in rats, leading to upregulation Nrf2 and its target antioxidant enzymes (Chapter 5). Hence, this demonstrates that sulforaphane is able to confer global protection to the brain. Studies highlighting the protective nature of sulforaphane when administered following ischaemic injury portray sulforaphane as an attractive post-stroke therapeutic strategy (Zhao *et al.*, 2006; Zhao *et al.*, 2007b).

Unfortunately, the occurrence of stroke is an unpredictable event, and furthermore, can affect any living human. A cohort of patients can be identified as being at an increased risk of experiencing a cerebral stroke. These include patients that suffer from diabetes, hypertension, atherosclerosis and other cardiovascular complications. Interestingly, statins have been shown to reduce damage following cerebral ischaemia and reperfusion injury *in vivo* (Laufs *et al.*, 2000; Amarenco, 2001; Laufs *et al.*, 2002; Gertz *et al.*, 2003; Amarenco *et al.*, 2004b; Bersano *et al.*, 2008). Furthermore, a meta-analysis studies by Amarenco *et al.* reports a 21% reduction

in strokes in patients receiving statins (Amarenco *et al.*, 2004a). This evidence strongly suggests that pre-conditioning in humans may be a useful strategy to protect the brain against ischaemia-reperfusion injury. Thus, advising high-risk patients to regularly take sulforaphane may improve neurological outcomes after cerebral stroke.

This present study only focused on the actions of one known dietary activator of Nrf2, however, other studies have also examined the effects of other dietary Nrf2 activators in rodent models of stroke. These include compounds such as, AITC (Xiang *et al.*, 2012), plumbagin (Son *et al.*, 2010), epicatechin-3-gallate (Shah *et al.*, 2010) and quercetin (Sumi *et al.*, 2013). Studies have only examined the protection afforded to the ischaemic brain when a single compound is administered, but there appear to be no reports on the effects of administering a cocktail of known Nrf2 activators. It is not known whether administration of multiple activators in combination would further enhance Nrf2 activity. Such studies are of relevance to the human environment, as food items are consumed in combination and multiple Nrf2 activators maybe present within the body at anyone time. Further studies could therefore examine the concentration-dependence of administering Nrf2 activators to determine whether actions are additive or potentiating.

7.7 Role of sulforaphane in pre-conditioning the brain against stroke

The use of pre-conditioning strategies cannot be described as a therapeutic strategy for treating stroke, but can be better referred to as a "safeguarding" technique, priming the Nrf2-defence system for battle against increased oxidative stress encountered in many disease states. This project examined the effects of the dietary isothiocyanate sulforaphane, a well characterised activator of the Nrf2 pathway (Thimmulappa *et al.*, 2002), as a pre-conditioning agent against cerebral ischaemia and reperfusion injury. This PhD thesis contains little information regarding the effects of sulforaphane pre-conditioning on animal behaviour following stroke, however published work from our research group demonstrated a reduction in IgG permeability and improved neurological outcome following stroke in rats pre-treated with sulforaphane for 1h prior to 70 min MCAo and 24h reperfusion injury (Alfieri *et al.*, 2013). The observed protection in pre-treated animals may be due to the rapid activation of Nrf2 by sulforaphane (Chapter 5), priming endogenous antioxidant defences prior to significant increases in ROS generation (Srivastava *et al.*, 2013). Once again emphasising points in Section 7.3, maintenance of the BBB is required for protection of the brain parenchyma. The present findings thus provide a clear demonstration that sulforaphane pre-conditioning primes the brain's antioxidant capacity, improving its efficiency to counteract increased oxidative stress.

Although our studies are the first to discuss the role of sulforaphane pre-conditioning strategies against cerebral ischaemia and reperfusion injury (Alfieri *et al.*, 2013; Srivastava *et al.*, 2013), sulforaphane has been employed to pre-condition the brain and its cells against other neurodegenerative disease states. Table 7.1 and 7.2 highlights *in vivo* and *in vitro* models of sulforaphane pre-conditioning respectively.

Sulforaphane pre-conditioning attenuates brain damage in multiple neurodegenerative diseases *in vivo* (Table 7.1), and moreover evidence strongly suggests that the observed protection is due to upregulation of the Nrf2 defence pathway. *In vitro* studies also highlight protection of cerebral cells by sulforaphane pre-conditioning, reducing cell death (Table 7.2). It is important to highlight the *in vitro* findings by Bergstrom *et al.* in astrocytes that were pre-treated transiently with repeated doses of sulforaphane over 4 days (Bergstrom *et al.*, 2011). The treatment regimes of sulforaphane applied to astrocytes *in vitro* closely mimic the intake of such dietary compounds by humans. Furthermore, cells were only exposed to sulforaphane for 4h, again closely mimicking the duration of sulforaphane in the plasma until clearance (Conaway *et al.*, 2000). Interestingly, Bergstrom and colleagues revealed rapid induction of Nrf2 upon transient sulforaphane stimulation (Bergstrom *et al.*, 2011), consistent with our findings of increased nuclear translocation of Nrf2 in bEnd.3 cells within 4h of sulforaphane treatment, and rapid induction of Nrf2 *in vivo* following sulforaphane administration. With regards to the downstream targets of Nrf2, Bergstrom *et al.* reported prolonged induction of NQO1, but not HO-1, following repeated transient stimulation of astrocytes with sulforaphane (Bergstrom *et al.*, 2011). This finding suggests that HO-1 may play a minor role in protection of astrocytes subjected to repeated transient sulforaphane treatment. Thus the observed effect maybe a consequence of the sensitisation of HO-1 to repeated sulforaphane treatment and hence warrants further investigation. There also remains a possibility that the modulation of co-factors that interact with Nrf2 to upregulate HO-1 mRNA expression, such as brahma related gene-1 (BRG1) (Zhang *et al.*, 2006) maybe affected by repeated sulforaphane treatment.

Table 7.1 *in vivo* studies of sulforaphane pre-conditioning

Species	***Model***	***SFN Dose***	***Findings***	***Reference***
Mice	Acute Alzheimers	30 mg/kg i.p.	• Sulforaphane administered 24h prior to injection of Amyloid beta peptide • Sulforaphane treatment improved behavioural outcomes after amyloid beta injections and aided in memory retention	(Kim *et al.*, 2013)
Mice	Epileptic Seizures	5 mg/kg i.p.	• Sulforaphane adminstered 30 min before electical stimulation of the brain to simulate epileptic seizures • Epileptic seizure associated oxidatiev stress was ameliorated following sulforaphane pre-treatment • Protection afforded via the upregulation of Nrf2, and its mediated defences, HO-1 and NQO1	(Wang *et al.*, 2014)
Mice	Parkinson's Disease	5 mg/kg i.p.	• Sulforaphane adminstered twice a week for 4 weeks prior to injection of 6-ODHA to induce neuronal degeneration • Sulforaphane pre-treatment protected cells against 6-ODHA induced neuronal apoptosis via the blockade of DNA fragmentation and caspase-3-activation • Protection is afforded via upregulation of intracellular GSH, and associated enzymes GST and GR	(Morroni *et al.*, 2013)
Rats	Hypoxia-Ischaemia	5 mg/kg i.p.	• Sulforaphane was administered 30 min before HI insult • Sulforaphane pre-treatment reduced infarction volume and cell loss • Sulforaphane pre-treatment resulted in reduced presence of oxidative stress markers (MDA) and also reduced caspase-3-activity • Sulforaphane treatment reduced microglia expression	(Ping *et al.*, 2010)

Table 7.2 *in vitro* studies of sulforaphane pre-conditioning

Cell type	*Model*	*SFN Dose*	*Duration of SFN treatment*	*Findings*	*Reference*
Mouse neuroblastoma Neuro2A cells	Hydrogen peroxide cytotoxicity	2.5 µM	8 - 24h	• Sulforaphane increased expression of NQO1, GCL and proteasomal subunits in following 8 and 24h treatment • 18h sulforaphane pre-treatment increased cell viability upon challenge with hydrogen peroxide • Inhibition of proteasomal subunits attenuated sulforaphane mediated protection of neuroblastoma cells	(Kwak *et al.*, 2007)
Mouse neuroblastoma Neuro2A cells	Amyloid Beta peptide	2.5 µM	18h	• Sulforaphane pre-incubation increased cell viability when exposed to amyloid beta peptide • Inhibition of proteasomal subunits using MG132 attenuated sulforaphane mediated protection • Sulforaphane mediated protection is owed to increased expression of proteasomal subunits and NQO1 at the mRNA and protein levels	(Park *et al.*, 2009)
Mouse primary cortical neurons	5-S-cysteinyl-dopamine (CysDA) induced toxicity	0.01 - 1µM	24h	• Sulforaphane pre-treatment exhibited a dose dependent increase in cell viability when challenged with CysDA • Sulforaphane treatment increased p-ERK 1/2 and p-AKT mediated activation of Nrf2 • Peak protein expression of Nrf2 recorded after 3h sulforaphane treatment, which also corresponded to increased nuclear translocation • Protection of neuroblastoma cells is owed to increased GST expression after sulforaphane treatment	(Vauzour *et al.*, 2010)

Rat astrocytes	Exogenous superoxide challenge	10µM	Repeated treatment of 4h/day for 4 days	• Sulforaphane mediated the upregulation of multiple Nrf2 gene targets with 4h treatment • Sulforaphane mediated protein indution remained elevated for 24h • Short durations of sulforaphane stimulation resulted in prolonged induction of NQO1 over 4 days • Short durations of sulforaphane stimulation does not prolong HO-1 protein expression, observing increased mRNA and protein after 1 day but not over days 2 -4 of stimulation • Short durations of sulforaphane stimulation offered increased protection to astrocytes upon challenge with superoxide	(Bergstrom *et al.*, 2011)
Mouse primary hippocampal neurons	Hemin toxicity	0.5µM	24h	• 10µM hemin treatment post sulforaphane pre-treatment reduced neuronal cell death	(Soane *et al.*, 2010)
Rat cortical astrocytes	OGD	5µM	48h	• Sulforaphane pre-treatment significantly reduced cell death after OGD and 48h re-oxygenation	(Danilov *et al.*, 2009)

Abbreviations: CysDA, 5-S-cysteinyl-dopamine; NQO1, NADPH Quinone Oxidoreductase1; HO-1, Heme oxygenase-1; GCL, Glutamate cysteine ligase; GST, Glutathione S transferase; OGD, Oxygen glucose deprivation

Current clinical focus is to increase public awareness of the beneficial effects of sulforaphane, and thus further research should ascertain the bioavailability of sulforaphane following dietary intake different vegetables. Glucoraphanin, a precursor of sulforaphane, is found in abundance in broccoli sprouts (Fahey *et al.*, 1997), and notably varying levels of glucoraphanin have been found in different broccoli sub-types (Gasper *et al.*, 2005). Clinical trails conducted in China assessed the bioavailability of sulforaphane, from patients who either consumed sulforaphane rich beverages for 5 says, followed by glucoraphanin, and the opposite protocol (Egner *et al.*, 2011). Bioavailability of sulforaphane was greater in patients during consumption of sulforaphane rich beverages compared to gluoraphanin rich beverages, following assessment of sulforaphane excretion in urine (Egner *et al.*, 2011). Glucoraphanin is hydrolysed by the enzyme myrosinase, also found in cruciferous vegetables and is converted to sulforaphane upon mechanical breakdown or chewing (Vermeulen *et al.*, 2008). Hence, the comsumption of glucoraphanin alone will yield low levels of sulforaphane. Furthermore, the bioavailability of sulforaphane is also influenced by the method of cooking (Conaway *et al.*, 2000; Vermeulen *et al.*, 2008), as long durations of heat exposure denature myrosinase, required for the hydrolysis of glucoraphanin to sulforaphane. Saha *et al.* also report increased bioavailability of sulforaphane in fresh broccoli soup, compared to soup prepared from frozen or blanched broccoli (Saha *et al.*, 2012), thus demonstrating the importance of myrosinase in sulforaphane bioavailability. Cramer *et al.* however show an increase in sulforaphane bioavailability in healthy subjects consuming a combination of fresh broccoli and rich glucoraphanin powder (Cramer *et al.*, 2011). The phenotype of individuals also influences the bioavailability of sulforaphane, as GSTM1 positive individual showed reduced urinary excretion of sulforaphane over 6h following consumption compared to GSTM1 null subjects (Gasper *et al.*, 2005). Hence, this finding thus indicates that the bioavailability of sulforaphane is also dependent upon the composition of the gut flora, thus increasing the difficulty for researcher to define the general concentration of broccoli that should be consumed by prospective patients.

7.8 Nrf2 and cross-talk with other redox sensitive transcription factors

In this project, temporal and spatial distribution of Nrf2 in the rat brain was monitored following ischaemia and reperfusion injury. Nrf2 attained peak nuclear accumulation and protein levels 24h after the induction of reperfusion injury (Alfieri *et al.*, 2013; Srivastava *et al.*, 2013). An increase in the protein expression of the Nrf2 target enzymes HO-1, NQO1 and Prx1 24h after the induction of reperfusion injury strongly suggests that Nrf2 may attain peak levels prior to 24h (Alfieri *et al.*, 2013). However, the late induction of phase II detoxifying enzymes and antioxidant stress proteins may be due to a delayed activation of Nrf2. The delayed upregulation of antioxidant stress proteins and phase II detoxifying enzymes implies that limited

protection is available to the brain at the point of reperfusion injury, characterised further by peak generation of ROS (Peters *et al.*, 1998).

It should be noted that oxidative stress following cerebral ischaemia and reperfusion injury *in vivo* results in the activation of other redox sensitive transcription factors, and therefore cross-talk between transcription factors may influence the time course of their activation and course of action. Two other transcription factors known to be modulated by cerebral ischaemia and reperfusion injury include nuclear factor kappa B (NF-κB), which regulates the expression of pro-inflammatory processes (O'Neill & Kaltschmidt, 1997), and hypoxia inducible factor 1α (HIF-1α), responsible for the upregulation of pro-angiogenic processes following the induction of ischaemia (Semenza, 2003a).

7.8.1 NF-κB and Nrf2

NF-κB is composed of either homo or hetrodimeric complexes which consists of either a combination of p65 (RelA), c-Rel, RelB, p50 and p52 (Liu *et al.*, 2008). NF-κB can be activated by a range of stimuli, which includes viruses, cytokines and oxidative stress (Schreck *et al.*, 1992; Blackwell & Christman, 1997). Upregulation of NF-κB activity results in the increased expression of pro-inflammatory markers such as cytokines (e.g. TNFα and IL-β) and vascular adhesion molecules (ICAM1 and VCAM1) (Stephenson *et al.*, 2000). In 1997, Clemens *et al.* established a detrimental role for NF-κB in the ischaemic brain, with activation of NF-κB noted in dying neurons after transient forebrain ischaemia in rats (Clemens *et al.*, 1997). Stephenson *et al.* demonstrated increased nuclear localisation and DNA binding activity of NF-κB following 6h reperfusion in rats, subjected to 2h MCAo, however, this was abrogated in animals treated with the exogenous antioxidant compound LY341122, a potent inhibitor of lipid peroxidation (Stephenson *et al.*, 2000). There is controversy whether the actions of NF-κB are neuroprotective or detrimental following stroke. With reference to this statement, many studies have highlighted a biphasic mode of NF-κB activation following cerebral stroke, with peak activation recorded following 0 – 3h and then again at 12h after injury (Castillo *et al.*, 2003; Nijboer *et al.*, 2008; You *et al.*, 2012). The delayed secondary activation of NF-κB has been implicated in the upregulation of anti-apoptotic factors, increasing the endogenous neuroprotection afforded to the brain (Nijboer *et al.*, 2008).

In Chapter 1, we highlighted that Nrf2 deficient mice exhibit greater infarct volumes in comparison to their wild type counterparts (Zhao *et al.*, 2006; Shah *et al.*, 2007; Zhao *et al.*, 2007a). However, NF-κB deficient mice demonstrate the opposite result, with an increased cerebral infarct volume following stroke (Schneider *et al.*, 1999). In 2004, Nurmi *et al.* reproduced the findings of Schneider and colleagues, and moreover showed that

pharmacological inhibition of NF-κB with pyrrolidine dithiocarbamate ammonium salt (PDTC) yielded similar results (Nurmi *et al.*, 2004). The observed difference in cerebral damage between Nrf2 and NF-κB deficient mice strongly suggests crosstalk between these two redox sensitive transcription factors. In 2008, Liu and colleagues reported the inhibition of Nrf2-mediated responses via NF-κB p65 subunit by two distinct mechanisms in HepG2 cells: (1) depriving the interaction of Nrf2 with its co-factor CBP, a crucial requirement for Nrf2-ARE binding, and (2) promoting the recruitment and interaction of histone deacetylase (HDAC3) with either CBP or MafK and leading to local histone hypoacetylation (Liu *et al.*, 2008). However, it is interesting to note the findings of Yang *et al.* who reported a reduction in the expression of the NF-κB subunit p50 in fibroblasts derived from Nrf2 knockout animals (Yang *et al.*, 2005). Hence, although the current literature provides an indication that Nrf2 regulates its own activity via NF-κB, there is clear and convincing evidence to suggest that NF-κB may play a role in dampening down the initial or "early" activation of Nrf2. Although this project did not explore the response of NF-κB to cerebral ischaemia, the highlighted studies suggest that early induction of NF-κB activity may in part explain the observed delay in Nrf2 activation. Hence further studies are required to understand and define the crosstalk between Nrf2 and NF-κB following stroke.

7.8.2 HIF-1α and Nrf2

HIF-1α is a basic helix-loop-helix domain transcription factor, which is subjected to tight regulation under normoxic conditions. Furthermore, HIF-1α also contains the PER-ARNT-SIM (PAS) domain, required for protein dimerisation prior to DNA binding (Semenza *et al.*, 1997). HIF-1α dimerises with aryl hydrocarbon receptor (AHR) nuclear translocator protein (ARNT) to form HIF-1 in cells subjected to hypoxia. HIF-1α is targeted for degradation by the 26S proteasome post ubiquitination by an E3 ligase complex formed by the von Hipple-Lindau (VHL) tumour suppressor protein (Semenza, 2000; Metzen *et al.*, 2003). The ubiquitination of HIF-1α is dependent upon the presence of O_2, used as a substrate for the hydroxylation of proline 402 and 564 by prolyl hydroxylase (PDH), in the presence of 2-oxoglutarate, allowing for binding of VHL to HIF-1α (Semenza *et al.*, 1997). Factor inhibiting HIF-1 (FIH-1) also utilises the presence of O_2 to add a hydroxyl group to asparagine 803, present in the transactivator domain of HIF-1α, preventing binding of P300/CBP and thus limiting transcriptional activity (Semenza, 2003b). Under conditions of hypoxia, limited hydroxylation and acetylation of HIF-1α reduces its degradation by the 26s proteasome, and induces its activation. Nuclear translocation of HIF-1 induces the expression of genes, which consists of the hypoxia-responsive elemens (HRE) in the promoter sequence. HIF-1 α results in the upregulation of approximately 100 target genes, which include proteins involved in

angiogenesis, iron and glucose metabolism, apoptosis, cell survival and proliferation and vascular tone.

Bergeron *et al.* identified an increase in HIF-1α protein 16h after permanent MCAo in rats, and furthermore, increased HIF-1α mRNA was observed 6 – 7h after permanent MCAo (Bergeron *et al.*, 1999). Baranova *et al.* argued that HIF-1 is protective following 30 min MCAo and reperfusion injury in mice, however, they identified a bisphasic increase in HIF-1 protein following stroke (Baranova *et al.*, 2007). The authors report a 4-fold increase in HIF-1α protein within 1h of MCAo and a 10-fold increase 6h after MCAo. Interestingly, HIF-1α protein expression declined transiently 24h but was raised and remained elevated 2 – 10 days after MCAo and reperfusion injury (Baranova *et al.*, 2007). Notably, neuron specific knockdown of HIF-1α *in vivo* decreases neuronal cell death following MCAo and reperfusion, indicating that HIF-1 α deficiency may confer protection to the ischaemic brain (Baranova *et al.*, 2007). However, the early rise in HIF-1α protein expression may affect and hamper the observed delay in Nrf2 activation following stroke.

Malec *et al*. has proposed a pathway of cross-talk involving Nrf2 and HIF-1α, observed in adinocarcenoma A549 epithelial cells (Malec *et al.*, 2010). The intermittent model of hypoxia demonstrated increased activity of Nrf2 in response to the generation of ROS by NOX1 at re-oxygenation, resulting in an increase in the expression of thioredoxin 1 (Trx1), thus leading to the activation of increase in the activation of HIF-1 α. Malec and colleagues also demonstrated decreases in HIF-1α in response to the ablation of Nrf2 and Trx1 (Malec *et al.*, 2010). Proposed mechanisms of HIF-1α induction by Trx1 include the regulation of cysteine residues in the transactivator domain of HIF -1α mediated by Trx1. Furthermore, the increased phosphorylation of translational activators P70S6K and 4E-BPI mediated by Trx1 results in an increase in the synthesis of HIF-1α (Malec *et al.*, 2010).

With regards to endothelial cells, Laboda *et al.* reported that the activation of HIF-1α by either hypoxia, or pharmacologically using dimethyloxloylglycine (DMOG), attenuated the expression of IL-8 and HO-1 in human microvascular endothelial cells (HMEC-1) and HUVEC (Loboda *et al.*, 2009). Interestingly, similar results were observed following the overexpression of HIF-1α *in vitro* (Loboda *et al.*, 2009). Notably, these authors also demonstrated that increased HIF-1α attenuated Nrf2 mRNA and protein expression, limiting the activation of HO-1 and IL-8 (Loboda *et al.*, 2009).

Based on the reported findings of Malec *et al.* and Loboda *et al.* upon implicating crosstalk between HIF-1 and Nrf2, it seems likely that pathways of communication between these two redox sensitive transcription factors exist in the brain. Furthermore, the time course of HIF-1 expression in the ischaemic brain reported by Baranova *et al.* indicates that the delayed increase

in Nrf2 observed after stroke may in part be attributed to early increases in HIF-1 activity. Figure 7.3 illustrates the potential crosstalk that exists between different redox sensitive transcription factors and Nrf2 (Figure 7.3). However, with regards to HIF-1 and NF-κB, there is strong evidence that these transcription factors may work in tandem to delay the upregulation of antioxidant defences mediated by Nrf2, although this hypothesis remains to be validated experimentally.

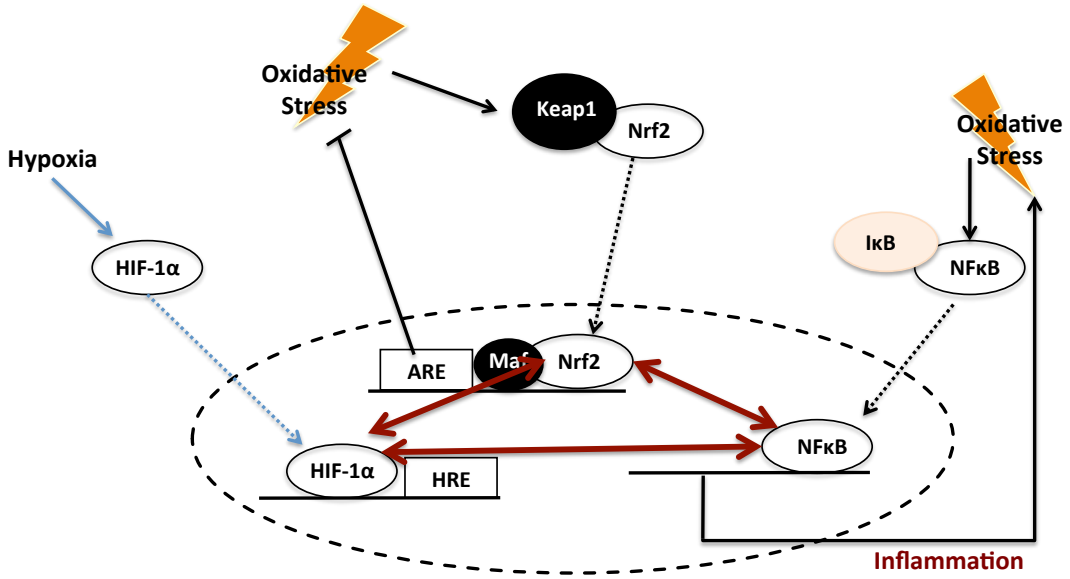

Figure 7.3 Potential cross-talk between redox-sensitive transcription factors.

7.9 Limitations of the project

Although the current study highlights novel and significant findings, experimental limitations were present in both the *in vivo* and *in vitro* studies. Firstly, this project focused on the protein expression of Nrf2 following cerebral ischaemia *in vivo* in male Sprague Dawley rats. Furthermore, this project examined whether sulforaphane pre-conditioning confers protection to the brain via Nrf2. Although pre-conditioning conferred protection to the brain following stroke, we have been unable to demonstrate that sulforaphane-mediated protection is mediated predominantly via Nrf2. Though it is possible to knockdown proteins of interest within rats *in vivo* using siRNA techniques, the cost coupled with employing such protocols were not viable during the course of this project. Furthermore, as mentioned previously, the expression of HO-1 may be driven by multiple transcription factors. Hence, the use of Nrf2 deficient animals would aid in determining whether Nrf2 predominantly regulates HO-1 protein expression.

The animals used in this study were between 3 – 4 months of age, which is representative of young adults. However, the incidence of cerebral stroke is greater in patients aged 60 and over. Hence, this factor also serves as another valid limitation of the current study. Reported studies highlight a decline in Nrf2-mediated defences with increasing age (Ungvari *et al.*, 2011; Valcarcel-Ares *et al.*, 2012; Rahman *et al.*, 2013; Sachdeva *et al.*, 2014).

Studies have demonstrated (1) decreased GSH levels and Nrf2 activity (Suh *et al.*, 2004), and (2) declining levels of Nrf2 nuclear accumulation and ARE binding in the liver of aged rats (Shenvi *et al.*, 2012), as well as dysfunction of Nrf2-mediated signalling in skeletal muscle with increase age (Miller *et al.*, 2012). With particular reference to the brain, increased incidence of Parkinson's and Alzheimer's disease is observed with increasing age. Notably, studies have highlighted increased ROS in the ageing brain associated to these diseases (Kumar *et al.*, 2012), and identified a significant decline in Nrf2 and its mediated antioxidant proteins in the aged brain (L'Episcopo *et al.*, 2013). Our current experimental design did not take into consideration the effects of ageing on stroke, and hence further experiments are required to determine whether the data are applicable to stroke in aged patients.

The identification of proteins in *ex vivo* brain sections was largely dependent upon the use of polyclonal antibodies. Although polyclonal antibodies are relatively inexpensive and commercially available, their ability to identify multiple epitopes on any one antigen and the lack specificity of antibodies limits the technique. Though the images presented in this thesis for HO-1, NQO1, Prx1 and Nrf2 show differential staining patterns, the specificities of these antibodies towards their targets were not validated due to the absence of tissue from respective knockout animals. However, this difference in staining patterns suugest that each antibody recognised different antigens of interest.

In Chapter 6, *in vitro* experiments were conducted using a mouse derived brain endothelial cell line, bEnd.3. The loss of paracrine interactions within an *in vitro* model of the BBB serves as a limitation, as other cell types involved in the neurovascular unit also influence the function of the cerebral endothelium. Furthermore, cerebral cell lines do not achieve the same levels of TEER or "tightness" as primary brain endothelial cells, hence the use of the bEnd.3 cell line also serves as a limitation for an *in vitro* model of the BBB.

7.10 Conclusion

The present studies revealed a significant delay (of up to 24h) in attaining peak protein expression of Nrf2 following MCAo and reperfusion injury in rats. Pre-treatment of rats with sulforaphane prior to MCAo and reperfusion injury attenuated latter increases in Nrf2 protein expression, improved neurological outcome after stroke. In the brain endothelium *in vitro*,

sulforaphane mediates an increase in HO-1 and NQO1 protein via the Nrf2 defence pathway. Moreover, sulforaphane pre-treatment of brain endothelial cells prior to OGD, an *in vitro* model of cerebral ischaemia, significantly attenuated cerebral endothelial cell death. These findings suggest that the Nrf2 defence pathway plays a key role in protecting the brain against ischaemia-reperfusion injury induced oxidative stress, and implicates Nrf2 as an important endogenous therapeutic target. Furthermore, pre-conditioning of Nrf2 by sulforaphane increased the antioxidant capacity of the brain, conferring protection to the vascular endothelium and brain parenchyma. Hence, pre-conditioning of the Nrf2 defence pathway with sulforaphane provides a potential therapeutic strategy to protect the brain from ischaemia-reperfusion injury induced damage in stroke.

7.11 Future studies

7.11.1 Future studies – in vivo

Although we provide the first quantitative measurements of the temporal and spatial distribution of Nrf2 in the naïve and sulforaphane pre-treated ischaemic rat brain, further experiments are required to determine the importance of Nrf2 in pre-conditioning. However, using our current model of *in vivo* experimental stroke will not allow us to determine the importance of Nrf2 conferring protection following sulforaphane preconditioning. Hence, the use of mice will allow greater access to Nrf2 deficient animals, which will then be used to determine whether sulforaphane pre-conditioning confers protection to Nrf2-deficient animals and their wild-type counterparts. Furthermore, Nrf2-deficient animals will also allow us to determine whether sulforaphane mediates the expression of HO-1, NQO1 and Prx1 via Nrf2, or other redox sensitive transcription factors. Furthermore, in this present study an increase in the protein expression of HO-1 and NQO1 in the rat brain was observed following ischaemia and reperfusion injury and sulforaphane treatment. However, increases in protein expression are not indicative of increase enzyme activity. Using activity assays for NQO1 and HO-1 it would be possible to assay enzyme activity of given enzymes in ischaemic and sulforaphane treated brains.

Our current *ex vivo* analysis has only focused on the protein expression of Nrf2 and its mediated protein targets. However, the effects of ischaemia-reperfusion injury, or sulforaphane pre-treatment on mRNA levels are yet to be determined. mRNA expression may be determined following the employment of *in situ* hybridisation protocols on *ex vivo* brain sections, or following RNA extraction from tissue, and quantified by RT-qRT-PCR.

Oxidative stress plays a major role in the pathophysiology of stroke and ROS may be generated from xanthine oxidase, mitochondria, NADPH oxidase and NOS. However the major source of

ROS following ischaemia and reperfusion injury remains to by elucidated. The use of pharmacological inhibitors may be used to determine the major source of ROS in the ischeamic brain. ROS generation may then be assessed using imaging techniques (Hyun *et al.*, 2013), electron spin resonance (ESR) (Lee, 2013), or by luminescence. Determining the source of ROS will aid in the design of therapeutic drugs that may be administered during ischaemia to limit oxidative stress upon reperfusion injury.

Current stroke research has focused on modulating Nrf2 in protection of astrocytes and neurons following cerebral ischaemia and reperfusion injury, however, our *in vitro* model of the BBB using bEnd.3 cells revealed that sulforaphane modulates expression of HO-1 and NQO1 via Nrf2. Hence, to further investigate the importance of Nrf2 linked defences activated by sulforaphane in the BBB endothelium, the effects of MCAo and reperfusion injury in endothelial specific Nrf2 deficient mice could be studied.

This project, focused on profiling the time of Nrf2 protein expression following ischaemia and reperfusion injury. As mentioned previously upregulation of Nrf2 following cerebral ischaemia and reperfusion injury occurs with a dealy of approximately 24h. Studies have shown a rapid induction in HIF-1 and NF-κB protein expression after ischaemia and reperfusion injury. Hence, to understand whether Nrf2 expression in regulated by other redox sensitive transcription, we propose to examine the expression of Nrf2 in HIF-1 and NF-κB deficient mice.

Nrf2 protein expression is regulated by is cytosolic repressor, Keap1, or Bach1. Limited information is available regarding the modulation of Keap1 and Bach1 protein in the ischaemic brain. Along with the reported increases in other redox-sensitive transcription factors that may affect the time-course of Nrf2 activation, it is possible that Keap1 and Bach1 may also influence Nrf2 protein expression. Hence it is important to examine the effects of ischaemia-reperfusion injury and sulforaphane treatment on mRNA and protein expression of these proteins in the rat brain.

A high incidence of cerebral stroke is observed in patients aged 60 or greater, however, this project and other studies have reported findings using animals similar in age with young human adults. Aging has been reported to affect the Nrf2-defence pathway, hence to further understand the role of aging in ischaemia-reperfusion injury, it is necessary to conduct experimental stroke in aged animals.

7.11.2 Future studies – in vitro

To compliment our *in vivo* studies and to further understand the molecular mechanism involved in protection of the BBB endothelium, further experiments *in vitro* experiments are also

required In this project, we illustrated that bEnd.3 cells cultured under 5% oxygen show increased cell death within 2h of OGD. Although cell death following ischaemia occurs within minutes, *in vitro* models show increased cell death after a minimum of 6h OGD. Hence, to produce and conduct *in vitro* experiments of relevance to *in vivo* models of stroke should examine cell death after 0 – 2h OGD in endothelial cells cultured under physiological oxygen tensions. *In vitro* models of stroke largely involve the study of a single cerebral cell type at any one time. Hence, to re-introduced paracrine interactions present *in vivo*, it would be important to establish a co-culture model of the neurovascular unit *in vitro* under physiological oxygen.

7.11.3 Investigating other sulforaphane mediated pathways

This project has not focused on the pathway of activation of Nrf2 following sulforaphane treatment both *in vivo* and *in vitro.* There is evidence to suggest that sulforaphane may activate Nrf2 via specific kinase pathways (Manandhar *et al.*, 2007; Leoncini *et al.*, 2011; Deng *et al.*, 2012; Lee *et al.*, 2012), hence future work will aim to elucidate the pathways of sulforaphane mediated Nrf2 activation in the brain and the cerebrovascular endothelium.

Chapter 8 – References

Chapter 8 - References

Abbott NJ, Patabendige AA, Dolman DE, Yusof SR & Begley DJ. (2010). Structure and function of the blood-brain barrier. *Neurobiol Dis* **37,** 13-25.

Abbott NJ, Ronnback L & Hansson E. (2006). Astrocyte-endothelial interactions at the blood-brain barrier. *Nat Rev Neurosci* **7,** 41-53.

Abramov AY, Scorziello A & Duchen MR. (2007). Three distinct mechanisms generate oxygen free radicals in neurons and contribute to cell death during anoxia and reoxygenation. *J Neurosci* **27,** 1129-1138.

Adams JC. (1992). Biotin amplification of biotin and horseradish peroxidase signals in histochemical stains. *J Histochem Cytochem* **40,** 1457-1463.

Agarwal R & Shukla GS. (1999). Potential role of cerebral glutathione in the maintenance of blood-brain barrier integrity in rat. *Neurochem Res* **24,** 1507-1514.

Agus DB, Gambhir SS, Pardridge WM, Spielholz C, Baselga J, Vera JC & Golde DW. (1997). Vitamin C crosses the blood-brain barrier in the oxidized form through the glucose transporters. *J Clin Invest* **100,** 2842-2848.

Agyeman AS, Chaerkady R, Shaw PG, Davidson NE, Visvanathan K, Pandey A & Kensler TW. (2012). Transcriptomic and proteomic profiling of KEAP1 disrupted and sulforaphane-treated human breast epithelial cells reveals common expression profiles. *Breast Cancer Res Treat* **132,** 175-187.

Akdemir H, Asik Z, Pasaoglu H, Karakucuk I, Oktem IS & Koc RK. (2001). The effect of allopurinol on focal cerebral ischaemia: an experimental study in rabbits. *Neurosurg Rev* **24,** 131-135.

Al Ahmad A, Gassmann M & Ogunshola OO. (2012). Involvement of oxidative stress in hypoxia-induced blood-brain barrier breakdown. *Microvasc Res* **84,** 222-225.

Alam J, Stewart D, Touchard C, Boinapally S, Choi AM & Cook JL. (1999). Nrf2, a Cap'n'Collar transcription factor, regulates induction of the heme oxygenase-1 gene. *J Biol Chem* **274,** 26071-26078.

Albers GW, Goldstein LB, Hess DC, Wechsler LR, Furie KL, Gorelick PB, Hurn P, Liebeskind DS, Nogueira RG, Saver JL & Consortium SV. (2011). Stroke Treatment Academic Industry Roundtable (STAIR) recommendations for maximizing the use of intravenous thrombolytics and expanding treatment options with intra-arterial and neuroprotective therapies. *Stroke* **42,** 2645-2650.

Alfieri A, Srivastava S, Siow RC, Cash D, Modo M, Duchen MR, Fraser PA, Williams SC & Mann GE. (2013). Sulforaphane preconditioning of the Nrf2/HO-1 defense pathway

protects the cerebral vasculature against blood-brain barrier disruption and neurological deficits in stroke. *Free Radic Biol Med* **65C,** 1012-1022.

Alfieri A, Srivastava S, Siow RC, Modo M, Fraser PA & Mann GE. (2011). Targeting the Nrf2-Keap1 antioxidant defence pathway for neurovascular protection in stroke. *J Physiol* **589,** 4125-4136.

Allen CL & Bayraktutan U. (2009). Oxidative stress and its role in the pathogenesis of ischaemic stroke. *Int J Stroke* **4,** 461-470.

Almeida A, Delgado-Esteban M, Bolanos JP & Medina JM. (2002). Oxygen and glucose deprivation induces mitochondrial dysfunction and oxidative stress in neurones but not in astrocytes in primary culture. *J Neurochem* **81,** 207-217.

Amarenco P. (2001). Hypercholesterolemia, lipid-lowering agents, and the risk for brain infarction. *Neurology* **57,** S35-44.

Amarenco P, Labreuche J, Lavallee P & Touboul PJ. (2004a). Statins in stroke prevention and carotid atherosclerosis: systematic review and up-to-date meta-analysis. *Stroke* **35,** 2902-2909.

Amarenco P, Lavallee P & Touboul PJ. (2004b). Statins and stroke prevention. *Cerebrovasc Dis* **17 Suppl 1,** 81-88.

Anderson MF, Nilsson M, Eriksson PS & Sims NR. (2004). Glutathione monoethyl ester provides neuroprotection in a rat model of stroke. *Neurosci Lett* **354,** 163-165.

Andjelkovic AV, Stamatovic SM & Keep RF. (2003). The protective effects of preconditioning on cerebral endothelial cells in vitro. *J Cereb Blood Flow Metab* **23,** 1348-1355.

Aoyama K, Watabe M & Nakaki T. (2008). Regulation of neuronal glutathione synthesis. *J Pharmacol Sci* **108,** 227-238.

Appleton SD, Lash GE, Marks GS, Nakatsu K, Brien JF, Smith GN & Graham CH. (2003). Effect of glucose and oxygen deprivation on heme oxygenase expression in human chorionic villi explants and immortalized trophoblast cells. *Am J Physiol Regul Integr Comp Physiol* **285,** R1453-1460.

Aronowski J, Strong R & Grotta JC. (1997). Reperfusion injury: demonstration of brain damage produced by reperfusion after transient focal ischemia in rats. *J Cereb Blood Flow Metab* **17,** 1048-1056.

Arthur FE, Shivers RR & Bowman PD. (1987). Astrocyte-mediated induction of tight junctions in brain capillary endothelium: an efficient in vitro model. *Brain Res* **433,** 155-159.

Astrup J, Siesjo BK & Symon L. (1981). Thresholds in cerebral ischemia - the ischemic penumbra. *Stroke* **12,** 723-725.

Attwell D & Laughlin SB. (2001). An energy budget for signaling in the grey matter of the brain. *J Cereb Blood Flow Metab* **21,** 1133-1145.

Backos DS, Franklin CC & Reigan P. (2012). The role of glutathione in brain tumor drug resistance. *Biochem Pharmacol* **83,** 1005-1012.

Bandera E, Botteri M, Minelli C, Sutton A, Abrams KR & Latronico N. (2006). Cerebral blood flow threshold of ischemic penumbra and infarct core in acute ischemic stroke: a systematic review. *Stroke* **37,** 1334-1339.

Bannai S & Tateishi N. (1986). Role of membrane transport in metabolism and function of glutathione in mammals. *J Membr Biol* **89,** 1-8.

Baranova O, Miranda LF, Pichiule P, Dragatsis I, Johnson RS & Chavez JC. (2007). Neuron-specific inactivation of the hypoxia inducible factor 1 alpha increases brain injury in a mouse model of transient focal cerebral ischemia. *J Neurosci* **27,** 6320-6332.

Barone FC, White RF, Spera PA, Ellison J, Currie RW, Wang X & Feuerstein GZ. (1998). Ischemic preconditioning and brain tolerance: temporal histological and functional outcomes, protein synthesis requirement, and interleukin-1 receptor antagonist and early gene expression. *Stroke* **29,** 1937-1950; discussion 1950-1931.

Basten GP, Bao Y & Williamson G. (2002). Sulforaphane and its glutathione conjugate but not sulforaphane nitrile induce UDP-glucuronosyl transferase (UGT1A1) and glutathione transferase (GSTA1) in cultured cells. *Carcinogenesis* **23,** 1399-1404.

Basuroy S, Bhattacharya S, Leffler CW & Parfenova H. (2009). Nox4 NADPH oxidase mediates oxidative stress and apoptosis caused by TNF-alpha in cerebral vascular endothelial cells. *Am J Physiol Cell Physiol* **296,** C422-432.

Basuroy S, Bhattacharya S, Tcheranova D, Qu Y, Regan RF, Leffler CW & Parfenova H. (2006). HO-2 provides endogenous protection against oxidative stress and apoptosis caused by TNF-alpha in cerebral vascular endothelial cells. *Am J Physiol Cell Physiol* **291,** C897-908.

Beetsch JW, Park TS, Dugan LL, Shah AR & Gidday JM. (1998). Xanthine oxidase-derived superoxide causes reoxygenation injury of ischemic cerebral endothelial cells. *Brain Res* **786,** 89-95.

Behrens MM, Ali SS, Dao DN, Lucero J, Shekhtman G, Quick KL & Dugan LL. (2007). Ketamine-induced loss of phenotype of fast-spiking interneurons is mediated by NADPH-oxidase. *Science* **318,** 1645-1647.

Bell KF, Fowler JH, Al-Mubarak B, Horsburgh K & Hardingham GE. (2011). Activation of Nrf2-regulated glutathione pathway genes by ischemic preconditioning. *Oxid Med Cell Longev* **2011,** 689524.

Benavides A, Pastor D, Santos P, Tranque P & Calvo S. (2005). CHOP plays a pivotal role in the astrocyte death induced by oxygen and glucose deprivation. *Glia* **52,** 261-275.

Bergeron M, Yu AY, Solway KE, Semenza GL & Sharp FR. (1999). Induction of hypoxia-inducible factor-1 (HIF-1) and its target genes following focal ischaemia in rat brain. *Eur J Neurosci* **11,** 4159-4170.

Bergers G & Song S. (2005). The role of pericytes in blood-vessel formation and maintenance. *Neuro Oncol* **7,** 452-464.

Bergstrom P, Andersson HC, Gao Y, Karlsson JO, Nodin C, Anderson MF, Nilsson M & Hammarsten O. (2011). Repeated transient sulforaphane stimulation in astrocytes leads to prolonged Nrf2-mediated gene expression and protection from superoxide-induced damage. *Neuropharmacology* **60,** 343-353.

Bersano A, Ballabio E, Lanfranconi S, Mazzucco S, Candelise L & Monaco S. (2008). Statins and stroke. *Curr Med Chem* **15,** 2380-2392.

Betz AL. (1985). Identification of hypoxanthine transport and xanthine oxidase activity in brain capillaries. *J Neurochem* **44,** 574-579.

Betz AL. (1986). Transport of ions across the blood-brain barrier. *Fed Proc* **45,** 2050-2054.

Bhattacharjee P, Paul S, Banerjee M, Patra D, Banerjee P, Ghoshal N, Bandyopadhyay A & Giri AK. (2013). Functional compensation of glutathione S-transferase M1 (GSTM1) null by another GST superfamily member, GSTM2. *Sci Rep* **3,** 2704.

Blackwell TS & Christman JW. (1997). The role of nuclear factor-kappa B in cytokine gene regulation. *American journal of respiratory cell and molecular biology* **17,** 3-9.

Boado RJ, Li JY, Nagaya M, Zhang C & Pardridge WM. (1999). Selective expression of the large neutral amino acid transporter at the blood-brain barrier. *Proc Natl Acad Sci U S A* **96,** 12079-12084.

Botelho GG, Bufalo AC, Boareto AC, Muller JC, Morais RN, Martino-Andrade AJ, Lemos KR & Dalsenter PR. (2009). Vitamin C and resveratrol supplementation to rat dams treated with di(2-ethylhexyl)phthalate: impact on reproductive and oxidative stress end points in male offspring. *Arch Environ Contam Toxicol* **57,** 785-793.

Bradbury MW. (1993). The blood-brain barrier. *Exp Physiol* **78,** 453-472.

Bradbury MW & Deane R. (1993). Permeability of the blood-brain barrier to lead. *Neurotoxicology* **14,** 131-136.

Bragin DE, Zhou B, Ramamoorthy P, Muller WS, Connor JA & Shi H. (2010). Differential changes of glutathione levels in astrocytes and neurons in ischemic brains by two-photon imaging. *J Cereb Blood Flow Metab* **30,** 734-738.

Brahmachari S, Fung YK & Pahan K. (2006). Induction of glial fibrillary acidic protein expression in astrocytes by nitric oxide. *J Neurosci* **26,** 4930-4939.

Bramlett HM & Dietrich WD. (2004). Pathophysiology of cerebral ischemia and brain trauma: similarities and differences. *J Cereb Blood Flow Metab* **24,** 133-150.

Brathwaite S & Macdonald RL. (2013). Current Management of Delayed Cerebral Ischemia: Update from Results of Recent Clinical Trials. *Transl Stroke Res*.

Bulbarelli A, Lonati E, Brambilla A, Orlando A, Cazzaniga E, Piazza F, Ferrarese C, Masserini M & Sancini G. (2012). Abeta42 production in brain capillary endothelial cells after oxygen and glucose deprivation. *Mol Cell Neurosci* **49,** 415-422.

Bustin SA, Benes V, Garson JA, Hellemans J, Huggett J, Kubista M, Mueller R, Nolan T, Pfaffl MW, Shipley GL, Vandesompele J & Wittwer CT. (2009). The MIQE guidelines: minimum information for publication of quantitative real-time PCR experiments. *Clin Chem* **55,** 611-622.

Candelario-Jalil E. (2009). Injury and repair mechanisms in ischemic stroke: considerations for the development of novel neurotherapeutics. *Curr Opin Investig Drugs* **10,** 644-654.

Castillo J, Moro MA, Blanco M, Leira R, Serena J, Lizasoain I & Davalos A. (2003). The release of tumor necrosis factor-alpha is associated with ischemic tolerance in human stroke. *Ann Neurol* **54,** 811-819.

Chakravarthi S, Jessop CE & Bulleid NJ. (2006). The role of glutathione in disulphide bond formation and endoplasmic-reticulum-generated oxidative stress. *EMBO Rep* **7,** 271-275.

Chan SL & Baumbach GL. (2013). Nox2 deficiency prevents hypertension-induced vascular dysfunction and hypertrophy in cerebral arterioles. *Int J Hypertens* **2013,** 793630.

Chang EF, Wong RJ, Vreman HJ, Igarashi T, Galo E, Sharp FR, Stevenson DK & Noble-Haeusslein LJ. (2003). Heme oxygenase-2 protects against lipid peroxidation-mediated cell loss and impaired motor recovery after traumatic brain injury. *J Neurosci* **23,** 3689-3696.

Chang SH, Barbosa-Tessmann I, Chen C, Kilberg MS & Agarwal A. (2002). Glucose deprivation induces heme oxygenase-1 gene expression by a pathway independent of the unfolded protein response. *J Biol Chem* **277,** 1933-1940.

Chapple SJ, Siow RC & Mann GE. (2012). Crosstalk between Nrf2 and the proteasome: therapeutic potential of Nrf2 inducers in vascular disease and aging. *Int J Biochem Cell Biol* **44,** 1315-1320.

Charoensuk L, Pinlaor P, Prakobwong S, Hiraku Y, Laothong U, Ruangjirachuporn W, Yongvanit P & Pinlaor S. (2011). Curcumin induces a nuclear factor-erythroid 2-related factor 2-driven response against oxidative and nitrative stress after praziquantel treatment in liver fluke-infected hamsters. *Int J Parasitol* **41,** 615-626.

Chaturvedi RK & Flint Beal M. (2013). Mitochondrial diseases of the brain. *Free Radic Biol Med* **63,** 1-29.

Chen H, Yoshioka H, Kim GS, Jung JE, Okami N, Sakata H, Maier CM, Narasimhan P, Goeders CE & Chan PH. (2011). Oxidative stress in ischemic brain damage: mechanisms of cell death and potential molecular targets for neuroprotection. *Antioxid Redox Signal* **14,** 1505-1517.

Chen L, Wang L, Zhang X, Cui L, Xing Y, Dong L, Liu Z, Li Y, Zhang X, Wang C, Bai X, Zhang J, Zhang L & Zhao X. (2012). The protection by octreotide against experimental ischemic stroke: up-regulated transcription factor Nrf2, HO-1 and down-regulated NF-kappaB expression. *Brain Res* **1475,** 80-87.

Chen S, Wu K & Knox R. (2000). Structure-function studies of DT-diaphorase (NQO1) and NRH: quinone oxidoreductase (NQO2). *Free Radic Biol Med* **29,** 276-284.

Chen Z, Siu B, Ho YS, Vincent R, Chua CC, Hamdy RC & Chua BH. (1998). Overexpression of MnSOD protects against myocardial ischemia/reperfusion injury in transgenic mice. *J Mol Cell Cardiol* **30,** 2281-2289.

Cheng X, Ku CH & Siow RC. (2013). Regulation of the Nrf2 antioxidant pathway by microRNAs: New players in micromanaging redox homeostasis. *Free Radic Biol Med*.

Cheng X, Siow RC & Mann GE. (2011). Impaired redox signaling and antioxidant gene expression in endothelial cells in diabetes: a role for mitochondria and the nuclear factor-E2-related factor 2-Kelch-like ECH-associated protein 1 defense pathway. *Antioxid Redox Signal* **14,** 469-487.

Chew EH, Nagle AA, Zhang Y, Scarmagnani S, Palaniappan P, Bradshaw TD, Holmgren A & Westwell AD. (2010). Cinnamaldehydes inhibit thioredoxin reductase and induce Nrf2: potential candidates for cancer therapy and chemoprevention. *Free Radic Biol Med* **48,** 98-111.

Cho HY, Jedlicka AE, Reddy SP, Kensler TW, Yamamoto M, Zhang LY & Kleeberger SR. (2002). Role of NRF2 in protection against hyperoxic lung injury in mice. *Am J Respir Cell Mol Biol* **26,** 175-182.

Choi DH, Cristovao AC, Guhathakurta S, Lee J, Joh TH, Beal MF & Kim YS. (2012). NADPH oxidase 1-mediated oxidative stress leads to dopamine neuron death in Parkinson's disease. *Antioxid Redox Signal* **16,** 1033-1045.

Chowdhry S, Zhang Y, McMahon M, Sutherland C, Cuadrado A & Hayes JD. (2013). Nrf2 is controlled by two distinct beta-TrCP recognition motifs in its Neh6 domain, one of which can be modulated by GSK-3 activity. *Oncogene* **32,** 3765-3781.

Chowdhury I, Mo Y, Gao L, Kazi A, Fisher AB & Feinstein SI. (2009). Oxidant stress stimulates expression of the human peroxiredoxin 6 gene by a transcriptional mechanism involving an antioxidant response element. *Free Radic Biol Med* **46,** 146-153.

Christophe M & Nicolas S. (2006). Mitochondria: a target for neuroprotective interventions in cerebral ischemia-reperfusion. *Curr Pharm Des* **12,** 739-757.

Clark D, Tuor UI, Thompson R, Institoris A, Kulynych A, Zhang X, Kinniburgh DW, Bari F, Busija DW & Barber PA. (2012). Protection against recurrent stroke with resveratrol: endothelial protection. *PLoS One* **7,** e47792.

Clarke JD, Hsu A, Williams DE, Dashwood RH, Stevens JF, Yamamoto M & Ho E. (2011). Metabolism and tissue distribution of sulforaphane in Nrf2 knockout and wild-type mice. *Pharm Res* **28,** 3171-3179.

Clarkson AN, Clarkson J, Jackson DM & Sammut IA. (2007). Mitochondrial involvement in transhemispheric diaschisis following hypoxia-ischemia: Clomethiazole-mediated amelioration. *Neuroscience* **144,** 547-561.

Clemens JA, Stephenson DT, Smalstig EB, Dixon EP & Little SP. (1997). Global ischemia activates nuclear factor-kappa B in forebrain neurons of rats. *Stroke* **28,** 1073-1080; discussion 1080-1071.

Conaway CC, Getahun SM, Liebes LL, Pusateri DJ, Topham DK, Botero-Omary M & Chung FL. (2000). Disposition of glucosinolates and sulforaphane in humans after ingestion of steamed and fresh broccoli. *Nutr Cancer* **38,** 168-178.

Conaway CC, Yang YM & Chung FL. (2002). Isothiocyanates as cancer chemopreventive agents: their biological activities and metabolism in rodents and humans. *Curr Drug Metab* **3,** 233-255.

Coons AH & Kaplan MH. (1950). Localization of antigen in tissue cells; improvements in a method for the detection of antigen by means of fluorescent antibody. *J Exp Med* **91,** 1-13.

Cordon-Cardo C, O'Brien JP, Casals D, Rittman-Grauer L, Biedler JL, Melamed MR & Bertino JR. (1989). Multidrug-resistance gene (P-glycoprotein) is expressed by endothelial cells at blood-brain barrier sites. *Proc Natl Acad Sci U S A* **86,** 695-698.

Coyoy A, Valencia A, Guemez-Gamboa A & Moran J. (2008). Role of NADPH oxidase in the apoptotic death of cultured cerebellar granule neurons. *Free Radic Biol Med* **45,** 1056-1064.

Cramer JM, Teran-Garcia M & Jeffery EH. (2011). Enhancing sulforaphane absorption and excretion in healthy men through the combined consumption of fresh broccoli sprouts and a glucoraphanin-rich powder. *The British journal of nutrition***,** 1-6.

Cui W, Bai Y, Miao X, Luo P, Chen Q, Tan Y, Rane MJ, Miao L & Cai L. (2012). Prevention of diabetic nephropathy by sulforaphane: possible role of Nrf2 upregulation and activation. *Oxid Med Cell Longev* **2012,** 821936.

Dai G, Vaughn S, Zhang Y, Wang ET, Garcia-Cardena G & Gimbrone MA, Jr. (2007). Biomechanical forces in atherosclerosis-resistant vascular regions regulate endothelial redox balance via phosphoinositol 3-kinase/Akt-dependent activation of Nrf2. *Circ Res* **101,** 723-733.

Damiano S, Fusco R, Morano A, De Mizio M, Paterno R, De Rosa A, Spinelli R, Amente S, Frunzio R, Mondola P, Miot F, Laccetti P, Santillo M & Avvedimento EV. (2012). Reactive oxygen species regulate the levels of dual oxidase (Duox1-2) in human neuroblastoma cells. *PLoS One* **7,** e34405.

Dang J, Brandenburg LO, Rosen C, Fragoulis A, Kipp M, Pufe T, Beyer C & Wruck CJ. (2012). Nrf2 expression by neurons, astroglia, and microglia in the cerebral cortical penumbra of ischemic rats. *J Mol Neurosci* **46,** 578-584.

Danilov CA, Chandrasekaran K, Racz J, Soane L, Zielke C & Fiskum G. (2009). Sulforaphane protects astrocytes against oxidative stress and delayed death caused by oxygen and glucose deprivation. *Glia* **57,** 645-656.

Dawson J, Lees JS, Chang TP, Walters MR, Ali M, Davis SM, Diener HC, Lees KR, Gain & Investigators V. (2007). Association between disability measures and healthcare costs after initial treatment for acute stroke. *Stroke* **38,** 1893-1898.

Dayer R, Fischer BB, Eggen RI & Lemaire SD. (2008). The peroxiredoxin and glutathione peroxidase families in Chlamydomonas reinhardtii. *Genetics* **179,** 41-57.

Dayon L, Turck N, Garci-Berrocoso T, Walter N, Burkhard PR, Vilalta A, Sahuquillo J, Montaner J & Sanchez JC. (2011). Brain extracellular fluid protein changes in acute stroke patients. *J Proteome Res* **10,** 1043-1051.

del Zoppo GJ. (2010). The neurovascular unit in the setting of stroke. *J Intern Med* **267,** 156-171.

del Zoppo GJ, Poeck K, Pessin MS, Wolpert SM, Furlan AJ, Ferbert A, Alberts MJ, Zivin JA, Wechsler L, Busse O & et al. (1992). Recombinant tissue plasminogen activator in acute thrombotic and embolic stroke. *Ann Neurol* **32,** 78-86.

Deng C, Tao R, Yu SZ & Jin H. (2012). Sulforaphane protects against 6-hydroxydopamine-induced cytotoxicity by increasing expression of heme oxygenase-1 in a PI3K/Akt-dependent manner. *Mol Med Rep* **5,** 847-851.

Di Piero V, Chollet F, Dolan RJ, Thomas DJ & Frackowiak R. (1990). The functional nature of cerebellar diaschisis. *Stroke* **21,** 1365-1369.

Dinkova-Kostova AT, Fahey JW, Wade KL, Jenkins SN, Shapiro TA, Fuchs EJ, Kerns ML & Talalay P. (2007). Induction of the phase 2 response in mouse and human skin by sulforaphane-containing broccoli sprout extracts. *Cancer Epidemiol Biomarkers Prev* **16,** 847-851.

Dinkova-Kostova AT, Holtzclaw WD, Cole RN, Itoh K, Wakabayashi N, Katoh Y, Yamamoto M & Talalay P. (2002). Direct evidence that sulfhydryl groups of Keap1 are the sensors regulating induction of phase 2 enzymes that protect against carcinogens and oxidants. *Proc Natl Acad Sci U S A* **99,** 11908-11913.

Dinkova-Kostova AT & Kostov RV. (2012). Glucosinolates and isothiocyanates in health and disease. *Trends Mol Med* **18,** 337-347.

Dirnagl U. (2012). Pathobiology of injury after stroke: the neurovascular unit and beyond. *Ann N Y Acad Sci* **1268,** 21-25.

Dirnagl U, Iadecola C & Moskowitz MA. (1999). Pathobiology of ischaemic stroke: an integrated view. *Trends Neurosci* **22,** 391-397.

Dirnagl U, Simon RP & Hallenbeck JM. (2003). Ischemic tolerance and endogenous neuroprotection. *Trends Neurosci* **26,** 248-254.

Dohi Y, Alam J, Yoshizumi M, Sun J & Igarashi K. (2006). Heme oxygenase-1 gene enhancer manifests silencing activity in a chromatin environment prior to oxidative stress. *Antioxid Redox Signal* **8,** 60-67.

Donnan GA, Fisher M, Macleod M & Davis SM. (2008). Stroke. *Lancet* **371,** 1612-1623.

Dringen R. (2000). Metabolism and functions of glutathione in brain. *Prog Neurobiol* **62,** 649-671.

Duelli R & Kuschinsky W. (2001). Brain glucose transporters: relationship to local energy demand. *News Physiol Sci* **16,** 71-76.

Dykxhoorn DM, Novina CD & Sharp PA. (2003). Killing the messenger: short RNAs that silence gene expression. *Nat Rev Mol Cell Biol* **4,** 457-467.

Egner PA, Chen JG, Wang JB, Wu Y, Sun Y, Lu JH, Zhu J, Zhang YH, Chen YS, Friesen MD, Jacobson LP, Munoz A, Ng D, Qian GS, Zhu YR, Chen TY, Botting NP, Zhang Q, Fahey JW, Talalay P, Groopman JD & Kensler TW. (2011). Bioavailability of Sulforaphane from two broccoli sprout beverages: results of a short-term, cross-over clinical trial in Qidong, China. *Cancer prevention research* **4,** 384-395.

Endres M & Dirnagl U. (2002). Ischemia and stroke. *Adv Exp Med Biol* **513,** 455-473.

Endres M, Engelhardt B, Koistinaho J, Lindvall O, Meairs S, Mohr JP, Planas A, Rothwell N, Schwaninger M, Schwab ME, Vivien D, Wieloch T & Dirnagl U. (2008). Improving outcome after stroke: overcoming the translational roadblock. *Cerebrovasc Dis* **25,** 268-278.

Ernst IM, Wagner AE, Schuemann C, Storm N, Hoppner W, Doring F, Stocker A & Rimbach G. (2011). Allyl-, butyl- and phenylethyl-isothiocyanate activate Nrf2 in cultured fibroblasts. *Pharmacol Res* **63,** 233-240.

Erttmann SF, Bast A, Seidel J, Breitbach K, Walther R & Steinmetz I. (2011). PGD2 and PGE2 regulate gene expression of Prx 6 in primary macrophages via Nrf2. *Free Radic Biol Med* **51,** 626-640.

Fahey JW, Zhang Y & Talalay P. (1997). Broccoli sprouts: an exceptionally rich source of inducers of enzymes that protect against chemical carcinogens. *Proc Natl Acad Sci U S A* **94,** 10367-10372.

Feeney DM & Baron JC. (1986). Diaschisis. *Stroke* **17,** 817-830.

Ferrando-Miguel R, Cheon MS, Yang JW & Lubec G. (2003). Overexpression of transcription factor BACH1 in fetal Down syndrome brain. *J Neural Transm Suppl***,** 193-205.

Ferris CD, Jaffrey SR, Sawa A, Takahashi M, Brady SD, Barrow RK, Tysoe SA, Wolosker H, Baranano DE, Dore S, Poss KD & Snyder SH. (1999). Haem oxygenase-1 prevents cell death by regulating cellular iron. *Nat Cell Biol* **1,** 152-157.

Forstermann U. (2008). Oxidative stress in vascular disease: causes, defense mechanisms and potential therapies. *Nat Clin Pract Cardiovasc Med* **5,** 338-349.

Fraser PA. (2011). The role of free radical generation in increasing cerebrovascular permeability. *Free Radic Biol Med* **51,** 967-977.

Friedman B, Schachtrup C, Tsai PS, Shih AY, Akassoglou K, Kleinfeld D & Lyden PD. (2009). Acute vascular disruption and aquaporin 4 loss after stroke. *Stroke* **40,** 2182-2190.

Fu R, Zhao ZQ, Zhao HY, Zhao JS & Zhu XL. (2006). Expression of heme oxygenase-1 protein and messenger RNA in permanent cerebral ischemia in rats. *Neurol Res* **28,** 38-45.

Fukuda AM & Badaut J. (2012). Aquaporin 4: a player in cerebral edema and neuroinflammation. *J Neuroinflammation* **9,** 279.

Furuse M, Hirase T, Itoh M, Nagafuchi A, Yonemura S, Tsukita S & Tsukita S. (1993). Occludin: a novel integral membrane protein localizing at tight junctions. *J Cell Biol* **123,** 1777-1788.

Gan Y, Ji X, Hu X, Luo Y, Zhang L, Li P, Liu X, Yan F, Vosler P, Gao Y, Stetler RA & Chen J. (2012). Transgenic overexpression of peroxiredoxin-2 attenuates ischemic neuronal injury via suppression of a redox-sensitive pro-death signaling pathway. *Antioxid Redox Signal* **17,** 719-732.

Garbuzova-Davis S, Rodrigues MC, Hernandez-Ontiveros DG, Tajiri N, Frisina-Deyo A, Boffeli SM, Abraham JV, Pabon M, Wagner A, Ishikawa H, Shinozuka K, Haller E, Sanberg PR, Kaneko Y & Borlongan CV. (2013). Blood-brain barrier alterations provide evidence of subacute diaschisis in an ischemic stroke rat model. *PLoS One* **8,** e63553.

Gasper AV, Al-Janobi A, Smith JA, Bacon JR, Fortun P, Atherton C, Taylor MA, Hawkey CJ, Barrett DA & Mithen RF. (2005). Glutathione S-transferase M1 polymorphism and metabolism of sulforaphane from standard and high-glucosinolate broccoli. *Am J Clin Nutr* **82,** 1283-1291.

Gauden V, Hu DE, Kurokawa T, Sarker MH & Fraser PA. (2007). Novel technique for estimating cerebrovascular permeability demonstrates capsazepine protection following ischemia-reperfusion. *Microcirculation* **14,** 767-778.

Gaziano TA. (2005). Cardiovascular disease in the developing world and its cost-effective management. *Circulation* **112,** 3547-3553.

Geddes JW, Pettigrew LC, Holtz ML, Craddock SD & Maines MD. (1996). Permanent focal and transient global cerebral ischemia increase glial and neuronal expression of heme oxygenase-1, but not heme oxygenase-2, protein in rat brain. *Neurosci Lett* **210,** 205-208.

Gehrmann J, Matsumoto Y & Kreutzberg GW. (1995). Microglia: intrinsic immuneffector cell of the brain. *Brain Res Brain Res Rev* **20,** 269-287.

Genovese T, Mazzon E, Paterniti I, Esposito E, Bramanti P & Cuzzocrea S. (2011). Modulation of NADPH oxidase activation in cerebral ischemia/reperfusion injury in rats. *Brain Res* **1372,** 92-102.

Gertz K, Laufs U, Lindauer U, Nickenig G, Bohm M, Dirnagl U & Endres M. (2003). Withdrawal of statin treatment abrogates stroke protection in mice. *Stroke* **34,** 551-557.

Girouard H, Park L, Anrather J, Zhou P & Iadecola C. (2006). Angiotensin II attenuates endothelium-dependent responses in the cerebral microcirculation through nox-2-derived radicals. *Arterioscler Thromb Vasc Biol* **26,** 826-832.

Godman CA, Joshi R, Giardina C, Perdrizet G & Hightower LE. (2010). Hyperbaric oxygen treatment induces antioxidant gene expression. *Ann N Y Acad Sci* **1197,** 178-183.

Goemaere J & Knoops B. (2012). Peroxiredoxin distribution in the mouse brain with emphasis on neuronal populations affected in neurodegenerative disorders. *J Comp Neurol* **520,** 258-280.

Goldberg MP & Choi DW. (1993). Combined oxygen and glucose deprivation in cortical cell culture: calcium-dependent and calcium-independent mechanisms of neuronal injury. *J Neurosci* **13,** 3510-3524.

Gomez-Guzman M, Jimenez R, Sanchez M, Zarzuelo MJ, Galindo P, Quintela AM, Lopez-Sepulveda R, Romero M, Tamargo J, Vargas F, Perez-Vizcaino F & Duarte J. (2012). Epicatechin lowers blood pressure, restores endothelial function, and decreases oxidative stress and endothelin-1 and NADPH oxidase activity in DOCA-salt hypertension. *Free Radic Biol Med* **52,** 70-79.

Gonzales RA & Jaworski JN. (1997). Alcohol and glutamate. *Alcohol Health Res World* **21,** 120-127.

Graham RC, Jr. & Karnovsky MJ. (1966a). The early stages of absorption of injected horseradish peroxidase in the proximal tubules of mouse kidney: ultrastructural cytochemistry by a new technique. *J Histochem Cytochem* **14,** 291-302.

Graham RC, Jr. & Karnovsky MJ. (1966b). Glomerular permeability. Ultrastructural cytochemical studies using peroxidases as protein tracers. *J Exp Med* **124,** 1123-1134.

Grau AJ, Weimar C, Buggle F, Heinrich A, Goertler M, Neumaier S, Glahn J, Brandt T, Hacke W & Diener HC. (2001). Risk factors, outcome, and treatment in subtypes of ischemic stroke: the German stroke data bank. *Stroke* **32,** 2559-2566.

Gravanis I & Tsirka SE. (2005). Tissue plasminogen activator and glial function. *Glia* **49,** 177-183.

Greenwood J. (1991). Mechanisms of blood-brain barrier breakdown. *Neuroradiology* **33,** 95-100.

Griffin S, Clark JB & Canevari L. (2005). Astrocyte-neurone communication following oxygen-glucose deprivation. *J Neurochem* **95,** 1015-1022.

Groschner LN, Waldeck-Weiermair M, Malli R & Graier WF. (2012). Endothelial mitochondria--less respiration, more integration. *Pflugers Arch* **464,** 63-76.

Gu L, Huang B, Shen W, Gao L, Ding Z, Wu H & Guo J. (2013). Early activation of nSMase2/ceramide pathway in astrocytes is involved in ischemia-associated neuronal damage via inflammation in rat hippocampi. *J Neuroinflammation* **10,** 109.

Guichard C, Moreau R, Pessayre D, Epperson TK & Krause KH. (2008). NOX family NADPH oxidases in liver and in pancreatic islets: a role in the metabolic syndrome and diabetes? *Biochem Soc Trans* **36,** 920-929.

Gustafson DL, Siegel D, Rastatter JC, Merz AL, Parpal JC, Kepa JK, Ross D & Long ME. (2003). Kinetics of NAD(P)H:quinone oxidoreductase I (NQO1) inhibition by mitomycin C in vitro and in vivo. *J Pharmacol Exp Ther* **305,** 1079-1086.

Halliwell B. (1992). Reactive oxygen species and the central nervous system. *J Neurochem* **59,** 1609-1623.

Halliwell B. (2001). Role of free radicals in the neurodegenerative diseases: therapeutic implications for antioxidant treatment. *Drugs Aging* **18,** 685-716.

Halliwell B. (2006). Oxidative stress and neurodegeneration: where are we now? *J Neurochem* **97,** 1634-1658.

Halliwell B. (2007). Biochemistry of oxidative stress. *Biochem Soc Trans* **35,** 1147-1150.

Hansen JM, Moriarty-Craige S & Jones DP. (2007). Nuclear and cytoplasmic peroxiredoxin-1 differentially regulate NF-kappaB activities. *Free Radic Biol Med* **43,** 282-288.

Harrison R. (2002). Structure and function of xanthine oxidoreductase: where are we now? *Free Radic Biol Med* **33,** 774-797.

Hawkes HJ, Karlenius TC & Tonissen KF. (2013). Regulation of the human thioredoxin gene promoter and its key substrates: A study of functional and putative regulatory elements. *Biochim Biophys Acta*.

Hawkins BT & Davis TP. (2005). The blood-brain barrier/neurovascular unit in health and disease. *Pharmacol Rev* **57,** 173-185.

Hayashi Y, Nomura M, Yamagishi S, Harada S, Yamashita J & Yamamoto H. (1997). Induction of various blood-brain barrier properties in non-neural endothelial cells by close apposition to co-cultured astrocytes. *Glia* **19,** 13-26.

Hayes JD & Dinkova-Kostova AT. (2014). The Nrf2 regulatory network provides an interface between redox and intermediary metabolism. *Trends Biochem Sci* **39,** 199-218.

Hazell AS. (2007). Excitotoxic mechanisms in stroke: an update of concepts and treatment strategies. *Neurochem Int* **50,** 941-953.

He X, Kan H, Cai L & Ma Q. (2009). Nrf2 is critical in defense against high glucose-induced oxidative damage in cardiomyocytes. *J Mol Cell Cardiol* **46,** 47-58.

Heiss WD. (2000). Ischemic penumbra: evidence from functional imaging in man. *J Cereb Blood Flow Metab* **20,** 1276-1293.

Hira S, Tomita T, Matsui T, Igarashi K & Ikeda-Saito M. (2007). Bach1, a heme-dependent transcription factor, reveals presence of multiple heme binding sites with distinct coordination structure. *IUBMB Life* **59,** 542-551.

Hirase T, Staddon JM, Saitou M, Ando-Akatsuka Y, Itoh M, Furuse M, Fujimoto K, Tsukita S & Rubin LL. (1997). Occludin as a possible determinant of tight junction permeability in endothelial cells. *J Cell Sci* **110 (Pt 14),** 1603-1613.

Hong F, Freeman ML & Liebler DC. (2005). Identification of sensor cysteines in human Keap1 modified by the cancer chemopreventive agent sulforaphane. *Chem Res Toxicol* **18,** 1917-1926.

Hong H, Lu Y, Ji ZN & Liu GQ. (2006a). Up-regulation of P-glycoprotein expression by glutathione depletion-induced oxidative stress in rat brain microvessel endothelial cells. *J Neurochem* **98,** 1465-1473.

Hong H, Zeng JS, Kreulen DL, Kaufman DI & Chen AF. (2006b). Atorvastatin protects against cerebral infarction via inhibition of NADPH oxidase-derived superoxide in ischemic stroke. *Am J Physiol Heart Circ Physiol* **291,** H2210-2215.

Hong Y, Yan W, Chen S, Sun CR & Zhang JM. (2010). The role of Nrf2 signaling in the regulation of antioxidants and detoxifying enzymes after traumatic brain injury in rats and mice. *Acta Pharmacol Sin* **31,** 1421-1430.

Hsu WH, Lee BH, Li CH, Hsu YW & Pan TM. (2013). Monascin and AITC Attenuate Methylglyoxal-Induced PPARgamma Phosphorylation and Degradation through Inhibition of the Oxidative Stress/PKC Pathway Depending on Nrf2 Activation. *J Agric Food Chem* **61,** 5996-6006.

Huang TC, Chung YL, Wu ML & Chuang SM. (2011). Cinnamaldehyde enhances Nrf2 nuclear translocation to upregulate phase II detoxifying enzyme expression in HepG2 cells. *J Agric Food Chem* **59,** 5164-5171.

Huber JD, Egleton RD & Davis TP. (2001). Molecular physiology and pathophysiology of tight junctions in the blood-brain barrier. *Trends Neurosci* **24,** 719-725.

Hyun H, Lee K, Min KH, Jeon P, Kim K, Jeong SY, Kwon IC, Park TG & Lee M. (2013). Ischemic brain imaging using fluorescent gold nanoprobes sensitive to reactive oxygen species. *Journal of controlled release : official journal of the Controlled Release Society* **170,** 352-357.

Iadecola C. (2004). Neurovascular regulation in the normal brain and in Alzheimer's disease. *Nat Rev Neurosci* **5,** 347-360.

Iadecola C & Anrather J. (2011). The immunology of stroke: from mechanisms to translation. *Nat Med* **17,** 796-808.

Igarashi K & Sun J. (2006). The heme-Bach1 pathway in the regulation of oxidative stress response and erythroid differentiation. *Antioxid Redox Signal* **8,** 107-118.

Ikonomidou C & Kaindl AM. (2011). Neuronal death and oxidative stress in the developing brain. *Antioxid Redox Signal* **14,** 1535-1550.

Ishii T, Itoh K, Ruiz E, Leake DS, Unoki H, Yamamoto M & Mann GE. (2004). Role of Nrf2 in the regulation of CD36 and stress protein expression in murine macrophages: activation by oxidatively modified LDL and 4-hydroxynonenal. *Circ Res* **94,** 609-616.

Ishii T, Itoh K, Takahashi S, Sato H, Yanagawa T, Katoh Y, Bannai S & Yamamoto M. (2000). Transcription factor Nrf2 coordinately regulates a group of oxidative stress-inducible genes in macrophages. *J Biol Chem* **275,** 16023-16029.

Ishii T, Warabi E & Yanagawa T. (2012). Novel roles of peroxiredoxins in inflammation, cancer and innate immunity. *J Clin Biochem Nutr* **50,** 91-105.

Itoh K, Chiba T, Takahashi S, Ishii T, Igarashi K, Katoh Y, Oyake T, Hayashi N, Satoh K, Hatayama I, Yamamoto M & Nabeshima Y. (1997). An Nrf2/small Maf heterodimer mediates the induction of phase II detoxifying enzyme genes through antioxidant response elements. *Biochem Biophys Res Commun* **236,** 313-322.

Itoh K, Wakabayashi N, Katoh Y, Ishii T, Igarashi K, Engel JD & Yamamoto M. (1999). Keap1 represses nuclear activation of antioxidant responsive elements by Nrf2 through binding to the amino-terminal Neh2 domain. *Genes Dev* **13,** 76-86.

Itoh K, Wakabayashi N, Katoh Y, Ishii T, O'Connor T & Yamamoto M. (2003). Keap1 regulates both cytoplasmic-nuclear shuttling and degradation of Nrf2 in response to electrophiles. *Genes Cells* **8,** 379-391.

Itoh T, Kawakami M, Yamauchi Y, Shimizu S & Nakamura M. (1986). Effect of allopurinol on ischemia and reperfusion-induced cerebral injury in spontaneously hypertensive rats. *Stroke* **17,** 1284-1287.

Jain A, Lamark T, Sjottem E, Larsen KB, Awuh JA, Overvatn A, McMahon M, Hayes JD & Johansen T. (2010a). p62/SQSTM1 is a target gene for transcription factor NRF2 and creates a positive feedback loop by inducing antioxidant response element-driven gene transcription. *J Biol Chem* **285,** 22576-22591.

Jain V, Langham MC & Wehrli FW. (2010b). MRI estimation of global brain oxygen consumption rate. *J Cereb Blood Flow Metab* **30,** 1598-1607.

James D, Devaraj S, Bellur P, Lakkanna S, Vicini J & Boddupalli S. (2012). Novel concepts of broccoli sulforaphanes and disease: induction of phase II antioxidant and detoxification enzymes by enhanced-glucoraphanin broccoli. *Nutr Rev* **70,** 654-665.

Jazwa A, Rojo AI, Innamorato NG, Hesse M, Fernandez-Ruiz J & Cuadrado A. (2011). Pharmacological targeting of the transcription factor Nrf2 at the basal ganglia provides disease modifying therapy for experimental parkinsonism. *Antioxid Redox Signal* **14,** 2347-2360.

Jean WC, Spellman SR, Nussbaum ES & Low WC. (1998). Reperfusion injury after focal cerebral ischemia: the role of inflammation and the therapeutic horizon. *Neurosurgery* **43,** 1382-1396; discussion 1396-1387.

Jiang F, Zhang Y & Dusting GJ. (2011). NADPH oxidase-mediated redox signaling: roles in cellular stress response, stress tolerance, and tissue repair. *Pharmacol Rev* **63,** 218-242.

Jin MH, Lee YH, Kim JM, Sun HN, Moon EY, Shong MH, Kim SU, Lee SH, Lee TH, Yu DY & Lee DS. (2005). Characterization of neural cell types expressing peroxiredoxins in mouse brain. *Neurosci Lett* **381,** 252-257.

Johansen JS, Harris AK, Rychly DJ & Ergul A. (2005). Oxidative stress and the use of antioxidants in diabetes: linking basic science to clinical practice. *Cardiovasc Diabetol* **4,** 5.

Johansson BB. (1999). Hypertension mechanisms causing stroke. *Clin Exp Pharmacol Physiol* **26,** 563-565.

Juge N, Mithen RF & Traka M. (2007). Molecular basis for chemoprevention by sulforaphane: a comprehensive review. *Cell Mol Life Sci* **64,** 1105-1127.

Juurlink BH & Sweeney MI. (1997). Mechanisms that result in damage during and following cerebral ischemia. *Neurosci Biobehav Rev* **21,** 121-128.

Jyrkkanen HK, Kuosmanen S, Heinaniemi M, Laitinen H, Kansanen E, Mella-Aho E, Leinonen H, Yla-Herttuala S & Levonen AL. (2011). Novel insights into the regulation of antioxidant-response-element-mediated gene expression by electrophiles: induction of the transcriptional repressor BACH1 by Nrf2. *Biochem J* **440,** 167-174.

Kahles T, Kohnen A, Heumueller S, Rappert A, Bechmann I, Liebner S, Wittko IM, Neumann-Haefelin T, Steinmetz H, Schroeder K & Brandes RP. (2010). NADPH oxidase Nox1 contributes to ischemic injury in experimental stroke in mice. *Neurobiol Dis* **40,** 185-192.

Kahles T, Luedike P, Endres M, Galla HJ, Steinmetz H, Busse R, Neumann-Haefelin T & Brandes RP. (2007). NADPH oxidase plays a central role in blood-brain barrier damage in experimental stroke. *Stroke* **38,** 3000-3006.

Kam KY, Yu SJ, Jeong N, Hong JH, Jalin AM, Lee S, Choi YW, Lee CK & Kang SG. (2011). p-Hydroxybenzyl alcohol prevents brain injury and behavioral impairment by activating Nrf2, PDI, and neurotrophic factor genes in a rat model of brain ischemia. *Mol Cells* **31,** 209-215.

Kang SW, Chae HZ, Seo MS, Kim K, Baines IC & Rhee SG. (1998). Mammalian peroxiredoxin isoforms can reduce hydrogen peroxide generated in response to growth factors and tumor necrosis factor-alpha. *J Biol Chem* **273,** 6297-6302.

Kapinya KJ, Harms U, Harms C, Blei K, Katchanov J, Dirnagl U & Hortnagl H. (2003). Role of NAD(P)H:quinone oxidoreductase in the progression of neuronal cell death in vitro and following cerebral ischaemia in vivo. *J Neurochem* **84,** 1028-1039.

Kaspar JW, Niture SK & Jaiswal AK. (2009). Nrf2:INrf2 (Keap1) signaling in oxidative stress. *Free Radic Biol Med* **47,** 1304-1309.

Kataoka K, Noda M & Nishizawa M. (1994). Maf nuclear oncoprotein recognizes sequences related to an AP-1 site and forms heterodimers with both Fos and Jun. *Mol Cell Biol* **14,** 700-712.

Katoh Y, Itoh K, Yoshida E, Miyagishi M, Fukamizu A & Yamamoto M. (2001). Two domains of Nrf2 cooperatively bind CBP, a CREB binding protein, and synergistically activate transcription. *Genes Cells* **6,** 857-868.

Kevil CG, Pruitt H, Kavanagh TJ, Wilkerson J, Farin F, Moellering D, Darley-Usmar VM, Bullard DC & Patel RP. (2004). Regulation of endothelial glutathione by ICAM-1: implications for inflammation. *FASEB J* **18,** 1321-1323.

Keyt BA, Paoni NF, Refino CJ, Berleau L, Nguyen H, Chow A, Lai J, Pena L, Pater C, Ogez J & et al. (1994). A faster-acting and more potent form of tissue plasminogen activator. *Proc Natl Acad Sci U S A* **91,** 3670-3674.

Kido Y, Tamai I, Uchino H, Suzuki F, Sai Y & Tsuji A. (2001). Molecular and functional identification of large neutral amino acid transporters LAT1 and LAT2 and their pharmacological relevance at the blood-brain barrier. *J Pharm Pharmacol* **53,** 497-503.

Kim HV, Kim HY, Ehrlich HY, Choi SY, Kim DJ & Kim Y. (2013). Amelioration of Alzheimer's disease by neuroprotective effect of sulforaphane in animal model. *Amyloid* **20,** 7-12.

Kim YJ, Ahn JY, Liang P, Ip C, Zhang Y & Park YM. (2007). Human prx1 gene is a target of Nrf2 and is up-regulated by hypoxia/reoxygenation: implication to tumor biology. *Cancer Res* **67,** 546-554.

Kingwell K. (2010). Neurotransmission: A new take on glutamate. *Nat Rev Neurosci* **11,** 732.

Kinouchi H, Epstein CJ, Mizui T, Carlson E, Chen SF & Chan PH. (1991). Attenuation of focal cerebral ischemic injury in transgenic mice overexpressing CuZn superoxide dismutase. *Proc Natl Acad Sci U S A* **88,** 11158-11162.

Kinuta Y, Kimura M, Itokawa Y, Ishikawa M & Kikuchi H. (1989). Changes in xanthine oxidase in ischemic rat brain. *J Neurosurg* **71,** 417-420.

Klatzo I. (1987). Blood-brain barrier and ischaemic brain oedema. *Z Kardiol* **76 Suppl 4,** 67-69.

Kleinschnitz C, Grund H, Wingler K, Armitage ME, Jones E, Mittal M, Barit D, Schwarz T, Geis C, Kraft P, Barthel K, Schuhmann MK, Herrmann AM, Meuth SG, Stoll G, Meurer S, Schrewe A, Becker L, Gailus-Durner V, Fuchs H, Klopstock T, de Angelis MH, Jandeleit-Dahm K, Shah AM, Weissmann N & Schmidt HH. (2010). Post-stroke inhibition of induced NADPH oxidase type 4 prevents oxidative stress and neurodegeneration. *PLoS Biol* **8**.

Kochanski R, Peng C, Higashida T, Geng X, Huttemann M, Guthikonda M & Ding Y. (2013). Neuroprotection conferred by post-ischemia ethanol therapy in experimental stroke: an

inhibitory effect on hyperglycolysis and NADPH oxidase activation. *J Neurochem* **126,** 113-121.

Koehler RC, Gebremedhin D & Harder DR. (2006). Role of astrocytes in cerebrovascular regulation. *J Appl Physiol (1985)* **100,** 307-317.

Kohen R & Nyska A. (2002). Oxidation of biological systems: oxidative stress phenomena, antioxidants, redox reactions, and methods for their quantification. *Toxicol Pathol* **30,** 620-650.

Konior A, Schramm A, Czesnikiewicz-Guzik M & Guzik TJ. (2013). NADPH Oxidases in Vascular Pathology. *Antioxid Redox Signal*.

Koopman G, Reutelingsperger CP, Kuijten GA, Keehnen RM, Pals ST & van Oers MH. (1994). Annexin V for flow cytometric detection of phosphatidylserine expression on B cells undergoing apoptosis. *Blood* **84,** 1415-1420.

Krejsa CM, Franklin CC, White CC, Ledbetter JA, Schieven GL & Kavanagh TJ. (2010). Rapid activation of glutamate cysteine ligase following oxidative stress. *J Biol Chem* **285,** 16116-16124.

Kuchler-Bopp S, Delaunoy JP, Artault JC, Zaepfel M & Dietrich JB. (1999). Astrocytes induce several blood-brain barrier properties in non-neural endothelial cells. *Neuroreport* **10,** 1347-1353.

Kumar H, Lim HW, More SV, Kim BW, Koppula S, Kim IS & Choi DK. (2012). The role of free radicals in the aging brain and Parkinson's disease: convergence and parallelism. *Int J Mol Sci* **13,** 10478-10504.

Kunz A, Dirnagl U & Mergenthaler P. (2010). Acute pathophysiological processes after ischaemic and traumatic brain injury. *Best Pract Res Clin Anaesthesiol* **24,** 495-509.

Kuper H, Adami HO, Theorell T & Weiderpass E. (2007). The socioeconomic gradient in the incidence of stroke: a prospective study in middle-aged women in Sweden. *Stroke* **38,** 27-33.

Kwak JY, Takeshige K, Cheung BS & Minakami S. (1991). Bilirubin inhibits the activation of superoxide-producing NADPH oxidase in a neutrophil cell-free system. *Biochim Biophys Acta* **1076,** 369-373.

Kwak MK, Cho JM, Huang B, Shin S & Kensler TW. (2007). Role of increased expression of the proteasome in the protective effects of sulforaphane against hydrogen peroxide-mediated cytotoxicity in murine neuroblastoma cells. *Free Radic Biol Med* **43,** 809-817.

Kwak MK, Itoh K, Yamamoto M & Kensler TW. (2002). Enhanced expression of the transcription factor Nrf2 by cancer chemopreventive agents: role of antioxidant response element-like sequences in the nrf2 promoter. *Mol Cell Biol* **22,** 2883-2892.

L'Episcopo F, Tirolo C, Testa N, Caniglia S, Morale MC, Impagnatiello F, Pluchino S & Marchetti B. (2013). Aging-induced Nrf2-ARE pathway disruption in the subventricular zone drives neurogenic impairment in parkinsonian mice via PI3K-Wnt/beta-catenin dysregulation. *J Neurosci* **33,** 1462-1485.

Lagreze HL, Levine RL, Pedula KL, Nickles RJ, Sunderland JS & Rowe BR. (1987). Contralateral flow reduction in unilateral stroke: evidence for transhemispheric diaschisis. *Stroke* **18,** 882-886.

Lakhan SE, Kirchgessner A, Tepper D & Leonard A. (2013). Matrix metalloproteinases and blood-brain barrier disruption in acute ischemic stroke. *Front Neurol* **4,** 32.

Laufs U, Gertz K, Dirnagl U, Bohm M, Nickenig G & Endres M. (2002). Rosuvastatin, a new HMG-CoA reductase inhibitor, upregulates endothelial nitric oxide synthase and protects from ischemic stroke in mice. *Brain Res* **942,** 23-30.

Laufs U, Gertz K, Huang P, Nickenig G, Bohm M, Dirnagl U & Endres M. (2000). Atorvastatin upregulates type III nitric oxide synthase in thrombocytes, decreases platelet activation, and protects from cerebral ischemia in normocholesterolemic mice. *Stroke* **31,** 2442-2449.

Lavrovsky Y, Schwartzman ML & Abraham NG. (1993). Novel regulatory sites of the human heme oxygenase-1 promoter region. *Biochem Biophys Res Commun* **196,** 336-341.

Lavrovsky Y, Schwartzman ML, Levere RD, Kappas A & Abraham NG. (1994). Identification of binding sites for transcription factors NF-kappa B and AP-2 in the promoter region of the human heme oxygenase 1 gene. *Proc Natl Acad Sci U S A* **91,** 5987-5991.

Le LL, Li XY, Meng D, Liang QJ, Wang XH, Li N, Quan J, Xiang M, Jiang M, Sun J & Chen SF. (2013). Heme Oxygenase-1 Mediated Memorial and Revivable Protective Effect of Ischemic Preconditioning on Brain Injury. *CNS Neurosci Ther*.

Leak RK, Zhang L, Luo Y, Li P, Zhao H, Liu X, Ling F, Jia J, Chen J & Ji X. (2013). Peroxiredoxin 2 battles poly(ADP-ribose) polymerase 1- and p53-dependent prodeath pathways after ischemic injury. *Stroke* **44,** 1124-1134.

Lee JH, Lee J, Seo GH, Kim CH & Ahn YS. (2007). Heparin inhibits NF-kappaB activation and increases cell death in cerebral endothelial cells after oxygen-glucose deprivation. *J Mol Neurosci* **32,** 145-154.

Lee JM, Calkins MJ, Chan K, Kan YW & Johnson JA. (2003). Identification of the NF-E2-related factor-2-dependent genes conferring protection against oxidative stress in

primary cortical astrocytes using oligonucleotide microarray analysis. *J Biol Chem* **278,** 12029-12038.

Lee MC. (2013). Assessment of oxidative stress and antioxidant property using electron spin resonance (ESR) spectroscopy. *J Clin Biochem Nutr* **52,** 1-8.

Lee YJ, Jeong HY, Kim YB, Lee YJ, Won SY, Shim JH, Cho MK, Nam HS & Lee SH. (2012). Reactive oxygen species and PI3K/Akt signaling play key roles in the induction of Nrf2-driven heme oxygenase-1 expression in sulforaphane-treated human mesothelioma MSTO-211H cells. *Food Chem Toxicol* **50,** 116-123.

Lehner C, Gehwolf R, Tempfer H, Krizbai I, Hennig B, Bauer HC & Bauer H. (2011). Oxidative stress and blood-brain barrier dysfunction under particular consideration of matrix metalloproteinases. *Antioxid Redox Signal* **15,** 1305-1323.

Leoncini E, Malaguti M, Angeloni C, Motori E, Fabbri D & Hrelia S. (2011). Cruciferous vegetable phytochemical sulforaphane affects phase II enzyme expression and activity in rat cardiomyocytes through modulation of Akt signaling pathway. *J Food Sci* **76,** H175-181.

Lewandowsky M. (1900). Zur lehre der cerebrospinalflussigkeit. *Z klin Med* **40,** l900.

Li L, Zhang X, Cui L, Wang L, Liu H, Ji H & Du Y. (2013). Ursolic acid promotes the neuroprotection by activating Nrf2 pathway after cerebral ischemia in mice. *Brain Res* **1497,** 32-39.

Li Y, Paonessa JD & Zhang Y. (2012a). Mechanism of chemical activation of Nrf2. *PLoS One* **7,** e35122.

Li Z, Pang L, Fang F, Zhang G, Zhang J, Xie M & Wang L. (2012b). Resveratrol attenuates brain damage in a rat model of focal cerebral ischemia via up-regulation of hippocampal Bcl-2. *Brain Res* **1450,** 116-124.

Liang BA, Lew R & Zivin JA. (2008). Review of tissue plasminogen activator, ischemic stroke, and potential legal issues. *Arch Neurol* **65,** 1429-1433.

Liedtke W, Edelmann W, Bieri PL, Chiu FC, Cowan NJ, Kucherlapati R & Raine CS. (1996). GFAP is necessary for the integrity of CNS white matter architecture and long-term maintenance of myelination. *Neuron* **17,** 607-615.

Lin HJ, Probst-Hensch NM, Louie AD, Kau IH, Witte JS, Ingles SA, Frankl HD, Lee ER & Haile RW. (1998). Glutathione transferase null genotype, broccoli, and lower prevalence of colorectal adenomas. *Cancer Epidemiol Biomarkers Prev* **7,** 647-652.

Lin X, Yang H, Zhou L & Guo Z. (2011). Nrf2-dependent induction of NQO1 in mouse aortic endothelial cells overexpressing catalase. *Free Radic Biol Med* **51,** 97-106.

Lindsay S, Liu TH, Xu JA, Marshall PA, Thompson JK, Parks DA, Freeman BA, Hsu CY & Beckman JS. (1991). Role of xanthine dehydrogenase and oxidase in focal cerebral ischemic injury to rat. *Am J Physiol* **261,** H2051-2057.

Liu GH, Qu J & Shen X. (2008). NF-kappaB/p65 antagonizes Nrf2-ARE pathway by depriving CBP from Nrf2 and facilitating recruitment of HDAC3 to MafK. *Biochim Biophys Acta* **1783,** 713-727.

Liu Y, Zhang Z, Luo B, Schluesener HJ & Zhang Z. (2013a). Lesional accumulation of heme oxygenase-1+ microglia/macrophages in rat traumatic brain injury. *Neuroreport* **24,** 281-286.

Liu ZJ, Liu W, Liu L, Xiao C, Wang Y & Jiao JS. (2013b). Curcumin Protects Neuron against Cerebral Ischemia-Induced Inflammation through Improving PPAR-Gamma Function. *Evid Based Complement Alternat Med* **2013,** 470975.

Loboda A, Stachurska A, Florczyk U, Rudnicka D, Jazwa A, Wegrzyn J, Kozakowska M, Stalinska K, Poellinger L, Levonen AL, Yla-Herttuala S, Jozkowicz A & Dulak J. (2009). HIF-1 induction attenuates Nrf2-dependent IL-8 expression in human endothelial cells. *Antioxid Redox Signal* **11,** 1501-1517.

Lochhead JJ, McCaffrey G, Quigley CE, Finch J, DeMarco KM, Nametz N & Davis TP. (2010). Oxidative stress increases blood-brain barrier permeability and induces alterations in occludin during hypoxia-reoxygenation. *J Cereb Blood Flow Metab* **30,** 1625-1636.

Lonze BE & Ginty DD. (2002). Function and regulation of CREB family transcription factors in the nervous system. *Neuron* **35,** 605-623.

Love S. (1999). Oxidative stress in brain ischemia. *Brain Pathol* **9,** 119-131.

Lu SC. (2009). Regulation of glutathione synthesis. *Mol Aspects Med* **30,** 42-59.

Ludtmann MH, Angelova PR, Zhang Y, Abramov AY & Dinkova-Kostova AT. (2014). Nrf2 affects the efficiency of mitochondrial fatty acid oxidation. *Biochem J* **457,** 415-424.

MacLeod AK, McMahon M, Plummer SM, Higgins LG, Penning TM, Igarashi K & Hayes JD. (2009). Characterization of the cancer chemopreventive NRF2-dependent gene battery in human keratinocytes: demonstration that the KEAP1-NRF2 pathway, and not the BACH1-NRF2 pathway, controls cytoprotection against electrophiles as well as redox-cycling compounds. *Carcinogenesis* **30,** 1571-1580.

Maines MD. (1988). Heme oxygenase: function, multiplicity, regulatory mechanisms, and clinical applications. *FASEB J* **2,** 2557-2568.

Maines MD. (1997). The heme oxygenase system: a regulator of second messenger gases. *Annu Rev Pharmacol Toxicol* **37,** 517-554.

Malec V, Gottschald OR, Li S, Rose F, Seeger W & Hanze J. (2010). HIF-1 alpha signaling is augmented during intermittent hypoxia by induction of the Nrf2 pathway in NOX1-expressing adenocarcinoma A549 cells. *Free Radic Biol Med* **48,** 1626-1635.

Manandhar S, Cho JM, Kim JA, Kensler TW & Kwak MK. (2007). Induction of Nrf2-regulated genes by 3H-1, 2-dithiole-3-thione through the ERK signaling pathway in murine keratinocytes. *Eur J Pharmacol* **577,** 17-27.

Manley GT, Fujimura M, Ma T, Noshita N, Filiz F, Bollen AW, Chan P & Verkman AS. (2000). Aquaporin-4 deletion in mice reduces brain edema after acute water intoxication and ischemic stroke. *Nat Med* **6,** 159-163.

Mann GE, Bonacasa B, Ishii T & Siow RC. (2009). Targeting the redox sensitive Nrf2-Keap1 defense pathway in cardiovascular disease: protection afforded by dietary isoflavones. *Curr Opin Pharmacol* **9,** 139-145.

Manning AS, Coltart DJ & Hearse DJ. (1984). Ischemia and reperfusion-induced arrhythmias in the rat. Effects of xanthine oxidase inhibition with allopurinol. *Circ Res* **55,** 545-548.

Mark LP, Prost RW, Ulmer JL, Smith MM, Daniels DL, Strottmann JM, Brown WD & Hacein-Bey L. (2001). Pictorial review of glutamate excitotoxicity: fundamental concepts for neuroimaging. *AJNR Am J Neuroradiol* **22,** 1813-1824.

Markovic J, Borras C, Ortega A, Sastre J, Vina J & Pallardo FV. (2007). Glutathione is recruited into the nucleus in early phases of cell proliferation. *J Biol Chem* **282,** 20416-20424.

Martin SJ, Reutelingsperger CP, McGahon AJ, Rader JA, van Schie RC, LaFace DM & Green DR. (1995). Early redistribution of plasma membrane phosphatidylserine is a general feature of apoptosis regardless of the initiating stimulus: inhibition by overexpression of Bcl-2 and Abl. *J Exp Med* **182,** 1545-1556.

Martz D, Rayos G, Schielke GP & Betz AL. (1989). Allopurinol and dimethylthiourea reduce brain infarction following middle cerebral artery occlusion in rats. *Stroke* **20,** 488-494.

Matkowskyj KA, Schonfeld D & Benya RV. (2000). Quantitative immunohistochemistry by measuring cumulative signal strength using commercially available software photoshop and matlab. *J Histochem Cytochem* **48,** 303-312.

Matusheski NV & Jeffery EH. (2001). Comparison of the bioactivity of two glucoraphanin hydrolysis products found in broccoli, sulforaphane and sulforaphane nitrile. *J Agric Food Chem* **49,** 5743-5749.

Matz PG, Weinstein PR & Sharp FR. (1997). Heme oxygenase-1 and heat shock protein 70 induction in glia and neurons throughout rat brain after experimental intracerebral hemorrhage. *Neurosurgery* **40,** 152-160; discussion 160-152.

McCord JM. (1985). Oxygen-derived free radicals in postischemic tissue injury. *N Engl J Med* **312,** 159-163.

McCoubrey WK, Jr., Huang TJ & Maines MD. (1997). Isolation and characterization of a cDNA from the rat brain that encodes hemoprotein heme oxygenase-3. *Eur J Biochem* **247,** 725-732.

McMahon M, Itoh K, Yamamoto M & Hayes JD. (2003). Keap1-dependent proteasomal degradation of transcription factor Nrf2 contributes to the negative regulation of antioxidant response element-driven gene expression. *J Biol Chem* **278,** 21592-21600.

McMahon M, Lamont DJ, Beattie KA & Hayes JD. (2010). Keap1 perceives stress via three sensors for the endogenous signaling molecules nitric oxide, zinc, and alkenals. *Proc Natl Acad Sci U S A* **107,** 18838-18843.

McWalter GK, Higgins LG, McLellan LI, Henderson CJ, Song L, Thornalley PJ, Itoh K, Yamamoto M & Hayes JD. (2004). Transcription factor Nrf2 is essential for induction of NAD(P)H:quinone oxidoreductase 1, glutathione S-transferases, and glutamate cysteine ligase by broccoli seeds and isothiocyanates. *J Nutr* **134,** 3499S-3506S.

Meister A & Anderson ME. (1983). Glutathione. *Annu Rev Biochem* **52,** 711-760.

Meldrum BS. (2000). Glutamate as a neurotransmitter in the brain: review of physiology and pathology. *J Nutr* **130,** 1007S-1015S.

Metzen E, Zhou J, Jelkmann W, Fandrey J & Brune B. (2003). Nitric oxide impairs normoxic degradation of HIF-1alpha by inhibition of prolyl hydroxylases. *Mol Biol Cell* **14,** 3470-3481.

Middeldorp J & Hol EM. (2011). GFAP in health and disease. *Prog Neurobiol* **93,** 421-443.

Miller CJ, Gounder SS, Kannan S, Goutam K, Muthusamy VR, Firpo MA, Symons JD, Paine R, 3rd, Hoidal JR & Rajasekaran NS. (2012). Disruption of Nrf2/ARE signaling impairs antioxidant mechanisms and promotes cell degradation pathways in aged skeletal muscle. *Biochim Biophys Acta* **1822,** 1038-1050.

Miller DS, Bauer B & Hartz AM. (2008). Modulation of P-glycoprotein at the blood-brain barrier: opportunities to improve central nervous system pharmacotherapy. *Pharmacol Rev* **60,** 196-209.

Miyamoto N, Izumi H, Miyamoto R, Kondo H, Tawara A, Sasaguri Y & Kohno K. (2011). Quercetin induces the expression of peroxiredoxins 3 and 5 via the Nrf2/NRF1 transcription pathway. *Invest Ophthalmol Vis Sci* **52,** 1055-1063.

Mizusawa H, Ishii T & Bannai S. (2000). Peroxiredoxin I (macrophage 23 kDa stress protein) is highly and widely expressed in the rat nervous system. *Neurosci Lett* **283,** 57-60.

Modo M, Stroemer RP, Tang E, Veizovic T, Sowniski P & Hodges H. (2000). Neurological sequelae and long-term behavioural assessment of rats with transient middle cerebral artery occlusion. *J Neurosci Methods* **104,** 99-109.

Moi P, Chan K, Asunis I, Cao A & Kan YW. (1994). Isolation of NF-E2-related factor 2 (Nrf2), a NF-E2-like basic leucine zipper transcriptional activator that binds to the tandem NF-E2/AP1 repeat of the beta-globin locus control region. *Proc Natl Acad Sci U S A* **91,** 9926-9930.

Molofsky AV, Krencik R, Ullian EM, Tsai HH, Deneen B, Richardson WD, Barres BA & Rowitch DH. (2012). Astrocytes and disease: a neurodevelopmental perspective. *Genes Dev* **26,** 891-907.

Moreira TJ, Cebere A, Cebers G, Ostenson CG, Efendic S & Liljequist S. (2007). Reduced HO-1 protein expression is associated with more severe neurodegeneration after transient ischemia induced by cortical compression in diabetic Goto-Kakizaki rats. *J Cereb Blood Flow Metab* **27,** 1710-1723.

Morgello S, Uson RR, Schwartz EJ & Haber RS. (1995). The human blood-brain barrier glucose transporter (GLUT1) is a glucose transporter of gray matter astrocytes. *Glia* **14,** 43-54.

Morrison SJ, Csete M, Groves AK, Melega W, Wold B & Anderson DJ. (2000). Culture in reduced levels of oxygen promotes clonogenic sympathoadrenal differentiation by isolated neural crest stem cells. *J Neurosci* **20,** 7370-7376.

Morroni F, Tarozzi A, Sita G, Bolondi C, Zolezzi Moraga JM, Cantelli-Forti G & Hrelia P. (2013). Neuroprotective effect of sulforaphane in 6-hydroxydopamine-lesioned mouse model of Parkinson's disease. *Neurotoxicology* **36,** 63-71.

Mosmann T. (1983). Rapid colorimetric assay for cellular growth and survival: application to proliferation and cytotoxicity assays. *J Immunol Methods* **65,** 55-63.

Motohashi H, Katsuoka F, Engel JD & Yamamoto M. (2004). Small Maf proteins serve as transcriptional cofactors for keratinocyte differentiation in the Keap1-Nrf2 regulatory pathway. *Proc Natl Acad Sci U S A* **101,** 6379-6384.

Motohashi H & Yamamoto M. (2004). Nrf2-Keap1 defines a physiologically important stress response mechanism. *Trends Mol Med* **10,** 549-557.

Muir SW, Harrow C, Dawson J, Lees KR, Weir CJ, Sattar N & Walters MR. (2008). Allopurinol use yields potentially beneficial effects on inflammatory indices in those with recent ischemic stroke: a randomized, double-blind, placebo-controlled trial. *Stroke* **39,** 3303-3307.

Mukherjee S, Lekli I, Ray D, Gangopadhyay H, Raychaudhuri U & Das DK. (2010). Comparison of the protective effects of steamed and cooked broccolis on ischaemia-reperfusion-induced cardiac injury. *Br J Nutr* **103,** 815-823.

Mulcahy RT, Wartman MA, Bailey HH & Gipp JJ. (1997). Constitutive and beta-naphthoflavone-induced expression of the human gamma-glutamylcysteine synthetase heavy subunit gene is regulated by a distal antioxidant response element/TRE sequence. *J Biol Chem* **272,** 7445-7454.

Murakami A & Ohnishi K. (2012). Target molecules of food phytochemicals: food science bound for the next dimension. *Food Funct* **3,** 462-476.

Murakami K, Kondo T, Kawase M, Li Y, Sato S, Chen SF & Chan PH. (1998). Mitochondrial susceptibility to oxidative stress exacerbates cerebral infarction that follows permanent focal cerebral ischemia in mutant mice with manganese superoxide dismutase deficiency. *J Neurosci* **18,** 205-213.

Nada SE & Shah ZA. (2012). Preconditioning with Ginkgo biloba (EGb 761(R)) provides neuroprotection through HO1 and CRMP2. *Neurobiol Dis* **46,** 180-189.

Nakane PK & Pierce GB, Jr. (1966). Enzyme-labeled antibodies: preparation and application for the localization of antigens. *J Histochem Cytochem* **14,** 929-931.

Naughton P, Hoque M, Green CJ, Foresti R & Motterlini R. (2002). Interaction of heme with nitroxyl or nitric oxide amplifies heme oxygenase-1 induction: involvement of the transcription factor Nrf2. *Cell Mol Biol (Noisy-le-grand)* **48,** 885-894.

Nawashiro H, Brenner M, Fukui S, Shima K & Hallenbeck JM. (2000). High susceptibility to cerebral ischemia in GFAP-null mice. *J Cereb Blood Flow Metab* **20,** 1040-1044.

Nebert DW, Roe AL, Vandale SE, Bingham E & Oakley GG. (2002). NAD(P)H:quinone oxidoreductase (NQO1) polymorphism, exposure to benzene, and predisposition to disease: a HuGE review. *Genet Med* **4,** 62-70.

Nguyen T, Sherratt PJ, Nioi P, Yang CS & Pickett CB. (2005). Nrf2 controls constitutive and inducible expression of ARE-driven genes through a dynamic pathway involving nucleocytoplasmic shuttling by Keap1. *J Biol Chem* **280,** 32485-32492.

Nijboer CH, Heijnen CJ, Groenendaal F, May MJ, van Bel F & Kavelaars A. (2008). A dual role of the NF-kappaB pathway in neonatal hypoxic-ischemic brain damage. *Stroke* **39,** 2578-2586.

Nimmerjahn A, Kirchhoff F & Helmchen F. (2005). Resting microglial cells are highly dynamic surveillants of brain parenchyma in vivo. *Science* **308,** 1314-1318.

Niture SK, Khatri R & Jaiswal AK. (2013). Regulation of Nrf2-an update. *Free Radic Biol Med*.

Nurmi A, Lindsberg PJ, Koistinaho M, Zhang W, Juettler E, Karjalainen-Lindsberg ML, Weih F, Frank N, Schwaninger M & Koistinaho J. (2004). Nuclear factor-kappaB contributes to infarction after permanent focal ischemia. *Stroke* **35,** 987-991.

O'Brien PJ. (1988). Radical formation during the peroxidase catalyzed metabolism of carcinogens and xenobiotics: the reactivity of these radicals with GSH, DNA, and unsaturated lipid. *Free Radic Biol Med* **4,** 169-183.

O'Neill LA & Kaltschmidt C. (1997). NF-kappa B: a crucial transcription factor for glial and neuronal cell function. *Trends Neurosci* **20,** 252-258.

Okouchi M, Okayama N & Aw TY. (2009). Preservation of cellular glutathione status and mitochondrial membrane potential by N-acetylcysteine and insulin sensitizers prevent carbonyl stress-induced human brain endothelial cell apoptosis. *Curr Neurovasc Res* **6,** 267-278.

Ono T, Tsuruta R, Fujita M, Aki HS, Kutsuna S, Kawamura Y, Wakatsuki J, Aoki T, Kobayashi C, Kasaoka S, Maruyama I, Yuasa M & Maekawa T. (2009). Xanthine oxidase is one of the major sources of superoxide anion radicals in blood after reperfusion in rats with forebrain ischemia/reperfusion. *Brain Res* **1305,** 158-167.

Ozkul A, Akyol A, Yenisey C, Arpaci E, Kiylioglu N & Tataroglu C. (2007). Oxidative stress in acute ischemic stroke. *J Clin Neurosci* **14,** 1062-1066.

Paemeleire K & Leybaert L. (2000). ATP-dependent astrocyte-endothelial calcium signaling following mechanical damage to a single astrocyte in astrocyte-endothelial co-cultures. *J Neurotrauma* **17,** 345-358.

Panahian N, Yoshiura M & Maines MD. (1999). Overexpression of heme oxygenase-1 is neuroprotective in a model of permanent middle cerebral artery occlusion in transgenic mice. *J Neurochem* **72,** 1187-1203.

Parfenova H & Leffler CW. (2008). Cerebroprotective functions of HO-2. *Curr Pharm Des* **14,** 443-453.

Park HM, Kim JA & Kwak MK. (2009). Protection against amyloid beta cytotoxicity by sulforaphane: role of the proteasome. *Arch Pharm Res* **32,** 109-115.

Paterson PG & Juurlink BH. (1999). Nutritional regulation of glutathione in stroke. *Neurotox Res* **1,** 99-112.

Patt A, Harken AH, Burton LK, Rodell TC, Piermattei D, Schorr WJ, Parker NB, Berger EM, Horesh IR, Terada LS & et al. (1988). Xanthine oxidase-derived hydrogen peroxide contributes to ischemia reperfusion-induced edema in gerbil brains. *J Clin Invest* **81,** 1556-1562.

Payne RS, Akca O, Roewer N, Schurr A & Kehl F. (2005). Sevoflurane-induced preconditioning protects against cerebral ischemic neuronal damage in rats. *Brain Res* **1034,** 147-152.

Pekny M, Stanness KA, Eliasson C, Betsholtz C & Janigro D. (1998). Impaired induction of blood-brain barrier properties in aortic endothelial cells by astrocytes from GFAP-deficient mice. *Glia* **22,** 390-400.

Pendlebury ST. (2009). Stroke-related dementia: rates, risk factors and implications for future research. *Maturitas* **64,** 165-171.

Pendlebury ST. (2012). Review: depression is associated with an increased risk of developing stroke. *Evid Based Ment Health* **15,** 32.

Pendlebury ST & Rothwell PM. (2009a). Prevalence, incidence, and factors associated with pre-stroke and post-stroke dementia: a systematic review and meta-analysis. *Lancet Neurol* **8,** 1006-1018.

Pendlebury ST & Rothwell PM. (2009b). Risk of recurrent stroke, other vascular events and dementia after transient ischaemic attack and stroke. *Cerebrovasc Dis* **27 Suppl 3,** 1-11.

Perez-de-Puig I, Martin A, Gorina R, de la Rosa X, Martinez E & Planas AM. (2013). Induction of hemeoxygenase-1 expression after inhibition of hemeoxygenase activity promotes inflammation and worsens ischemic brain damage in mice. *Neuroscience* **243,** 22-32.

Peters A, Schweiger U, Pellerin L, Hubold C, Oltmanns KM, Conrad M, Schultes B, Born J & Fehm HL. (2004). The selfish brain: competition for energy resources. *Neurosci Biobehav Rev* **28,** 143-180.

Peters O, Back T, Lindauer U, Busch C, Megow D, Dreier J & Dirnagl U. (1998). Increased formation of reactive oxygen species after permanent and reversible middle cerebral artery occlusion in the rat. *J Cereb Blood Flow Metab* **18,** 196-205.

Petzold GC & Murthy VN. (2011). Role of astrocytes in neurovascular coupling. *Neuron* **71,** 782-797.

Piantadosi CA & Zhang J. (1996). Mitochondrial generation of reactive oxygen species after brain ischemia in the rat. *Stroke* **27,** 327-331; discussion 332.

Ping Z, Liu W, Kang Z, Cai J, Wang Q, Cheng N, Wang S, Wang S, Zhang JH & Sun X. (2010). Sulforaphane protects brains against hypoxic-ischemic injury through induction of Nrf2-dependent phase 2 enzyme. *Brain Res* **1343,** 178-185.

Plateel M, Dehouck MP, Torpier G, Cecchelli R & Teissier E. (1995). Hypoxia increases the susceptibility to oxidant stress and the permeability of the blood-brain barrier endothelial cell monolayer. *J Neurochem* **65,** 2138-2145.

Pomerleau J, Lock K & McKee M. (2006). The burden of cardiovascular disease and cancer attributable to low fruit and vegetable intake in the European Union: differences between old and new Member States. *Public Health Nutr* **9,** 575-583.

Poynton RA & Hampton MB. (2013). Peroxiredoxins as biomarkers of oxidative stress. *Biochim Biophys Acta*.

Prochaska HJ & Santamaria AB. (1988). Direct measurement of NAD(P)H:quinone reductase from cells cultured in microtiter wells: a screening assay for anticarcinogenic enzyme inducers. *Anal Biochem* **169,** 328-336.

Qi H, Han Y & Rong J. (2012). Potential roles of PI3K/Akt and Nrf2-Keap1 pathways in regulating hormesis of Z-ligustilide in PC12 cells against oxygen and glucose deprivation. *Neuropharmacology* **62,** 1659-1670.

Rada P, Rojo AI, Chowdhry S, McMahon M, Hayes JD & Cuadrado A. (2011). SCF/{beta}-TrCP promotes glycogen synthase kinase 3-dependent degradation of the Nrf2 transcription factor in a Keap1-independent manner. *Mol Cell Biol* **31,** 1121-1133.

Rahman MM, Sykiotis GP, Nishimura M, Bodmer R & Bohmann D. (2013). Declining signal dependence of Nrf2-MafS-regulated gene expression correlates with aging phenotypes. *Aging Cell* **12,** 554-562.

Raichle ME. (1983). The pathophysiology of brain ischemia. *Ann Neurol* **13,** 2-10.

Raichle ME & Gusnard DA. (2002). Appraising the brain's energy budget. *Proc Natl Acad Sci U S A* **99,** 10237-10239.

Ralay Ranaivo H, Hodge JN, Choi N & Wainwright MS. (2012). Albumin induces upregulation of matrix metalloproteinase-9 in astrocytes via MAPK and reactive oxygen species-dependent pathways. *J Neuroinflammation* **9,** 68.

Ramos-Cabrer P, Campos F, Sobrino T & Castillo J. (2011). Targeting the ischemic penumbra. *Stroke* **42,** S7-11.

Ray R & Shah AM. (2005). NADPH oxidase and endothelial cell function. *Clin Sci (Lond)* **109,** 217-226.

Reinecke S, Lutzenburg M, Hagemann G, Bruehl C, Neumann-Haefelin T & Witte OW. (1999). Electrophysiological transcortical diaschisis after middle cerebral artery occlusion (MCAO) in rats. *Neurosci Lett* **261,** 85-88.

Reinehr R, Gorg B, Becker S, Qvartskhava N, Bidmon HJ, Selbach O, Haas HL, Schliess F & Haussinger D. (2007). Hypoosmotic swelling and ammonia increase oxidative stress by NADPH oxidase in cultured astrocytes and vital brain slices. *Glia* **55,** 758-771.

Reisman SA, Yeager RL, Yamamoto M & Klaassen CD. (2009). Increased Nrf2 activation in livers from Keap1-knockdown mice increases expression of cytoprotective genes that detoxify electrophiles more than those that detoxify reactive oxygen species. *Toxicol Sci* **108,** 35-47.

Ren J, Fan C, Chen N, Huang J & Yang Q. (2011). Resveratrol pretreatment attenuates cerebral ischemic injury by upregulating expression of transcription factor Nrf2 and HO-1 in rats. *Neurochem Res* **36,** 2352-2362.

Rhee SG, Kang SW, Chang TS, Jeong W & Kim K. (2001). Peroxiredoxin, a novel family of peroxidases. *IUBMB Life* **52,** 35-41.

Rhee SG, Yang KS, Kang SW, Woo HA & Chang TS. (2005). Controlled elimination of intracellular H(2)O(2): regulation of peroxiredoxin, catalase, and glutathione peroxidase via post-translational modification. *Antioxid Redox Signal* **7,** 619-626.

Ribatti D, Nico B, Crivellato E & Artico M. (2006). Development of the blood-brain barrier: a historical point of view. *Anat Rec B New Anat* **289,** 3-8.

Richmon JD, Fukuda K, Maida N, Sato M, Bergeron M, Sharp FR, Panter SS & Noble LJ. (1998). Induction of heme oxygenase-1 after hyperosmotic opening of the blood-brain barrier. *Brain Res* **780,** 108-118.

Rizzardi AE, Johnson AT, Vogel RI, Pambuccian SE, Henriksen J, Skubitz AP, Metzger GJ & Schmechel SC. (2012). Quantitative comparison of immunohistochemical staining measured by digital image analysis versus pathologist visual scoring. *Diagn Pathol* **7,** 42.

Robertson CA, McCabe C, Gallagher L, Lopez-Gonzalez Mdel R, Holmes WM, Condon B, Muir KW, Santosh C & Macrae IM. (2011). Stroke penumbra defined by an MRI-based oxygen challenge technique: 1. Validation using [14C]2-deoxyglucose autoradiography. *J Cereb Blood Flow Metab* **31,** 1778-1787.

Rosenthal RE, Hamud F, Fiskum G, Varghese PJ & Sharpe S. (1987). Cerebral ischemia and reperfusion: prevention of brain mitochondrial injury by lidoflazine. *J Cereb Blood Flow Metab* **7,** 752-758.

Ross D, Kepa JK, Winski SL, Beall HD, Anwar A & Siegel D. (2000). NAD(P)H:quinone oxidoreductase 1 (NQO1): chemoprotection, bioactivation, gene regulation and genetic polymorphisms. *Chem Biol Interact* **129,** 77-97.

Rothwell PM, Algra A & Amarenco P. (2011). Medical treatment in acute and long-term secondary prevention after transient ischaemic attack and ischaemic stroke. *Lancet* **377,** 1681-1692.

Rothwell PM, Coull AJ, Giles MF, Howard SC, Silver LE, Bull LM, Gutnikov SA, Edwards P, Mant D, Sackley CM, Farmer A, Sandercock PA, Dennis MS, Warlow CP, Bamford JM, Anslow P & Oxford Vascular S. (2004). Change in stroke incidence, mortality, case-fatality, severity, and risk factors in Oxfordshire, UK from 1981 to 2004 (Oxford Vascular Study). *Lancet* **363,** 1925-1933.

Ruetzler CA, Furuya K, Takeda H & Hallenbeck JM. (2001). Brain vessels normally undergo cyclic activation and inactivation: evidence from tumor necrosis factor-alpha, heme oxygenase-1, and manganese superoxide dismutase immunostaining of vessels and perivascular brain cells. *J Cereb Blood Flow Metab* **21,** 244-252.

Rushmore TH, Morton MR & Pickett CB. (1991). The antioxidant responsive element. Activation by oxidative stress and identification of the DNA consensus sequence required for functional activity. *J Biol Chem* **266,** 11632-11639.

Ryter SW, Alam J & Choi AM. (2006). Heme oxygenase-1/carbon monoxide: from basic science to therapeutic applications. *Physiol Rev* **86,** 583-650.

Sa-Pereira I, Brites D & Brito MA. (2012). Neurovascular unit: a focus on pericytes. *Mol Neurobiol* **45,** 327-347.

Sacco RL, Kasner SE, Broderick JP, Caplan LR, Connors JJ, Culebras A, Elkind MS, George MG, Hamdan AD, Higashida RT, Hoh BL, Janis LS, Kase CS, Kleindorfer DO, Lee JM, Moseley ME, Peterson ED, Turan TN, Valderrama AL, Vinters HV, American Heart Association Stroke Council CoCS, Anesthesia, Council on Cardiovascular R, Intervention, Council on C, Stroke N, Council on E, Prevention, Council on Peripheral Vascular D, Council on Nutrition PA & Metabolism. (2013). An updated definition of stroke for the 21st century: a statement for healthcare professionals from the American Heart Association/American Stroke Association. *Stroke* **44,** 2064-2089.

Sacco RL, Wolf PA & Gorelick PB. (1999). Risk factors and their management for stroke prevention: outlook for 1999 and beyond. *Neurology* **53,** S15-24.

Sachdeva MM, Cano M & Handa JT. (2014). Nrf2 signaling is impaired in the aging RPE given an oxidative insult. *Experimental eye research* **119,** 111-114.

Saha S, Hollands W, Teucher B, Needs PW, Narbad A, Ortori CA, Barrett DA, Rossiter JT, Mithen RF & Kroon PA. (2012). Isothiocyanate concentrations and interconversion of sulforaphane to erucin in human subjects after consumption of commercial frozen broccoli compared to fresh broccoli. *Molecular nutrition & food research* **56,** 1906-1916.

Saka O, McGuire A & Wolfe C. (2009). Cost of stroke in the United Kingdom. *Age Ageing* **38,** 27-32.

Sakoda E, Igarashi K, Sun J, Kurisu K & Tashiro S. (2008). Regulation of heme oxygenase-1 by transcription factor Bach1 in the mouse brain. *Neurosci Lett* **440,** 160-165.

Saleem S, Zhuang H, Biswal S, Christen Y & Dore S. (2008). Ginkgo biloba extract neuroprotective action is dependent on heme oxygenase 1 in ischemic reperfusion brain injury. *Stroke* **39,** 3389-3396.

Satoh T, Okamoto SI, Cui J, Watanabe Y, Furuta K, Suzuki M, Tohyama K & Lipton SA. (2006). Activation of the Keap1/Nrf2 pathway for neuroprotection by electrophilic [correction of electrophillic] phase II inducers. *Proc Natl Acad Sci U S A* **103,** 768-773.

Schinkel AH, Smit JJ, van Tellingen O, Beijnen JH, Wagenaar E, van Deemter L, Mol CA, van der Valk MA, Robanus-Maandag EC, te Riele HP & et al. (1994). Disruption of the mouse mdr1a P-glycoprotein gene leads to a deficiency in the blood-brain barrier and to increased sensitivity to drugs. *Cell* **77,** 491-502.

Schneider A, Martin-Villalba A, Weih F, Vogel J, Wirth T & Schwaninger M. (1999). NF-kappaB is activated and promotes cell death in focal cerebral ischemia. *Nat Med* **5,** 554-559.

Schreck R, Albermann K & Baeuerle PA. (1992). Nuclear factor kappa B: an oxidative stress-responsive transcription factor of eukaryotic cells (a review). *Free radical research communications* **17,** 221-237.

Schreibelt G, van Horssen J, Haseloff RF, Reijerkerk A, van der Pol SM, Nieuwenhuizen O, Krause E, Blasig IE, Dijkstra CD, Ronken E & de Vries HE. (2008). Protective effects of peroxiredoxin-1 at the injured blood-brain barrier. *Free Radic Biol Med* **45,** 256-264.

Schulz JB, Lindenau J, Seyfried J & Dichgans J. (2000). Glutathione, oxidative stress and neurodegeneration. *Eur J Biochem* **267,** 4904-4911.

Semenza GL. (2000). HIF-1: mediator of physiological and pathophysiological responses to hypoxia. *J Appl Physiol (1985)* **88,** 1474-1480.

Semenza GL. (2003a). Angiogenesis in ischemic and neoplastic disorders. *Annu Rev Med* **54,** 17-28.

Semenza GL. (2003b). Targeting HIF-1 for cancer therapy. *Nat Rev Cancer* **3,** 721-732.

Semenza GL, Agani F, Booth G, Forsythe J, Iyer N, Jiang BH, Leung S, Roe R, Wiener C & Yu A. (1997). Structural and functional analysis of hypoxia-inducible factor 1. *Kidney Int* **51,** 553-555.

Senft AP, Dalton TP & Shertzer HG. (2000). Determining glutathione and glutathione disulfide using the fluorescence probe o-phthalaldehyde. *Anal Biochem* **280,** 80-86.

Seng S, Avraham HK, Birrane G, Jiang S, Li H, Katz G, Bass CE, Zagozdzon R & Avraham S. (2009). NRP/B mutations impair Nrf2-dependent NQO1 induction in human primary brain tumors. *Oncogene* **28,** 378-389.

Sermet A, Tasdemir N, Deniz B & Atmaca M. (2000). Time-dependent changes in superoxide dismutase, catalase, xanthine dehydrogenase and oxidase activities in focal cerebral ischaemia. *Cytobios* **102,** 157-172.

Shah ZA, Li RC, Ahmad AS, Kensler TW, Yamamoto M, Biswal S & Dore S. (2010). The flavanol (-)-epicatechin prevents stroke damage through the Nrf2/HO1 pathway. *J Cereb Blood Flow Metab* **30,** 1951-1961.

Shah ZA, Li RC, Thimmulappa RK, Kensler TW, Yamamoto M, Biswal S & Dore S. (2007). Role of reactive oxygen species in modulation of Nrf2 following ischemic reperfusion injury. *Neuroscience* **147,** 53-59.

Shah ZA, Nada SE & Dore S. (2011). Heme oxygenase 1, beneficial role in permanent ischemic stroke and in Gingko biloba (EGb 761) neuroprotection. *Neuroscience* **180,** 248-255.

Shan Y, Lambrecht RW, Donohue SE & Bonkovsky HL. (2006). Role of Bach1 and Nrf2 in up-regulation of the heme oxygenase-1 gene by cobalt protoporphyrin. *FASEB J* **20,** 2651-2653.

Shapiro AL, Vinuela E & Maizel JV, Jr. (1967). Molecular weight estimation of polypeptide chains by electrophoresis in SDS-polyacrylamide gels. *Biochem Biophys Res Commun* **28,** 815-820.

Shen KK, Ji LL, Chen Y, Yu QM & Wang ZT. (2011a). Influence of glutathione levels and activity of glutathione-related enzymes in the brains of tumor-bearing mice. *Biosci Trends* **5,** 30-37.

Shen XD, Ke B, Uchida Y, Ji H, Gao F, Zhai Y, Busuttil RW & Kupiec-Weglinski JW. (2011b). Native macrophages genetically modified to express heme oxygenase 1 protect rat liver transplants from ischemia/reperfusion injury. *Liver Transpl* **17,** 201-210.

Shenvi SV, Smith E & Hagen TM. (2012). Identification of age-specific Nrf2 binding to a novel antioxidant response element locus in the Gclc promoter: a compensatory means for the loss of glutathione synthetic capacity in the aging rat liver? *Aging Cell* **11,** 297-304.

Shichita T, Hasegawa E, Kimura A, Morita R, Sakaguchi R, Takada I, Sekiya T, Ooboshi H, Kitazono T, Yanagawa T, Ishii T, Takahashi H, Mori S, Nishibori M, Kuroda K, Akira S, Miyake K & Yoshimura A. (2012a). Peroxiredoxin family proteins are key initiators of post-ischemic inflammation in the brain. *Nat Med* **18,** 911-917.

Shichita T, Sakaguchi R, Suzuki M & Yoshimura A. (2012b). Post-ischemic inflammation in the brain. *Front Immunol* **3,** 132.

Shih AY, Li P & Murphy TH. (2005). A small-molecule-inducible Nrf2-mediated antioxidant response provides effective prophylaxis against cerebral ischemia in vivo. *J Neurosci* **25,** 10321-10335.

Shivakumar BR, Kolluri SV & Ravindranath V. (1995). Glutathione and protein thiol homeostasis in brain during reperfusion after cerebral ischemia. *J Pharmacol Exp Ther* **274,** 1167-1173.

Shohami E, Beit-Yannai E, Horowitz M & Kohen R. (1997). Oxidative stress in closed-head injury: brain antioxidant capacity as an indicator of functional outcome. *J Cereb Blood Flow Metab* **17,** 1007-1019.

Siegel D, Yan C & Ross D. (2012). NAD(P)H:quinone oxidoreductase 1 (NQO1) in the sensitivity and resistance to antitumor quinones. *Biochem Pharmacol* **83,** 1033-1040.

Siow RC & Mann GE. (2010). Dietary isoflavones and vascular protection: activation of cellular antioxidant defenses by SERMs or hormesis? *Mol Aspects Med* **31,** 468-477.

Siow RC, Richards JP, Pedley KC, Leake DS & Mann GE. (1999a). Vitamin C protects human vascular smooth muscle cells against apoptosis induced by moderately oxidized LDL containing high levels of lipid hydroperoxides. *Arterioscler Thromb Vasc Biol* **19,** 2387-2394.

Siow RC, Sato H & Mann GE. (1999b). Heme oxygenase-carbon monoxide signalling pathway in atherosclerosis: anti-atherogenic actions of bilirubin and carbon monoxide? *Cardiovasc Res* **41,** 385-394.

Smith PK, Krohn RI, Hermanson GT, Mallia AK, Gartner FH, Provenzano MD, Fujimoto EK, Goeke NM, Olson BJ & Klenk DC. (1985). Measurement of protein using bicinchoninic acid. *Anal Biochem* **150,** 76-85.

Soane L, Li Dai W, Fiskum G & Bambrick LL. (2010). Sulforaphane protects immature hippocampal neurons against death caused by exposure to hemin or to oxygen and glucose deprivation. *J Neurosci Res* **88,** 1355-1363.

Sokoloff L, Mangold R, Wechsler RL, Kenney C & Kety SS. (1955). The effect of mental arithmetic on cerebral circulation and metabolism. *J Clin Invest* **34,** 1101-1108.

Solenski NJ, diPierro CG, Trimmer PA, Kwan AL & Helm GA. (2002). Ultrastructural changes of neuronal mitochondria after transient and permanent cerebral ischemia. *Stroke* **33,** 816-824.

Son TG, Camandola S, Arumugam TV, Cutler RG, Telljohann RS, Mughal MR, Moore TA, Luo W, Yu QS, Johnson DA, Johnson JA, Greig NH & Mattson MP. (2010). Plumbagin, a novel Nrf2/ARE activator, protects against cerebral ischemia. *J Neurochem* **112,** 1316-1326.

Song HY, Ju SM, Seo WY, Goh AR, Lee JK, Bae YS, Choi SY & Park J. (2011). Nox2-based NADPH oxidase mediates HIV-1 Tat-induced up-regulation of VCAM-1/ICAM-1 and subsequent monocyte adhesion in human astrocytes. *Free Radic Biol Med* **50,** 576-584.

Song W, Huo T, Guo F, Wang H, Wei H, Yang Q, Dong H, Wang Q & Xiong L. (2013). Globular adiponectin elicits neuroprotection by inhibiting NADPH oxidase-mediated oxidative damage in ischemic stroke. *Neuroscience* **248C,** 136-144.

Srivastava S, Alfieri A, Siow RC, Mann GE & Fraser PA. (2013). Temporal and spatial distribution of Nrf2 in rat brain following stroke: quantification of nuclear to cytoplasmic Nrf2 content using a novel immunohistochemical technique. *J Physiol* **591,** 3525-3538.

Stagliano NE, Perez-Pinzon MA, Moskowitz MA & Huang PL. (1999). Focal ischemic preconditioning induces rapid tolerance to middle cerebral artery occlusion in mice. *J Cereb Blood Flow Metab* **19,** 757-761.

Stamatovic SM, Keep RF & Andjelkovic AV. (2008). Brain endothelial cell-cell junctions: how to "open" the blood brain barrier. *Curr Neuropharmacol* **6,** 179-192.

Stanimirovic DB & Friedman A. (2012). Pathophysiology of the neurovascular unit: disease cause or consequence? *J Cereb Blood Flow Metab* **32,** 1207-1221.

Steele ML, Fuller S, Patel M, Kersaitis C, Ooi L & Munch G. (2013). Effect of Nrf2 activators on release of glutathione, cysteinylglycine and homocysteine by human U373 astroglial cells. *Redox Biol* **1,** 441-445.

Stephenson D, Yin T, Smalstig EB, Hsu MA, Panetta J, Little S & Clemens J. (2000). Transcription factor nuclear factor-kappa B is activated in neurons after focal cerebral ischemia. *J Cereb Blood Flow Metab* **20,** 592-603.

Stoewsand GS. (1995). Bioactive organosulfur phytochemicals in Brassica oleracea vegetables--a review. *Food Chem Toxicol* **33,** 537-543.

Stringer JL, Gaikwad A, Gonzales BN, Long DJ, Jr., Marks LM & Jaiswal AK. (2004). Presence and induction of the enzyme NAD(P)H: quinone oxidoreductase 1 in the central nervous system. *J Comp Neurol* **471,** 289-297.

Suh JH, Shenvi SV, Dixon BM, Liu H, Jaiswal AK, Liu RM & Hagen TM. (2004). Decline in transcriptional activity of Nrf2 causes age-related loss of glutathione synthesis, which is reversible with lipoic acid. *Proc Natl Acad Sci U S A* **101,** 3381-3386.

Sukumari-Ramesh S, Laird MD, Singh N, Vender JR, Alleyne CH, Jr. & Dhandapani KM. (2010). Astrocyte-derived glutathione attenuates hemin-induced apoptosis in cerebral microvascular cells. *Glia* **58,** 1858-1870.

Sumi M, Tateishi N, Shibata H, Ohki T & Sata M. (2013). Quercetin glucosides promote ischemia-induced angiogenesis, but do not promote tumor growth. *Life Sci*.

Sun Z, Wu T, Zhao F, Lau A, Birch CM & Zhang DD. (2011). KPNA6 (Importin {alpha}7)-mediated nuclear import of Keap1 represses the Nrf2-dependent antioxidant response. *Mol Cell Biol* **31,** 1800-1811.

Sun Z, Zhang S, Chan JY & Zhang DD. (2007). Keap1 controls postinduction repression of the Nrf2-mediated antioxidant response by escorting nuclear export of Nrf2. *Mol Cell Biol* **27,** 6334-6349.

Sutherland BA, Rahman RM, Clarkson AN, Shaw OM, Nair SM & Appleton I. (2009). Cerebral heme oxygenase 1 and 2 spatial distribution is modulated following injury from hypoxia-ischemia and middle cerebral artery occlusion in rats. *Neurosci Res* **65,** 326-334.

Taguchi K, Motohashi H & Yamamoto M. (2011). Molecular mechanisms of the Keap1-Nrf2 pathway in stress response and cancer evolution. *Genes Cells* **16,** 123-140.

Takahashi S, Takahashi Y, Yoshimi T & Miura T. (1998). Oxygen tension regulates heme oxygenase-1 gene expression in mammalian cell lines. *Cell Biochem Funct* **16,** 183-193.

Takeda K, Lin J, Okubo S, Akazawa-Kudoh S, Kajinami K, Kanemitsu S, Tsugawa H, Kanda T, Matsui S & Takekoshi N. (2004). Transient glucose deprivation causes upregulation of heme oxygenase-1 and cyclooxygenase-2 expression in cardiac fibroblasts. *J Mol Cell Cardiol* **36,** 821-830.

Takuwa H, Tajima Y, Kokuryo D, Matsuura T, Kawaguchi H, Masamoto K, Taniguchi J, Ikoma Y, Seki C, Aoki I, Tomita Y, Suzuki N, Kanno I & Ito H. (2013). Hemodynamic changes during neural deactivation in awake mice: A measurement by laser-Doppler flowmetry in crossed cerebellar diaschisis. *Brain Res*.

Tanaka N, Ikeda Y, Ohta Y, Deguchi K, Tian F, Shang J, Matsuura T & Abe K. (2011). Expression of Keap1-Nrf2 system and antioxidative proteins in mouse brain after transient middle cerebral artery occlusion. *Brain Res* **1370,** 246-253.

Tao RR, Wang H, Hong LJ, Huang JY, Lu YM, Liao MH, Ye WF, Lu NN, Zhu DY, Huang Q, Fukunaga K, Lou YJ, Shoji I, Wilcox CS, Lai EY & Han F. (2013). Nitrosative stress induces peroxiredoxin 1 ubiquitination during ischemic insult via E6AP activation in endothelial cells both in vitro and in vivo. *Antioxid Redox Signal*.

Thimmulappa RK, Mai KH, Srisuma S, Kensler TW, Yamamoto M & Biswal S. (2002). Identification of Nrf2-regulated genes induced by the chemopreventive agent sulforaphane by oligonucleotide microarray. *Cancer Res* **62,** 5196-5203.

Tiede LM, Cook EA, Morsey B & Fox HS. (2011). Oxygen matters: tissue culture oxygen levels affect mitochondrial function and structure as well as responses to HIV viroproteins. *Cell Death Dis* **2,** e246.

Todd NV, Picozzi P, Crockard HA & Russell RR. (1986). Reperfusion after cerebral ischemia: influence of duration of ischemia. *Stroke* **17,** 460-466.

Tontsch U & Bauer HC. (1991). Glial cells and neurons induce blood-brain barrier related enzymes in cultured cerebral endothelial cells. *Brain Res* **539,** 247-253.

Toyokuni S, Tanaka T, Hattori Y, Nishiyama Y, Yoshida A, Uchida K, Hiai H, Ochi H & Osawa T. (1997). Quantitative immunohistochemical determination of 8-hydroxy-2'-deoxyguanosine by a monoclonal antibody N45.1: its application to ferric nitrilotriacetate-induced renal carcinogenesis model. *Lab Invest* **76,** 365-374.

Travis LH, Flemming KD, Brown RD, Jr., Meissner I, McClelland RL & Weigand SD. (2003). Awareness of stroke risk factors, symptoms, and treatment is poor in people at highest risk. *J Stroke Cerebrovasc Dis* **12,** 221-227.

Turrens JF. (1997). Superoxide production by the mitochondrial respiratory chain. *Biosci Rep* **17,** 3-8.

Ungvari Z, Bailey-Downs L, Sosnowska D, Gautam T, Koncz P, Losonczy G, Ballabh P, de Cabo R, Sonntag WE & Csiszar A. (2011). Vascular oxidative stress in aging: a homeostatic failure due to dysregulation of NRF2-mediated antioxidant response. *American journal of physiology Heart and circulatory physiology* **301,** H363-372.

Valcarcel-Ares MN, Gautam T, Warrington JP, Bailey-Downs L, Sosnowska D, de Cabo R, Losonczy G, Sonntag WE, Ungvari Z & Csiszar A. (2012). Disruption of Nrf2 signaling impairs angiogenic capacity of endothelial cells: implications for microvascular aging. *The journals of gerontology Series A, Biological sciences and medical sciences* **67,** 821-829.

Valko M, Leibfritz D, Moncol J, Cronin MT, Mazur M & Telser J. (2007). Free radicals and antioxidants in normal physiological functions and human disease. *Int J Biochem Cell Biol* **39,** 44-84.

Vallet P, Charnay Y, Steger K, Ogier-Denis E, Kovari E, Herrmann F, Michel JP & Szanto I. (2005). Neuronal expression of the NADPH oxidase NOX4, and its regulation in mouse experimental brain ischemia. *Neuroscience* **132,** 233-238.

Vandesompele J, De Preter K, Pattyn F, Poppe B, Van Roy N, De Paepe A & Speleman F. (2002). Accurate normalization of real-time quantitative RT-PCR data by geometric averaging of multiple internal control genes. *Genome Biol* **3,** RESEARCH0034.

Vauzour D, Buonfiglio M, Corona G, Chirafisi J, Vafeiadou K, Angeloni C, Hrelia S, Hrelia P & Spencer JP. (2010). Sulforaphane protects cortical neurons against 5-S-cysteinyl-dopamine-induced toxicity through the activation of ERK1/2, Nrf-2 and the upregulation of detoxification enzymes. *Mol Nutr Food Res* **54,** 532-542.

Velichkova M & Hasson T. (2005). Keap1 regulates the oxidation-sensitive shuttling of Nrf2 into and out of the nucleus via a Crm1-dependent nuclear export mechanism. *Mol Cell Biol* **25,** 4501-4513.

Vermes I, Haanen C, Steffens-Nakken H & Reutelingsperger C. (1995). A novel assay for apoptosis. Flow cytometric detection of phosphatidylserine expression on early apoptotic cells using fluorescein labelled Annexin V. *J Immunol Methods* **184,** 39-51.

Vermeulen M, Klopping-Ketelaars IW, van den Berg R & Vaes WH. (2008). Bioavailability and kinetics of sulforaphane in humans after consumption of cooked versus raw broccoli. *J Agric Food Chem* **56,** 10505-10509.

Vivancos PD, Dong Y, Ziegler K, Markovic J, Pallardo FV, Pellny TK, Verrier PJ & Foyer CH. (2010). Recruitment of glutathione into the nucleus during cell proliferation adjusts whole-cell redox homeostasis in Arabidopsis thaliana and lowers the oxidative defence shield. *Plant J* **64,** 825-838.

von Lohneysen K, Noack D, Wood MR, Friedman JS & Knaus UG. (2010). Structural insights into Nox4 and Nox2: motifs involved in function and cellular localization. *Mol Cell Biol* **30,** 961-975.

Wagner AE, Boesch-Saadatmandi C, Dose J, Schultheiss G & Rimbach G. (2012). Anti-inflammatory potential of allyl-isothiocyanate--role of Nrf2, NF-(kappa) B and microRNA-155. *J Cell Mol Med* **16,** 836-843.

Wakabayashi N, Dinkova-Kostova AT, Holtzclaw WD, Kang MI, Kobayashi A, Yamamoto M, Kensler TW & Talalay P. (2004). Protection against electrophile and oxidant stress by induction of the phase 2 response: fate of cysteines of the Keap1 sensor modified by inducers. *Proc Natl Acad Sci U S A* **101,** 2040-2045.

Wakabayashi N, Itoh K, Wakabayashi J, Motohashi H, Noda S, Takahashi S, Imakado S, Kotsuji T, Otsuka F, Roop DR, Harada T, Engel JD & Yamamoto M. (2003). Keap1-null mutation leads to postnatal lethality due to constitutive Nrf2 activation. *Nat Genet* **35,** 238-245.

Wang B, Zhu X, Kim Y, Li J, Huang S, Saleem S, Li RC, Xu Y, Dore S & Cao W. (2012). Histone deacetylase inhibition activates transcription factor Nrf2 and protects against cerebral ischemic damage. *Free Radic Biol Med* **52,** 928-936.

Wang H, Liu K, Geng M, Gao P, Wu X, Hai Y, Li Y, Li Y, Luo L, Hayes JD, Wang XJ & Tang X. (2013a). RXRalpha inhibits the NRF2-ARE signaling pathway through a direct interaction with the Neh7 domain of NRF2. *Cancer Res* **73,** 3097-3108.

Wang H, Luo M, Li C & Wang G. (2011). Propofol post-conditioning induced long-term neuroprotection and reduced internalization of AMPAR GluR2 subunit in a rat model of focal cerebral ischemia/reperfusion. *J Neurochem* **119,** 210-219.

Wang JJ & Cui P. (2013). Neohesperidin attenuates cerebral ischemia-reperfusion injury via inhibiting the apoptotic pathway and activating the Akt/Nrf2/HO-1 pathway. *J Asian Nat Prod Res*.

Wang W, Wu Y, Zhang G, Fang H, Wang H, Zang H, Xie T & Wang W. (2014). Activation of Nrf2-ARE signal pathway protects the brain from damage induced by epileptic seizure. *Brain Res* **1544,** 54-61.

Wang X, Tsuji K, Lee SR, Ning M, Furie KL, Buchan AM & Lo EH. (2004). Mechanisms of hemorrhagic transformation after tissue plasminogen activator reperfusion therapy for ischemic stroke. *Stroke* **35,** 2726-2730.

Wang YF, Tsirka SE, Strickland S, Stieg PE, Soriano SG & Lipton SA. (1998). Tissue plasminogen activator (tPA) increases neuronal damage after focal cerebral ischemia in wild-type and tPA-deficient mice. *Nat Med* **4,** 228-231.

Wang Z, Wei X, Liu K, Zhang X, Yang F, Zhang H, He Y, Zhu T, Li F, Shi W, Zhang Y, Xu H, Liu J & Yi F. (2013b). NOX2 deficiency ameliorates cerebral injury through reduction of complexin II-mediated glutamate excitotoxicity in experimental stroke. *Free Radic Biol Med* **65,** 942-951.

Watanabe T, Dohgu S, Takata F, Nishioku T, Nakashima A, Futagami K, Yamauchi A & Kataoka Y. (2013). Paracellular barrier and tight junction protein expression in the immortalized brain endothelial cell lines bEND.3, bEND.5 and mouse brain endothelial cell 4. *Biol Pharm Bull* **36,** 492-495.

Wegiel B, Nemeth Z, Correa-Costa M, Bulmer A & Otterbein L. (2013). Heme Oxygenase-1: A Metabolic Nike. *Antioxid Redox Signal*.

Weir NU & Dennis MS. (1997). Meeting the challenge of stroke. *Scott Med J* **42,** 145-147.

Werner C & Engelhard K. (2007). Pathophysiology of traumatic brain injury. *Br J Anaesth* **99,** 4-9.

Wolburg H & Lippoldt A. (2002). Tight junctions of the blood-brain barrier: development, composition and regulation. *Vascul Pharmacol* **38,** 323-337.

Wolf PA. (1985). Risk factors for stroke. *Stroke* **16,** 359-360.

Wondrak GT, Cabello CM, Villeneuve NF, Zhang S, Ley S, Li Y, Sun Z & Zhang DD. (2008). Cinnamoyl-based Nrf2-activators targeting human skin cell photo-oxidative stress. *Free Radic Biol Med* **45,** 385-395.

Woo HA, Yim SH, Shin DH, Kang D, Yu DY & Rhee SG. (2010). Inactivation of peroxiredoxin I by phosphorylation allows localized H(2)O(2) accumulation for cell signaling. *Cell* **140,** 517-528.

Woodfin A, Hu DE, Sarker M, Kurokawa T & Fraser P. (2011). Acute NADPH oxidase activation potentiates cerebrovascular permeability response to bradykinin in ischemia-reperfusion. *Free Radic Biol Med* **50,** 518-524.

Wu J, Li Q, Wang X, Yu S, Li L, Wu X, Chen Y, Zhao J & Zhao Y. (2013). Neuroprotection by curcumin in ischemic brain injury involves the Akt/Nrf2 pathway. *PLoS One* **8,** e59843.

Wu KC, Cui JY & Klaassen CD. (2011a). Beneficial role of Nrf2 in regulating NADPH generation and consumption. *Toxicol Sci* **123,** 590-600.

Wu ML, Ho YC & Yet SF. (2011b). A central role of heme oxygenase-1 in cardiovascular protection. *Antioxid Redox Signal* **15,** 1835-1846.

Wuest DM, Wing AM & Lee KH. (2013). Membrane configuration optimization for a murine in vitro blood-brain barrier model. *J Neurosci Methods* **212,** 211-221.

Xiang J, Alesi GN, Zhou N & Keep RF. (2012). Protective effects of isothiocyanates on blood-CSF barrier disruption induced by oxidative stress. *Am J Physiol Regul Integr Comp Physiol* **303,** R1-7.

Xie R, Li X, Ling Y, Shen C, Wu X, Xu W & Gao X. (2012). Alpha-lipoic acid pre- and post-treatments provide protection against in vitro ischemia-reperfusion injury in cerebral endothelial cells via Akt/mTOR signaling. *Brain Res* **1482,** 81-90.

Xu J, He L, Ahmed SH, Chen SW, Goldberg MP, Beckman JS & Hsu CY. (2000). Oxygen-glucose deprivation induces inducible nitric oxide synthase and nitrotyrosine expression in cerebral endothelial cells. *Stroke* **31,** 1744-1751.

Yamagata K, Tagami M, Nara Y, Mitani M, Kubota A, Fujino H, Numano F, Kato T & Yamori Y. (1997). Astrocyte-conditioned medium induces blood-brain barrier properties in endothelial cells. *Clin Exp Pharmacol Physiol* **24,** 710-713.

Yang C, Zhang X, Fan H & Liu Y. (2009). Curcumin upregulates transcription factor Nrf2, HO-1 expression and protects rat brains against focal ischemia. *Brain Res* **1282,** 133-141.

Yang G, Chan PH, Chen J, Carlson E, Chen SF, Weinstein P, Epstein CJ & Kamii H. (1994). Human copper-zinc superoxide dismutase transgenic mice are highly resistant to reperfusion injury after focal cerebral ischemia. *Stroke* **25,** 165-170.

Yang H, Magilnick N, Lee C, Kalmaz D, Ou X, Chan JY & Lu SC. (2005). Nrf1 and Nrf2 regulate rat glutamate-cysteine ligase catalytic subunit transcription indirectly via NF-kappaB and AP-1. *Mol Cell Biol* **25,** 5933-5946.

Yang J, Shi QD, Song TB, Feng GF, Zang WJ, Zong CH & Chang L. (2013). Vasoactive intestinal peptide increases VEGF expression to promote proliferation of brain vascular endothelial cells via the cAMP/PKA pathway after ischemic insult in vitro. *Peptides*.

Ye L, Dinkova-Kostova AT, Wade KL, Zhang Y, Shapiro TA & Talalay P. (2002). Quantitative determination of dithiocarbamates in human plasma, serum, erythrocytes and urine: pharmacokinetics of broccoli sprout isothiocyanates in humans. *Clin Chim Acta* **316,** 43-53.

You WC, Li W, Zhuang Z, Tang Y, Lu HC, Ji XJ, Shen W, Shi JX & Zhou ML. (2012). Biphasic activation of nuclear factor-kappa B in experimental models of subarachnoid hemorrhage in vivo and in vitro. *Mediators Inflamm* **2012,** 786242.

Zafar KS, Inayat-Hussain SH, Siegel D, Bao A, Shieh B & Ross D. (2006). Overexpression of NQO1 protects human SK-N-MC neuroblastoma cells against dopamine-induced cell death. *Toxicol Lett* **166,** 261-267.

Zhai X, Lin M, Zhang F, Hu Y, Xu X, Li Y, Liu K, Ma X, Tian X & Yao J. (2013). Dietary flavonoid genistein induces Nrf2 and phase II detoxification gene expression via ERKs and PKC pathways and protects against oxidative stress in Caco-2 cells. *Mol Nutr Food Res* **57,** 249-259.

Zhang DD & Hannink M. (2003). Distinct cysteine residues in Keap1 are required for Keap1-dependent ubiquitination of Nrf2 and for stabilization of Nrf2 by chemopreventive agents and oxidative stress. *Mol Cell Biol* **23,** 8137-8151.

Zhang H, Gerson T, Varney ML, Singh RK & Vinogradov SV. (2010). Multifunctional peptide-PEG intercalating conjugates: programmatic of gene delivery to the blood-brain barrier. *Pharm Res* **27,** 2528-2543.

Zhang J, Ohta T, Maruyama A, Hosoya T, Nishikawa K, Maher JM, Shibahara S, Itoh K & Yamamoto M. (2006). BRG1 interacts with Nrf2 to selectively mediate HO-1 induction in response to oxidative stress. *Mol Cell Biol* **26,** 7942-7952.

Zhang Y, Talalay P, Cho CG & Posner GH. (1992). A major inducer of anticarcinogenic protective enzymes from broccoli: isolation and elucidation of structure. *Proc Natl Acad Sci U S A* **89,** 2399-2403.

Zhang Y & Tang L. (2007). Discovery and development of sulforaphane as a cancer chemopreventive phytochemical. *Acta Pharmacol Sin* **28,** 1343-1354.

Zhao J, Kobori N, Aronowski J & Dash PK. (2006). Sulforaphane reduces infarct volume following focal cerebral ischemia in rodents. *Neurosci Lett* **393,** 108-112.

Zhao J, Moore AN, Redell JB & Dash PK. (2007a). Enhancing expression of Nrf2-driven genes protects the blood brain barrier after brain injury. *J Neurosci* **27,** 10240-10248.

Zhao J, Yu S, Zheng W, Feng G, Luo G, Wang L & Zhao Y. (2010). Curcumin improves outcomes and attenuates focal cerebral ischemic injury via antiapoptotic mechanisms in rats. *Neurochem Res* **35,** 374-379.

Zhao X, Sun G, Zhang J, Strong R, Dash PK, Kan YW, Grotta JC & Aronowski J. (2007b). Transcription factor Nrf2 protects the brain from damage produced by intracerebral hemorrhage. *Stroke* **38,** 3280-3286.

Zhu J, Aja S, Kim EK, Park MJ, Ramamurthy S, Jia J, Hu X, Geng P & Ronnett GV. (2012). Physiological oxygen level is critical for modeling neuronal metabolism in vitro. *J Neurosci Res* **90,** 422-434.

Zlokovic BV. (2008). The blood-brain barrier in health and chronic neurodegenerative disorders. *Neuron* **57,** 178-201.

Appendix

Appendix 1 – Components of cell culture medium

High glucose with phenol red DMEM, D5671, Sigma UK

Inorganic Salts	**mM**
CaCl2	0.2
Fe(NO3)3 • 9H2O	0.0001
MgSO4	0.09767
KCl	0.4
NaHCO3	0.37
NaCl	6.4
NaH2PO4	0.109
Amino Acids	
L-Alanyl-L-Glutamine	-
L-Arginine • HCl	0.084
L-Cysteine • 2HCl	0.626
L-Glutamine	-
Glycine	0.03
L-Histidine • HCl • H2O	0.042
L-Isoleucine	0.105
L-Leucine	0.105
L-Lysine • HCl	0.146
L-Methionine	0.03
L-Phenylalanine	0.066
L-Serine	0.042
L-Threonine	0.095
L-Tryptophan	0.016
L-Tyrosine • 2Na • 2H2O	0.10379
L-Valine	0.094

Vitamins	**mM**
Choline Chloride	0.004
Folic Acid	0.004
myo-Inositol	0.0072
Niacinamide	0.004
D-Pantothenic Acid • 1⁄2Ca	0.004
Pyridoxal • HCl	-
Pyridoxine • HCl	0.00404
Riboflavin	0.0004
Thiamine • HCl	0.004
Other	
D-Glucose	4.5
HEPES	-
Phenol Red • Na	0.0159
Pyruvic Acid • Na	

Low glucose, phenol red free DMEM, D5921, Sigma, UK

Inorganic Salts	**mM**
CaCl2	0.265
Fe(NO3)3 • 9H2O	0.0001
MgSO4	0.09767
KCl	0.4
NaHCO3	0.37
NaCl	6.4
NaH2PO4	0.109
Amino Acids	
L-Alanyl-L-Glutamine	-
L-Arginine • HCl	0.084
L-Cysteine • 2HCl	0.626
L-Glutamine	-
Glycine	0.03
L-Histidine • HCl • H2O	0.042
L-Isoleucine	0.105
L-Leucine	0.105
L-Lysine • HCl	0.146
L-Methionine	0.03
L-Phenylalanine	0.066
L-Serine	0.042
L-Threonine	0.095
L-Tryptophan	0.016
L-Tyrosine • 2Na • 2H2O	0.12037
L-Valine	0.094

Vitamins	**mM**
Choline Chloride	0.004
Folic Acid	0.004
myo-Inositol	0.0072
Niacinamide	0.004
D-Pantothenic Acid • 1⁄2Ca	0.004
Pyridoxal • HCl	-
Pyridoxine • HCl	0.00404
Riboflavin	0.0004
Thiamine • HCl	0.004
Other	
D-Glucose	4.5
HEPES	-
Phenol Red • Na	0.0159
Pyruvic Acid • Na	

Appendix 2 – Composition of SDS-PAGE

Resolving gel:

Reagent	8% (x2)	10% (x2)	12% (x2)	13% (x2)	Final con.
4xTris-SDS pH 8.8 (mL)	4.8	4.8	4.8	4.8	1x (375mM Tris0.1% SDS)
30% Acrylamide (mL)	5.12	6.4	7.68	8.32	13, 12, 10 or 8%, respectively
dd H2O (mL)	9.28	8	6.72	6.08	
10% APS *(µL)	70	70	70	70	0.04%
TEMED *(µL)	15	15	15	15	0.08%

* Toxic- use in hood

Stacking gel:

Reagent	Amount	Final Concentration
4xTris-SDS pH 8.8 (mL)	2	1x (375mM Tris 0.1% SDS)
30% Acrylamide (mL)	1.04	4%
dd H2O (mL)	4.88	
10% APS *(µL)	40	0.05%
TEMED *(µL)	5	0.06%

Appendix 3 – Composition of transfer buffer for SDS-PAGE

Reagent	**Concentration**	**Amount required for 500 mL**
Tris Base	25 mM	1.5g
Glycine	192 mM	7.2g
Methanol	-	100 mL
ddH2O	-	400 mL

Appendix 4 – Control staining in brain sections

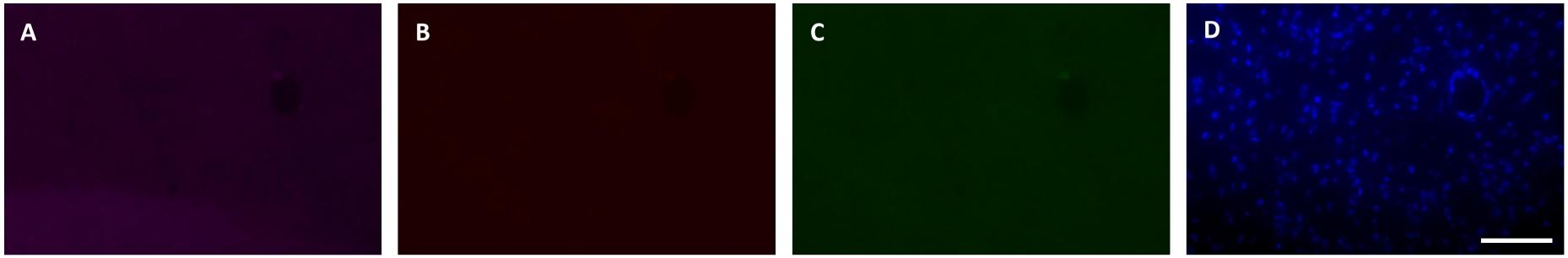

Negative control staining of brain sections. Coronal 10µm brain sections were incubated with donkey anti rabbit or donkey anti goat (**A**) Cy5, (**B**) Alexa 555 and (**C**) Alexa 488 fluorescent secondary antibodies for 1 hour at room temperature. Brain sections were washed and a coverslip applied using vectashield mounting medium with DAPI (**D**). Brain Sections were visualised using a Nikon diaphot microscope adapted for fluorescence. Scale bar represents 10µm.

Appendix 5 – Neurological score in rats following MCAo

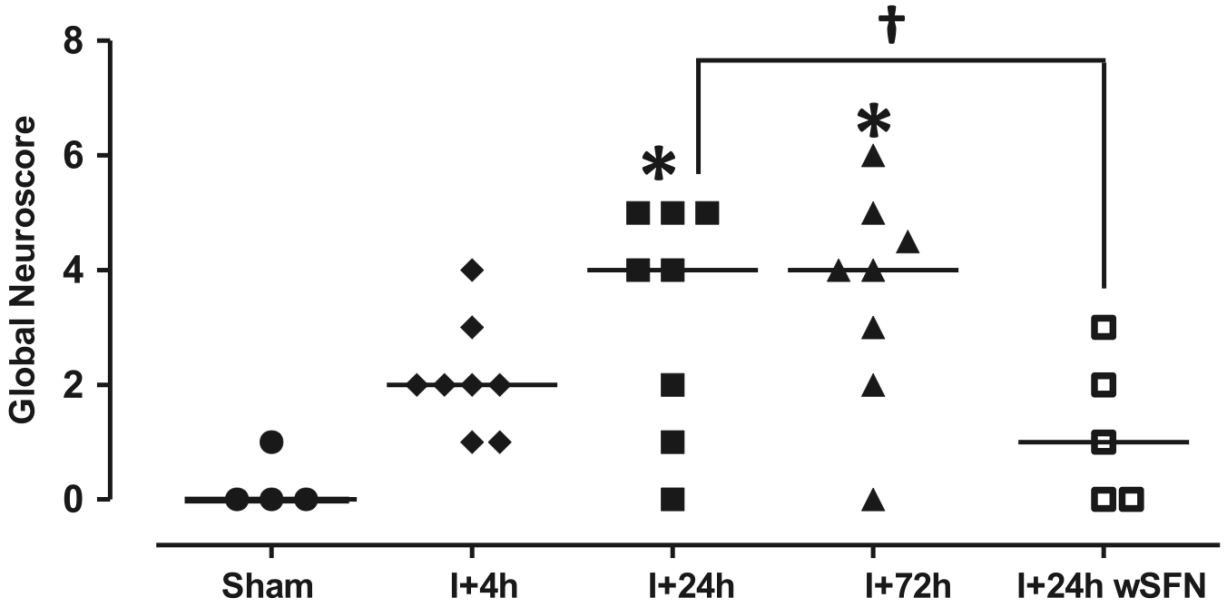

Sulforaphane pre-treatment of rats attenuates neurological dysfunction after MCAo. Neurological dysfunction was measured in sham rats, in rats subjected to 70 min MCAo and 4h (I+4h), 24h (I+24h) and 72h (I+72h) reperfusion, and in rats pre-treated with sulforaphane (5 mg/kg *i.p.*) for 1h before 70 min MCAo and 24h reperfusion (I+24h wSFN). Neurological dysfunction is increases following 24h and 72h reperfusion, however, neurological dysfunction is reduced in SFN pre-treated animals. n= 4-8 animals, * $P<0.05$ vs Sham; † $P<0.05$ I+24h. Figure taken from (Alfieri *et al.*, 2013).

Appendix 6 – Effects of sulforaphane treatment on mRNA levels of Nrf2 regulated genes

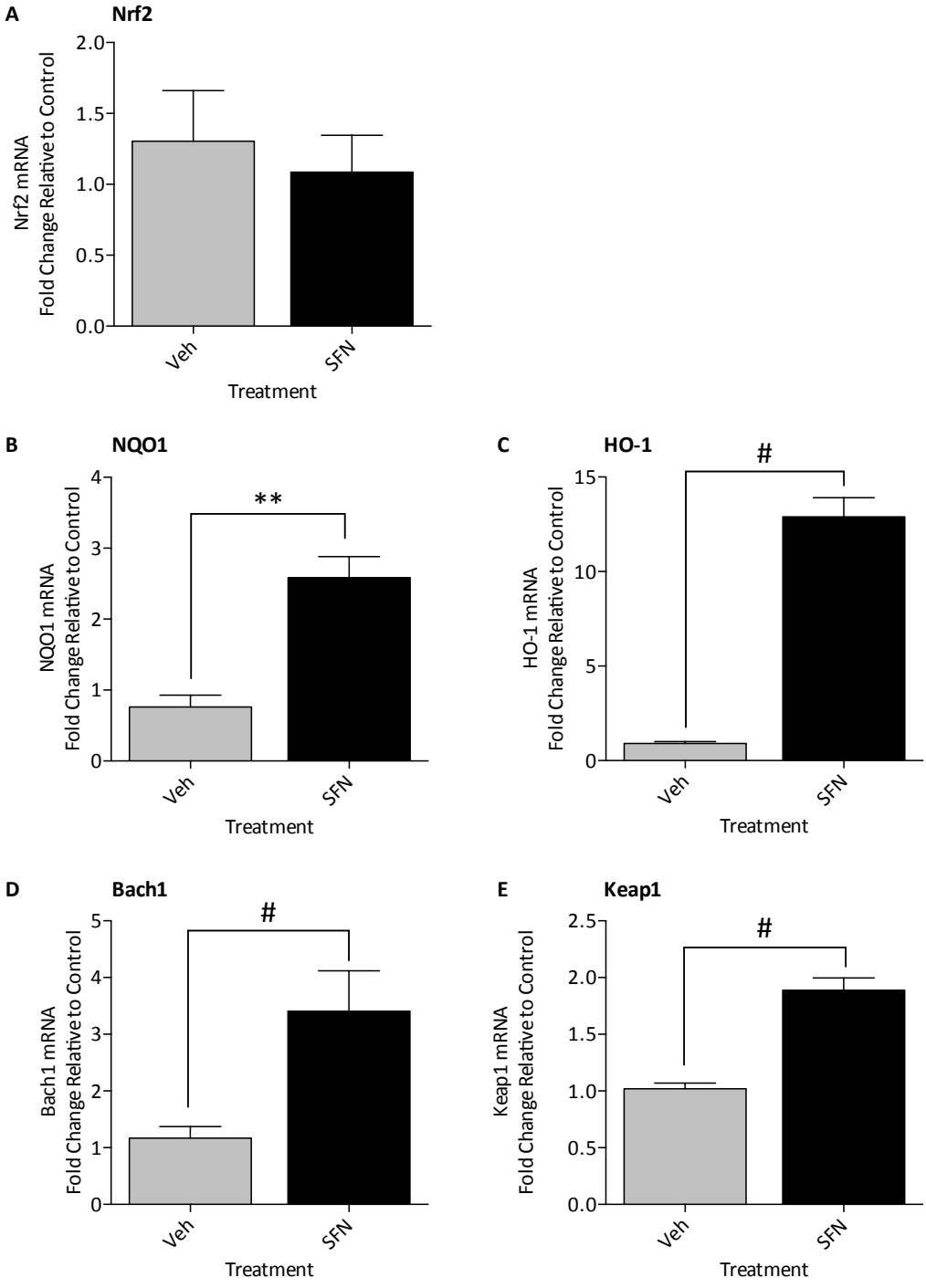

Confluent monolayers of bEnd.3 cells, equilibrated in DMEM supplemented with 10% FCS and 5.5m M glucose, were treated with either vehicle (0.01% DMSO) or 2.5µM sulforaphane (SFN) for 4h and RNA collected. qRT-PCR was employed to determine mRNA copy numbers for (A) Nrf2, (B) NQO1, (C) HO-1, (D) Bach1 and (E) Keap1 following normalization to three house keeping genes (SDHA, RPL13A and B2M). Data are presented as fold change relative to control. Data denote mean ± S.E.M., and were analysed by students t-test, # $P<0.0001$, ** $P<0.01$, n = 5 bEnd.3 cultures passage 10 – 19.